Alpha-synuclein post-translational modifications and abnormal network oscillations in Lewy body dementias

Nelson de Oliveira Manzanza

A thesis submitted for the degree of Doctor of Philosophy

Institute of Translational and Clinical research

Faculty of Medicine

at Newcastle University, UK

December 2020

Thesis abstract

Lewy body dementias (LBDs) are age related neurodegenerative diseases characterized by the presence of abnormal alpha-synuclein (αSyn) inclusions termed Lewy Bodies (LBs) and Lewy Neurites (LNs) and represent the second most common form of neurodegenerative dementia after Alzheimer's disease. LBDs are progressive pathologic conditions with variable clinical signs and symptoms including dementia and abnormal neuronal network oscillations, with no currently available treatment. The interaction between αSyn post-translational modifications (PTMs) and neuronal dysfunction is a core concept in LBDs. Accumulating evidence shows that, αSyn PTMs, such as, phosphorylation, ubiquitination and nitration, are events that occur in the context of synucleinopathies. I hypothesised that these PTMs lead to the formation of toxic/aggregated forms of αSyn that causes neuronal dysfunctions/death and impair neuronal network oscillations. The aim of this thesis was to Identify the PTMs of αSyn, analyse their distribution in LBDs, correlate them with the distribution of parvalbumin expressing interneurons in in post-mortem brain tissues of LBD patients, and analyse its links with mitochondrial dysfunction and neuronal network impairments. Using, electrophysiological and immunohistochemical protocols in selected cases that fulfilled the neuropathological criteria for LBDs and control cases, sourced from Newcastle Brain Tissue Resource (NBTR), and Transgenic A30P and control C57BL6 mice from comparative biology centre (CBC), I found that aged A30P mice had greater sensitivity to the mitochondrial inhibition by reducing the area power of the gamma frequency oscillations. In addition, parvalbumin expressing cells are significantly altered in humans, specifically in areas associated with the development of prodromal stages of LBDs, these same areas correlated with regions that presented higher Burden of αSyn phosphorylation. In conclusion, this thesis demonstrates that, reduction in density of parvalbumin cells depicts the impairments in gamma frequency oscillations and correlates with an increase in αSyn PTMs in some regions of LBD patients.

Acknowledgements

Health Services Research at Durham University], who I am proud to call him a father, because he has been there for me in all the turbulences and provided me full and unconditional support), and his wife Ann (for giving me unconditional motherly love, in all times) , and family Laura and Mark who I am proud to call brother and sister.

To Judy Francis (grandma), Aunties Silvia, Auntie Marlin Mils and Auntie Margaret for the continuous and unparalleled support and unconditional love. The seme appreciation I extend to my family in the USA, my brother Rosario Luis and family, Tayengo's family (Albano, Tony, Elijah and Jillian "aka the doctor"), Dra. Hilda Viktor Msaki. Not forgetting my friends (Dra. Marlene Tagide, my brother Mutegui, Shelton, Dra. Elsa silva, Dra. Raissa Afonso, Dr Katebe, Dra. Dayanis Andrew, Dra. Hayde Jordao, Arlete Nkoko, Gabriel Tchivelekete, Abreu Passos, Chouna, and Isha. I would also extend my greatest appreciation and feelings of gratitude to Santos' family, specifically to (Adelina, Catila, tia Bia), for being always there for me, regardless of the circumstances. Special thanks also to Dr. Cafala Neto and Junior Pangue for their trust and continuous support. Words are not enough to express my gratitude to you all. A very special thanks to my Auntie Joana Mbambi and Julia Van-Dunem.

Finally, I would like to dedicate this PhD to all my biological family, especially for mama Maria and to my grandparents Oliveira Ganga and Amelia Zacarias Ngola for being my greatest role model and inspiration. Although, they are no longer in the land of the living I am comforted to know that this PhD is the fulfilment of the dream they had for me.

List of abbreviations

DLB   Dementia with Lewy Bodies

LBD   Lewy body disorders

LBs   Lewy bodies

LNs-   Lewy neurites

PD-   Parkinson's disease

PDD-   Parkinson's disease dementia

ETC-   Electron transport chain

PTMs-   Posttranslational modifications

α-syn   Alpha synuclein

AA   Amino acid

CSP   α-Cysteine Stirring Protein alpha

SNARE   Soluble NSF attachment receptor

UPS   Ubiquitin proteasome system

VDAC   Voltage-dependent anion channel

ROS-   Reactive oxygen species

MT   Microtubules

ER   Endoplasmic reticulum

TLR2-   Toll-like receptor2

GABA   Gama amino butyric acid

kDa   Kilo Daltons

ErbB4   Receptor tyrosine-protein kinase erbB-4

NRG1   Neuregulin 1

AD   Alzheimer's disease

5XFAS   Mouse model

PNN   Perineuronal nets

AMPA   α-amino-3-hydroxy-5-methyl-4-isoxazoleprpionic acid

NeK7   NIMA-related kinases7

IPSPs   Inhibitory post synaptic potentials

CCK.   Cholecystokinin

SST.   Somatostatin

VIP   Vasoactive intestinal peptide

GAD65/67   glutamate decarboxylase 65/67

AB   Amyloid beta

EPSPs   Excitatory post synaptic potentials

PTMs   Posttranslational modifications

aSyn   Alpha synuclein

AD   Alzheimer's disease

UPS   Ubiquitin proteasome system

PV   Parvalbumin

PV+   Parvalbumin positive

NBTR   Newcastle brain tissue resource

Pser129   Phosphorylated alpha synuclein at serine 129

AT   Array tomography

STED   Stimulation emission depletion

EDTA   Ethylenediamine tetraacetic acid

DAPI   4′,6-diamidino-2-phenylindole

DAB   3'-Diaminobenzidine

TMA   Tissue microarray

NMDA	N-methyl D aspartate
NMDAr	N-methyl D aspartate receptor
REM	Rapid eye movement
DMNV	The dorsal motor nucleus of vagus
OB	Olfactory bulb
iRt	Intermediate reticular zone
LC	Locus coeruleus
MoRa	Lower raphe nuclei
SN	The substantia nigra
PnRa	Upper raphe nuclei
PTG	Pedunculopontine tegmental nucleus
HT	Hypothalamic
BF	Basal forebrain
DA	Dopamine
PET	Positron emission tomography
SPECT	Single photon emission computed tomography
CBD	Corticobasal degeneration
PSNP	Progressive supranuclear palsy
MRI	Magnetic resonance imaging
EEG	Electroencephalograph
LFPs	Local field potentials
PING	Principal cell interneuron network gamma model
ING	Interneuron network gamma
AP	Action potential
CA3	*cornu ammonis* 3

SNCA	αSyn gene
NAC	Non-amyloid beta component
DOPA	3,4-dihydroxyphenylacetaldehyde
TOM20	Translocase of outer membrane 20
Rab1	Ras-related protein 1
E1-UBA	Ubiquitin-activating enzyme
E2-UBC	Ubiquitin-conjugating enzyme
E3-UBL	Ubiquitin ligase
SIAH	Seven in absentia homologue
DMSO	Dimethyl sulfoxide
Cidia	Clinical diagnosis,
Padia	Pathological diagnosis.
PFC	Prefrontal cortex
MFC	Mid-frontal cortex
CC	Cingulate cortex
MC	Motor cortex
PC	Parietal cortex
OC	Occipital cortex
IC	Insular cortex
EC	Entorhinal cortex (
BG	Basal ganglia
WM	White matter
APES	3-aminopropyltriethoxysilane
EDTA	Ethylenediaminetetraacetic acid
TBS	Tris buffered saline

TBST   Tris buffered saline with tween 20®

H_2O_2 Hydrogen peroxide

HRP   Horseradish peroxidase

DPX   DePex destrene

ROI   Region of interest

RI   Rhythm index

ETC   Electron transport chain

ATP   Adenosine triphosphate

NADH   Nicotinamide adenine dinucleotide

LTP   Long term potentiation

PA   Action potentials

Table of Contents

List of figures

List of tables

Chapter 1: Introduction

1.1 Ageing, neurodegeneration and dementia

Population ageing is a global phenomenon that is affecting many countries as a result of the increase in life expectancy and the reduction of fertility rates in the global population. Ageing is now the driving force propelling the current rise of dementia, which in turn, is causing an increase in socio-economic burden affecting many countries (Sosa-Ortiz et al., 2012, Olshansky, 1985). This parallel increase in prevalence of dementia, together with its socio-economic burden, is predicted to cost the global economy, up to $1.117 billion by the year 2030 (Lakey, 2012, Wittenberg et al., 2019). In the UK alone, it is estimated that approximately 690,000 people over the age of 60 are affected with some form of dementia, costing the National Health Service approximately £23 billion a year (Lakey, 2012, Wittenberg et al., 2019). In addition to other chronic non-transmissible diseases, such as, diabetes, chronic respiratory and cerebrovascular diseases that are known to be frequent in the elderly populations, the neurodegenerative dementias introduce a unique set of challenges, as they are associated with high social and financial costs, with the potential of decreasing the economic growth of a country. Therefore, governments are now forced to prioritise strategies to address this issue (Daar et al., 2007).

Neurodegenerative disease, is an umbrella term used to describe a group of pathologic conditions that affects primarily the nerve tissue (Przedborski et al., 2003). They are characterized by a plethora of complex pathogenic pathways, which culminate with the chronic progressive dysfunction and degeneration of nerve cells (Herrero and Morelli, 2017). The similitude in the pathogenic pathways among the neurodegenerative diseases and their predilection for anatomically related structures, leads them to share common clinical features (Dugger and Dickson, 2017). This overlap in clinical features among different neurodegenerative diseases, is thought to be directly proportional to the regional and anatomically related areas within the brain rather than molecular mechanisms that underlie the pathological lesion (Gelder et al., 1989, Jackson, 2012). This aspect is explored in this thesis.

Neurodegenerative diseases are mainly sporadic in their occurrence and multifactorial in their aetiology (Elbaz et al., 2007). Multiple lines of evidence suggest that the common molecular pathological characteristic of these pathologies is the aggregation of a specific set of proteins. These proteins are thought to misfold as a result of genetic errors or modifications due to radiation, oxidation, glycation or other influences, which then leads to abnormal accumulation of the protein within the neuronal tissues, resulting in cellular dysfunction and death. (Carrell and Lomas, 1997, Dobson, 1999, Skovronsky et al., 2006). The type of pathological protein deposit, its molecular characteristics together with its cellular effects and topographical localization/distribution, constitute the basis of the neuropathological classification of the respective diseases (Carrell and Lomas, 1997, Dobson, 1999, Skovronsky et al., 2006). Despite the advances in understanding the pathogenesis of neuronal degeneration, the exact causes that leads to formation of these proteinaceous inclusions remain poorly understood. It is suggested, however, that the volume of aggregated proteins, together with their location and distribution are determinants of the onset, the progression of these diseases, as well as the manifestation of the clinical symptoms (Jellinger and Attems, 2013).

More recent evidence suggests that in some neurodegenerative diseases, such as, the synucleinopathies, the pathogenic cascade starts before the proteins forms aggregates (Visanji et al., 2019). In addition, a certain degree of neuropathological lesions was also detected in non-demented individuals, although the number and size of these aggregates is lower, when compared to the disease-affected individuals. In fact, in some individuals, the neurodegenerative processes (aggregate formation) correlate with clear symptoms of dementia, while in others they appear to be inert with no impact on cognition and limited pathology (Kosaka, 2014, Kosaka et al., 1988). These observations have sparked a debate as to why some aged individuals do not develop dementia, and whether neurodegenerative diseases are a direct consequence of ageing or of a distinctive disease caused by an identifiable molecular pathology (Stern, 2012, Attems et al., 2005). Thus, understanding the molecular mechanism underlying these clinical manifestations may help elucidate these questions.

Dementia is defined as a non-specific syndrome that characterises an extensive group of brain disorders, which progress with a gradual decrease of the cognitive functions,

affecting the individual's ability to function in the society independently. It brings forth a devastating impact to the affected individuals, their family, including non-family members entrusted with the care of these patients (Prince et al., 2013, Sosa-Ortiz et al., 2012). According to the time of the onset, dementias are classified into two main types, early onset dementias (EOD) and late onset dementias (LOD). EOD are often more aggressive and rapidly progressing, in which the clinical symptoms develop before the age of 65. They are less common, and are often attributed to brain injuries, toxic-metabolic/hypoxic complications and genetic causes (Prince et al., 2013, Sosa-Ortiz et al., 2012). LOD/ progressive dementias are commonly known as age-related dementias as their clinical manifestations usually present after the age of 65 (it can also occur before 65 years of age). In most cases, it occurs as a result of neurodegenerative or cerebrovascular diseases. Less common causes of this type of dementia include paraneoplastic, infectious and autoimmune diseases (Prince et al., 2013, Sosa-Ortiz et al., 2012). It is the sporadic nature and lack of clear correlation between protein aggregates and the development of dementias in neuronal degeneration that are explored in this thesis.

1.2   Synucleinopathies and Lewy body dementias

Synucleinopathies is a term used for a group of neurodegenerative disorders characterised by the pathological aggregation of alpha synuclein (αSyn) protein forming Lewy bodies (LBs) and Lewy neurites (LNs) inclusions within the neuron or neuroglia (Goedert et al., 2013, Spillantini et al., 1998, Spillantini et al., 1997). They are clinically characterised by chronic and progressive cognitive dysfunction, motor impairments, autonomic and behavioural dysfunction. In parallel with the anatomical distribution of the aggregates (LB/LN) (figure1.1), the nosological entities that are included in this group are: Parkinson's disease (PD), Parkinson's disease dementia (PDD), dementia with Lewy bodies (DLB), pure autonomic failure (PAF), and multiple system atrophy (MSA) (Bras et al., 2020) (table 1.1). These disorders share common genetic and pathogenic mechanisms and their clinical spectrum often overlaps, making it difficult to establish a clear differential diagnosis (Marti et al., 2003). In fact, the overlap in clinical presentation is considerable among DLB and PDD as dementia is one of their main symptoms.

Table 1. 1: showing the summary of the synucleinopathies and their main clinical and pathological features.

Disease	Aggregates	Cell type	Region affected	Main Clinical features
DLB	LBs/LNs	Neurons	Cortex	Cognitive decline
PD	LBs/LNs	Neurons	Substantia Nigra	Motor impairment
PDD	LBs/LNs	Neurons	Substantia Nigra, Cortex	Motor impairment, cognitive decline
MSA	LBs/LNs	Glia	Cerebellum, Substantia Nigra	Cerebellar ataxia, Motor impairment
PAF	LBs/LNs	Neurons	Sympathetic ganglia	Orthostatic hypotension

DLB, PD and PDD are a subgroup of the synucleinopathies that are collectively termed Lewy body disorders (LBDs) (Outeiro et al., 2019). They are characterized by the pathological aggregation of αSyn protein as intra-neuronal inclusions and named as LBs and LNs, which are the pathological hallmarks of this group of diseases. LBDs account for 22% of all dementias in the geriatric population (McKeith et al., 2017, Spillantini et al., 1997, Braak et al., 1999) and are second only to Alzheimer's disease (AD) in prevalence (Outeiro et al., 2019). Although, LBDs share the same pathological hallmarks, they are distinguished by the anatomical distribution of the pathology, and accordingly to the symptomatic profile presented (Hansen et al., 2019, McKeith et al., 2005). The nature and correlation of aggregates in DLB, PD and PDD, their anatomical distribution is also investigated in this thesis.

1.2.1 Parkinson's disease

Parkinson's disease is a chronic disorder that affects approximately 2% of the aged population (de Rijk et al., 1997). It is the most common neurodegenerative disease, which progresses with movement disorder (Kumar et al., 2012, Fahn, 2011). The disease can result from a combination of genetic (Fahn, 2011) and environmental factors (Kumar et al., 2012). Clinically, a classical trilogy consisting of bradykinesia, rigidity and resting tremor characterises PD. In addition to this, patients may also

develop some non-motor symptoms such as hyposmia, constipation, anxiety, mood disorders and rapid eye movement (REM) sleep behaviour disorder (Ravina et al., 2007, Jankovic, 2010, Hely et al., 2008). Habitually, these symptoms may precede the classical trilogy, and are therefore considered a risk factor for the later development of the classical symptoms that define the disease (Ravina et al., 2007, Jankovic, 2010, Hely et al., 2008).

Macroscopically, PD cases tends to show unremarkable changes in the CNS tissue, except for the changes observed in the locus coeruleus, motor nucleus of the vagus nerve and the substantia nigra (figure 1.1) (Ma et al., 1996, Kalaitzakis et al., 2008). The main microscopic alterations in PD brains, as well in DLB and in PDD are the neuronal loss, macrophages filled with neuro melanin inclusions and gliosis (Damier et al., 1999). In PD the neuronal cell loss is usually observed in the ventral tier of the substantia nigra (SN), which can be observed as the loss of the pigmented nuclei (Damier et al., 1999, Ma et al., 1996). In addition, the classical pathological hallmark (LBs and LNs) of the disease can also be observed in substantia nigra, motor nucleus of the vagus and the locus ceruleus (Maiti et al., 2017).
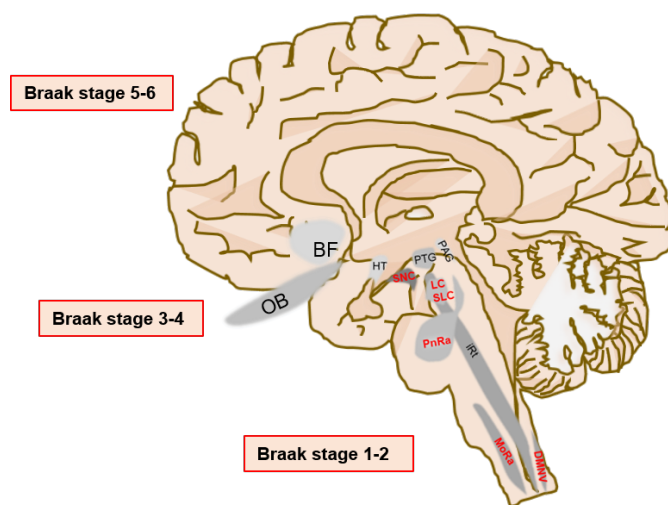
Figure 1. 1 Brain regions affected in Parkinson's disease. The dorsal motor nucleus of vagus (DMNV), the olfactory bulb (OB) and the intermediate reticular zone (iRt) are affected in Braak stage 1. Locus coeruleus (LC), the lower raphe nuclei (MoRa), affected in braak stage 2. The substantia nigra (SN), the upper raphe nuclei (PnRa), thee pedunculopontine tegmental nucleus (PTG) are affected in the braak stage 3, including other hypothalamic (HT) nucleus and structures in the basal forebrain (BF).

The SN is abundant in dopaminergic (DA) neurons, which produces neuro-melanin, a substance that gives the dark appearance of these nuclei. This cluster of neurons forms projections that forms the nigro-striatal pathways (Damier et al., 1999). The loss of these neurons leads to the reduction of projection to the striatum, therefore to motor dysfunctions (Damier et al., 1999). The loss of the nigro-striatal connections subsequently leads to a loss of inhibition output from the SN par reticulate and the internal Globus pallidum to the sub-thalamic nucleus. On the other hand, this loss of inhibition leads to a relative hyperexcitability output from the sub-thalamic nucleus, inhibiting the thalamic regions to the motor cortex, resulting in akinetic rigidity, a core symptom of PD (Mark et al., Damier et al., 1999, Dickson, 2012, Alexander, 2004).

Although, there are no effective diagnostic tests for PD a number of investigations has recently focused on identifying a biomarker for PD. Olfactory impairment is a prodromal symptom that occurs in most PD patients and often precedes the motor symptoms (figure 1) (Boesveldt et al., 2008, Attems et al., 2014). An olfactory test that is based in analysing the functions of the olfactory nerve was developed, and its sensitivity and specificity, has been reported to be between 75-100% specific for the differential diagnosis of PD (Doty et al., 1995, Katzenschlager et al., 2004). Second, DA loss and the loss of projection from the SN to the striatum can be identified by imaging tests such as the positron emission tomography (PET) or the single photon emission computed tomography (SPECT) (Colloby et al., 2012, Rakshi et al., 1999). Nonetheless, these methods are proven to be inefficient for the clear differential diagnosis of PD from other neurodegenerative diseases that present with SN degeneration such as MSA, DLB, corticobasal degeneration (CBD) and progressive supranuclear palsy (PSNP) (Miki et al., 2010, Doppler et al., 2014b). In addition, extra-axial deposits of αSyn were found in the skin and the small nerve fibres in the intra-epidermal tissue. However, to date, the validity of these biopsies is still a matter of debate (Miki et al., 2010, Doppler et al., 2014b).

1.2.2 Parkinson's disease dementia

PDD is not considered a single nosolgical entity in itself, but rather a common complication of PD (Jellinger and Korczyn, 2018, Richard et al., 2002, Hely et al., 2008). It is estimated that 80% of patients with parkinsonian symptoms develop dementia in the advanced stages of their disease. A 20-yearlong prospective study on

136 patients suffering from PD reported that 75% of the autopsy of these patients reported to have had dementia before death and 83% of the living patients presented dementia. These findings suggest that PDD is a late complication of PD (Hely et al., 2008). Contrariwise, some longitudinal studies reported dementia-free at the time of death in individuals with PD (Docherty and Burn, 2010). Whether this is because some individuals have higher cognitive reserve or is simply a matter of time i.e., death occurs before the individuals fully develop dementia, more investigations are required to address this issue. Nevertheless, the risk of developing dementia increases six-fold in PD patients compared to healthy individuals (Aarsland et al., 2003), adding an extra burden to the disease by increasing the need for patient placement into the nursing homes (Aarsland et al., 2001, Levy et al., 2002).

1.2.3 Dementia with Lewy bodies

DLB is the second most common type of dementia that results from neuronal degeneration after AD, accounting for 4.2% of all dementia cases in the community (Vann Jones and O'Brien, 2014). DLB also represents 10-15% of all cases of neurodegenerative dementia proven by autopsy (McKeith et al., 2004). The clinical hallmarks of DLB include core clinical features of progressive dementia, visual hallucination, sleep abnormalities and Parkinsonism. In addition, supportive features, such as hypersomnia, hyposmia and severe sensitivity to antipsychotic drugs may also be present (Gurd et al., 2000, McKeith, 2006, McKeith et al., 2017, Goedert et al., 2013, Spillantini et al., 1998, Spillantini et al., 1997). Some patients may present with recurrent syncope and falls, which is suggestive of the involvement of the autonomic nervous system in the development of DLB (McKeith et al., 2003). Moreover, individuals with DLB present with greater attention and visual processing deficits in comparison to AD patients, with relative preservation of naming and memory (Hansen, 1997, Ferman et al., 2006). Currently, age remains the strongest risk factor for the development of DLB (McKeith et al., 1996).

Similarly to PD, the most notable macroscopic characteristic of DLB is the depigmentation of the SN due to the loss of the neuromelanin-expressing DA neurons (Bozzali et al., 2005). Nevertheless, other changes similar to those observed in AD, such as broad cerebral atrophy can also be observed (Bozzali et al., 2005). The macroscopical difference between DLB and AD comes from the relative preservation

of the frontal lobe observed in structural magnetic resonance imaging (MRI) in DLB patients (Burton et al., 2009). The assessment of cortical thickness through MRI has also been proven effective in differentiating DLB from other dementing disorders, by showing atrophy pattern that primarily affects subcortical structures in DLB (Watson et al., 2009). The yearly cerebral atrophy rate in DLB is 1.4% that is three times higher than in the age matched non-DLB patients, however, this is slightly less when compared to AD, in which the yearly cerebral atrophy rate is 2% (O'Brien et al., 2001). For instance, Watson et al, found that in DLB, cortical thinning is more accentuated in brain regions such as posterior cingulate gyrus, inferior parietal and fusiform gyrus. In contrast, cortical thinning is more accentuated in parietal, temporal and frontal lobes in AD (Watson et al., 2015). The structural changes in DLB are consistent with the predominate affectation on the limbic and cortical areas, with Lewy pathology present in the principal glutamatergic neurons, particularly those of layer III and V of the neocortex (Rezaie et al., 1996) (Wakabayashi et al., 1995, Marui et al., 2003 and Bernstien et al., 2011).

In practice, the clinical and pathological profiles of PD and DLB demonstrate considerable overlap. Many DLB cases present with parkinsonism associated with brainstem and midbrain pathology, indeed many PD cases present with dementia owing to limbic and cortical invasion by pathology, known as PDD (figure 2) (Jellinger and Korczyn, 2018). Currently, the differential diagnosis between PDD and DLB is done using the temporal profile, i.e., the time of onset of cognitive symptoms from the presentation of parkinsonism (McKeith et al., 2004, McKeith et al., 2017). The diagnosis of PDD requires the onset of dementia to occur at least one year after the onset of the initial PD related symptoms (McKeith et al., 2017). In contrast, if the onset of dementia begins within one year of the development of parkinsonism, then the profile is considered to be consistent with DLB (Gurd et al., 2000, McKeith, 2006, McKeith et al., 2017, Goedert et al., 2013, Spillantini et al., 1998, Spillantini et al., 1997). Nevertheless, if dementia develops in the context of established PD, then it is consistent with PDD (McKeith et al., 2017). Generally, PDD occurs after at least 10 years of the onset of PD (McKeith et al., 2017, Aarsland et al., 2003). However, the neuropsychological profile of PDD is phenotypically not very different when compared with DLB (Aarsland et al., 2003). Despite progress in our understanding and identification of the variable symptoms, which may be indicative of either PD or DLB

disease progression, a definitive clinical diagnosis remains difficult to achieve. At present, a confirmed diagnosis is only provided through post-mortem examination via the detection of intraneuronal inclusions, consistent with LB pathology within the neuronal soma and LN pathology within the neuronal processes (figure 1.2).
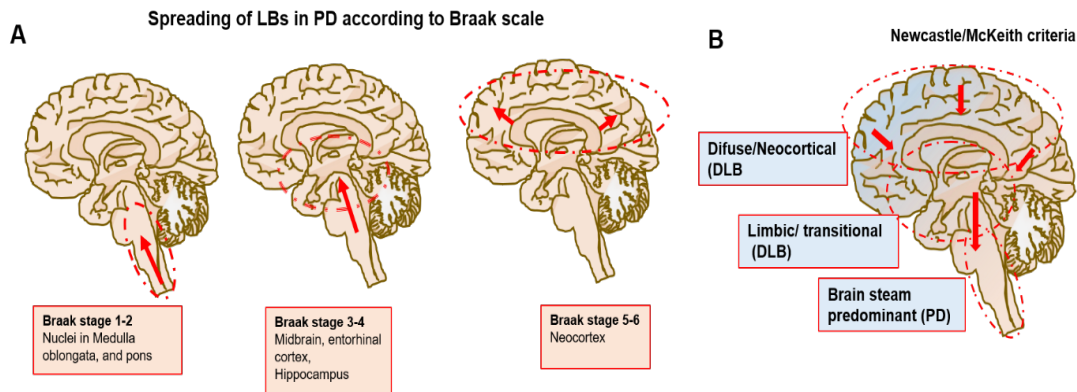
Figure 1. 2: Topographical distribution of LBs according to Braak and Newcastle/McKeith scales. A In Braak stage LBs initially affects the medulla oblongata (stage I), then gradually spreads to Pons (stage II), midbrain (stage III), Hippocampus and entorhinal cortex (stage IV), and finally the neocortex (stages V-VI). **B** the Newcastle/McKeith criteria differentiates between Brain stem Predominant (PD), Limbic (transitional DLB) and diffuse neocortical DLB. It has been proposed that in PD LBs spreads from caudal to cephalic regions in the neuroaxis. On the other hand, the topographical progression in DLB has been proposed to start from the cephalic to caudal regions of the neuroaxis.

1.3   High Frequency oscillations in synucleinopathies

The role of pathological αSyn in disrupting the synaptic integrity has been described in sections below. Synaptic impairment could underlie the characteristic changes in the neuronal network oscillations observed in many neurodegenerative diseases. This is supported by electroencephalograph (EEG) studies from both human patients and animal models (Nimmrich et al., 2015). In our Lab, we have previously demonstrated the involvement of the pathological αSyn in impairing the neuronal network oscillations and causing mitochondrial dysfunction (Robson et al., 2018b). However, the knowledge about the pathophysiology of the neuronal network oscillations in synucleopathies is still highly incomplete.

The mammalian EEG is a non-invasive method that record brain electrical activity by placing the electrodes at the surface of the scalp in physiological and pathological states (Lopes da Silva, 2013, Skinner et al., 1994, Wood, 1996, Berger et al., 2010). The measured electrical activity in the EEG is the result of the electrical potential difference recorded at the surface of the scalp, generated by the precise timing and synchronous firing of a group of neurons when processing information across different brain regions, which results in different frequency ranges (Wood, 1996, Light et al., 2010). These neuronal oscillations reflect the excitatory activity of a group of neurons that present as rhythmic fluctuations over time. It is electrically manifested as cyclic changes in voltage, and it is seen as a combination of sine waves of different frequencies (Mathalon and Sohal, 2015, Basar, 2013)(Daniel, Et al., 2015). Oscillations represent synchronized activity between group of neurons within a brain region or across different brain regions (Mathalon and Sohal, 2015, Basar, 2013). Neuronal oscillations can be detected at different levels using intracranial or surface EEG, local field potentials (LFPs), multi-unit recordings, and intracellular recordings (Buzsáki et al., 2012, Sohal, 2012b). Based on frequency, cortical neuronal network oscillations are classified into delta (0.5-4Hz) theta (4-10Hz), alpha (8-12Hz), beta (10-30Hz), and gamma (30-100Hz) oscillations (Buzsáki, 2005, Sohal, 2012b).

1.3.1 Gamma frequency oscillations and cognition

Gamma frequency oscillations are believed to be essential for cognitive function and different behavioural states. Crucially, many studies have found abnormal gamma network oscillations in a range of neurodegenerative and neuropsychiatric diseases (Buzsáki, 2005, Sohal, 2012b, Mably and Colgin, 2018). Therefore, it is important to understand how oscillatory activity might be altered in neurodegenerative disease such as LBDs and AD (Bonanni et al., 2008). Alterations in network oscillations seen in patients with LBDs and AD, underlie the cognitive impairments observed in these patients (Bonanni et al., 2016, Bonanni et al., 2008, Thomas et al., 2008). In fact, cognitive impairment, such as fluctuations in cognitive ability and function, have been linked to an abnormal EEG burst patterns seen in the frontal brain regions of the DLB patients (Delli Pizzi et al., 2015, Cromarty et al., 2016, Peraza et al., 2018, Crystal et al., 1990).

The prefrontal cortex and the hippocampal activities orchestrate a precise interplay in the generation of complex cognitive functions such as memory (Preston and Eichenbaum, 2013, Sigurdsson and Duvarci, 2015). Although cognitive dysfunction linked with LBD is thought to be in nature more related to the prefrontal cortex (PFC) than the hippocampus, an overall slowing of the oscillation frequency to lower frequency bands was observed in the individuals affected with the DLB (Bonanni et al., 2008, Andersson et al., 2010, Morris et al., 2015). In addition, gamma frequency oscillations are thought to play an important role in selecting and combining inputs from the sensory cortex to allow the brain to process multimodal stimuli (Uhlhaas and Singer, 2006). Moreover, high frequency oscillations are essential for the rapid processing and transfer of information across different brain regions and are frequently implicated in the cognitive processing (Lu et al., 2012). A single neuron is not suited to orchestrate cognitive functions by itself. It needs the participation of multiple neurons to act in synchrony as a group, to generate measurable electrical fluctuations in the LFP that can be detected (Quiroga, 2013), in such way gamma frequency oscillations is detected in the LFP.

1.3.2 The role of the inhibitory interneurons in generation of fast network oscillations

The source of the gamma frequency oscillations (30-100Hz) that exceed the firing of pyramidal cells (1-3Hz) was not clearly understood until the implication of gamma amino-butyric acid (GABA)ergic interneurons, which fire at a frequency rate up to 40Hz (Whittington et al., 1995). GABAergic interneurons are classified into Retzius-Cajal cells, Martolini cells and Basket cells (Table1.2) (Sultan et al., 2013). A subgroup of GABAergic interneurons are parvalbumin (PV) expressing fast spiking interneurons, representing 40% of all GABAergic interneurons (Rudy et al., 2011) (Table 1.2). Since the frequency of the neuronal network, oscillations are reliant to the decay kinetics of GABA, GABAergic interneurons project inhibitory inputs to both inhibitory and excitatory pyramidal cells (Otis and Mody, 1992, Heistek et al., 2010, Lee and Jones, 2013). Hence, based on their interaction with the two types of pyramidal cells, two models of gamma network oscillations generated by the GABAergic interneurons have been proposed (figure 3): The principal cell interneuron network gamma model (PING) and the interneuron network gamma (ING) (Börgers and Kopell, 2005).

Table 1. 2: Comparative table for interneurons population.

Molecular Marker	Interneuron types	Interneuron circuitry	Electrical properties	Firing properties	Oscillatory activity	Potential malfunction in DLB
PV	Chandelier cells Basket cells	Perisomatic inhibition into pyramidal	Fast, reliable, short term depression	Fast spiking	Gamma 40-100Hz	Impact on cognition, behavioural and motor functions
Cholecystokinin (CCK)	Basket cells	Perisomatic inhibition into pyramidal	Fast, unreliable, variable short-term plasticity	Regular spiking/ low treshold spiking	Gamma 40-100Hz	-
Somatostatin (SST)	Martinotti cells	Dendritic inhibition	Low-threshold spiking	Fast, reliable, short term depression	Theta 4-8Hz	-
Nitric oxide synthase (NOS)	Neuoroglioform cells (NG)	Axonic inhibition	Slow, unreliable	Late spiking	Theta 4-8Hz	-
Vasoactive intestinal peptide(VIP)	Bipolar Vasoactive intestinal peptide (VIP)	Axonic inhibition	-	Burst spiking		-

*The table lists some of the properties of GABAergic interneurons and it is not completely exhaustive. References (DeFelipe et al., 2013, Ascoli et al., 2008, Markram et al., 2004, Kawaguchi and Kubota, 1997, Freund and Katona, 2007, Armstrong and Soltesz, 2012, Daw et al., 2009, Kuhlman et al., 2013).

The ING model (figure 1. 3) suggests that gamma oscillations can be locally generated by interneurons where the oscillation cycles are stabilised by gap junctions of axonal plexus that provides fast electrical transmission (Traub et al., 1996, Traub et al., 1999). This model, however, does not clarify the gamma frequency oscillations that project over longer distances within the hippocampus or across different brain regions. The PING model (figure 1. 3) better explains these long-range oscillations.

PING is a model that explains the interconnection between pyramidal cells and the interneurons. In this model, it is suggested that the pyramidal cells firing excitatory post synaptic potential (EPSP) occur earlier than the interneurons, in cycle, which causes the interneurons to generate rhythmic trains of inhibitory postsynaptic potential (IPSPs). This then produce an inhibitory feedback which ends the cycle of the excitatory cell action potential (AP) firing, and then later the pyramidal cell cycle

restarts once the IPSP has dissipated (Langmoen and Andersen, 1983).
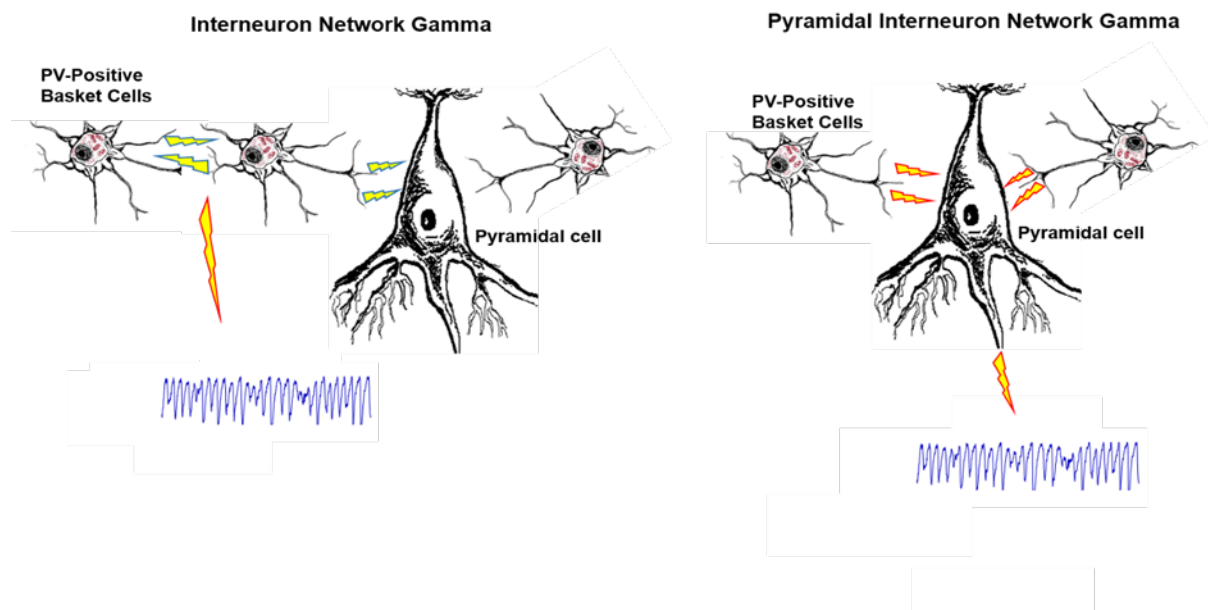
Figure 1. 3: A representation of the ING (left) and PING (right) models of gamma frequency oscillations in the CA3 region of the hippocampus.

PV+ fast spiking interneurons are thought to play a key role in the generation of the gamma frequency oscillations. The involvement of these interneurons was demonstrated in an *in vivo* optogenetic study in mice, where gamma oscillations were abolished when fast spiking PV+ interneurons were silenced (Sohal et al., 2009). In rodent *cornu ammonis* 3 (CA3) region of the hippocampus, gamma frequency oscillations are also found to be dependent on the PV+ cells (Traub et al., 2000, Ferando and Mody, 2015, Fuchs et al., 2007). The results of these studies have led to the hypothesis that the reduction of number or loss in function of the PV+ interneurons, may be at the basis of the network connectivity impairment and the subsequent cognitive dysfunction (Fuchs et al., 2007), that is observed in many neuropsychiatric disorders, including schizophrenia (Nakazawa et al., 2012), and neurodegenerative disorders, including DLB (Robson et al., 2018a), and AD (Brady and Mufson, 1997).

1.3.3 Invitro study of the gamma frequency oscillations

The study of the association between neuronal network oscillations and their underlying cellular activity in a determined region of the brain can now be made through the investigations of the oscillations *in vitro*. These studies are possible thanks to improved protocols of the cellular preservation and viability used in the current

electrophysiology methods (Pietersen et al., 2009, Robson et al., 2018b). With the use of the interface chamber, a more persistent gamma oscillations can be induced successfully using cholinergic agonists such as carbachol (CCH), which activates the muscarinic and nicotinic receptors of the acetylcholine neurotransmitter (Traub et al., 1992), or the ionotropic glutamatergic kainite receptor agonist kainate (KA) (Hájos et al., 2000, Hormuzdi et al., 2001), which provides excitation input to the network. The peak frequencies and the power of spontaneous, KA- and CCH-induced hippocampal gamma frequency models may vary, depending on the region and the layer of the hippocampus that is being investigated and the interneuron types that are recruited, due to the variability of the expression of the receptors (Pálhalmi et al., 2004, Vreugdenhil and Toescu, 2005).

1.4 The molecular pathology in neurodegenerative diseases

1.4.1 LB and LN inclusions

LBs and LNs are insoluble proteinaceous aggregates comprised of many cellular components including dysmorphic organelles, vesicular structures and membranes (Spillantini et al., 1998, Shults, 2006, Shahmoradian et al., 2018, Braak et al., 1999). Whilst proteomic analysis of LBs reported over 90 potential co-aggregates, αSyn was identified as the most abundant constituent of the inclusion (figure 1. 4) (Spillantini et al., 1998, Spillantini et al., 1997, Marques and Outeiro, 2012). αSyn is ubiquitously expressed in the nervous system, encompasses 1% of the total cytosolic protein, and is predominantly located in the presynaptic terminals of neurons (Kahle, 2008). In immunohistochemistry studies, αSyn is found to be robustly present within the LBs and LNs, often forming a halo-like structure around the inclusions (Spillantini et al., 1998, Spillantini et al., 1997, Baba et al., 1998). The involvement of αSyn in PD pathology was confirmed in studies of the familiar forms of PD, in which five common mutations. i.e., p.A30P, p.E46K, p.H50Q p.G51D and p.A53T within the αSyn gene (*SNCA*), was fund to cause the formation of LBs and LNs (Kruger et al., 2001, Pasanen et al., 2014, Proukakis et al., 2013, Zarranz et al., 2004, Polymeropoulos et al., 1997, Lesage et al., 2013, Bussell and Eliezer, 2001, Kumar et al., 2012, Albin et al., 1989). In addition, these intraneuronal inclusions are immunoreactive to αSyn antibodies and are the main histopathological features of all LBDs. Crucially, the differential regional and cellular distribution of aggregated αSyn distinguishes the

various forms of LBDs (Mattila et al., 2000, Goedert et al., 2013, Spillantini et al., 1998, Spillantini et al., 1997). In addition to αSyn mutations, it is now understood that posttranslational modifications (PTMs) impair the native state of the protein, which consequently induces the protein to misfold and aggregate, forming LBs and LNs inclusions within the nervous system (Villar-Pique et al., 2016).

Although, the exact mechanisms that trigger pathological aggregation of αSyn and the consequent formation of LBs and LNs in DLB are not clearly understood, the assessment of disease associated PTMs of αSyn is thought to be key in the comprehension and elucidation of potential reasons of the aggregation (Pajarillo et al., 2019). Moreover, understanding the anatomical and regional distribution of PTMs of αSyn, in line with the established neuropathological schemes of pathological progression, may provide an insight of the temporal sequence of the occurrence of toxic PTMs at different stages of the disease. For example, if αSyn modifications were to occur early in the subcortical regions including the medulla, olfactory tract and mesencephalon, prior to the axial progression to the cortical regions, may highlight the modification as a potential facilitator of LB and LN formation in subsequent regions, thus, it may help in understanding the observed differences in anatomical and distribution patterns of LBs as evident in various synucleinopathies (Moors et al., 2018, Jellinger and Korczyn, 2018). The elucidation of this mechanism of disease-causing PTMs on αSyn structure, function and localization may help to better aid the development of new treatments for LBDs.
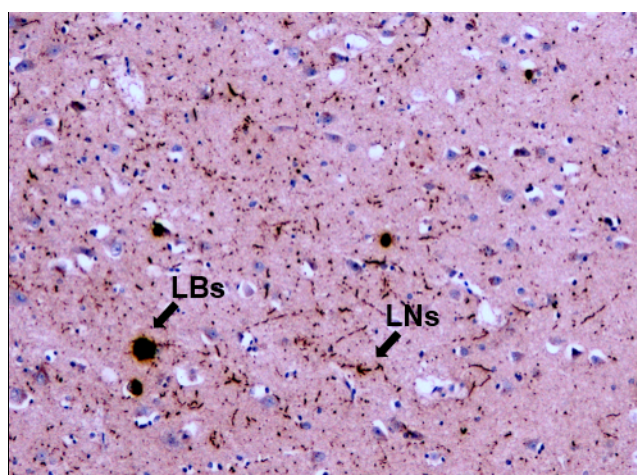
Figure 1. 4: A representation of brain histology showing LBs and LNs inclusions labelled by an antibody recognizing αSyn phosphorylated at serine 129 (Pser[129]) co stained with haematoxylin in the amygdala.

1.4.2 αSyn structure and function

αSyn is a small 14.5kDa protein, a member of the synuclein family, which also includes γ-synuclein and ß-synuclein (Maroteaux et al., 1988, Ueda et al., 1993). αSyn is a product of the *SNCA* gene located at position 21 of the long arm of chromosome 4. This gene encodes 140 highly charged amino acid (aa) residues that do not adopt a defined structure in an aqueous solution (Polymeropoulos et al., 1997, Wales et al., 2013). αSyn consists of three distinct domains: The *N-terminal domain, the Central domain* and the *C-terminal domain.* The *N-terminal domain* or *the amino terminus,* (aa 1-60) contains four 11-mer repeats that have a KTKEGV consensus sequence. This region is predisposed to fold into alpha helices, and it is thought to be linked with the lipid binding capacity of the protein (Wales et al., 2013, Polymeropoulos et al., 1997, Marui et al., 2004). The *Central domain*, also called the *non-amyloid beta component (NAC)* (aa 61-95) is a particularly hydrophobic and amyloidogenic region (Maroteaux et al., 1988, Ueda et al., 1993). Studies have reported that this domain is associated with αSyn aggregation when it adopts a beta-sheet structure (Lesage et al., 2013, Polymeropoulos et al., 1997, Proukakis et al., 2013). Additionally, identified PTMs, such as phosphorylation, linked with synucleinopathies are also found in this region (Lesage et al., 2013, Polymeropoulos et al., 1997, Proukakis et al., 2013). Lastly, the *C terminal domain* or *the carboxyl terminus* (aa 96-140), provides flexibility to the polypeptide, because of its abundance in proline residues, which are known to disrupt the secondary structure of the region (Ueda et al., 1993, Maroteaux et al., 1988). This region is highly acidic and intrinsically unstructured, and it is believed to be the target of diverse PTMs (figure 1.5; 1.6) (Bussell and Eliezer, 2001, Bussell and Eliezer, 2003, Davidson et al., 1998). Furthermore, this region is thought to be involved in protein-protein interactions, polyamine binding, protection from protein aggregation and modulation of membrane-binding properties of the protein (Oueslati et al., 2010, Fernandez et al., 2004, Brown, 2007, Nielsen et al., 2001, Bodner et al., 2009, Sevcsik et al., 2011, Park et al., 2002, Crowther et al., 1998).

The exact function of αSyn remains a focus of intense debate and research efforts. Nonetheless, the predominant neuronal expression of αSyn and its localization in the presynaptic terminal, suggests a regulatory function in the synapse (Burre, 2015). In fact, changes in αSyn expression, either overexpression, knockdown or knockout led to alterations in synaptic vesicle trafficking and maintenance, neurotransmitter

compartmentalization, storage, as well as recycling and accordingly, alterations in synaptic activity and plasticity (Lashuel et al., 2012, Burre et al., 2013, Allen Reish and Standaert, 2015). Given the extensive nature of the synaptic parameters affected, it may be speculated that αSyn acts as an accessory protein within these processes. Precisely, αSyn is thought to act as a scaffold and as such, assists various proteins in their cellular functions. For instance, αSyn supports the soluble N-ethylmaleimide-sensitive factor attachment protein receptor (SNARE) proteins in their role, potentially acting with some level of functional redundancy with cysteine stirring protein alpha (CSP-alpha) (Goda, 1997, Gerst, 1999). αSyn is thought to interact with the SNARE proteins by acting as molecular chaperone that assists in folding and refolding of these proteins (Burre et al., 2010) by directly binding to synaptobrevin 2 (a SNARE protein) to promote the formation of the SNARE complex. Its interaction with SNAREs ultimately leads to the regulation of the synaptic vesicle's dynamics during the process of neurotransmitter release in the synapse (Burre et al., 2010). This finding is further supported by the study of Fortin et al. (2005), that demonstrated that during neuronal activity, fluorescently labelled αSyn retracts from the synaptic vesicles and returns progressively to the vesicles, thus regulating the neurotransmitter release. Despite various efforts to understand the functions of αSyn, the full extent of αSyn function remains poorly understood.

1.4.3   αSyn aggregation and its role in cellular dysfunction

αSyn aggregates are the main constituents of LBs and LNs, the neuropathological hallmarks of the synucleinopathies, also present in mixed neuropathological cases where both LBs and atypical AD beta-amyloid and tau pathology are present (Spillantini et al., 1998, Spillantini et al., 1997). Multiple studies have shown that unstructured soluble monomers of αSyn are transformed into oligomers, then the oligomers aggregate to form mature insoluble fibrils, to then form the LBs (Harper et al., 1997, Lambert et al., 1998, Miake et al., 2002, Walsh et al., 1997). An *in vitro* study demonstrated that the αSyn aggregation process occurs in three different stages, named respectively as the *lag, elongation* and *stationary* phases (Buell et al., 2014). The *lag phase* is defined by key structural changes that result in the formation of misfolded monomers, followed by monomer aggregation and oligomer formation. In the *elongation phase*, an exponential growth of oligomers into insoluble fibrils is achieved by a continued addition of αSyn monomers. Finally, in the *stationary phase*,

the depletion of monomeric aggregates culminates into reduction of the fibril growth rate (Buell et al., 2014, Invernizzi et al., 2012). This sequence of events that starts from the natively unfolded protein and terminates with the formation of fibrils is termed αSyn aggregation which forms LBs and LNs in LBDs.

It is believed that aggregation is the core pathogenic feature of αSyn (Periquet et al., 2007). However, it is unclear if whether the end-stage products of the aggregation (LBs/LNs) are the most disease relevant toxic forms of αSyn. It is widely assumed that the process of aggregation is critical and its intermediates including pre-fibrils and oligomers formed during the aggregation process may in fact be more relevant to disease pathology (Periquet et al., 2007). This view is supported by a study which showed that αSyn and ß-synuclein that do not contain the *NAC* domain (which promotes aggregation) are resistant to aggregation (Periquet et al., 2007). Moreover, αSyn oligomers and aggregated fibrils exhibit toxicity, and have been associated with progressive motor impairment and neuronal cell death (Periquet et al., 2007). Cell culture and *in vitro* studies in αSyn models have shown that the introduction of exogenous aggregated fibrils can cause further aggregation of αSyn monomers that consequently translocate between cells in prion-like manner (Hansen et al., 2011, Desplats et al., 2009, Wood et al., 1999). Likewise, aggregated αSyn was shown to affect various cellular pathways, by impairing the adaptation of neurons to endoplasmic reticulum (ER) stress, inducing dysfunction of the proteasomal degradation process, promoting mitochondrial dysfunction, and leading to membrane damage as well as loss of synaptic function (figure 1.6) (Hansen et al., 2011, Desplats et al., 2009, Wood et al., 1999). Overall, whether the end products of the aggregation (LBs and LNs) or the pre-aggregated forms of αSyn are the main pathogenic cause, is till elusive. In this thesis, I address this question by investigating the role of PTMs in synuclein pathology.

1.4.4 αSyn and Synaptic dysfunction

Synaptic impairment is an early event in the development of DLB and other neurodegenerative diseases (Schulz-Schaeffer, 2010). Considering the hypothesized physiological role of αSyn at the synapse, it is predicted that aggregated αSyn induces synaptic dysfunction and neurotoxicity. In contrast to physiological αSyn, which facilitates the formation of the SNARE complexes (as discussed above), oligomeric

species of αSyn that also associate with synaptobrevin appears to inhibit SNARE complex formation, preventing the fusion of the synaptic membrane with the cytoplasmic membrane and thus inhibiting the release of neurotransmitters (Choi et al., 2013). Moreover, in COS-7 cells, αSyn overexpression was shown to cause disruption of the Golgi apparatus, the site of synaptic vesicle formation, and led to synaptic dysfunction by depletion of synaptic vesicles (Gosavi et al., 2002). In addition, oligomeric species of αSyn were found to cause a reduction in neurotransmitter release by inducing premature intracellular rupture of synaptic vesicles (Figure 5) (Danzer et al., 2007). In a similar manner, αSyn oligomers promote increased calcium influx due to cell membrane permeabilization with consequent result of increased neuronal excitotoxicity (Danzer et al., 2007). Lastly, αSyn oligomers decrease the stability of microtubules (MT), which are fundamental for axonal transport of vesicles and organelles and the regulation of neuronal homeostasis (Goldstein et al., 2008, Prots et al., 2013).

In vitro studies demonstrated that the interaction of αSyn with 3,4-dihydroxyphenylacetaldehyde (DOPA), a toxic product of dopamine degradation, promotes αSyn oligomerization (Burke, 2003). The consequence of this interaction is permeabilization of cholesterol-rich lipid membranes, including synaptic vesicles (Burke, 2003). Altogether, these studies suggest a synergistic effect of DOPA production and αSyn toxicity, might explain the selective vulnerability of DA neurons to the rupture of synaptic vesicles (Lima et al., 2019, Burke, 2003, Plotegher et al., 2017). Overall, the effects of aggregated and oligomeric forms of αSyn can be epitomized in decrease of neurotransmitter release, inhibition of synaptic vesicle recycling, and loss of presynaptic proteins and redistribution of the SNARE proteins (Chung et al., 2009, Garcia-Reitbock et al., 2010, Nemani et al., 2010).

1.4.5 αSyn and Proteasome system dysfunction

The ubiquitin proteasome system (UPS) is a major protein degradation pathway that contributes to cellular proteostasis by the identification and degradation of misfolded proteins (Tanaka and Chiba, 1998, Tanaka, 2009). The process is mediated by tri-enzymatic reaction leading to the attachment of ubiquitin (ubiquitination) to protein lysine residues (Tanaka and Chiba, 1998, Tanaka, 2009). Protein poly-ubiquitination is associated with protein degradation by the 29s proteasome and requires substrate

recognition by the 19s proteasome subunit prior to the degradation by the proteolytic core of the 20s proteasome complex (Finley, 2009). Within the LBs, αSyn is highly ubiquitinated (Wakabayashi et al., 2000, Lowe et al., 1990, Hasegawa et al., 2002, Tofaris et al., 2003, Anderson et al., 2006b). In fact, major components of the proteolytic 20S proteasome are also present in LBs (Lindersson et al., 2004), and can therefore, be considered as sequestrated from their physiological role of proteostasis. The incorporation of the 20S proteasome into LBs, could be preceded by an impairment of its protein degradation capacity as a result of αSyn oligomer binding and thus blockage of the catalytic core (Nielsen et al., 2001, Tanaka, 2009). This was demonstrated in PC12 cells, in which the mutant A53T αSyn oligomers impaired the proteasomal activity (Emmanouilidou et al., 2010). This inhibition was reversed upon supplementation of Congo red, an αSyn oligomerization inhibitor (Emmanouilidou et al., 2010). Other studies have demonstrated the selective vulnerability of the substantia nigra to proteasome inhibition in PD patients, occur as a result of proteasomal inhibition by the oligomeric species of αSyn (McNaught and Jenner, 2001, McNaught et al., 2001, Olanow and McNaught, 2006). In addition, lysosome mediated-autophagy contributes to proteostasis by recycling proteins and organelles, as lysosomes are thought impaired by toxic species of αSyn, because, αSyn was found to be linked with the deregulation of the autophagic lysosomal clearance pathways (Zhang et al., 2012).

1.4.6 αSyn mitochondrial and membrane dysfunction

Mitochondria are intracellular double membraned organelles and hubs of cellular energy metabolism and cell fate determination. Although, they contain their own genome, they depend critically on the protein import from the cytosol for the majority of their proteomes that supports their function (Xia et al., 2019). A growing body of evidence has confirmed the presence of endogenous and/or overexpressed αSyn within the mitochondria (Li et al., 2007b, Liu et al., 2009, Loeb et al., 2010, Nakamura et al., 2008). Some studies proposed that αSyn binds to and inhibits the function of translocase of outer membrane 20 (TOM20), a subunit of the mitochondrial protein import system (Wiedemann et al., 2004, Wurm et al., 2011, Di Maio et al., 2016). Rostovtseva et al. (2015) showed that, αSyn monomers reversibly inhibit the voltage-dependent anion channel (VDAC), an outer mitochondrial membrane channel that regulates the flux of small hydrophilic molecules and calcium in and out of the

mitochondria, in a voltage dependent manner (Rostovtseva et al., 2015). Although it is responsible for the flux of anion from across the outer mitochondrial membrane, it is worthy of mention that at high membrane potential VDAC is cation specific and as such conduct calcium into the membrane (Rostovtseva et al., 2015). This high influx of calcium into the mitochondria facilitated by αSyn oligomers propels mitochondrial swelling, which occurs as a result of depolarisation, and retention of exogenous calcium in the mitochondrial matrix (Luth et al., 2014). In another study, using a dopaminergic SH-SY5Y cell line model, it was observed that, overexpression and subsequent oligomerization of αSyn led to mitochondrial fragmentation (Plotegher et al., 2014). Moreover, mutant forms of αSyn were also found to induce mitochondrial fragmentation and excessive mitochondrial recycling, mitophagy (Nakamura et al., 2011, Choubey et al., 2011). Furthermore, toxic αSyn species are thought to cause downregulation of complex I in the electron transport chain (ETC) of mitochondria, which consequently leads to mitochondrial dysfunction and energetic imbalance (Loeb et al., 2010, Nakamura et al., 2008). These effects on mitochondria, importantly the inhibition of complex I of the ETC, is thought to induce the production of reactive oxygen species (ROS) and oxidative stress with the consequent upregulation of the apoptotic signals (Hsu et al., 2000, Ryan et al., 2015).

The stability of the cell and its biochemical reactions rely on the integrity of the cell membrane that functions as a barrier between intracellular and extracellular environments and controls the movement of metabolites. When incubated with natural and synthetic phospholipids or other lipid bilayer membranes *in vitro*, αSyn quickly formed aggregates and oligomeric species (Haque et al., 2010, Grey et al., 2011). Extracellular oligomeric αSyn species were shown to form pores on the membrane, which facilitated the influx of excess exogenous calcium that precedes cellular disruption and death (Danzer et al., 2007). Similarly, unfolded monomeric and the resulting oligomeric species of αSyn were found to cause calcium dysregulation by interacting with the calcium membrane signalling (Angelova et al., 2016). Importantly, both studies demonstrated that only oligomeric species are capable of inducing cell death (Danzer et al., 2007, Angelova et al., 2016). Additionally, NPT100-18A, a new compound that can displace αSyn from the lipid bilayer membrane was found to reduce the toxicity of oligomeric αSyn (Wrasidlo et al., 2016). Likewise, endosulfine-alpha, a compound that selectively binds to membrane-associated α-syn, was found

to block the formation of toxic aggregated forms of αSyn and reduce the death of DA neurons (Ysselstein et al., 2017). This suggests the interaction of toxic αSyn impairs cellular membrane integrity and function.

1.4.7 αSyn and endoplasmic reticulum stress

ER may be a primary target of αSyn toxicity, as it is the cellular site of protein synthesis, folding, modification and release to the secretory pathway. Perturbation at any these stages of ER-mediated proteostasis leads to ER stress (Hampton, 2000). In fact, ER stress is an event that is thought to occur early in the development of αSyn pathology (Smith et al., 2005). In a study using A53T αSyn mutant in PC12 cell lines, authors reported reduced effects of αSyn neurotoxicity in cells treated with cyclosporine A, a pharmacological inhibitor for ER stress and mitochondrial permeability transition process (Smith et al., 2005). In support of this finding, another study in SH-SY5Y cells showed that ER stress was linked with overexpressed αSyn (Castillo-Carranza et al., 2012). The use of a transgenic mouse models of synucleinopathy further confirmed that oligomeric αSyn species trigger increased levels of chronic ER stress (Colla et al., 2012, Colla, 2019). Furthermore, a study using a yeast model of synucleinopathy, and Ras-related protein 1 (Rab1), (a protein that regulates the membrane trafficking, associated with cytoplasmic αSyn inclusions, important in αSyn mediated neurotoxicity in a variety of disease models), showed that αSyn blocks ER-Golgi vesicular trafficking (figure 5) (Cooper et al., 2006).

1.4.8 αSyn and Immune response

Increased levels of aggregated αSyn trigger a neuronal protective response. Many studies have demonstrated that αSyn can directly affect the immune cells, triggering a localized response that culminates with neuronal cell death. It is believed that this process could also translate into a peripheral immune response (Ferreira and Romero-Ramos, 2018). Moreover, dying neurons were shown to release toxic αSyn species into the extracellular space (Qiao et al., 2012). The release of extracellular αSyn is associated with the activation of the inflammatory response. For instance, microglia activation, has been observed in response to monomeric αSyn (Park et al., 2008). This may potentially occur via the synergic interaction with Toll-like receptor2 (TLR2), which is a potent microglia activator (Stivers et al., 2017, Kim et al., 2013, Qiao et al., 2012). In addition, the activation of microglia is also boosted by monomeric αSyn (Park et al.,

2008). Thus, αSyn can activate the immune system to destroy the dying neurons. Recent evidence has highlighted the lack of chronic activation of the microglia and the subsequent reduction in neuroinflammation in DLB. For instance, Surendranathan et al., has demonstrated early microglia activation and peripheral inflammation in DLB. This was later confirmed by Amin et al., showed that neuro inflammation is a pathogenic aspect in DLB. Other studies in human post-mortem cases have also confirmed the presence of neuroinflammation in DLB. (Surendranathan et al., 2018, Amin et al., 2020, Shepherd et al., 2000, Streit and Xue, 2016).

Microtubules
Mitochondria
Nucleus
Nucleolus
Rough ER

DNA & RNA

Translation

Protein

ER over reactive 3

Apoptotic signal

Caspases

Cytochrome C

Ca+

ATP 2

ROS RNS

PTMs

GA

Folding

Unfolding

Dysfunctional aSyn

Misfoldings

ROS RNS

Vacuoles

Membrane Lysis 4

Organelles Are expelled 6

Impaired cellular trafficking
(5,7)   Protein sequestration
Altered neurotransmission
Inhibition of UPS
Synaptic dysfunction

1 aSyn Monomers   aSyn Oligomers   aSyn fibrils   Lewy body

Golgi apparatus

Synapsis 8

Presynaptic neuron

Axoplasm

Voltage-gated Ca+ channel

↓aSyn

NMDA

Na+

Mitochondria

Synaptic vesicles

Synaptic bulb

Synaptic cleft

TH

VMAT

DA

Ca+

ATP

Glut

DA toxicity

DAT

↑glut

Neurotransmitter

Neurotransmitter receptor

9

Ligand-Gated channel

Ca+ Ca+ Ca+
Ca+ Ca+ Ca+
Ca+ Ca+ Ca+
Ca+ Ca+
Ca+ Ca+
Ca+
Ca+

Hyperexcitability

Activated microgiia

ROS NOS

Lysis

↓UPS   PTMs

Fast neuronal network Impairments

Postsynaptic neuron

44

Figure 1. 5: A schematic representation, of the potential mechanisms by which αSyn aggregates lead to neurotoxicity and cell death in neurodegenerative diseases. Monomeric αSyn assemble into oligomeric species that form mature fibrils. **(i) LBs and LNs formation:** fibril forms of αSyn are segregated to proteinaceous inclusions that contain intracellular membranes, proteins, vesicular structures as well as dysmorphic organelles. **(ii) Proteasome impairment (iii) Mitochondrial impairment:** Altered αSyn can translocate inside the mitochondria, causing oxidative stress by increasing the production of reactive oxygen species (ROS), due to impairment of energy production at complex I. Mitochondrial damage can also trigger the release of cytochrome c, which activates the cytoplasmic apoptosomes and initiates apoptotic response. **(iv) ER dysfunction and protein trafficking inhibition:** the depletion of ATP due to mitochondrial dysfunction, causes ER over reactivity that leads to and increased release of calcium in the cytosol. This also causes blockage of the protein trafficking from ER to Golgi, leading to Golgi fragmentation. **(v) Membrane pore formation:** toxic forms of αSyn can penetrate cellular membranes, altering their permeability, causing excess of calcium and other ions to enter the cytosol. **(vi) Impaired autophagy:** the adhesion of αSyn to the membrane of the lysosomes alter the autophagy pathway, resulting in the aggregation of the substrates. Moreover, impairments of the proteasome system are also reported. **(vii) Release of toxic αSyn and other cellular components into extracellular space:** toxic αSyn may be passively or actively released to the extracellular space by dying neurons and consequently be taken up by adjacent neurons, resulting in seeding aggregation and synaptic impairments. **(viii) Defects in axonal transport:** toxic αSyn triggers Tau hyperphosphorylation, resulting in inhibition of the modulation of microtubule assembly and thus impairment of the cellular transport. **(ix) Synaptic terminal dysfunction:** toxic αSyn alters the distribution of the proteins in the synaptic terminal, reduces the synaptic vesicle release, which leads to changes of the synaptic protein release and hyperexcitability. **(x) Impairments in dopamine (DA) metabolism:** aggregation of αSyn impairs the metabolism of DA, which induces ROS that increases oxidative stress. Figure was assembled using information from   (Shahmoradian et al., 2018, Li et al., 2007b, Hampton, 2000, Danzer et al., 2007, Lindersson et al., 2004, Prots et al., 2013, Haggerty et al., 2011).

1.5 The PTMs of αSyn

PTMs are chemical modifications of amino acid residues that carry a potential to modify protein structure and regulate protein localization, activity, binding affinity and degradation (Beck-Sickinger and Mörl, 2006, Prabakaran et al., 2012, Schmid et al., 2013). To date, the majority of αSyn PTMs have been studied in isolation and of all PTMs, the most studied is αSyn phosphorylation at serine 129 (pSer[129]) (Oueslati et al., 2010). Other PTMs, including ubiquitination, nitration (Oueslati et al., 2010), acetylation (Fauvet et al., 2012, Maltsev et al., 2012, Theillet et al., 2016), truncation (Li et al., 2005, Beyer and Ariza, 2013), SUMOylation (Wilkinson and Henley, 2010, Dorval and Fraser, 2006, Krumova et al., 2011), glutathionylation (Kim et al., 2012, Zhang et al., 2018), glycosylation (Spiro, 2002), and fatty acid acylation (Resh, 2016, Robinson et al., 1970) have also been reported (figure 1. 6). Nevertheless, the precise involvement of these PTMs in the pathogenesis of synucleinopathies is still not well understood.

Table 1. 3: Known PTMs in α-syn, sites, enzymes and effects.

Known PTMs	α-syn residue	enzymes	cytotoxicity	References
Phosphorylation	Y39, Y126, S129 Y133, Y136	CKII GRK2 PLK2 SIAH	Aggregation Oligomerization Degradation Aggregation	(Mahul-Mellier et al., 2014, Paleologou et al., 2010, Oueslati et al., 2010, Waxman and Giasson, 2008, Okochi et al., 2000, Fujiwara et al., 2002, Arawaka et al., 2006)
Ubiquitination	M1, K6, K10, K12, K21, K23 K32, K34, K43 K45, K96, K102	SIAH CHIP	Aggregation Degradation	(Lee et al., 2008, Rott et al., 2008, Shin et al., 2005, Tetzlaff et al., 2008)
Nitration	Y39, Y125, S129 Y133, Y136	-	aggregation	(Hodara et al., 2004a)
Truncation	K58, V74, K80 G84, A89, K97 E110, K102, P120, Y125	Calpin I Neurosin Neurosin	Aggregation Polymerization Degradation	(Mishizen-Eberz et al., 2005, Kasai et al., 2008)
SUMOylation	K96 K102	PIAS2	Aggregation	(Rott et al., 2017)
o-GlcNAcylation	T33, T59, T64 T72, T75, T81 S87	OGT	Aggregation	(Levine et al., 2019b, Lewis et al., 2017)
N-Acetylation	-	-	No difference in aggregation or membrane binding	(Runfola et al., 2020)

*PIAS= protein inhibitor of activated STAT; CK II= casein kinase II; GRK2= G protein coupled receptor kinases; PLK2= polo like kinases 2; SIAH=seven in absentia homologue; CHIP= carboxyl terminus of Hsp 7-interacting; PIAS2= protein inhibitor of activated STAT 2; OGT= o-linked N-acetyl glucosamine (GlcNAc) transferase.
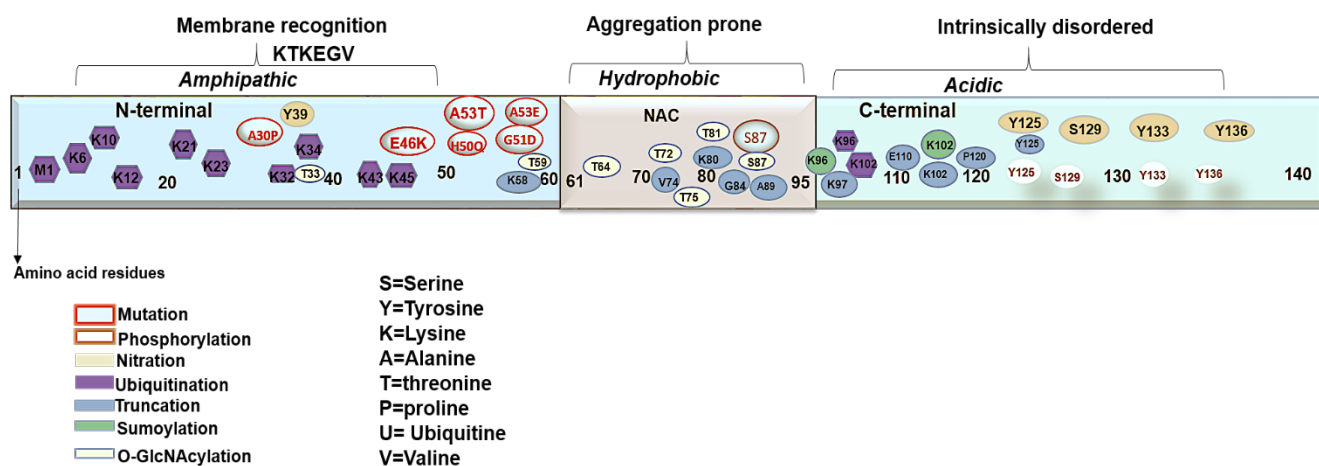
Figure 1. 6: A representation αSyn structure and the main sites of mutations and PTMs.

1.5.1 αSyn Phosphorylation

The enzymatic addition of a negatively charged phosphate group on the amino acids of a protein at serine (Ser), threonine (T) or tyrosine (Y) is known as protein phosphorylation (Manning et al., 2002a, Manning et al., 2002b). Under physiological conditions, protein phosphorylation is a form of reversible PTMs that plays an essential role in the regulation of protein function and is traditionally utilized in pathways including but not limited to differentiation, cellular metabolism, gene expression, cell cycle progression, intercellular communication, cellular motility, migration and cytoskeletal arrangements (Manning et al., 2002a, Manning et al., 2002b). In healthy individuals, the level of αSyn phosphorylation is very low, and the presence of pY^{39}, pSer^{87} and pY^{125} (phosphorylated residues) are almost absent (Okochi et al., 2000, Anderson et al., 2012, Fujiwara et al., 2002). However, under pathologic conditions phosphorylation of threonine (pT^{125}, pT^{133}, pT^{135}), serine (pSer^{87}, Pser^{129}) and tyrosine (pY^{125}, pY^{133}, pY^{136}) was detected in αSyn aggregates (Fujiwara et al., 2002, Takahashi et al., 2003). Most phosphorylated residues are found on residues within the *C terminus* (Chen et al., 2010, Chen et al., 2009, Xu et al., 2015, Venda et al., 2010). The most abundant phosphorylation PTM in post-mortem brain tissue occurs at pSer^{129}, which is now considered an important marker for synucleinopathies (Fujiwara et al., 2002, Anderson et al., 2006a, Okochi et al., 2000, Takahashi et al., 2003). In addition, phosphorylated αSyn, was also identified in cingulate and temporal

and motor cortex of post-mortem brain of PD and LBD patients (Takahashi et al., 2003, Zhou et al., 2011, Walker et al., 2013). In this thesis, I address the phosphorylation of αSyn (Pser [129]) within the LBs/LNs in the corresponding region of the disease.

Multiple lines of evidence support the idea that αSyn phosphorylation is linked to formation of the toxic species of αSyn that underlies the formation LBs and LNs (Okochi et al., 2000, Anderson et al., 2006a, Fujiwara et al., 2002, Kahle et al., 2000a, Kahle et al., 2000b). For instance, in PD, over 90% of endogenous αSyn is found to be phosphorylated at Ser[129]; in direct contrast to only 4% αSyn phosphorylation detected in healthy individuals (Kahle et al., 2000b, Fujiwara et al., 2002). Similarly, Pser[129] was also found in post-mortem brain tissues of DLB, PD, PDD patients and in SH-SY5Y cells that overexpress wild type αSyn (Swirski et al., 2014). It is believed that Pser[129] may occur in late stages of the aggregation leading to fibrillization, and it is crucial for the modulation of disease progression (Paleologou et al., 2010, Waxman and Giasson, 2011, Wales et al., 2013). In addition, other studies suggest that different forms of phosphorylation may upregulate each other (Paleologou et al., 2010).

In contrast to non-phosphorylated forms, phosphorylated αSyn is linked with the impairment of different clearance mechanisms of the cells (Mahul-Mellier et al., 2014, Oueslati et al., 2013, Arawaka et al., 2017). This suggests that normal αSyn is recruited to degradation machinery more readily under physiologic conditions. In addition, proteasomal inhibition was also reported to increase the toxicity of pS[129] αSyn, as well as its toxicity in DA neurons in PD (Chau et al., 2009). Furthermore, αSyn Pser[129] binds to vesicular trafficking proteins, cytoskeletal proteins and other enzymes (McFarland et al., 2009), suggesting further disruptions of these cellular systems. This could also be related to Pser[129] αSyn interfering with the function of these proteins by their sequestration into aggregates that forms LBs/LNs, echoing the interrelationship among these pathways in the pathogenesis of the synucleinopathy. Hence, it can be assumed that Pser[129] αSyn, may be a key factor in LBs/LNs formation and LBD pathogenesis.

1.5.2 Oxidative stress in αSyn phosphorylation

Several studies support the idea the αSyn phosphorylation may be enhanced by oxidative stress (Chau et al., 2009). While non-phosphorylated forms of αSyn were found to co-localize with complexes I, III and IV of the mitochondrial, It is assumed that

any impairments of these complexes and the resulting ETC dysfunctions, leads to the ROS production, which consequently promotes αSyn phosphorylation (Kahle et al., 2000b, McFarland et al., 2009). In SH-SY5Y cell line, treatment with low doses of rotenone, an ETC complex I inhibitor that results in ROS production, led to increased levels of Pser[129] αSyn (Sugeno et al., 2008). Similarly, an *in vitro* study of a synucleinopathy model, demonstrated that αSyn phosphorylation increases when exposed to rotenone and ferrous iron (Perfeito et al., 2014). The increase of αSyn phosphorylation was also observed in SH-SY5Y cells upon exposure to toxic factors, such as, 6-hydroxidopamine, as well as epoxomycin (a proteasome inhibitor), and paraquat (an environmental toxin that inhibits the ETC) leading to increased ROS production (Ganapathy et al., 2016, Chau et al., 2009). Perfeito et al. hypothesized that stimuli that promote mitochondrial dysfunction and the formation of ROS, may be associated with mutant A53T αSyn phosphorylated at Ser[129], which may underlie neuronal degeneration in PD and DLB. They found correlation between rotenone Pser[129] αSyn in the formation of ROS, where the overexpression of αSyn triggered ROS release, as well as both the exposure of rotenone and the ROS release lead to greater phosphorylation of αSyn (Perfeito et al., 2014). Hence, biochemical changes linked with DLB pathogenesis such as oxidative stress, mitochondrial complex I dysfunction and proteasome impairment, could underlie the changes in αSyn phosphorylation and promote pathology (Lashuel et al., 2012, Lee and Trojanowski, 2006, Robson et al., 2018a).

1.5.3 Phosphorylated αSyn as biomarker of synucleinopathies

The role of phosphorylated αSyn as a potential biomarker has also been widely studied. The quantification of total αSyn in the cerebrospinal fluid (CSF) in patients diagnosed with synucleinopathies and related disorders was proposed as a potential biomarker (Hong et al., 2010, Mollenhauer et al., 2008). Nevertheless, Flouds et al. have shown that the total αSyn in the blood plasma of PD patients was similar to that in non-PD controls (Foulds et al., 2013). In contrast, the levels of Pser[129] αSyn were significantly higher in PD patients when compared to non-PD controls (Foulds et al., 2013). Another important diagnostic test that could also be used for synucleinopathies is the detection of phosphorylated αSyn in the peripheral nervous system. Extra-axial biopsies, such as skin biopsies performed in PD subjects, revealed aggregation of phosphorylated αSyn in large and small skin fibres (Stewart et al., 2015, Wang et al.,

2012, Doppler et al., 2014a). Moreover, aggregation of phosphorylated αSyn was detected in the gastrointestinal tract of PD individuals (Pouclet et al., 2012, Hilton et al., 2014). These studies highlight the importance of investigation of pαSyn in the development of diagnostic and therapeutic strategies.

1.5.4 αSyn ubiquitination

Ubiquitin is a 76 residue protein that is ubiquitously expressed in the nervous system (Varshavsky, 2001), however, it is not limited to it, as it is present in all the tissues as well. Ubiquitination, is a process by which ubiquitin is covalently conjugated to a substrate protein in a reaction that requires the activity of a ubiquitin-activating enzyme (E1-UBA), a ubiquitin-conjugating enzyme (E2-UBC) and a ubiquitin ligase (E3-UBL) (Stone, 2016). This process terminates in the formation of an amide bond between ubiquitin and lysine or in other instances with cysteine, serine or threonine residues of the substrate protein (Vosper et al., 2009, Wang et al., 2007a). When the conjugation culminates with the single molecule of ubiquitin attached to the residue protein, the process is referred to as monoubiquitination. If the process is not terminated at this stage, the addition several ubiquitin molecules lead to formation of a poly-ubiquitin chain (Wang and Pickart, 2005, Hochstrasser, 2006, Li et al., 2007a, Deshaies and Joazeiro, 2009, Maspero et al., 2011).

Similar to phosphorylation, protein ubiquitination is a an important mechanism that regulates various cellular processes such as cell cycle, transcription, transduction, antigen presentation and apoptosis (Hershko and Ciechanover, 1998). In contrast, protein poly-ubiquitination (addition of four and more ubiquitin molecules in a single chain) leads to protein degradation primarily by the UPS. The UPS together with the autophagy-lysosomal pathways constitute the two major degradation pathways systems that direct the elimination of misfolded, aggregated and damaged proteins (Blasiak et al., 2019, Seglen et al., 1996, Ciechanover and Kwon, 2015, Bustamante et al., 2018). An alternative pathway linked to degradation of long-lived ubiquitinated proteins, protein aggregates and organelles is macroautophagy (Chen et al., 2019). UPS, chaperone-mediated autophagy and macro-autophagy are the three main proteolytic pathways that are believed to mediate degradation of αSyn. However, macroautophagy seems to be the main system involved in αSyn clearance (Bennett et al., 1999, Webb et al., 2003, Paxinou et al., 2001).

Ubiquitinated αSyn (ub-αSyn) is often present in LB inclusions. Multiple lines of evidence demonstrate the presence of monoubituitinated αSyn (mub-αSyn) as the predominant ubiquitinated species in LBs (Wakabayashi et al., 2000, Lowe et al., 1990, Hasegawa et al., 2002, Tofaris et al., 2003, Anderson et al., 2006b). Indeed, in synucleinopathies such as LBDs, the cells are heavily loaded with proteasome subunits and ubiquitinated structures (Kuzuhara et al., 1988, Bentea et al., 2017, Lehtonen et al., 2019). Nevertheless, monoubiquitination mechanisms that underlie the modulation of αSyn aggregation are still unknown. A step towards understanding was achieved in a study of isolated LBs from PD patients, that demonstrated the presence of the seven in absentia homologue (SIAH), an E3-UBL enzyme, previously reported to interact with and ubiquitinate αSyn (Liani et al., 2004, Engelender, 2008, Lee et al., 2008). De facto, lysine 12, 21 and 23 (K^{12}, K^{21} and K^{23}) residues (figure 1.6), the common targets of αSyn monoubiquitination, are also ubiquitinated by SIAH (Anderson et al., 2006a). This suggests that SIAH is involved in the pathogenesis of the synucleinopathies. However, these findings are a matter of debate, as some studies have found that only a small fraction of αSyn is ubiquitinated in LBs (Hasegawa et al., 2002). In this thesis, I demonstrate that αSyn Ubiquitination is present within the LBs/LNs within the corresponding regions affected by the disease.

1.5.5 αSyn nitration

Protein nitration is a nitrosative stress-related PTM that affects the tyrosine (Y) residues (Radi, 2004, Bartesaghi and Radi, 2018). αSyn is nitrated (n-αSyn) at its C-terminal in residues Y^{125}, Y^{133}, Y^{136} and at N-terminal residue Y^{39} (these are the same residues that are also found to be phosphorylated) (figure.1.6) (Souza et al., 2000, Giasson et al., 2000). Tyrosine residues are necessary for αSyn aggregation under oxidative stress conditions (Souza et al., 2000). In fact, it was found that αSyn exposure to nitrating agents leads to the formation of covalently stabilized oligomers through the oxidation of tyrosine to 0, 0'-dityrosine (Souza et al., 2000). Although a high rate of oligomerization was observed upon n-Y^{39} αSyn formation, studies have shown that Y^{125} is more relevant to αSyn dimer formation (Yu et al., 2004, Olteanu and Pielak, 2004, Danielson et al., 2011, Takahashi et al., 2002). Moreover, fibril formation is increased by both, monomeric and dimeric, n-αSyn (Hodara et al., 2004).

1.5.6 αSyn nitration-mediated interaction with membranes and oxidative stress

The association of αSyn with membranes may lead to peroxidation of polyunsaturated fatty acids. Membrane lipid peroxidation can be triggered by ROS and RNS (Trostchansky et al., 2006, Qin et al., 2007). αSyn incubation with 4-hydroxy-2-nonenal (4HNE), a lipid peroxidation compound, leads to formation of αSyn-HNE adducts (Trostchansky et al., 2006, Qin et al., 2007). Indeed, the interaction of αSyn with membrane phospholipids and polyunsaturated fatty acids is necessary for the formation of αSyn oligomers (Assayag et al., 2007, Perrin et al., 2001, Beyer and Ariza, 2013). In addition, αSyn promotes nitric oxide synthase (NOS) activity at the plasma membrane, which leads to production of excess nitric oxide (NO). NOS in turns, may inhibit the ETC, thus increasing the production of superoxide (Lashuel et al., 2002). This is thought to create a vicious cycle that facilitates nitration and oxidation that potentiate cellular dysfunction and loss of viability (Radi, 2004, Radi et al., 2002). Furthermore, αSyn oxidation and nitration impedes αSyn degradation by chaperone mediate autophagy, therefore inhibiting the degradation of n-αSyn (Martinez-Vicente et al., 2008). This resistance to degradation of n-αSyn promotes an increase in its half-life and consequently its concentration, which boosts the toxicity of the protein potentially leading to neurodegeneration (Chavarria and Souza, 2013).

1.6 Mouse model of synucleinopathies (Thy-1A30P mouse model)

Several missense mutations in the human αSyn gene were linked to early onset synucleinopathies (Polymeropoulos et al., 1997). Thus, various transgenic mouse lines that overexpress either human or mutant αSyn were generated for the study of synucleinopathies. However, in this project, I used the A30P mouse model for the assessment of the effects of abnormal αSyn on cortical neuronal network oscillations. A30P, is an autosomal dominant missense mutation in the *SNCA* gene where the guanine nucleotide substitutes a cytosine nucleotide at the position 88, which in turns, leads to an exchange of alanine to proline at the position 30 in αSyn protein, under the control of Thy-1 promoter. This mouse model was first used to study the transport of αSyn to synapses, where the pathological αSyn was found to preferentially accumulate in the soma (Kahle et al., 2000a), and seemed to show reduced tendency to bind the synaptic vesicles (Jensen et al., 1998). Later, the same model was used for the study of several synucleinopathies. In addition, the A30P mouse was proven to

show higher expression of human αSyn than the endogenous murine αSyn, which does not have the same expression and aggregation properties as the human αSyn (Kahle et al., 2000b). This makes the model suitable to simulate human disease. Furthermore, the A30P mutation is found to be linked to many pathogenic mechanisms such as reduced membrane binding capacity (Bussell and Eliezer, 2004), reduced interaction with the cytoskeleton (Esposito et al., 2007, Sousa et al., 2009), impairments in synaptic vesicle trafficking (Dalfó et al., 2004), and a reduced capacity of DA storage (Yavich et al., 2004).

Clinically, the A30P mouse model presents with motor symptoms form the early stage of life and shows decline of spatial memory by 12 months of age, which turns severe at the age of 16 months (Ekmark-Lewén et al., 2018b). The A30P mice develop paralysis and die prematurely by the age of 17-18 months (Freichel et al., 2007). It was recently reported that the A30P mouse exhibits unsteady gait, abnormal tail posture and movement, and weakening of the extremities, prior to the development of the parkinsonian symptoms (Gaugler et al., 2012). The cognitive deficits observed in these mice, seems to develop independently from the motor and visual impairments. Freichel et al., reported cognitive decline and amygdala pathology develops independently of other symptoms in mouse model of synucleinopathy. It has been suggested that early motor disfunction was distinguished from cognitive disfunction, as it was demonstrated to result from the down regulation of the dopaminergic system disfunction in A30P mice (Paumier et al., 2013, Freichel et al., 2007). Hence, the use of Thy-1 A30P mouse line appears to be clearly suited for this study. In our recent *in vitro* work, we have demonstrated a reduction in the power of carbachol-induced gamma frequency oscillations, and mitochondrial dysfunction in A30P mice aged over 9 months old (Robson et al., 2018b). In opposition of the early results, it was suggested that the motor symptoms exhibited by the A30P mouse line are not purely parkinsonian in nature (Neuner et al., 2014). Authors of this study demonstrated that virally expressed wild type (WT) αSyn in rat SN resulted in parkinsonian symptoms, whilst A30P αSyn did not. The authors concluded that this may be due to A30P reduced binding to the presynaptic membranes of DA neurons (Gaugler et al., 2012). Hence, the use of Thy-1 A30P mouse line appears to be clearly suited for the study of the hippocampal and cortical neuronal network oscillations linked with the overexpression of human A30P αSyn as demonstrated in this thesis.

Table 1. 4: Representation of the chronological spectrum of clinical manifestation and oscillatory impairments in A30P mouse model of alpha synucleinopathy.

Age	Pathology	Motor	Cognition	References
1-4 Months	• Insoluble αSyn expressed in the whole brain • No loss of cholinergic neurons	• Fine Motor impairments	-	(Kahle, Neumann et al. 2002) (Ekmark-Lewén, Lindström et al. 2018)
6-8 Months	• Aggregation of oligomeric forms of αSyn • Loss of serotoninergic neurons	• Motor impairments	-	(Ekmark-Lewén, Lindström et al. 2018) (Neumann, Kahle et al. 2002)
10-14 Months	• αSyn aggregates • Reduction of GABAergic neurons • Microglia activation	• Motor impairments	• Cognitive dysfunction • Abnormal network oscillations • Mitochondrial dysfunction	(Neumann, Kahle et al. 2002)(Freichel, Neumann et al. 2007) (Ekmark-Lewén, Lindström et al. 2018)
16-18 Months	• αSyn aggregates	• Severe motor impairments	• Cognitive dysfunction • Abnormal network oscillations • Mitochondrial dysfunction • Death	(Schell, Hasegawa et al. 2009) (Neumann, Kahle et al. 2002)(Freichel, Neumann et al. 2007) (Ekmark-Lewén, Lindström et al. 2018)

1.7 Thesis hypothesis

This thesis addresses four major questions in the field: (i) where are different PTMs of αSyn distributed in the brains of LBD patients and in which regions these modifications take place in relation to the disease progression? (ii) What is the involvement of PV+ interneurons in the disease pathogenesis? (iii) What are the pathogenic correlations between αSyn PTMs and PV+ interneuron dysfunctions/deficits? (iv) What are the effects of pathological αSyn on gamma frequency oscillations?

The main hypothesis for this thesis is:

PTMs are one of the early events that trigger the aggregation and/or dysfunction of αSyn, possibly altering its physiological sub-cellular distribution (e.g., in the nucleus or mitochondria), causing the dysfunction of subcellular organelles such as the mitochondria. These changes in αSyn produce the pathogenic cascade of αSyn that culminates in neuronal dysfunction and death. This may primarily affect a specific group of neurons that are highly energy dependent such as PV+ interneurons, resulting in the impairments of gamma network oscillations, that underlie cognitive dysfunction and motor impairment which characterize the LBDs.

The sub-hypotheses of the work presented in this thesis are:

- Different PTMs may occur at different stages of disease progression, according to Braak LB pathology / McKeith scales. These changes may affect more significantly brain regions such as the locus coeruleus, the substantia nigra, the reticular formation, the amygdala, hippocampus, thalamus and neocortex, due to the high sensitivity of these regions to changes in homeostasis. Moreover, early occurring PTMs may emerge in those regions, which are affected earliest in the disease according to Braak LB pathology / McKeith stages, and identifying those, which occur earliest, may provide an insight on the mechanism of disease progression. In addition, the identification of key modifications within post-mortem tissue may enable their manipulation and reproduction in animal models, allowing for an insight into both the mechanism of aSyn-mediated neurodegeneration and into potential therapeutic targets for future drug development.
- Mouse models of synucleinopathies, such as the A30P transgenic mice, may develop mitochondrial dysfunction and abnormal network oscillations, in an

age-dependent manner. Mitochondrial dysfunction in synucleinopathies may occur as a result of aSyn PTMs and important mutations in the genes that could take place either in the mitochondrial or nuclear DNA.

- In addition, fast neuronal network oscillations are important for cognitive functions and may become impaired in LBD. These oscillations are intrinsically dependent on the reciprocal interaction between PV+ fast spiking interneurons and excitatory pyramidal cells (Whittaker et al., 2011a, Robson et al., 2018b). Considering that fast network oscillations underlie the high cognitive and motor functions impaired in DLB (Zheng et al., 2016, Thomas et al., 2008), the malfunctioning or death of these interneurons may be causative in disease symptomology (Whittington and Traub, 2003). Therefore, I hypothesised that the number of these interneurons may be reduced in important regions of the brain that are essential for cognitive functions, in correlation with the presence of αSyn PTMs.

1.8 Aims and Objectives

This thesis investigates the involvement of different PTMs of αSyn as described in many synucleinopathies, with a particular focus on αSyn phosphorylation, ubiquitination and nitration, which are thought to occur in the context of synucleinopathies. Moreover, it studies changes in PV+ cells, and correlates these with an impairment in gamma frequency oscillations and an increase in αSyn PTMs in some regions of DLB patients' brains.

Specific aims and objectives of this this thesis are:

Aim 1: Identify disease associated PTMs of αSyn such as phosphorylation, ubiquitination and nitration in LBD post-mortem brain tissues and analyse their distribution in LBDs.

- **Objective 1.1**: To determine the correlation between different PTMs.

Aim 2: Quantify the distribution of PV+ fast spiking interneurons in brain tissue of LBD patients.

- **Objective 2.1:** To determine the correlation of PV+ interneurons with different PTMs.

Aim 3: Investigate links between αSyn and mitochondrial dysfunction, its links with the gamma network oscillations impairment in a mouse model of alpha synucleinopathy.

- **Objective 3.1:** Investigate the effects of memantine and sodium pyruvate treatments on gamma frequency of the network oscillations in A30P mice.
- **Objective 3.2:** Investigate whether the inhibition of the mitochondrial ETC has an effect on gamma oscillation in the A30P mice.
- **Objective 3.3:** Analyse the correlation of alpha synuclein overexpression with mitochondrial dysfunction in A30P mice.

Chapter 2: Mitochondrial dysfunction impairs gamma frequency oscillations in A30P mouse model of alpha-synucleinopathy: partial restoration of gamma frequency oscillations with memantine and sodium pyruvate
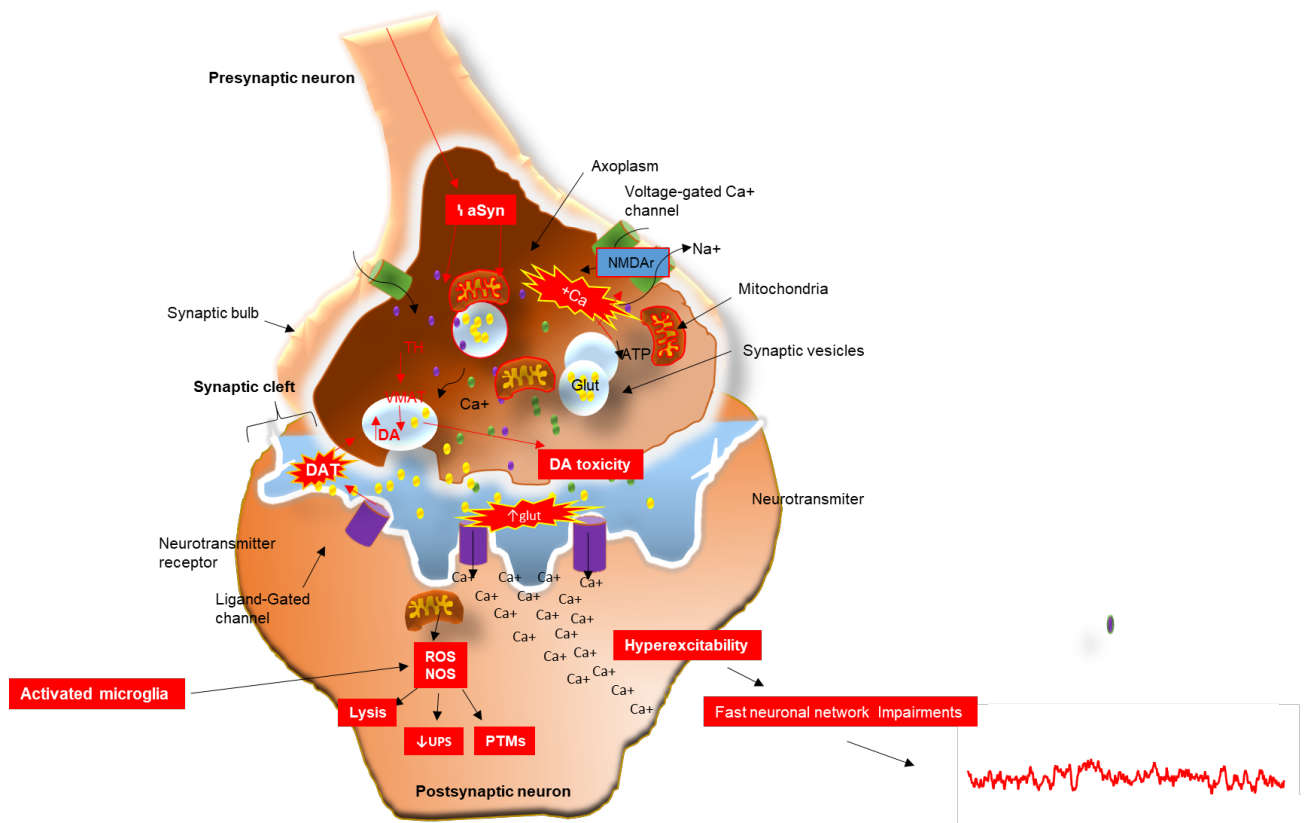
2.1 Introduction

Abnormal αSyn aggregation occurs in all the stages of LBDs, as putative toxic forms of αSyn are ubiquitously found in the brain, including within the hippocampus and the neocortex (Rieker et al., 2011, Braak et al., 2003a). In pathologic conditions, such as DLB, αSyn is thought to cause mitochondrial dysfunction and synaptic impairment, concomitantly with other pathogenic cascades (see chapter 1 mitochondria and gamma oscillations), which together underlie the polymorphic clinical signs and symptoms including cognitive impairments and the significant cortical neuronal network alterations (Peraza et al., 2018, Bonanni et al., 2016, McKeith et al., 2017). Nevertheless, the link between abnormal αSyn aggregation and the impaired neuronal network oscillations is still not completely understood (Nimmrich et al., 2015). Despite the fact that many studies have demonstrated a slowing in the frequency of neuronal network oscillation in the EEG of AD and DLB patients, within the lower frequency oscillations bands, including delta (1-4Hz), theta (4-8Hz) and alpha (8-12Hz) (Bonanni et al., 2016, Morris et al., 2015), as well as other lines of evidence demonstrated impaired gamma frequency oscillations (30-100Hz) (Herrmann and Demiralp, 2005, Basar et al., 2016, Robson et al., 2018b), that are linked to cognitive functions including attention and memory (Clayton et al., 2015, Watrous et al., 2015, Zheng et al., 2016), the alterations of fast network oscillations bands have not been widely studied in DLB.

Normal mitochondrial function is required for the generation of fast neuronal network oscillations, as these type of oscillations are highly energy dependent (Whittaker et al., 2011a). In fact, previous studies have demonstrated that an acute inhibition of complex I of the mitochondrial ETC in slices from normal animals can cause oxidative stress and impairments of gamma frequency of the neuronal network oscillations (Kann et al., 2011). However, the process by which mitochondrial dysfunction and the resulting oxidative stress may underlie gamma frequency impairments and neuronal cell death, remains unclear. It is currently hypothesized that abnormal αSyn can invade the inner mitochondrial membrane, thus impairing ETC function that then leads to accumulation of ROS. Additionally, the resulting oxidative stress might then promote membrane lipid peroxidation (Nakamura et al., 2011, Reeve et al., 2015, Devi et al., 2008, Birben et al., 2012), adding an extra burden to the pathology. In addition, previous studies have shown that NMDA receptor antagonist increases the gamma

oscillations, since excess NMDA receptor activation can lead to excitotoxicity in neurons, and therefore, impairing gamma frequency oscillations (Dreyer et al., 1995, Tenneti et al., 1998, Okamoto et al., 2002). In line with this, I have assessed the mitochondrial function by blocking the ETC complex I and II, I also assessed the therapeutic potentials of memantine, which is an NMDA antagonist that is currently used in the treatment of patients with dementia, to observe whether they have any positive effect in gamma frequency oscillations (Lo and Grossberg, 2011). Thus, the experimental results presented here characterise the degree to which neuronal gamma frequency oscillations are dependent on the normal functioning of the mitochondria as well as in the integrity of the NMDA receptors, building on observations published in Robson et al. (2018).

Here, I first observed that inhibition of complex I and complex IV of the mitochondrial ETC leads to compromised bioenergetics by depleting the availability of ATP production, consequently leading to a decrease of the power of the gamma frequency oscillations. The addition of energy supplements such as sodium pyruvate which enters the glycolytic pathways, produced a slight increase in the area power of the gamma frequency oscillations. Since I predicted that mice that overexpress toxic forms of αSyn would present with mitochondrial dysfunction, which would then lead to impairments in the fast neuronal network oscillations, specifically on the gamma band, and that this impairment precedes the cognitive decline. I further hypothesized that addition of an energy supplement pyruvate and antagonising the effects of NMDA receptors would help restore the deficits in the generation of gamma frequency oscillations. I therefore went on to assess the effects of mitochondrial blockers such as rotenone and KCN, to study the mitochondrial function, complemented by the addition of sodium pyruvate. In addition, I verified the effects of memantine on gamma network oscillations. Thus, the aims of the chapter are: To investigate the mitochondrial dysfunctions, its links with the gamma oscillations in A30P mice; To Investigate the effects of memantine and sodium pyruvate on gamma frequency oscillations, and then, investigate whether the inhibition of the mitochondrial ETC has an effect on gamma oscillation in the A30P mice.

2.2 Methods:

All procedures described in this thesis relating to animals were carried out according to the UK Animals Act 1986 (Scientific Procedures), and European Union directive 2010/63EU, with the appropriate provision project and personal licences (PPI and PPL).

2.2.1 Animal model

Transgenic (Thy-1)-h[A30P] αSyn mice C57BL/6 background, both male and female that overexpressed human mutant A30P αSyn under the Thy-1 CNS specific promoter (Kahle et al., 2000b, Neumann et al., 2002), were supplied by Dr. Khale (University of Tubigen). Upon arrival, the mice were transported, bred and maintained in-house in a homozygous colony, in the comparative behavioural centre animal facility (CBC) Newcastle University, on a 12-hour dark/light cycle, with lights on from 7 a.m., in an enriched environment with free access to food and water. All procedures done according to the animal research reporting of *in vivo* experiments (ARRIVE) guidelines, as described in (Robson et al., 2018b). Animals were kept in number of 1-6 same-sex groups and aged 2-16 months old. The crossing over homozygous mice (Kahle et al., 2000a, Neumann et al., 2002)with C57BL/6 and wild type mice produced F1 generation. After ~21 days, mice were ear notched previous to the formation of two separate lines (wild type and homozygous A30P). Next, the samples were genotyped externally, and for preliminary electrophysiological studies, we used homozygous mice. The obtained three lines (wild type, A30P and heterozygous) were kept separately, and when needed, they were crossed again to be used for the subsequent experiments. In this thesis, all mice were divided into age groups referred to as WT/A30P2+ (2-6 months) and WT/A30P9+ (9-16months) and WT/A30P16+ (15-17months) as referred in the result section. Although, based on the clinical spectrum, a30P mice is more suitable for PD and PDD studies, this model was chosen for DLB studies, mainly because of presenting overexpressed aSyn as the main causative factor of the different clinical phenotypes, in addition to the great degree of overlap of these clinical manifestations among LBDs (Ekmark-Lewén et al., 2018a, Kahle, 2008). In addition, moe recent evidence have been reporting a plethora of cognitive deficitis in A30P mice (Freichel et al., 2007, Kilpeläinen et al., 2019, Crabtree and Zhang, 2012). The cognitive deficits observed in these mice, seems to develop independently

from the motor and visual impairments (Paumier et al., 2013, Freichel et al., 2007). Therefore, I believe it can also be suitable for DLB studies.

2.2.2 Brain extraction and preparation of the solutions

Before being euthanized, the animals were anesthetized with inhaled isoflurane (100% w/w, Zoetis, UK), followed by an intramuscular injection of ketamine (0.25ml ≥100mg/kg -1, Vetoquinol Group, Buckinghamshire, UK) and xylazine (0.25ml ≥10mg/kg-1, Animal care Ltd, York, UK) as previously described (Driver et al., 2007, Robson et al., 2018b). Once the response to noxious stimuli (tail pinch, corneal and pedal withdrawal reflexes) were abolished, laparotomy and thoracotomy were performed, and the heart of the animals was exposed, to be intracardially perfused with chilled sucrose artificial cerebrospinal fluid (SACSF) 25~mls (for mice), ~50mls (for rats) at a rate of ~0.5ml/sec. The composition of SACSF was 252 mM sucrose, 3.0 mM KCl, 1.25 mM NaH_2PO_4, 24 mM $NaHCO_3$, 2.0 mM $MgSO_4$, 2.0 mM $CaCl_2$ and 10 mM glucose (Table 2.1). The procedure of high sucrose perfusion in animals was proven to improve the viability of the fast-spiking interneurons and the brain cytoarchitecture in general (Aghajanian and Rasmussen, 1989). For regular artificial cerebrospinal fluid (ACSF), 252 mM of sucrose was substituted with 126 mM NaCl. Stock solutions were kept for 2 weeks, and fresh ACSF was prepared on a daily basis from the stock solutions. After SACSF solution was made, it was used within 48 hours.

Following perfusion in SACSF cervico-myelotomy was performed, following by sagittal craniotomy, to remove the brain from the skull. The brain was placed in a petri dish containing chilled carbogenated SACSF. The brain was then excised with a razor blade, in coronal planes to obtain anterior cingulate (ACC) cortices, and in horizontal planes to obtain hippocampal slices. The respective portions of the brain were glued to the chuck of a Leica VT1000 microtome (Leica Microsystems, Germany) and covered in chilled carbogenated SACSF. 450 µm thick transverse slices were cut using a Leica VT1000S Vibratome. The slices were then trimmed and the hippocampal or ACC slices were observed.

Table 2. 1: Components of the ACSF solution

Chemical Name	Chemical formula	Dosage used	Vendor
Potassium chloride	KCl	3 mM	VWR International (307164T)
Sodium dihydrogen orthophosphate	NaH_2PO_4	1.25 mM	VWR International (101985M)
Sodium bicarbonate	$NaHCO_3$	24 mM	Tocris (3152)
Magnesium sulphate	$MgSO_4$	2 mM	Sigma-Aldrich (M7506-M))
Sodium chloride	NaCl	126 mM	Sigma-Aldrich (S7653)
Calcium chloride	$CaCl_2$	2 mM	VWR International (275844L)
Glucose	$C_6H_{12}O_6$	10 mM	VWR International (101176K)
Sucrose	$C_{12}H_{22}O_{11}$	252 mM	Sigma-Aldrich (16104)

2.2.3 Slice preparation

Following brain extraction and slicing, the slices were transferred into a holding chamber containing carbogenated regular ACSF (126 mM NaCl in alternative to sucrose) and covered with paraffin for approximately 1 hour at room temperature to washout the water-soluble anaesthetics (ketamine, isoflurane and xylazine) (Dickinson et al., 2003). Next, the slices were transferred into a recording chamber, where they were maintained at an interface between regular ACSF supplied at a continuous flow of ~1.2 ml/min and humidified carbogen gas (95 % oxygen and 5 % CO_2) through a Gilson Minipils3 pump at temperature ranging between 30-31°C, using FH16-D heater (Grant Instruments Ltd, UK). The measurements of the temperature were taken using an infrared thermometer for the duration of the experiment. The slices were then left for another 30 min to equilibrate before recording. For rats, coronal slices of the PFC were determined using the rat and mouse brain (Franklin and Paxinos, 2013).

After brain extraction, 450 μM thick coronal slices of ACC (in rats) and *cornu amonis 3* (CA3) region of the hippocampus (in mice) were obtained. ACC is associated with different cognitive tasks of the brain and plays an important role for modulation of

NMDA receptors (Adams et al., 2017). The number of animals and slices are represented as N/n, because multiple slices can be generated from each animal. Whenever were possible, multiple rigs with two electrodes and one recording chamber were simultaneously used to maximise the use of the slices.

Thin hippocampal slices (150-180 μM) prepared without SACSF solution, were previously reported to survive in a submerged holding chamber for ~4 h (Fukuda et al., 1995). This survival rate is enhanced through transcardial perfusion of SACSF because of its neuroprotective effects (Aghajanian and Rasmussen, 1989). Therefore, the use of SACSF in this thesis intended to prolong the viability of the acute brain slices during the 6 hours of slice preparation to enhance the experimental design.
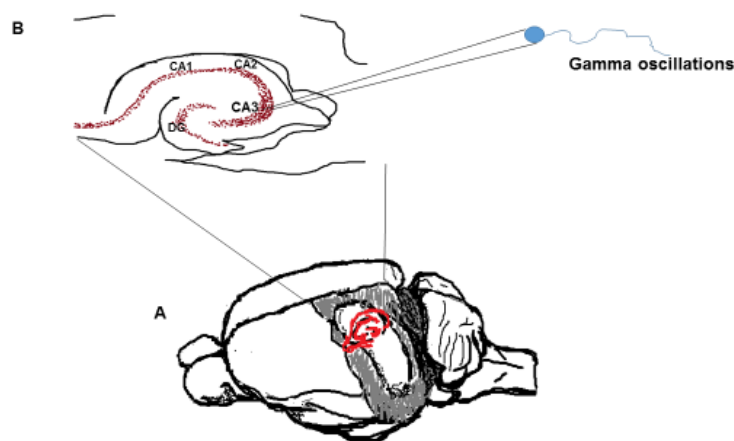
Figure 2. 1: (**A**) Schematic representation of the mouse brain and the region that the hippocampal slices were taken from, to be recorded in LFP. (**B**) Above, the diagram of the hippocampus showing the CA3 region where gamma oscillations were measured using microelectrodes.

2.2.4 Data acquisition and recording

Recordings of neuronal network oscillations for extracellular recordings local field potential (LFP) were measured using microelectrodes (1.2 mm OD,094 mm ID, 100 mml on the 30-0050 G120TF-10, Harvard Apparatus Ltd.,UK), pulled from borosilicate glass P-97 Flaming/Brown puller (Sutter Instrument Co., USA) (figure 2.1), which produced electrodes of 2-5 MΩ resistance that were filled with normal ACSF. A silver chloride electroplated wire was inserted into the microelectrodes and placed in an electrode holder adhered to a head stage preamplifier. Each electrode was positioned

manually in the corresponding slides using an operated micromanipulator, in either a superficial or a deep layer of the region of study. Each rig had two channels and two micromanipulators (figure 2.1). LFPs were recorded simultaneously from each slice using the corresponding number of microelectrodes placed on the slices under the microscope (Olympus, Japan) into the desired region of the hippocampus, CA3 (in mice) or ACC (in rats). In our experiments, the electrodes could be placed in the same or separate slices, to record the oscillations.

The signal recorded by electrodes was amplified 100 times using an axoclamp-2B amplifier (Axon instruments Inc., UK), and the neuronal activity was band-pass filtered at 0.001-0.4 kHz high-low using Neuralog external filters (figure 2.1). The background noise was subtracted using Humbug (Digitimer, Welwyn Garden City, Herts, UK) which removed 50 Hz of electrical mains noise. Signal were digitised in the Computer, at 10 kHz using an ITC-16 interface (Digitimer, Welwyn Garden City, UK) (figure 2.1). The data were converted into a digital waveform, recorded and analysed using AxoGraph 4.6 software (Version X, Axon instruments Inc., Union City, CA, USA), using a Fast Fourier Transform (FFT) algorithm, thus generating power spectrum where the frequency components were split from the waveform (figure 2.2). Subsequent analysis of the data was performed offline, using GRAPH Pad Prism 7.01 (La Jolla, CA, USA).
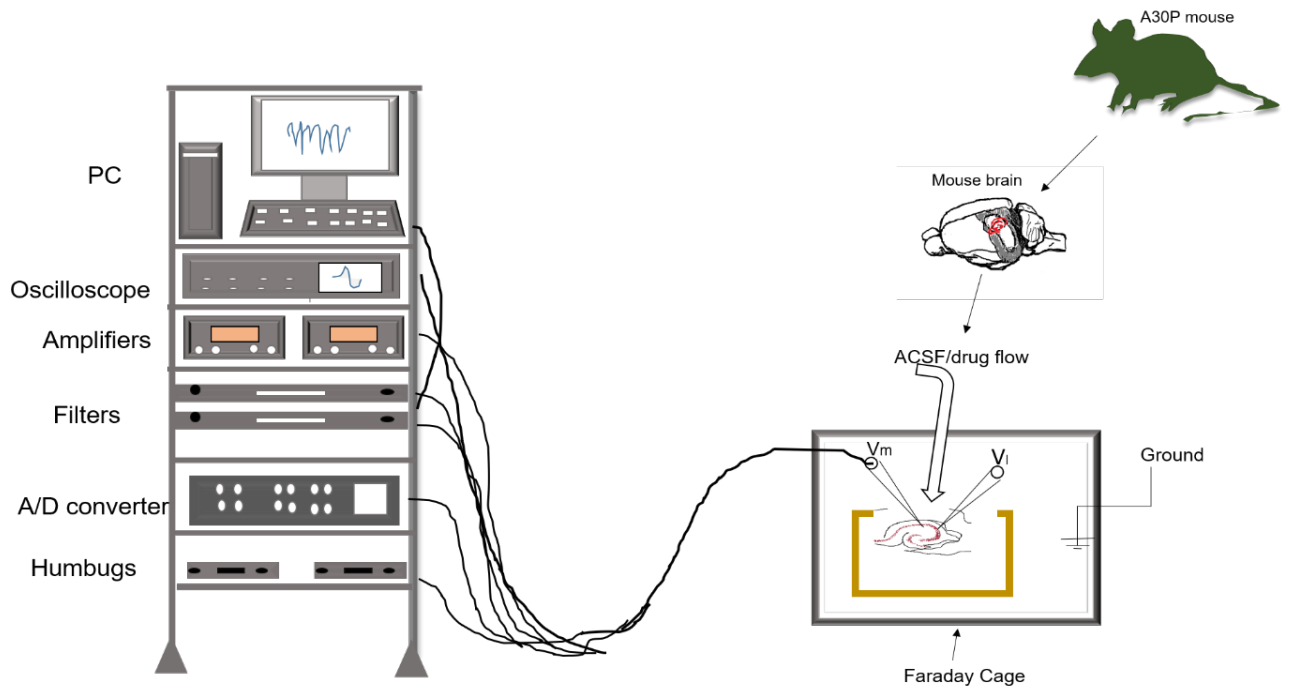
Figure 2. 2: Set up of the electrophysiology rig for LFP potentials recordings.

2.2.5 Data Analysis

AxoGraph 4.6 software (Axon instruments Inc., Union City, CA, USA) was first used to generate power spectra density by Fast Fourier Transform algorithms, by the analysis of 60-second epochs of recorded activity to produce a peak frequency of the measured oscillations. Data were plotted as frequency (Hz) over time (s) and power ($\mu V2/Hz$) using 8192 frequency bins. For each trace, the area under the peak (area power; $\mu V2$) in the power spectra between 15 and 45 Hz (representing the strength of the oscillations in this frequency band) were determined as the value for the area power (a combination of the amplitude and area). It was shown previously that gamma frequency oscillations in mice are 20-30 Hz lower frequency than in other primates (Driver et al., 2007). Frequency oscillations in mice are reported to occur between 20-80 Hz (Vreugdenhil and Toescu, 2005). Moreover, they are described to be temperature dependent in acute hippocampal slices (Dickinson et al., 2003). In this thesis, gamma frequency oscillations performed at relatively low temperature 30-31ºC. Therefore, we selected a gamma frequency band between 15-45 Hz for the recordings to detect all neuronal gamma frequency activity accurately.

The amplitude of the first side peak of the autocorrelations was performed over 1 second epoch of data to measure the value of the rhythmicity index (RI). The first side

peak amplitude provides a normalised RI value, giving the maximum of 1. Original signals were changed in time, to allow comparison of the similarity of the signals with the time-shifted version. To measure the time delay in milliseconds between regions (CA3-CA1), a cross-correlation analysis of a 1-second epoch was performed. The time delay between the two signals was represented by the central peak amplitude.

2.2.6 Statistical analysis

Data were analysed in sigma plot (v12.5) to determine whether the data are normally distributed. Normally distributed data were plotted as mean+-s.e.m and compared using t-test. Due to normal variability in the area power of the gamma frequency oscillations, the data were analysed using non-parametric tests on the raw data and described as percentage change or median and interquartile ranges (IQR). Here I used Mann-Whitney rank sum text when comparing two different groups. For comparisons before and after conditions in the same sample I used Wilcoxon signed rank test. Friedman's repeated measures ANOVA was used when performing repeated measures on the same sample. Kruskal-Wallis one-way ANOVA on ranks was used when comparing multiple groups. When significant difference was observed in the ANOVA test, a pair wise multiple comparison (Dunn's or Tukey) tests were performed to determine which parameters were significantly different. P value are reported significant if in the range between <0.05 and <0.001.

2.2.7 Compounds used

To measure the effects of mitochondrial modulation, drugs were added to the carbogenated ACSF that was continuously circulating to through the slices within the recording chamber. ACSF used for bath application in the slides was supplemented with the following compounds: Carbachol (10 µM); phosphate buffered saline (PBS); potassium cyanide (KCN, 50-100 µM); rotenone (250-1000 nM); sodium pyruvate (10 µM); memantine hydrochloride (20 mM), kinate 800 nM (Sigma-Aldrich, Gillingham, Dorset, UK), phencyclidine (PCP) (10 µM) (Tocris bioscience, Avonmouth, UK). All water-soluble drugs were prepared in distilled water, aliquoted and kept chilled at 4°C. Non-water-soluble drugs such as Rotenone, were dissolved in Dimethyl sulfoxide (DMSO) (Sigma-Aldrich, Gillingham, Dorset, UK) and stored at -20°C. The storage of the compounds was done according to the recommendation of the manufacturers.

Table 2. 2: List of compounds used in the electrophysiology for the mitochondrial activity modulation.

Commercial Name	Chemical name	Action	Supplier
Rotenone	(2R,6As,12As)-1,2,6,6a,12,12a hexahydro-2-isopropenyl-8,9-dimethoxychromeno[3,4-b]furo(2,3-h)chromen-6-one	Inhibition of complex I of the mitochondria electron transport chain	Sigma-Aldrich(***)
Potassium Cyanide	KCN	Blocks cytochrome C oxidase	Sigma-Aldrich (***)
Charbachol	Carbamylcholine chloride	Cholinergic agonist	Sigma-Aldrich (C4382)
Sodium Pyruvate	2-oxopropanoic acid sodium	Enhancement of Kreb's cycle	Sigma-Aldrich (P3662-25G)
Memantine	Memantine hydrochloride	NMDAr antagonist	Sigma-Aldrich (***)
Kainic acid	(2s,3s,4s)-3-(carboxymethyl)-4-prop-1-en-2-ylpyrrolidine-2-carboxic acid	Kainate receptor agonist, parcial AMPA receptor agonist	Sigma-Aldrich (K0250)

(***) means that that the catalogue number is not known.

2.3 Results

2.3.1 Rotenone causes mitochondrial dysfunction and impairs gamma frequency oscillations in the hippocampus of A30P mice.

The effects of mitochondrial inhibitors and their impact on the cortical neuronal network oscillations, was assessed in control and A30P mice. We previously reported impairments of gamma frequency oscillations in aged A30P mice (Robson et al., 2018b). The impaired gamma activity seen in these mice, reflected the age-dependent reduction of the mitochondrial function due to pathologic αSyn accumulation. I, therefore, predicted that this group of mice would show a greater sensitivity to the inhibition of mitochondrial function. In addition, the majority of the studies on gamma frequency oscillations was done using acute slices from hippocampus (Kann et al., 2011, Traub et al., 1996, Fisahn et al., 2002, Hajos et al., 2004), where persistent gamma activity, was induced by bath application of glutamatergic or cholinergic receptor agonists at lower molar concentration (Kann, 2011).

Taking all of the above into account, I compared the effects of rotenone on gamma frequency oscillations in both aged control 9+ (from 9 months above) and aged 9+ months old A30P mice to assess the impact of blocking complex I of the mitochondrial respiratory chain. In this set of experiments, control oscillations (within the 15-45 Hz frequency) were considered stable when the measurements of the area power for at least three consecutive recordings were within ±10-15 % at 10-to-15-minute intervals. For this work, I activated the cholinergic receptors (Wojtowicz et al., 2009, Kann, 2011) in the hippocampus slices of A30P and control mice, as it is thought that gamma activity is more prominent in in this region of the brain (figure.3.2) (Kann et al., 2011). I then bath applied rotenone (250, 500, and 1000 nM) to the slices, to block complex I of the mitochondrial ETC to inhibit the mitochondrial function and compare the effects with normal mice.

Gamma oscillations were induced with 10 µM carbachol, a cholinergic receptor agonist, and once stable values were reached, after approximately 3h of recordings (see methods, slice recordings), rotenone was bath applied, and its concentration was increased every 30 minutes with readings taken every 10 minutes (figure 2.3). I observed that in the control 9+ C57 group (7 mice/21 slices) there was a clear trend towards a concentration-dependent reduction in gamma frequency area power (figure

69

2.3). Nevertheless, not much change was observed in the frequency of the gamma oscillations. The values were not statistically different when compared with stable control levels (Friedman's repeated measures ANOVA on ranks followed by Tukey post hoc multiple comparisons test p<0.05).

In contrast, rotenone application at the higher concentration (500-1000 nM), caused a statistically significant decrease in the area power of gamma frequency oscillations in the 9+ A30P group (6 mice/18 slices) (Friedman's repeated measures ANOVA on ranks followed by Tukey post hoc multiple comparisons test p<0.05). Indeed, at 1 µM concentration, rotenone reduced the gamma oscillation power by -29.6 ± 9.8% in 9+C57 mice, and -41.9±8.8% in the 9+A30P mice. The significant decrease in gamma power of the oscillations in 9+ A30P mice by rotenone treatment, suggests that slices from 9+ A30P mice were more sensitive to inhibition of mitochondria complex I of the ETC with rotenone, suggesting an underlined dysfunction of the ETC due to the accumulation of pathological αSyn.

In this experiment, I have not performed the comparisons across concentration in the two genotypes. Although I attempted to make a direct comparison of C57 and A30P mice at a higher concentration of rotenone, I was not able to finalise it. Preferably I would like to perform 2-way ANOVA for this experiment like on the other experiments in the subsequent chapters. However, the circumstances were not favourable to be able to access the data as the statistical analysis was performed in conjunction with Dr. Fiona LeBeau for the paper already published, and all the electrophysiology data for these experiments would require access to the electrophysiology Lab software system. Because of the conflict of interest, it makes it more difficult to access them. Thus, this is a limitation of this thesis.
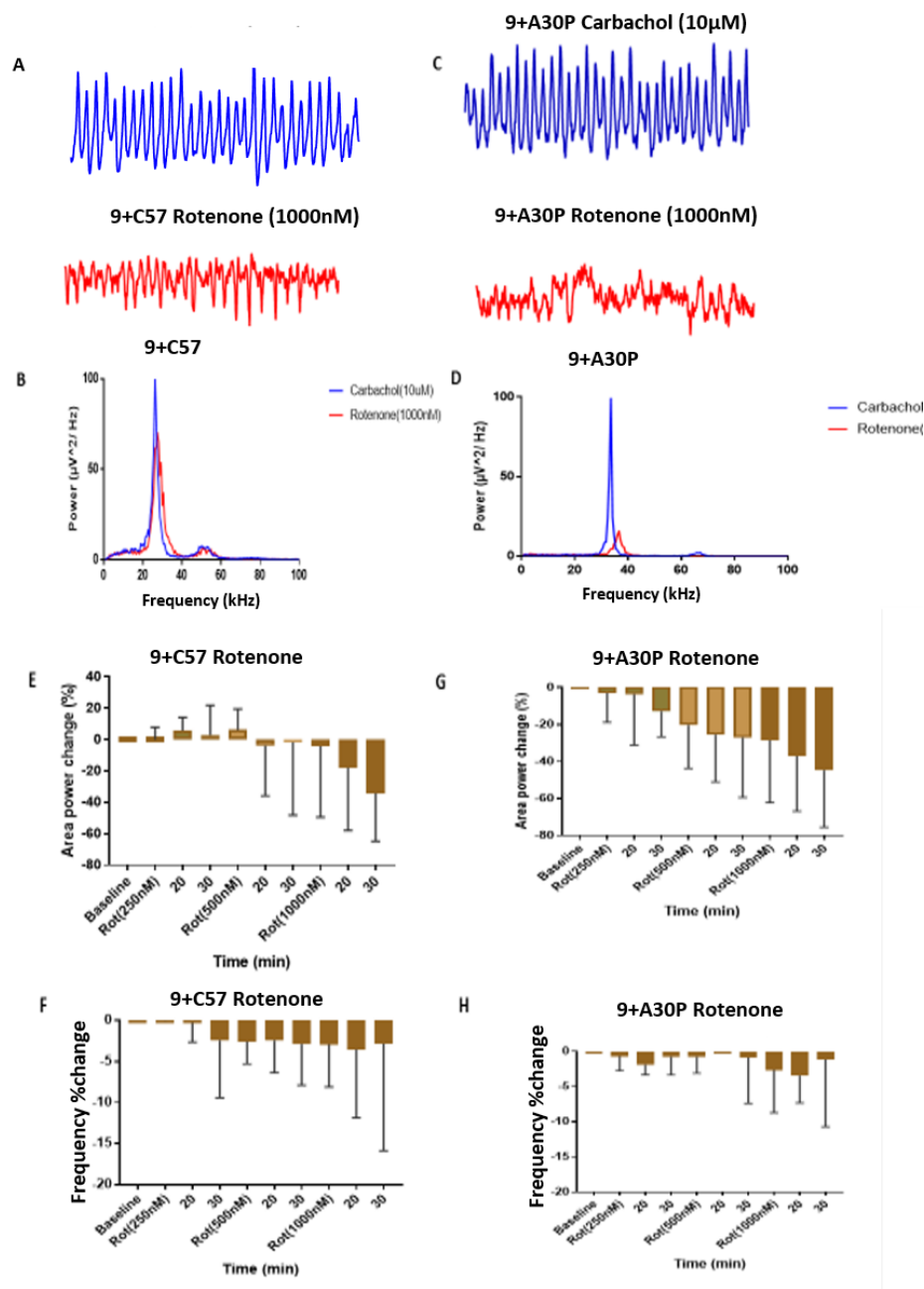
Figure 2. 3: Effects of rotenone in area power of gamma frequency oscillations in the hippocampus. (**A**) Raw traces comparing the frequency of the oscillations in C57 (left) stable gamma oscillations (in blue), impaired gamma (in red). (**B**) Area power of the gamma frequency oscillations in C57 mice, carbachol (in blue) and rotenone (in red). (**C**) Raw traces comparing the frequency of the oscillations in A30P (right) mice, in carbachol (blue) and rotenone (red). (**D**) (**E**) Bar graph showing percentage change in area power and frequency in C57 mice (left), after application of an increasing concentration of rotenone (250 nM, 500 nM, 1000 nM) in 9+ group. (**F**) The frequency

did not change in rotenone. (**G**) Histogram showing the same measurements with rotenone in A30P mice. (**H**) No significant change in frequency in rotenone. The readings were taken in every 10 minutes for 90 minutes.

2.3.2 Potassium cyanide causes mitochondrial dysfunction and impairs gamma frequency oscillations in the hippocampus of A30P mice.

Following the hypothesis, I believe the impaired gamma activity that occurred as a result of mitochondrial complex I inhibition with rotenone in mice aged 9+ months old reflected pathologic αSyn-related reduction of the mitochondrial function. Thus, I predicted that the A30P mice would also show a greater sensitivity to the inhibition of complex IV of mitochondrial ETC, since complex IV is the last stage of the last step of the ETC, which transforms oxygen molecules into water, hence by blocking this last step all the activity of the ETC may be abolished. The links between αSyn and and complex IV of the mitochondria ETC has been demonstrated, it is thought that this interaction is associated with the mitochondrial disfunction, which is an important pathogenic aspect of LBDs (Elkon et al., 2002). Hence, I used KCN in a concentration dependent manner (25, 50, 100 μM), to block complex IV of the ETC, and consequently, inhibit the mitochondrial function, to then compare its effects in both aged control 9+ (from 9 months above) and aged 9+ months old A30P mice.

Gamma frequency oscillations were induced with 10 μM carbachol, followed by bath application of KCN once the reading stabilized. KCN concentration was increased every 30 minutes with readings being taken every 10 minutes (figure 2.4). In control 9+ C57 group (7 mice/21 slices), there was a clear trend towards a concentration-dependent reduction of the area power of gamma oscillations upon KCN treatment (figure 3.4b), Nevertheless, not much change was observed in the frequency of the gamma oscillations. In fact, I observed a rapid reduction in the area power of the gamma frequency oscillation within 10 minutes of the bath application of KCN in both 9+ C57 and 9+ A30P mice (4 mice/6 slices) (figure 2.4), and statistically significant reductions from the baseline measurements were evident at 50 μM and 100 μM KCN in both groups (9+ C57 and 9+ A30P) (figure 2.4) (Friedman's repeated measures ANOVA on ranks followed by Tukey post hoc multiple comparisons test $p > 0.05$). The power of the gamma frequency oscillations was reduced by 77 % in the 9+ C57 group and 82.6 ± 8.3% in the 9+ A30P mice when the final concentration was added. These

changes were not statistically significant when comparing both groups. The frequency of the gamma oscillations was abolished only when the final drug concentration was added, when practically no activity was seen. Hence, KCN, appeared to be effective in reducing the area power of the oscillations in both diseased and control mice.
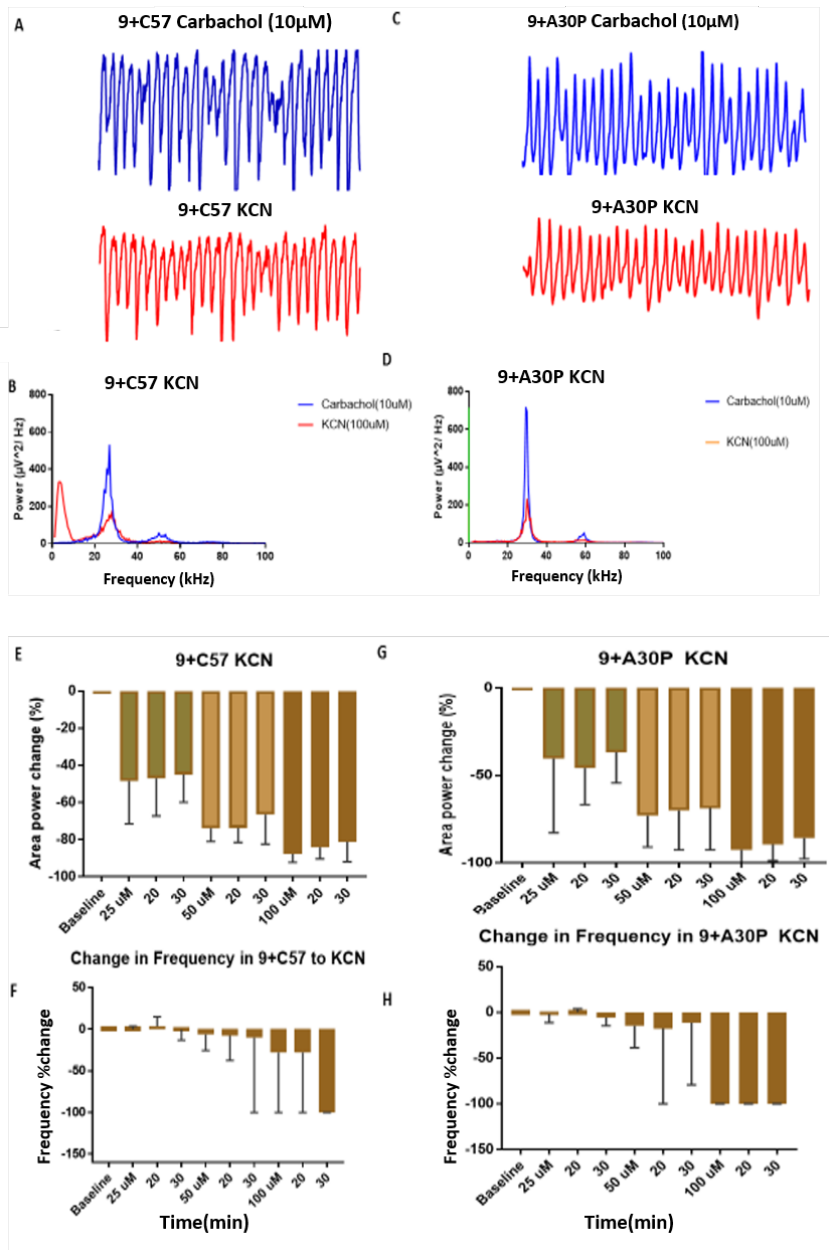
Figure 2. 4: Effects of KCN in area power of gamma oscillations in the hippocampus. (A) Raw traces comparing the frequency of the oscillations in C57 (left) stable gamma oscillations (in blue), impaired gamma (in red). (B) Area power of the gamma frequency oscillations in C57 mice, carbachol (in blue) and KCN (in red). (C) Raw traces comparing the frequency of the oscillations in A30P (right) mice, in carbachol (blue) and rotenone (red). (D) Power spectrum showing a higher peak in

gamma frequency in carbachol (blue) which greatly decreased when KCN (red) was added, in both C57 (left) and A30P (right) mice. (E) Histogram showing percentage changes in area power and frequency in C57 mice (left), after application of an increasing concentration of KCN (25 µM, 50 µM, 100µM) in 9+ group. (F) The frequency did not change in KCN. (G) Bar graph showing the same measurements with KCN in A30P mice. (H) Significant drop in frequency of the oscillations in A30P mice when 100 µM of KCN was added. The readings were taken in every 10 minutes for 90 minutes.

2.3.3 Sodium pyruvate improves gamma frequency oscillations in the hippocampus of both control and A30P mice

Since the results above described indicates impairments of the complex I and IV of the mitochondria, I hypothesised that they might underlie the deficits in neuronal gamma oscillations in A30P mice (Robson et al., 2018b). I therefore investigated whether, by supplementing sodium pyruvate into slices from A30P mice, would lead to the restoration of the observed mitochondrial impairments. Based on the observation of impairment in the mitochondrial ETC function in A30P mice (Robson et al 2018) I hypothesised that by administering an energy supplement, a cell permeable form of pyruvate (sodium pyruvate), might restore mitochondrial function, which could be reflected by an improvement in gamma frequency oscillations.

Slices from young and aged mice (2+C57 mice (5 mice/ 13 slices) and 2+A30P (5 mice/ 13 slices)) and aged (9+C57 mice (5 mice/ 13slices) and 9+A30P (4 mice/ 10 slices)) were used to ascertain gamma oscillations were again induced with 10 µM carbachol until after approximately 3 hours when the reading stabilized. I then bath applied 20 µM sodium pyruvate and recorded readings every 10 minutes for the duration of 2h. No significant effect of pyruvate addition was seen on gamma oscillation frequency or area power in slices taken from 2+C57 mice (figure 2.5). In contrast, in slices from the 2+A30P mice the area power of the gamma oscillations showed a slight improvement after 30 minutes in sodium pyruvate, which then decreased after 110 minutes (figure.2.5). Importantly, the changes in the frequency of gamma oscillations between the control and A30P mice were statistically significant when compared the basal stable oscillations upon addition of pyruvate (Freidman's repeated measures ANOVA on ranks followed by Tukey post hoc multiple

comparisons test p>0.05). In contrast, a significant increase was observed for the duration of the recordings in adult 9+C57 mice. However, the same beneficial effect of pyruvate was not present in the 9+A30P mice. These data suggest sodium pyruvate may have a small effect in improving gamma frequency oscillations specifically in old mice.
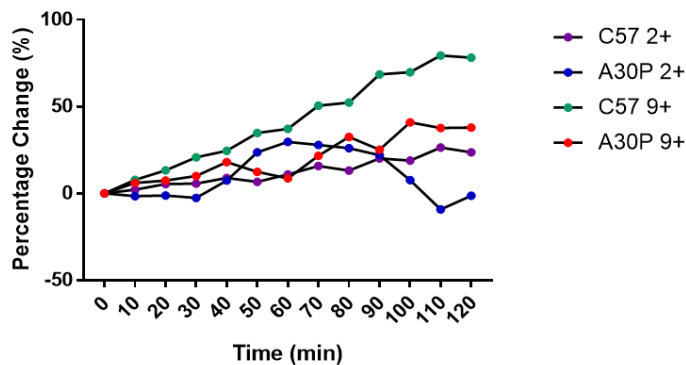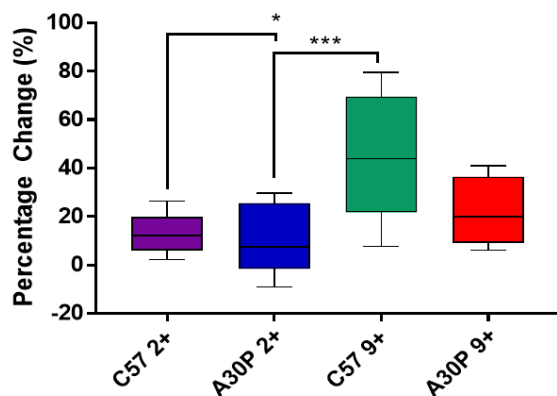
Figure 2. 5: Line charts representing the trend in area power of the gamma frequency oscillations with sodium pyruvate. Slices from young and aged mice (2+C57 mice (5 mice/ 13 slices) and 2+A30P (5 mice/ 13 slices)) and aged (9+C57 mice (5 mice/ 13slices) and 9+A30P (4 mice/ 10 slices)) were used to ascertain gamma oscillations were again induced with 10 μM carbachol until after approximately 3 hours when the reading stabilized. The area power of the gamma frequency oscillations shows a slight increase from the base line when pyruvate is added for 2h. Similar trend is observed in 2+A30P and 9+A30P mice where the area power of the gamma frequency oscillations shows also an increase when compared with the control, but with a lesser effect when compared to control cases. Box plot showing similar results observed in the line chart.

2.3.4 NMDA receptor antagonist memantine increases gamma frequency oscillations in the hippocampus of A30P mice

In this set of experiments, I assessed the effects of memantine, which is an NMDA receptor antagonist, that is widely used to treat cognitive and motor dysfunction in patients with dementia (Litvinenko et al., 2010). As in previous experiments, I have demonstrated impairments in the mitochondrial function in A30P mice (Robson et al 2018). I have also shown the effects of sodium pyruvate producing a slight increase in the area power of the gamma frequency oscillations. In addition, a work done in our lab demonstrated that young A30P mice develops early hyperexcitability, which is reduced in 10+ months of age mice, as seizure-like activity is reduced (Tweedy, 2019). In fact, some of the mice used in this work presented EEG epileptiform activity during the experiments, which I believe to be occurring long before the impairments of gamma network oscillations and the subsequent cognitive dysfunction, which is present in the A30P mice at 12 months of age (these hyperexcitability were not further explored here, as it was not the aim of this thesis). This is consistent with the recent study that used a similar transgenic (A53T) aSyn mouse, which showed epileptiform activity (Morris et al 2015), suggesting an excitatory-inhibitory imbalance due to hyperactivation of the NMDA receptors. Although, memantine does not improve cognition or gamma frequency oscillations in people with DLB, however, it was proven to reduce the rate of cognitive decline in Dementia (Folch et al., 2018). Therefore, I predicted that by antagonising the effects of the NMDA receptors with memantine in slices of control and A30P mice, the impaired gamma frequency oscillations may be restored in these mice. Indeed, *in vivo* studies have suggested that blocking these receptors with an NMDA receptor antagonist has led to an increase of gamma frequency oscillations in rat cerebral cortex (Pinault, 2008, Bian et al., 2009).

To determine whether a non-competitive NMDA antagonist, has an effect on gamma frequency oscillation of the neuronal network. Gamma oscillations were induced with 10 µM Carbachol for approximately 3h, in the hippocampal slices and then bathed in 20 µM of memantine for the duration of 2 hours with readings were taken every 10 minutes throughout the experiment in hippocampal slices of young (2+C57 mice (n 6/10 slices) and 2+A30P mice (n 6/12 slices) mice (figure.3.5). Memantine treatment induced a significant increase in the area power of the gamma oscillations in slices taken from 2+C57 mice, for approximately 1h:30 minutes. Although the effect seems

to cause a slight decrease of the area power after 1 hour, to increased again till the end of the experiment, the increase in the area power was clear when compared to the baseline oscillations. On the contrary, the frequency of the oscillations remained practically the same (Freidman's repeated measures ANOVA on ranks followed by Tukey post hoc multiple comparisons test $p>0.05$) (figure 2.6). On the other hand, after approximately 20 minutes in memantine, there was also a significant increase in the area power of the oscillations in 2+A30P mice. Notwithstanding, it followed with a gradual decrease in the frequency of the oscillations, after approximately 30 minutes in memantine and after 70 minutes. In the experiments the decrease in the frequency of the oscillation was accentuated (figure 2.6). one-way ANOVA $p>0.05$), and post-hoc analysis (Tukey pairwise comparison) showed statistically significant increase from the base line, in both control and A30P mice. However, the results were not significant when comparing both control and A30P mice, as there was a clear trend to an increase in the area power of the oscillations in both groups (figure 2.6).

Following the significant effect of memantine on the younger group of 2+A30P mice (when compared to the baseline), I went on trying the same experiments with the available older group of 14+A30P mice (n4/9 slices). Because of their scarce availability I was only able to do it in these group of mice. Memantine treatment in the 14+A30P mice had not significant effect on the area power of gamma oscillation when compared to the baseline (figure 3.6). However, we observed a clear trend to reduction of the frequency of the oscillations after 60 minutes of treatment in 14+A30P mice (Freidman's repeated measures ANOVA on ranks followed by Tukey post hoc multiple comparisons test $p>0.05$) (figure 2.7).

Although, I predicted that inhibition of NMDA receptors by memantine, can increase gamma frequency oscillatory power when compared to the baseline, the results from the young mice were not statistically different when comparing both disease and control groups, suggesting that NMDA receptor impairments may not play a key role in the disease pathogenesis in the young A30P mice. On the other hand, the experiments in the adult mice were also not finished. However, I can speculate that there seemed to be some trend to an increase in the area power of the oscillations, notwithstanding, more analyses are necessary to completely elucidate the effects of memantine in adult A30P mice. Overall, the study of memantine effects in the A30P

mice demands more experiments, as memantine results presented here it is not strongly suggestive of any clear change between the control and the diseased mice.
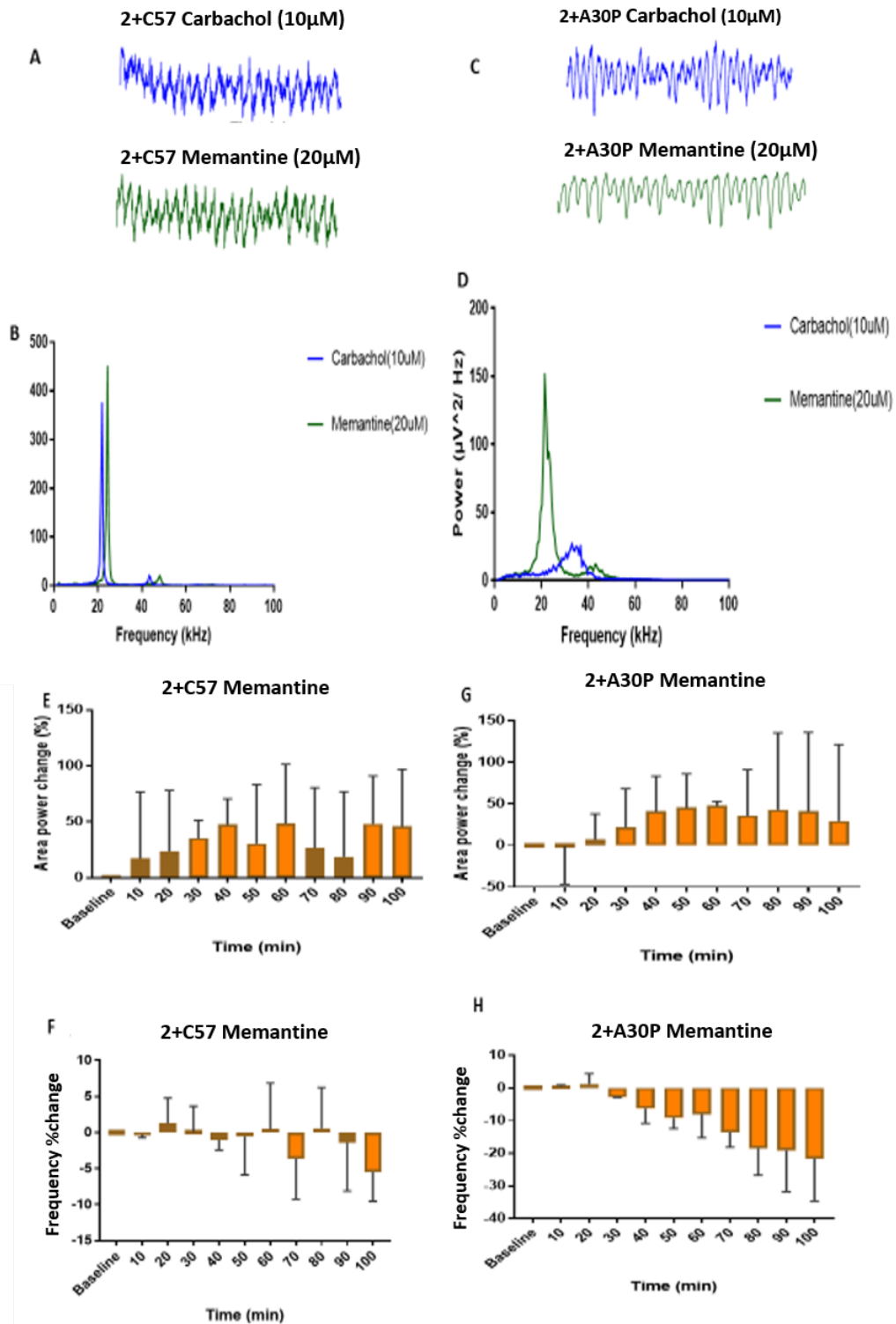
Figure 2. 6: Effects of memantine in area power of gamma oscillations in the hippocampus. (**A**) Raw traces comparing the frequency of the oscillations in C57 (left) stable gamma oscillations (in blue), improved gamma (in green) with memantine. (**B**) Area power of the gamma frequency oscillations in C57 mice, carbachol (in blue) and memantine (in green). (**C**) Raw traces comparing the frequency of the oscillations in A30P (right) mice, in carbachol (blue) and memantine (green). (**D**) Power spectrum showing a higher peak in gamma frequency in memantine (green) comparing to carbachol (blue). (**E**) Bar graph showing percentage changes in area power and frequency in C57 mice (left), after application of memantine. (**F**) The frequency of the oscillations did not have a significant change in memantine. (**H**) Histogram showing the same measurements with memantine in A30P mice. (**G**) Significant drop in frequency of the oscillations in A30P mice when memantine was added. The readings were taken every 10 minutes for 100 minutes.
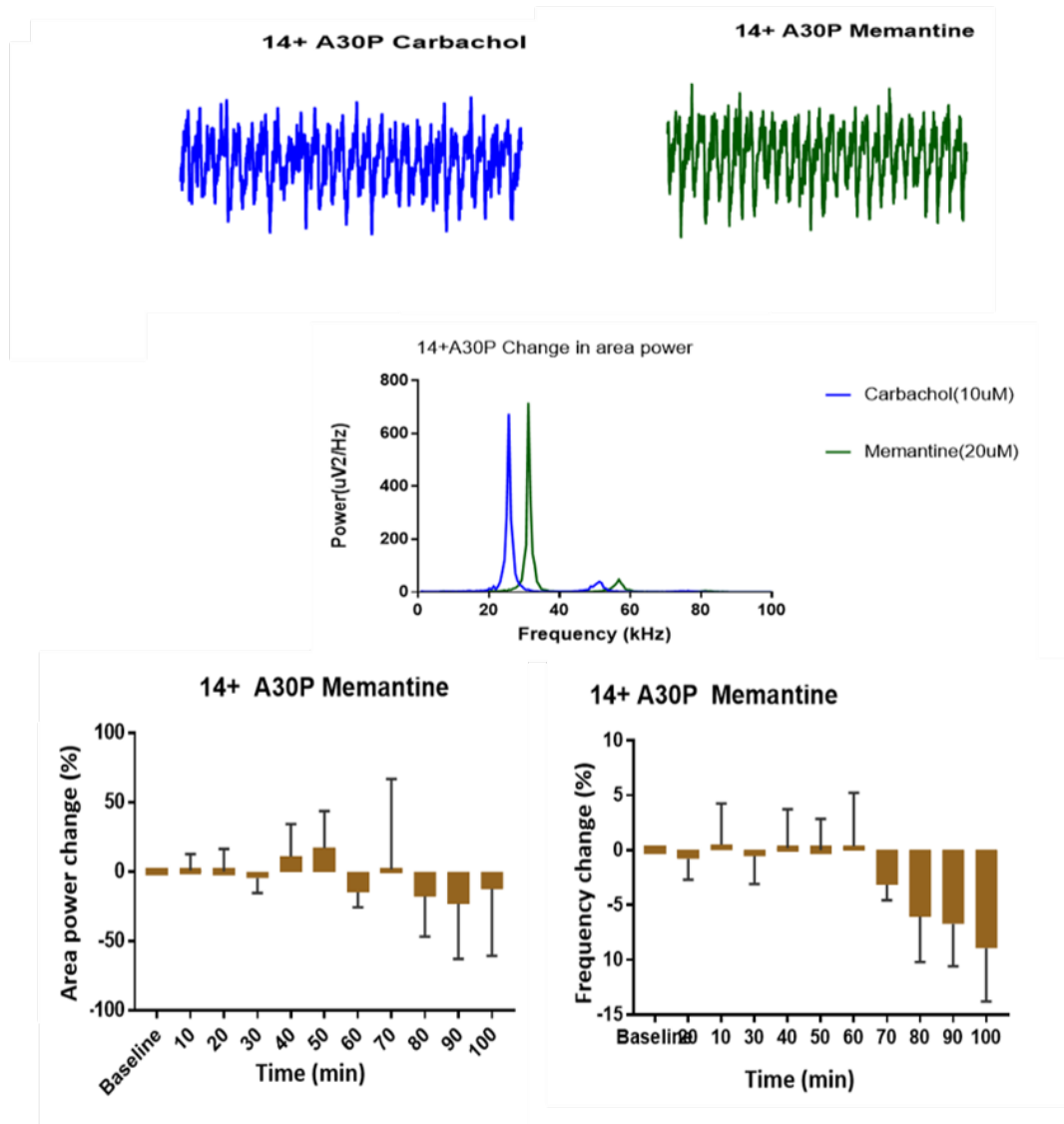
Figure 2. 7: Effects of Memantine in area power of gamma oscillations in the hippocampus of aged A30P mice. (**A**) Histogram chowing percentage changes in area power in adult A30P mice, after application of Memantine (20 µM). (**B**) Bar graph showing the frequency measurements with Memantine in 14+A30P mice. The area power did no change significantly after 30 minutes in the drug. However, the frequency seemed to reduce after 70 minutes. The readings were taken every 10 minutes for 2 hours. **C**) Raw traces comparing the frequency of the oscillations in carbachol (blue) and memantine (green). (**D**) Power spectrum showing similar peak in gamma frequency in carbachol (blue) and Memantine (green).

2.4 Discussion

2.4.1 Gamma frequency oscillations in the hippocampus

Gamma network oscillations have been well studied in the hippocampus, which has now become the prototype for neuronal oscillation studies, associated to cognitive functions. This region is thought to play important role in spatial navigation, episodic memory, additionally, its simple laminated architecture is simpler than the neocortex cytoarchitecture, and gamma oscillations recorded in this region presents larger amplitudes (Lisman et al., 2017, Buzsáki and Wang, 2012). In the hippocampus, persistent gamma oscillations can be reliably evoked by a glutamatergic or cholinergic agonist (acetylcholine, carbachol), which activate the metabotropic cholinergic receptors. On other occasions it can also be evoked by bath application of kainic acid (Kainate) which activates the ionotropic glutamatergic receptors (Pietersen et al., 2009, Dheerendra et al., 2018, Schneider et al., 2015a).

Moreover, *In vitro* induction of gamma frequency oscillations in the hippocampus are less prominent in the dentate gyrus, weaker in the CA1 subfield and more prominent in the CA3 subfield of neuronal network (Akam et al., 2012, Craig and McBain, 2015). Hence, the CA3 is commonly known to be the hippocampal generator of high-power gamma frequency oscillations, although neuroenergetical and the electrophysiological features of the CA3 network may not relate to the gamma oscillations properties recorded from other regions (Akam et al., 2012, Craig and McBain, 2015, Traub et al., 2000). Therefore, in this work, gamma frequency oscillations were studied in the CA3 region of the hippocampus evoked by the use of carbachol. In addition, the induction of gamma oscillations with carbachol are dependent on the mediation of AMPA receptor excitatory postsynaptic potentials (Traub et al., 2000). Hence, I was able to evoke gamma frequency oscillations in the hippocampus as a reliable region to study the impairments these oscillations in DLB.

2.4.2 Implication of mitochondrial inhibition and pyruvate supplementation on gamma frequency oscillations in the young A30P mice.

Mitochondria are cellular power plants of neurons, since they are the main source of energy for the cells, by providing adenosine triphosphate (ATP) that results from chemicals that are converted through the ETC and the oxidative phosphorylation

(Laird et al., 2013, Sheng, 2014, Zhu et al., 2012). In the human brain, a cortical neuron may utilize up to approximately 4.7 billion of ATP molecules per second to perform its function (Laird et al., 2013, Sheng, 2014, Zhu et al., 2012). Thus, the continuous supply of ATP is key for the function and the survival of the neurons (Nicholls et al., 2015), as the production of ATP helps to maintain the synapse assembly and synaptic transmission by buffering calcium (Medler and Gleason, 2002, Vos et al., 2010). In fact, it was proven that the absence of the mitochondria in the synapses causes an impairments in the synaptic transmission due to the insufficient ATP supply and impairment in calcium transients (Sheng, 2014). Therefore, normal mitochondrial function is required for the generation of fast neuronal network oscillations, such as gamma frequency oscillations, as they are thought to be highly energy dependent (Whittaker et al., 2011a).

Mitochondrial dysfunction has previously been demonstrated in mice that overexpress αSyn (Rothman et al., 2014, Chen et al., 2015). It is currently believed that αSyn can translocate inside the mitochondria and modulate mitochondria morphology and function in mouse models of synucleinopathy (Li et al., 2014, Martin et al., 2014). In fact the effect of impaired αSyn in the mitochondria is particularly worse in A53T mice (a different mouse model of synucleinopathy), compared to the A30P mice (used for my experiments) (Pozo Devoto et al., 2017). This discrepancy in study results from the mouse models, parallels with studies in human, in which authors showed that the A30P mutation is linked with the late onset of the development of synucleinopathy as well as the less severe clinical phenotypes of the disease (Kruger et al., 2001, Puschmann et al., 2009). The age-dependent reduction of mitochondrial activity and the resulting oxidative stress is what I believe to be associated with the age-dependent reduction in the area power of gamma activity observed in the hippocampal slices of adult A30P mice, that predates the development of cognitive deficits that arise after 12 months of age in these mice (Neumann et al., 2002).

Furthermore, gamma oscillations are impaired in the presence of hypoxia, oxidative stress, and inhibition of the mitochondrial oxidative phosphorylation, which depends on the normal functioning of the mitochondrial ETC (Kann et al., 2014b). The nicotinamide adenine dinucleotide (NADH): ubiquinone oxidoreductase also known as complex I, is the first enzyme in the ETC that catalyses the transfer of electrons from NADH produced during the Krebs cycle to coenzyme Q10 to be transferred to the

ETC. It also pumps protons directly into the mitochondrial intermembrane space, facilitating the synthesis of ATP (Baradaran et al., 2013). Inhibition of complex I of the ETC is therefore associated with the production of ROS and ATP depletion. Interestingly, inhibition of complex I in the substantia nigra, was found to be associated with the development of PD, as well as inhibition of the complex I in prefrontal cortex was found to be linked with cognitive decline (Gatt et al., 2016). Thus, significant impairments in mitochondrial function, linked with the impairments in the gamma frequency oscillations, could be consistent with the process of slow neurodegeneration seen in A30P mice. This is also supported by studies that have shown that complex I inhibition ETC with rotenone compromises the normal ATP production, while simultaneously triggering an increase in the production reactive oxygen species thus leading to elevated levels of oxidative stress (Heinz et al., 2017, Chou et al., 2010). In parallel with this, here I show that rotenone reduces the area power of the gamma frequency oscillations in a concentration dependent manner with a greater effect in aged A30P mice compared to aged controls. In fact, mice that overexpress misfolded human mutant αSyn protein (A30P), showed higher sensitivity to mitochondrial inhibition of complex I with rotenone, by showing a greater reduction in the area power of gamma frequency oscillations in adult 9+ A30P mice when compared with the control (9+C57) mice. suggesting that mitochondrial impairment may lead to the impaired gamma oscillations seen in these mice (Robson et al., 2018b).

KCN was shown to depolarize and abolish the activity of the fast-spiking interneurons, by reducing the inhibitory post synaptic potential (IPSP) on the pyramidal cells (Whittaker et al., 2011a). The same study also showed that a high concentration of KCN (100 µM) had no effect on the excitatory postsynaptic potential (EPSPs) in the pyramidal cells. This suggests that the changes in the neuronal network oscillations may not be associated with the diminution in glutamatergic neurotransmission. On the contrary, the same study found a diminution in the IPSPs on the pyramidal cell, thus, disrupting the PING model of generation of gamma frequency oscillation (figure. 3.3), as they observed that the PV+ expressing fast spiking interneurons were depolarised and their activity abolished (Whittaker et al., 2011b). Therefore, the observed changes in fast spiking interneurons (loss of action potential firing and the decrease of IPSPs amplitude) could be at the root of the reduction of gamma frequency oscillations observed in their studies, as well as seen in the findings that I present in this thesis.

The unparallel electrophysiological properties of the interneurons, particularly the high energy demand cells (PV+), which is reflected by their mitochondria and cytochrome *c* enriched ultrastructure, and are thought to be essential for the GABA metabolism and the extensive Ion transport (Kann et al., 2014b). This suggests a higher sensitivity of these groups of neurons (interneurons) to mitochondrial inhibition, and its correlation with their high metabolic demands (Kann, 2011, Kann, 2016). In parallel with the hypothesis that suggests that highly energized interneurons are key element for information processing which may be crucial for cognitive decline when the supply of energy is deprived or impaired, thus impairing the gamma frequency oscillations (Kann et al., 2011, Whittaker et al., 2011a). The evidence presented here, shows that treatment with KCN, which blocks the activity of complex IV, led to a greater reduction in area power of gamma frequency oscillations in both aged 9+C57 and 9+A30P mice. Indeed, previous studies have demonstrated that acute application of high concentration of both rotenone (1 µM) and KCN (100 µM) caused a quick collapse of the area power of gamma frequency oscillations (Kann et al., 2011, Whittaker et al., 2011a). Hence, I can speculate that the impairments of the gamma frequency oscillations in the synucleinopathy model, may be associated the existence of toxic species of αSyn.

In addition, sodium pyruvate, which is an energy supplement, is thought to possess positive effects in neurodegeneration, as it increases availability of brain glycogen in mouse brain of AD, and restores the behavioural impairments observed in AD patients (Koivisto et al., 2016). The preliminary results presented here in this topic, showed that the addition of sodium pyruvate in the neuronal network oscillations, elevates the tendency to produce a slight increase in the area power of gamma frequency oscillations in young A30P mice. Moreover, in young control and A30P mice, the area power of the gamma oscillations showed a slight improvement after 30 minutes in sodium pyruvate. However, these changes were observed in both adult control and aged A30P mice, casting more doubts to any possible beneficial effect of sodium pyruvate in restoring the gamma frequency oscillations. Although sodium pyruvate was shown, to have a therapeutic effect in myopathic mitochondrial DNA diseases and in patients with oxidative phosphorylation disorders by increasing the glycolytic pathways (Saito et al., 2012, Fujii et al., 2014), there are no current available literature studies that supports the hypothesis of positive the effects of sodium pyruvate in DLB.

Thus, it is unclear to whether sodium pyruvate may have any benefit effects that suggesting a potential therapeutic approach for the restoration of the gamma frequency oscillations.

2.4.3 The effect of memantine on gamma frequency oscillations

The results presented also demonstrate that memantine treatment leads to a slight increase in the area power of gamma frequency in both young control and DLB mice (figure 3.4). This suggests that the role of NMDA receptors needs further mechanistic investigations as the animals grow older. Here, I have noted an increase in the area power of gamma frequency in both control (C57) and A30P mice. This is consistent with the previous studies that showed that NMDA receptor antagonist increases the gamma oscillations, since excess NMDA receptor activation can lead to excitotoxicity in neurons (Dreyer et al., 1995, Tenneti et al., 1998, Okamoto et al., 2002). Altogether, these findings suggest that modulation of gamma frequency oscillations with memantine can be a therapeutic approach to consider in disease treatment or even for further studies. In addition, memantine is thought to increase long term potentiation (LTP) at the network and cellular level, particularly the LTP effect of memantine is thought to depend on the enhanced levels of tonic NMDA current (Liu et al., 2019), suggesting that the action of memantine in the NMDA receptor requires previous tonic activation of the receptor. Although, it was not an aim for this study to look at the changes in the receptor, I believe that this would be an interesting topic to pursue in the future. In fact, basal NMDA receptor mediated excitatory post synaptic currents (EPSCs) were shown to increase with bath application of αSyn oligomers, which consequently led to LTP impairments. These impairments were then rescued with the application of an NMDAR antagonist (Diógenes et al., 2012). This study suggests that toxic forms of αSyn can lead to a prejudicial increase in synaptic transmission mediated by NMDA receptor activation.

Moreover, the increase in the activation of the NMDA receptors due to exposure to toxic αSyn species, is also thought to be associated with the increase in the expression of calcium permeable AMPA receptors (Diógenes et al., 2012), which I believe to be related to the increase in the hyperexcitability. Additionally, gamma frequency oscillations in the hippocampus, that are evoked with bath application of carbachol is not substantially modulated by NMDA receptor antagonists (Fisahn et al., 1998). In

this study, I observed a significant increase of the area power in slices taken from both young 2+C57 and 2+A30P mice. However, the difference between control and 30P mice was not significant, as there was a clear increase in the area power of the oscillations in both groups (figure 3.6). Considering these studies together, the results suggest a change in NMDA receptor function, that may be detrimental to the generation of gamma frequency oscillations in the A30P mice. However, further studies are required to confirm this hypothesis. At present, it is unclear why memantine-induced potentiating effect in gamma frequency oscillations was observed in both control and the mutant mice. It has been suggested, however, that gamma frequency oscillations could be increased by increasing acetylcholine levels, independently of the blockage of an NMDA receptor (Betterton et al., 2017). As the data presented in this chapter shows an area power increase in both control and A30P mice treated with memantine, it is possible that the cholinergic drive on the NMDA receptor was maximal in the slices from both young groups of mice.

2.4.4 Study limitations and future directions

Within this study, all the recordings of gamma activity were done in the CA3 region of the hippocampus. Due to technical limitations of the experiments, simultaneous measurements within different regions of the hippocampus were not possible. I believe that comparing the results of simultaneous recordings with other hippocampal regions such as CA1, CA2 including the dentate gyrus, would offer important mechanistic insights on the extent of gamma oscillation impairments. Furthermore, within the scope of this study, I was not able to assess the impairment of mitochondrial impairments in young mice to compare with the results observed in adult mice.

As some observed that, mitochondrial impairments in mice that overexpress toxic forms of αSyn causes a reduction in the IPSPs, suggesting a reduction of inhibitory input onto pyramidal cells, that consequently causes an increase of the EPSPs. This suggests an excess in excitations inputs from the excitatory pyramidal cells, which I believe to lead to hyperexcitability. This early excitatory-inhibitory imbalance ultimately may lead to the progressive neuronal neurodegeneration observed in older mice, which includes activated microglia and reduced mitochondrial function and impairments in gamma frequency oscillations. In a work done in our lab, my colleague was able to demonstrate this early hyperexcitability in the young A30P mice (Tweedy,

2019). Hence, I can speculate that the presence of overexpressed αSyn may indeed be associated with the mitochondrial dysfunctions and the impairments of gamma frequency oscillations. In addition to other pathogenic cascades such as, neuroinflammation, I believe that mitochondrial impairment is potentially a mechanism behind the impairments in gamma frequency oscillations observed in the mouse model of synucleinopathies. However, to better understand the intrinsic mechanism that underlie this impairment, it would be useful to study the period of the early hyperexcitability that was also found to precede the gamma network oscillations impairments. At the same time, other therapeutic experiments could also be done to assess whether an early therapeutic intervention could potentially delay or even prevent the later network changes.

This study would also be enhanced by the assessment whether the impairment of the complex I is a result of an ongoing oxidative stress damage, as many studies suggest that oxidative damage may precede complex I impairments. In fact, some studies have suggested that oxidative damage, may be at the root of the development of synucleinopathies such as PD (Dias et al., 2013). However, it is not clear whether this is because of the reduction of other complex I subunits, that results from mDNA mutations (Keeney et al., 2006, Gatt et al., 2016). Hence, it would be worthwhile in future to study the impact of oxidative stress in these mouse models.

In addition, memantine is thought to be a non-specific NMDA receptor antagonist, since it can act on other receptors such as 5HT3Rs or even D2Rs. I believe that the results with memantine could be worth comparing with other more selective NMDA channel inhibitor, such as MK801. Alternatively, it could be worth extending the study and comparing a more reliable compound with a similar agonistic effect such as pregnenolone sulphate. Furthermore, due to time limitations and the availability of resources in the lab, in this work it was not possible to answer the question on to why the potentiating effects of memantine on gamma frequency oscillation were not observed in the adult A30P mice. Therefore, further studies are necessary to compare these effects in adult mice. Another limitation of memantine study, is the fact that, memantine data are too preliminary, and its direct effects on the gamma network oscillations could be backed up with an experiment extended on a similar compound (succinate or fatty acids), which I believe would strengthen the memantine data. I propose a similar approach for the experiments done with sodium pyruvate.

2.5 Conclusions

In this work, I hypothesized that A30P mice will develop mitochondrial dysfunction in an age-dependent manner. I therefore predicted that hippocampal slices from aged A30P mice would show greater sensitivity to lower concentrations of mitochondrial blockers. However, I did not find any significant differences in area power of gamma oscillations between aged C57 and 9+A30P upon treatment with KCN. In contrast to this, the results obtained with rotenone treatment, suggests a slightly higher effects on the mitochondrial, by reducing the area power of the oscillations and therefore inhibiting gamma frequency oscillations in 9+ A30P mice. In parallel to this, additional immunohistochemistry studies from our lab group, have shown alteration in mitochondrial complex IV in the adult A30P mice (Robson et al., 2018b). This suggests mitochondrial dysfunction in this model of synucleinopathy is linked with overexpression of αSyn, that may occur as a result of important mutations in the genes that codify the protein. To my knowledge, this is the first study reporting deficits in gamma frequency oscillations in the A30P mouse model of synucleinopathy. I have demonstrated a consistent deficit in the fast network oscillations in the aged mice that overexpress abnormal human mutant αSyn that precedes the reported cognitive and behavioural deficits and temporally correlates with the observed impairments of the mitochondrial function (Robson et al., 2018b). Furthermore, memantine has been widely used to treat cognitive and motor dysfunction in patients with dementia (Litvinenko et al., 2010). In my experiments, Although, memantine treatment produced a slight increase in the area power of gamma frequency oscillations in *in vitro* slices of A30P mice, these results are still not clear. Further studies are necessary to corroborate these findings. Notwithstanding, this work provides further mechanistic insights into the consequences of overexpression of αSyn, by confirming that mitochondrial dysfunction may be associated with the abnormal neuronal network oscillations observed in the A30P mouse model of synucleinopathies. Thus, suggesting that, it is possible that mitochondrial dysfunction may precede Lewy body pathology and contribute directly to cognitive decline.

Chapter 3: Parvalbumin interneurons in cortical and subcortical regions in A30P mouse and DLB patients
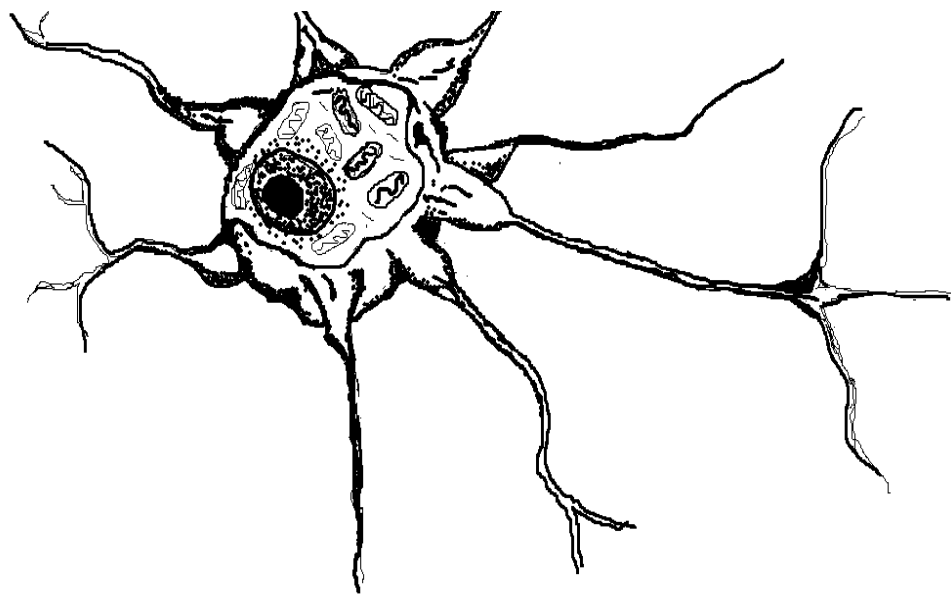
3.1 Introduction

Information processing in the brain neural circuitry, demands a precise spatiotemporal coordination of the activity between pyramidal cells and the inhibitory interneurons (Castejon and Nuñez, 2016, Cardin, 2018). This is because the electrical activity of the pyramidal cells are heavily regulated by fast spiking interneurons such as, parvalbumin positive (PV+) type, which are thought to generate action potentials (AP) at high frequency rate (Tremblay et al., 2016). This high frequency PA from the interneurons reflects the high-energy utilization and demand from this neuronal population, thus, highlighting their vulnerability at the presence of pathologic conditions that impairs neuronal metabolism such as neurodegeneration (Kann et al., 2014b, Tremblay et al., 2016). In fact, inhibitory interneurons such as GABAergic cells are involved in pathogenesis of many brain disorders including, neurodegenerative, neuropsychiatric and neurodevelopmental disorders, epilepsy and encephalopathies (Katsarou et al., 2017). However, this chapter focuses specifically on the vulnerability of PV+ cells in neurodegenerative disorders such as DLB. Although, little is known about the involvement of PV+ interneurons in DLB, the colocalization of overexpressed αSyn with PV+ fast spiking interneurons was found to be linked with the decrease of this group of neuronal populations in DLB (Bernstein et al., 2011b). This colocalization provides an insight on how the pathological burden of αSyn affects this group of interneurons, which affects negatively the function of the neuronal network oscillations, that are dependent on the normal function of these interneurons (Bernstein et al., 2011b). Indeed, the loss of PV+ interneurons is worthy of note, given their importance in forming the neuronal networks and their involvement in gamma rhythmogenesis, essential for cognitive and motor functions (Bernstein et al., 2011b, Bonanni et al., 2008, Whittington and Traub, 2003).

Cognitive decline and motor impairments are major symptoms of DLB (McKeith et al., 2017). They are thought to reflect the impairments in the neuronal network, expressed electrophysiologically as impaired oscillatory activity in gamma frequency oscillations, as observed in chapter 3 (Robson et al., 2018b, Kann et al., 2011, Kann et al., 2014b). Hence, the characteristic dementia profile of DLB is thought to resemble those impairments previously identified in the gamma frequency band (Robson et al., 2018b). This highlights the fundamental role of PV cells in gamma rhythmogenesis

and maintenance under physiological conditions (Kann, 2011, Kann et al., 2014a). Moreover, when the excitability of the interneurons is impaired, it critically contributes to the impairments of the neural oscillatory synchrony and rhythms of the fast oscillatory frequency bands (Morris et al., 2015, Verret et al., 2012). Likewise, when oxidative stress occurs and energy supply is limited, PV+ interneurons are critically affected, leading to the neuronal network impairments (Kann, 2016). Hence, I can speculate that PV+ interneuron loss/dysfunction may underpin the development of neurodegenerative disorders such as DLB.

Furthermore, fast neuronal network oscillations are thought to critically rely on the normal function of PV+ inhibitory interneurons, where they play key role by providing rhythm-based timing of the principal cells at multiple time scales, thus generating neuronal oscillations (Buzsáki and Wang, 2012, Kann, 2016). The important job of PV+ interneurons reside in swinging the membrane potential of principal cells by firing their PA in a completely restricted to perisomatic inhibition of the PV+ fast spiking interneurons onto the principal cells, resulting in gamma-band rhythmogenesis (Buzsáki et al., 2012, Buzsáki et al., 1983, Buzsáki and Wang, 2012). Hence, PV+ interneurons are essential for the synchronisation of the IPSPs in neuronal fast network oscillations (Buzsáki et al., 1983). In fact, PV+ interneurons are known to be very active during generation of gamma oscillations (Gonzalez-Burgos et al., 2015, Kann et al., 2014b). Thus, gamma activity consists of short lived rhythms emerging from the coordinated interaction between excitation and inhibition signals (Buzsáki et al., 2012).

The population of inhibitory interneurons in the cortex is highly diverse, and is largely represented by the GABAergic interneurons, in which PV+ cells represent the majority (Rudy et al., 2011). This group of interneurons is found to be most abundant in the hippocampus and neocortex (Booker and Vida, 2018, Kann, 2016). In fact, every layer of cortical pyramidal cells is under the specific control of a unique class of interneuron populations. Exceptions may be observed in the thalamus, BG and the cerebellum, where the degree of variability of the resident interneurons is low, consisting of few interneuron's types (Pelkey et al., 2017, Buzsáki et al., 1983, Buzsáki and Wang, 2012). It is believed that this diversity of the interneurons may be required for the achievement of the balance between excitation and inhibition in the cortex (Tremblay et al., 2016, Markram et al., 2004). Since, GABAergic interneurons are ubiquitous

throughout the brain, it is not surprising that fast network oscillations such as gamma, will appear in almost every part of the brain. This may be the reason why gamma band oscillations are the most ubiquitous neuronal network activity in the healthy brain (Buzsáki et al., 2012). Moreover, they provide important information about the dynamics of neuronal population in health and disease (Buzsáki et al., 2012).

Based on the functional point of view, the inhibitory interneurons can be classified into three different types. First, interneurons that regulate other interneurons. Second, dendritic targeting interneurons control synaptic inputs into the pyramidal cells, and finally, the perisomatic interneurons, which control the spiking activity of pyramidal cells (figure 3.1). The spiking neurons were the focus of study described in this chapter, particularly the fast-spiking interneurons which express calcium-binding protein PV. Indeed, fast spiking highly energised PV+ interneurons are fundamental elements for information processing in cortical regions of the brain (Kann et al., 2014b).

Figure 3. 1: Schematic representation of the connections of GABAergic interneurons in the cortex, based on functional classification. PV= Parvalbumin, SOM= somatostatin, NG= neuralgiform cells.

DLB and other types of dementias are associated with neuronal loss across the cortical and subcortical structures (Mak et al., 2014). Features such as cognitive decline and motor impairments (McKeith et al., 2017) that characterize DLB are thought to resemble those impairments previously identified in the gamma frequency band (Robson et al., 2018b). This impairment may be a result of pathological changes (in the density/function) of PV+ interneurons, due to their key role in the generation of gamma frequency oscillations (Kann, 2016, Trojsi et al., 2018, Honkanen et al., 2014, Li et al., 2019). The evidence presented in this chapter suggests that the density of the PV+ interneuron population is significantly affected in some areas of the brain, including, the perineuronal nets (PNN) of the cortex. The complexity of the relationship between different brain regions, which are differentially affected by the disease, but act in synchrony with others to complement brain functions, makes it difficult to study all. Here, I carried out neuroanatomical quantification of the PV cells in different brain regions to establish in which regions the PV+ interneuron density might be affected in DLB. Thus, this chapter provides evidence from a quantitative neuroanatomical analysis, yielding insights into the involvement of PV+ fast spiking interneurons in the generation of neuronal network oscillations, in parallel with the electrophysiological results presented in chapter 3. Since DLB is a disease in which gamma frequency oscillations are affected in certain regions of the brain, I hypothesised that this is due to the impairment of PV+ interneurons. Thus, I aimed to perform quantitative analysis of the distribution of PV+ fast spiking interneurons in brain tissue of DLB patients; to compare the PV+ interneuron density with the disease progression and analyse its links with the impaired gamma frequency network oscillations in the progression of DLB. I also investigated the extracellular matrix that ensheathes the PV+ fast spiking interneurons (the perineuronal network (PNN)) which is essential for the regulation of the functions of GABAergic interneurons (Wen et al., 2018). This would help to gain more insight into the involvement of PV+ interneurons in LBDs, as well as ideate how their dysfunction affects/contributes to DLB pathology.

3.2 Methods

All procedures described in this chapter relating to animals were carried out according to the UK Animals Act 1986 (Scientific Procedures), and European Union directive 2010/63EU, with the appropriate provision project and personal licences (PPI and PPL). All human tissues were obtained from the Newcastle Brain Tissue Resource (NBTR) in accordance with the Joint Ethics Committee of Newcastle and North Tyneside Health Authority approval and following the NBTR brain banking procedures.

3.2.1 Animals

Transgenic (Thy-1)-h[A30P] αSyn mice C57BL/6 background, both male and female that overexpressed human mutant A30P αSyn under the Thy-1 CNS specific promoter (Kahle et al., 2000b, Neumann et al., 2002), were supplied by Dr. Khale (University of Tubigen).

3.2.2 Immunohistochemistry- slice preparation

Upon completion of the electrophysiological recordings, slices were rapidly fixed in 4% buffered paraformaldehyde (PFA powder; Sigma-Aldrich P-6148) solution, and stored at 4°C, for at least 2 days. Alternatively, slices were obtained from animals following anaesthetics by transcardial perfusion of the brain with 4% buffered paraformaldehyde. Fixed brain tissues were then removed and stored in 30% sucrose PBS (PBS tablets; Sigma-Aldrich P4417) at temperature of 4°C for few days for cryoprotection. Before slicing further into 40 μm thick slices, which were then placed into 0.3% Triton-PBS.

In some cases, animals were anaesthetised and transcardially perfused with 4% buffered paraformaldehyde and the slices obtained were used for immunostaining. Before staining, the slices were transferred to 30% sucrose phosphate buffered saline for ~2-3 days for cryoprotection at 4ºC, before being sectioned to 40 μm thick slices with a freezing microtome or a Bright OTF 5000 cryostat and placed in a well plate containing 0.3% triton-PBS (TPBS; Triton X-100, Sigma-Aldrich T-8787) at room temperature. Then the slices were kept in 4% PBS at 4ºC. The appropriate primary antibody and the appropriate serum species (depending on where the antibody was raised) was added directly into each well plate containing PBS 4%, and stored at room temperature.

3.2.3 Immunohistochemistry staining for Anti-PV

Slices were then stained with a mouse monoclonal anti-4-hydroxinonenal (anti-4-HNE) antibody (1:5000; SWANT) (see appendix), or a mouse monoclonal parvalbumin (PV) antibody (1:5000), prepared in 4% PBS containing 0.3% Triton X-100 (Sigma) and 0.3% normal goat serum (S100, Vector Laboratories). Slices were incubated in primary antibody overnight at 4°C (18-20 h) on a shaking platform in the cold room. Next day, slices were incubated with anti-mouse IgG (Vector Laboratories BA1000), which was used as secondary antibody, then slices were left incubated for 2h at room temperature on a shaking platform (figure 2.2). Following three 5-minute washes with PBS, slices were incubated in 3, 3'diaminobenzidine peroxidase (DAB) and hydrogen peroxidase (Vector Laboratories Inc.), for 5 minutes to visualize the morphology of the cells followed by three 5-minute washes in PBS. DAB substrate was prepared in water (2 drops of DAB in 5 ml of H_2O), and the solution was added into the well plates that contained the slices. To stop DAB reaction, the solution was carefully removed, and the slices were washed 3x5 min in PBS.

The slices were then mounted onto gelatine-subbed microscope slides (Fisher Scientific, Super Frost slides 26x76x1mm) and left to dry overnight at room temperature. The following day, when the slices were completely dried, they were re-hydrated in dH_2O for 30 seconds, before ethanol-based dehydration protocol of successive 5 minutes incubations with 70%, 90%, and 2x 100% ethanol. The dry slides were then transferred to HistoChoice Clearing Agent I and II (National Diagnostics, HS200) for 10 minutes each. Next, the slides were covered with a cover glass (VWR cover glass 22x 50 mm, 631-0137) using an immmunohistomount (AgarSci, HS103) mounting solution and left to dry in the fume cupboard overnight.

The antibody signal was captured on an Olympus BX51 stereology microscope, mounted with an Olympus U-TV1X-2 T2 Camera that uses Picture Frame software (Softonic, Spain). The same protocol was used for staining for PV interneurons except that the primary antibody used was anti-PV 1:5000 (the result for these experiments is shown in the appendix).
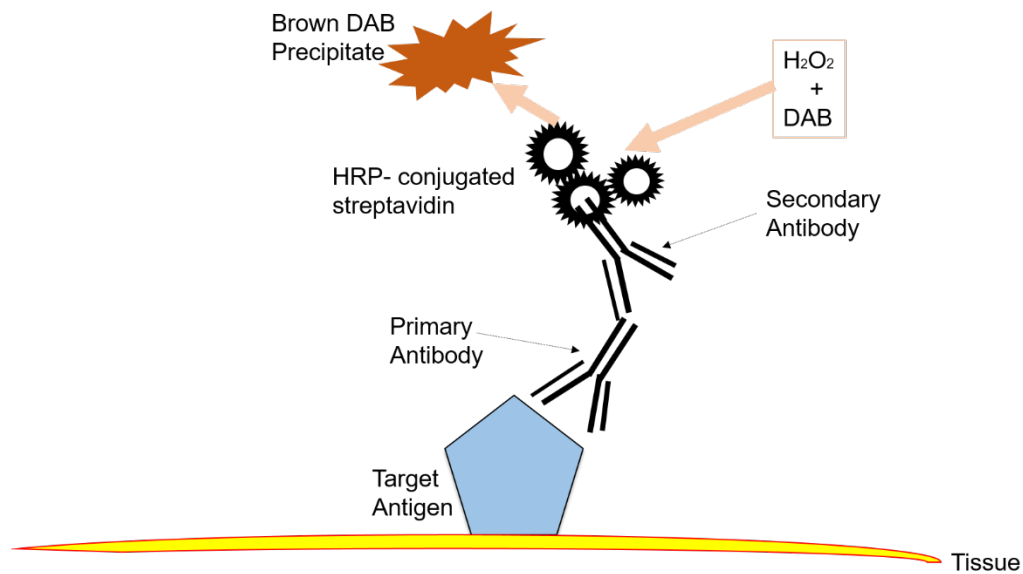
Figure 3. 1: Schematic representation of DAB peroxidase immunohistochemistry.

3.2.4 Immunofluorescence Staining for Lectin and PV (Animal tissues).

Brain sections were fixed with 4% PFA, after the brain removal from the animal skull. The tissues were sectioned in horizontal planes to obtain the hippocampal sections, and in coronal planes to obtain PFC sections (figures 3.2 A). Next, the sections were incubated in sucrose PBS for overnight, for cryoprotection. The slices were then transferred into the primary antibody solutions, containing anti-PV (mouse) (1:500) and biotinylated lectin (1:5000) to detect PNN. Non-specific binding was prevented by adding goat serum (3%) and 0.3% triton phosphate buffered saline (TPBS) (1 ml) was used as a diluent and incubated overnight at 4°C. After washing out the primary AB (3x 5 minutes each) the slices were then incubated with the appropriate secondary antibodies (Texas red streptavidin 499 nm (1:200), which binds to biotin (for lectin), and goat Ab to mouse IgG 488nm (1:200) were used with TPBS as diluent) for 2 hours (in the dark). Subsequently, the slices were washed 3 times for 5 minutes each and mounted onto slides with 4',6-diamino-2-phenylindole (DAPI) (1:10000, Sigma-Aldrich, D9542). The sections were visualized using an epifluorescence microscope Axio Imager M1 (Zeiss) mounted with an AxioCam MrM camera.

3.2.5 Immunofluorescence staining for calbindin and PV

For immunofluorescent analysis, hippocampal slices were fixed in 4% PFA after the removal of the brain from the animal or following electrophysiological recordings as indicated above. The brain tissue was cut to 40 μm thick slices and the selected area of interest was CA3 region. For staining, slices were transferred into different primary antibody solutions, one containing Parvalbumin (1:5000) and other anti-4-HNE (1:5000) and Calbindin (1:10000), respectively (Table 2.3). Non-specific binding was prevented by adding Goat Serum (3%) and 0.3% Triton in Phosphate Buffered Saline (TPBS) (1 ml) was used as a diluent and incubated for overnight in the cold room. The slices were then incubated with the appropriate secondary antibodies (Texas red streptavidin 499 nm (1:200), which binds to biotin, and Goat pAb to mouse IgG 488nm (1:200) were used with TPBS as diluent) for 2 hours in the dark. Subsequently, the slices were washed 3x 5 minutes each and mounted onto slides with 4',6-diamino-2-phenylindole (DAPI) (1:10000, Sigma-Aldrich, D9542) to stain the nucleus. The sections were visualized using an epifluorescence microscope Axio Imager M1 (Zeiss) mounted with an AxioCam MrM camera.

The antibodies used for this experiment are biotinylated wisteria Floribunda Lectin, mouse monoclonal anti-parvalbumin, sodium-3 hydroxybotyrate; All acquired from Sigma-Aldrich (Gillingham, Dorset, UK); mouse monoclonal anti-calbindin (Swant, Marly1 CH-1723 Switzerland), mouse anti-4-Hydroxinonenal (HNE) (R&D systems, MAB3249) anti-Mouse IgG (Vector Laboratories, Peterborough, UK). 3, 3'diaminobenzidine peroxidase (DAB) and hydrogen peroxidase from a kit (containing DAB, hydrogen peroxidase, buffer and nickel solutions; Vector Laboratories Inc.) (Table. 3.1).

Table 3. 1: List of the antibodies used for free-floating IHC experiments.

Target	Host	Serum	Concentration	Vendor
Parvalbumin (PV)	Mouse	Horse (S-2000, Vector Laboratories	1:5000 IP 1:2000 IF	Sigma-Aldrich (AB18108)
Biotinylated Wisteria Floribunda Lectin; N-acetylgalactosamine sugar (PNN)	N/A	N/A	1:500 IF	Vector Laboratories (B1355)
Calbindin D-28k (CB)	Rabbit	N/A	1:10000 IF	SWANT (CB38)
Lipid peroxidation (Anti-4HNE)	Mouse	NGS	1:500 IP	SWANT (MAB3249)

3.2.6 Tissue selection based on a neuropathological diagnosis (Human brain tissues)

Pathological examination of brain tissue sourced from the Newcastle Brain Tissue Resource (NBTR) was carried out on selected cases that fulfilled the neuropathological criteria for DLB, PD, and PDD and on non-diseased control tissues (Table 3.2). In total, 120 post-mortem brain tissues from neuropathological and clinically assessed diseased and non-diseased (CTRL) individuals were studied including both male (number of cases 71), and female (number of cases 49) with an overall mean age at death of 76.10 SE±1.20 years. Brain tissue samples were sourced from 11 non-diseases individuals (CTRL), 22 DLB, 14 PD and 13 PDD, were used for TMA studies. In addition, 15 CTR and 12 DLB cases were used to study the colocalization of the PTMs (Table 3.2). All tissues were obtained from the NBTR in accordance with the Joint Ethics Committee of Newcastle and North Tyneside Health Authority approval and following NBTR brain banking procedures. During life, these patients were carefully examined by a group of board-certified old age psychiatrist and neurologists. The diagnosis included the evaluation of cognitive functions including Mini-Mental State Examination (MMSE), and cognitive decline rate was used for cases with multiple MMSE (Folstein et al., 1975, Olichney et al., 1998). All pathological tissue was staged Braak stage 5-6 and non-pathological tissues were selected from Braak stage 0-1 Overall, 93 brain samples from 60 donors were used for TMA studies, and a total of 24 brain tissues (from both male and female) were used to study the colocalization of the PTMs. All cases were carefully examined by a group of board-certified old age psychiatrist and neurologist and pathologist.

Table 3. 2: Patient Demographics of Tissue Microarray samples. Main characteristic used for the cohort studies. Abbreviations: DLB, dementia with Lewy bodies; PD, Parkinson disease; PDD, Parkinson's disease dementia; CTRL, control; Cidia, clinical diagnosis; Padia, Pathological diagnosis.

	DLB	PD	PDD	CTRL
Number of cases (n)	22	14	13	11
Mean Age at death	76.1	78.1	77.60	80.1
Female %	20%	10%	40%	50%
Post-mortem interval	25-50h	18-105 h	18-125h	12-50 h
Clinical diagnosis	3	6	15	1
Braak stage diagnosis	5-6	5-6	5-6	0-1
McKeith Scale	Limbic-neocortical	Limbic-neocortical	Limbic-neocortical	Negative

*All synucleinopathy cases had clinical evidence of dementia and motor dysfunction. All dementias group represent all causes of dementia including DLB and PDD. There were no relationships between the post-mortem intervals and the pathological diagnostic groups or any of the subsequent measures (P>0.05). The samples were not always gender matched which is a limitation for this study.

The diagnosis of dementia in the selected patient donors, was made according to the standard international clinical criteria for DLB, PD and PDD based on the presence of core clinical manifestations such as Parkinsonism, cognitive fluctuations, and persistent visual hallucinations, and suggestive features including REM sleep behaviour disorder, neuroleptic sensitivity and positive dopaminergic imaging evidenced of LBD (Emre et al., 2007, McKeith et al., 2005). Post-mortem clinical assessments were carried out by Professors Johannes Attems or Ian McKeith and validated according to standard international clinical criteria (McKeith et al., 2017). Apart from the clinical diagnosis, a standardised neuropathological assessment was performed in all cases, blind to the clinical diagnosis. The neuropathological diagnoses were done based on a semi-quantitative assessment of the cases (Alafuzoff et al.,

2009, Whitfield et al., 2014), and it was determined using the conventional international neuropathological criteria including neuritic Braak stages (Braak et al., 2006, Braak et al., 1999), Thal amyloid phases (Thal et al., 2002b), CERAD scores (Mirra et al., 1991), McKeith criteria (McKeith et al., 2017), NIA-AA scores (Montine et al., 2012) and cerebral amyloid angiopathy (CAA) (Thal et al., 2002a).
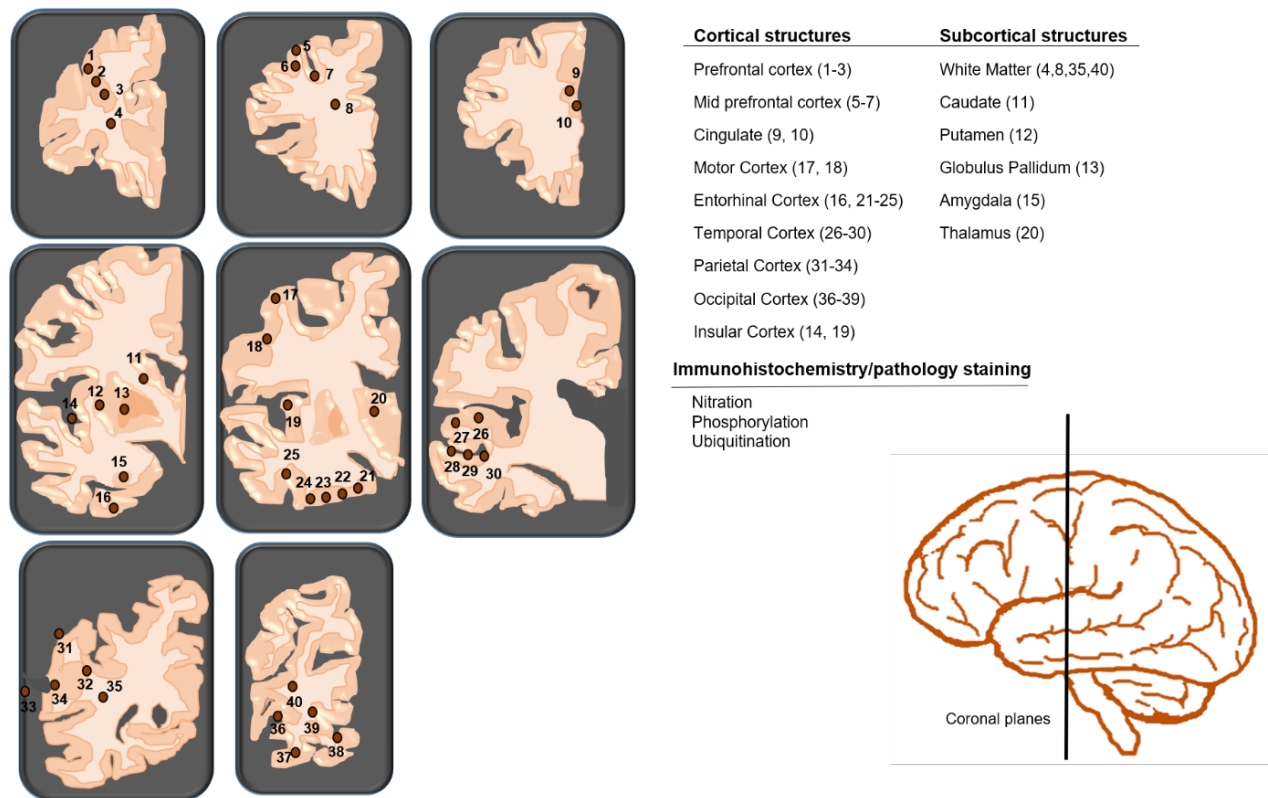
Figure 3. 2: Schematic diagram indicating the location of TMA diagnostic block extraction from brain tissue. Samples for TMA were taken from paraffin embedded blocks containing PFC (Brodmann area (BA), 10/46), MFC (BA 8, 9) CC (BA 24, 32), TC (BA 41/42), PC (BA 22, 40), OC (BA17, 18, 19, 19/37), MC (BA 4), IC (BA4), BG (BA4), Amygdala and thalamus (BA 21), entorhinal cortex (BA22).

3.2.7 Tissue microarray (TMA) Construction

Structures of brain tissue, processed and fixed at autopsy, including the cortical structures of prefrontal cortex (PFC), mid-frontal cortex (MFC), cingulate cortex (CC), motor cortex (MC), parietal cortex (PC), occipital cortex (OC), insular cortex (IC) entorhinal cortex (EC), and subcortical structures of basal nucleus (BN) (often referred to as basal ganglia), amygdala (Agd), thalamus and white matter (WM) were requested for the experiments presented in this thesis. All obtained regions of the brain

were sectioned at 6 μm and mounted onto 4% 3-aminopropyltriethoxysilane (APES)-coated glass slides.

Samples for TMA were taken from paraffin embedded blocks described above containing the PFC (Brodman area (BA), 10/46), MFC (BA 8, 9), CC (BA 24, 32), TC (BA 41/42), PC (BA 22,40), OC (BA17, 18, 19, 19/37), MC (BA 4), IC (BA4), BG (BA4), Agd and thalamus (BA 21), EC (BA22) (figure 2.3). The paraffin blocks were warmed for 1 h at 37ºC to allow for brain tissue removal. Next, using a handheld tissue sampler (Tissue-tek Quick-ray TMA system, Sakura, CA, USA), 3 mm cylindrical tissue cores were taken from the predefined positions. For the procedure, the tip of the handheld punch was inserted through the depth of the tissue and extracted along with the cylindrical core of the tissue (figure 3.4b). Each core of the tissue was then inserted into the correct spot of the single premade regular sized TMA paraffin block recipient (4 cm x 3 cm - made to match perfectly the Tissue-tek Quick Ray TMA system) in a numerical order (figure 3.4b). Empty spots were filled with molten wax if any donor blocks were missing, and the missing spots were accounted for in data analysis. To reduce wax tissue interface during sectioning, each punch was securely pushed into the recipient block by hand following the incubation of the block at 37ºC. A silicone mould, made specifically to fit TMA recipient blocks, was preheated for 1 h at 60ºC and paraffin wax (2-4 ml) was placed into the base. The TMA tissue recipient block was placed face down onto the molten wax for 5 minutes, followed by a 15 minute anneal incubation at 37 ºC (figure 3.4c) before removing the silicone mould and the wax. The block was allowed to completely refresh. Next, the TMA sections were cut and mounted onto glass slides (figure 3.4d). All this preparation was done by the Lab Technician in NBTR (for review please see (Kampf et al., 2012).
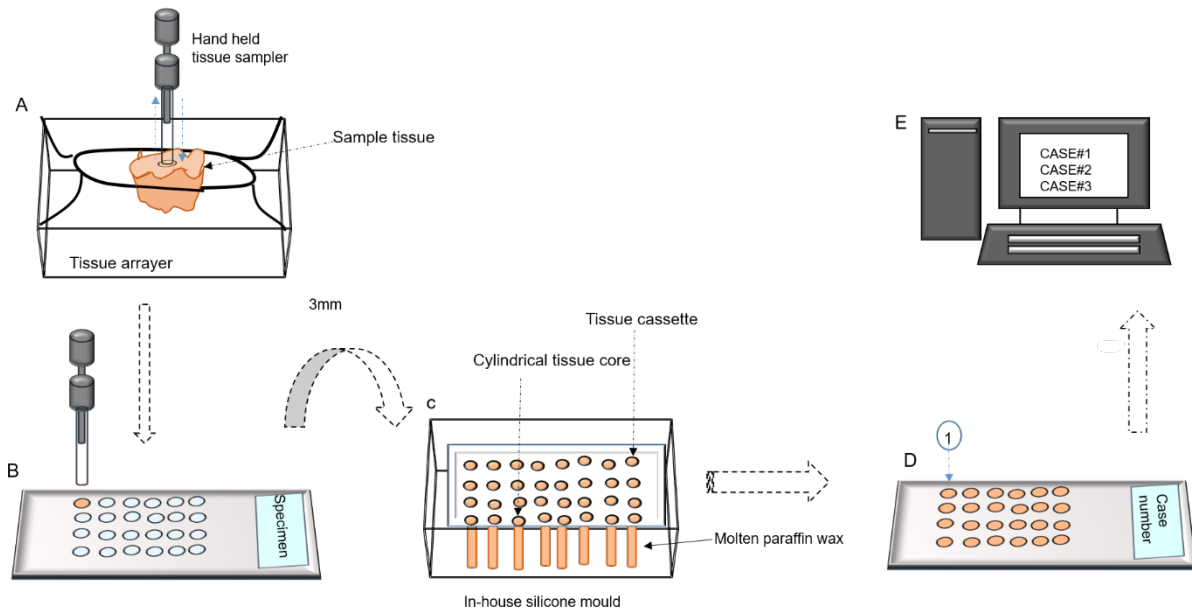
Figure 3. 3: Flow chart of TMA construction.

3.2.8 Human histology or histopathology

Sections were examined for the presence of PV+ interneurons using standard immunohistochemical staining. Slides were first pre-warmed in an LEEC oven for 30 minutes, then dewaxed and rehydrated in alcohol gradient 99%(2x), 80% and 70% for 5 minutes each, before immunostaining. The slices were then subjected to a microwave boiling procedure with citrate solution (11.4 mM, pH 6 (Figure 2.5)). Next, sections were washed with Tris-buffered saline (TBS) pH 7.6 and Tris buffered saline with tween 20® (TBST) pH 7.6 3 times, 5 minutes each, then hydrogen peroxide (H_2O_2) 10% was added to block the action of endogenous peroxidases. All the slides were then demarcated with a pap pen to avoid leakage of the antibody solution. Anti-PV antibody 1:500 (Abcam, UK) (Table. 2.3) was added as the primary antibody and incubated for 1 h at room temperature. Then, the slides were washed with TBST 3 times, 5 minutes each, and yellow cap universal probe (Menapath) was used as the secondary antibody and incubated for 30 minutes at room temperature. Once the slices were washed with TBST, avidin-biotinylated horseradish peroxidase (HRP)-Polymer (red) (Menapath HRP multipolymer) was added for 30 minutes at room temperature and slices were washed again with TBS 3 times, 5 minutes each and the chromogen DAB was added for 3 minutes. Next, slides were washed in running water for 10 minutes, and then submerged in haematoxylin (Menapath) for 20 seconds. Slides were then transferred into acid water (Menapath), for 2 seconds and into the

ammonia containing water (Menapath) for 2 seconds. Slides where washed again in flowing water for 2 seconds, to be then dehydrated in alcohol concentration 70% to 99% 5 minutes each (4 steps). The sections were then transferred to clearing xylene 1-2 (Menapath), for 10 minutes each, and then mounted with DePex destrene (DPX) (Menapath). For the negative controls, the primary antibodies were omitted but all other steps were followed as described above.
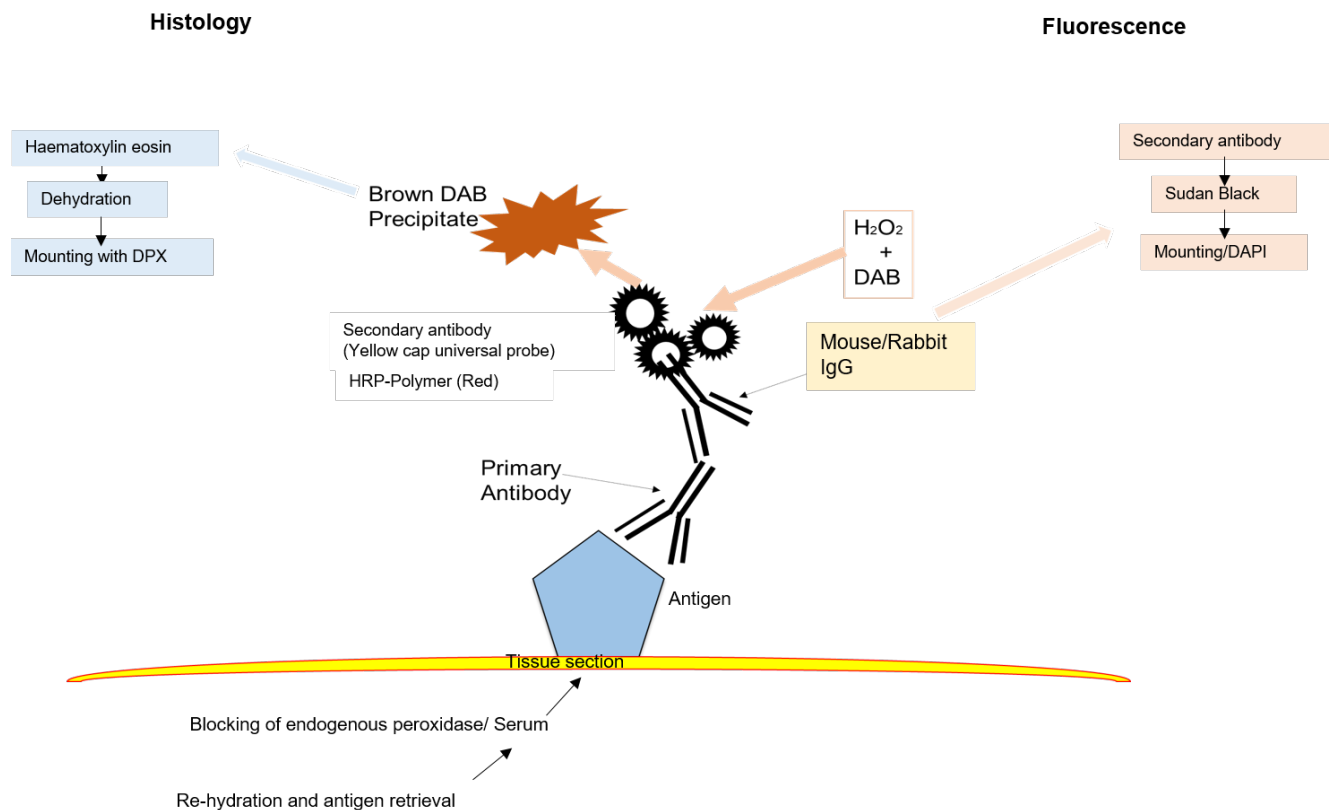
Figure 3. 4: Schematic diagram of the pathology staining protocols.

3.2.8.1 TMA – Immunohistochemical data capture and analysis

Tissue microarray (TMA) images were captured using an automated system consisting of Eclipse 90i microscope (Nikon), mounted with a DsFi1 camera (Nikon) and processed in NIS element software v 3.0 (Nikon). For these experiments, I examined only freshly stained samples. The microscope was firstly positioned at the centre of the first tissue core at 10x magnification for guidance and brought into focus at 100x magnification, after a background correction. Then, the lens of the microscope was positioned to the first cores of the TMA slide, to be automatically mapped the NIS element software, macro designed to take a map of the remaining 39 images of each

40-tissue cores that contains in a single TMA tissue slide (figure 2.3). After mapping all 40 tissue cores, the microscope was directed to the mapped co-ordinates of the first tissue core, and images of all the tissue cores were sequentially taken automatically. Following the completion of data capture, regions of interest (ROI) were applied to each image manually to exclude any sample abnormalities such as folded tissues, tears, and regions consisting of white matter. A restriction threshold was then applied to capture all immuno-positive foci. In cases when the slides were missing a tissue core or simply one or some tissue cores were too damaged to be included in the analysis, the tissue core number and position were noted manually, and captured data was excluded. The immuno-positive signal in each ROI was then calculated automatically after application of a pre-selected threshold. The red, green and blue (RGB) thresholds were set separately for each PTM-specific antibody signal, and the thresholds were set at a level that the immuno-positive pathological structures (LBs and LNs) were detected. The values of RGB intensity are measured on a scale between 0-255 (NIS elements user guide v 3.0, 2008, Nikon, Surrey UK) and were set as follows: Pser[129] (R25-170, G27-156, B11-126), nitrated -αSyn[Tyr125,133] (R50-180, G20-168, B8-139) and ubiquitinated-αSyn (R15-161, G7-139, B4-133) to minimize measurement of a non-specific background signal. The percentage area of the tissue covered by immuno-positive LBs and LNs were subsequently calculated and automatically exported. Mean values were then calculated for each brain region that was represented by more than one tissue core. All data graphs were generated and exported from Graph Pad prism.

TMA images were captured using an automated system consisting of Eclipse 90i microscope (Nikon), mounted with a DsFi1 camera (Nikon) and processed in NIS element software v 3.0 (Nikon). For these experiments, I examined only freshly stained samples. First, position of the first TMA section (figure 2.3) was mapped in the NIS element software, followed by a macro designed to take a map of the remaining 39 (figure 2.3). Image of each 40-tissue that contains in a single TMA tissue slide were taken. The microscope was firstly positioned at the centre of the first tissue core at 10x magnification for guidance and brought into focus at 100x magnification, after a background correction. After mapping all 40-tissue cores, the microscope was directed to the mapped co-ordinates of the first tissue core, and images of all the tissue cores were sequentially taken automatically. Following the completion of data capture, regions of interest (ROIs) were applied to each image manually to exclude any sample

abnormalities such as folded tissue, tissue tears, and regions consisting of white matter. A restriction threshold was then applied to capture all immuno-positive foci. In cases when the slides were missing a tissue core or simply one or some tissue cores were too damaged to be included in the analysis, the tissue core number and position were noted manually, and captured data was excluded. The immuno-positive signal in each ROI was then calculated automatically after application of a pre-selected threshold. The red, green and blue (RGB) thresholds were set separately for PV-specific antibody signal, and the thresholds were set at a level that the immuno-positive PV+ cells were detected. The values of RGB intensity were measured on a scale between 0-255 (NIS elements user guide v 3.0, 2008, Nikon, Surrey UK) and were set as follows: PV+ (R25-170, G27-156, B11-126), to minimize measurement of a non-specific background signal. The percentage area of the tissue covered by immuno-positive PV+ cells were subsequently calculated and automatically exported. Mean values for each slide/case were then calculated for each brain region that was represented by more than one tissue core. Normally distributed data (Shapiro-Wilk test) were plotted as mean ±SEM and compared using *t*-test. Non-normally distributed data were analysed using non-parametric tests and described as median and interquartile ranges (IQR) or percentage change and analysed using non-parametric statistics on the raw data. *P* values are reported as significant <0.05. All data graphs were generated and exported from Graph Pad prism.

3.2.8.2 Samples- Immunofluorescence data capture and analysis

For immunofluorescence, the images were taken using an automated system consisting of Nikon Eclipse 90i microscope, DsFi1 camera and NIS element software v 3.0 (Nikon). Image acquisition settings were kept constant. The exposure time for each fluorophore was kept constant between slides to allow for comparison. Bleed-through effects were minimized by acquiring the images exclusively by sequential scanning. The analysis was conducted using ImageJ, and ICY software workflow protocol, that generate an automatic spreadsheet that was exported to Excel software. For DAB analysis, ICY software was used to determine LB area staining. Images captured via 40 x objective were subject to intensity thresholding and subsequent size exclusion (items < 19794 Pixels were excluded as they were not representative of the

round inclusions that characterize the LBs) within a determined ROI that is automatically set in the Lab for the detection of LB and LN. For each section, 2 regions of interest where quantified and the number of immuno-positive items per section averaged and pooled across sections per disease category. Co-localisation analysis was carried out in the ImageJ software using a JACoP plugin. Captured images were split into RGB colour channels and intensity selected via individual constant RGB. The thresholds for each channel were kept between samples from the same experiment. Colocalisation was subsequently determined using Pearson's, Mander's and overlapping coefficients.

3.2.9 Statistical Analyses

All data were statistically analysed using GraphPad Prism 9 (GraphPad Software, Inc., version 9.1.0. USA) and Sigma Plot (Systat software, USA). Statistical significance was defined as significant $*p<0.05$, $**p<0.01$ and $***p<0.001$. To determine the normal distribution of the data and equal variance, the Shapiro-Wilk test and the Brown-Forsythe tests were used, respectively. The data were normally distributed and plotted as mean ± standard error of the mean (S.E.M.) as bar chart or box plot depicting median with interquartile range (IQR, Q1-Q3) or percentage change. When comparing multiple groups, I used Kruskal-Wallis one-way ANOVA. Pairwise multiple comparison (Dunn's or Tukey test) was used when p value (reported as significant, <0.05 and <0.001) if the ANOVA test showed significance to determine which parameters were significantly different. For the analysis of the effects of two independent variables in the same sample, I used a two-way ANOVA with Bonferroni post-test, to determine the interaction between the disease groups and regions of the brain. Error bars represented standard deviation and the data were reported with F-value, degree of freedom an p value (reported as significant, $*<0.05$ and $**<0.001$). Sample sizes are shown in the respective figure legends.

3.3   Results

3.3.1   Vulnerability of PV+ interneuron and PNN density in the hippocampus and PFC of the adult A30P mouse model of DLB

To corroborate the dysfunction of gamma frequency oscillations in the hippocampus of aged A30P mice, I first compared the density of the PV+ cells in the hippocampal sections in both aged control (9+C57) and aged DLB mice (9+A30P). The immunoreactivity of the PV+ interneurons can be identified by their round or oval soma with a widespread arborisation of the dendritic branches (figure 3.6A). Here, sections obtained from the A30P mice showed a trend of reduction in number of PV+ fast spiking interneurons in the CA3 regions (figure 3.6A, B). The immunoreactivity was also largely restricted in the pyramidal cell layer of the hippocampus CA3 region. However, this difference was not statistically significant when compared to the control mice (Mann-Whitney test) (figure 3.6A, B).

To further explore the density of PV+ interneurons in the 9+A30P mice, I determined the amount of PV+ cells and the density of PNN in the PFC. I hypothesized that a tendency to reduction in PNN density would be observed, which would correlate with the reduction of the PV+ cells as it was observed in the CA3 region. Consistent with the results observed in PV+ cells in the CA3 region of the hippocampal slices of 9+A30P mice (figure 3.6A, B), the PFC regions of 9+A30P mice showed a slight, though non-significant, reduction in PNN+ and PV+ cells (figure 3.6C, D), compared to the 9+C57 mice (Post-hoc power analysis showed that this experiment was underpowered), which is a limitation of this study, therefore, this study could be improved in the future by increasing sample size, as changes in density of PNN and PV+ cells were marginal. This work was carried out in collaboration with an undergraduate student (Nishaal Ajmera) that I supervised for a summer project work, Nishaal participated in cutting the section, and helping with the staining of some slices and processing the images. I did the rest of the work including the statistical quantifications. In addition, the work was presented in a poster in the Anatomical society conference in London 2018.

A

9+Ctrl   9+A30P

200μM   200μM

B

1
2/3
5
6
ACAd
PL
ILA

C

9+C57   9+A30P

PV

Lectin

Merged

D

Density of PV+ cells

ns

PV+

# of PV+ / Image

CONTROL   DLB

Groups

Density of PV+ cells and PNN

ns

PV+

# of overlap / Image

CONTROL   DLB

Groups
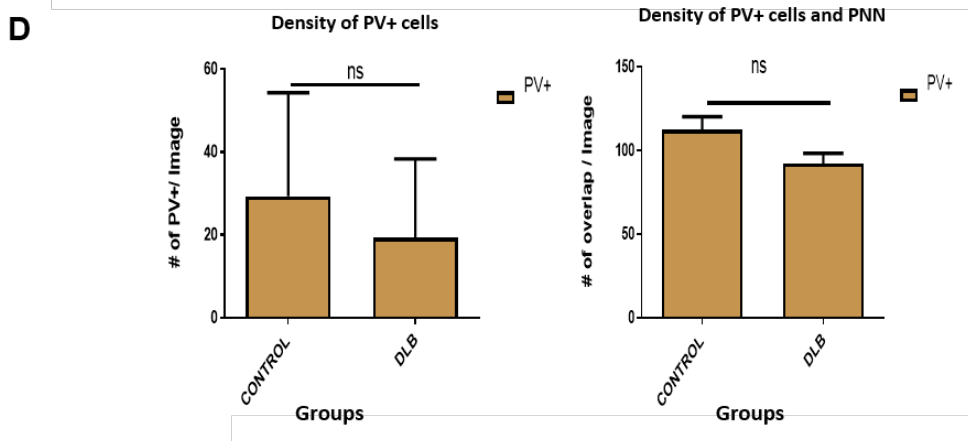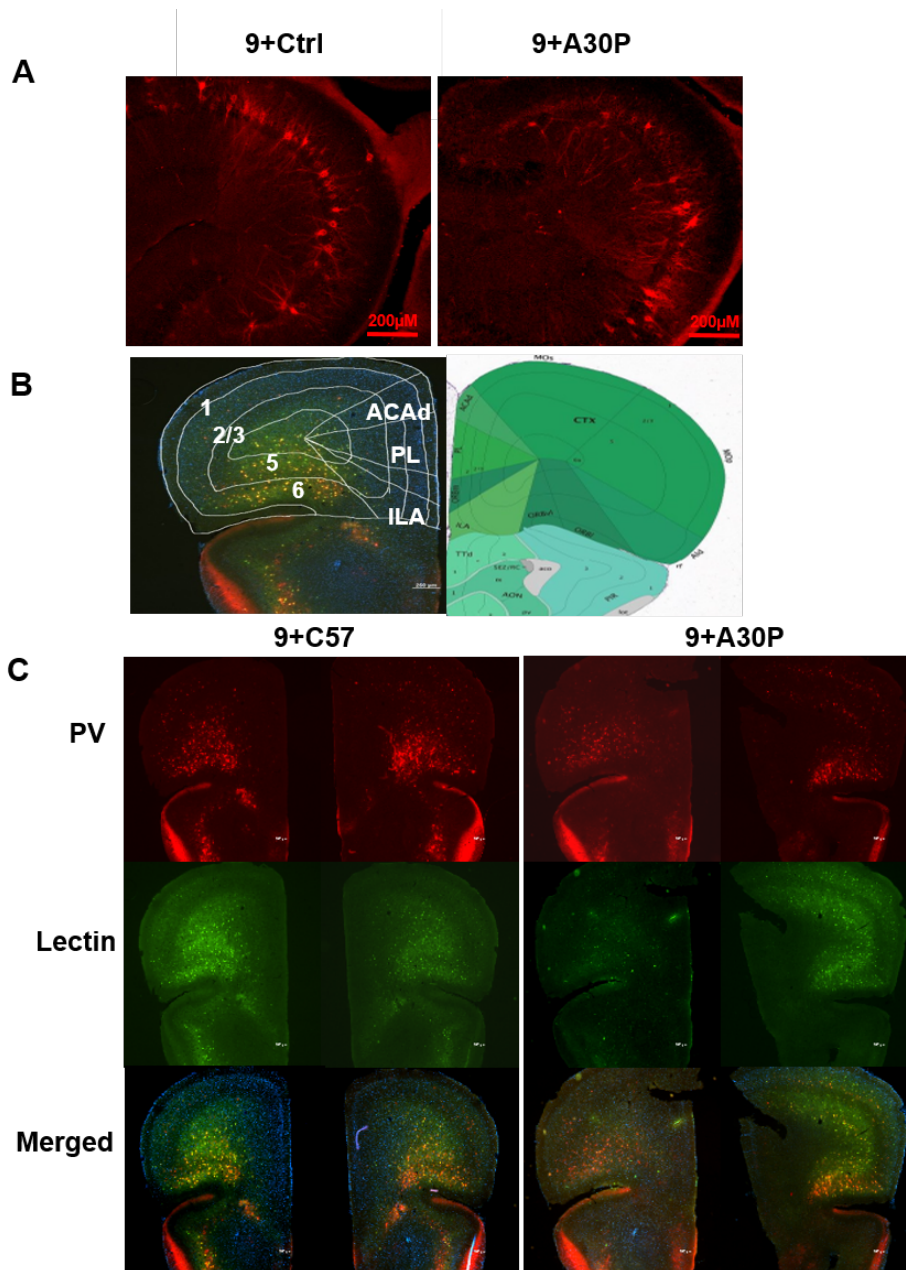
Figure 3. 6: Density of PV+ cells and PNN in hippocampus and PFC of A30P mouse. (**A**) Representative immunofluorescence images at x10 magnification show immunoreactivity in the 9+Ctrl mice (left) (N= 3 mice, n= 6 slices) and 9+A30P (right) (N= 3 mice, n= 6 slices) mice in CA3 region of the hippocampus. (**B**) Representative image of the mouse brain and the area of the brain where PFC slices were taken. (**C**) Representative images of PNN and PV expression in the PFC of 9+C57 (control) (N= 3 mice, n= 5 slices), 9+A30P (N= 3 mice, n= 8 slices). (**D**) Bar chart (left) shows the number of PV+ fast spiking interneurons in the hippocampus of 9+A30P mice compared to the 9+control mice. The percentage coverage of PV+ cells in both control and DLB were not statistically significant (P>0.05). Bar chart (right) showing the degree of overlap of PNN+ and PV+ cells in PFC of control and A30P mouse. Although, the immunoreactivity was slightly greater in the Control mice, the results were not statistically significant when compared to the A30P mice (P>0.05).

3.3.2 Vulnerability of PV+ fast spiking interneurons in cortical regions of human post-mortem brain tissue

3.3.2.1 Density of PV+ interneurons in the frontal lobe of DLB patients

To further explore the relative status of PV+ interneurons, I quantified PV+ interneurons in the frontal lobe in DLB patients compared to healthy control individuals. Following the immunostaining with anti-PV antibody, PV+ cells with/ without neuronal processes were observed in PFC of brain tissues from both control and DLB patients. However, no significant changes were observed in the number of PV+ interneurons between control and DLB cases (P>0.6991, Mann-Whitney test) (figure 4.3).

Taking into account that no loss of PV+ cells was observed in the rostral area of the frontal cortex, I continued to assess the neuroanatomical distribution of PV+ interneurons in the medial region of the frontal lobe, the mid-frontal cortex (MFC) for both DLB and control cases. PV+ cells were observed in this area in both control and DLB patients. Although there appeared to be a trend toward higher number of PV+ cells in control, compared to DLB cases, this difference was found to be not statistically significant (P>0.4641, Mann-Whitney test) (figure 3.7). I then extended the analysis to the motor cortex (MC). Interestingly, here I found less PV+ fast spiking interneurons present in the DLB compared to the control cases (figure 3.7) and the results were

statistically significant in the percentage change of the number of PV+ calculated in each ROI, between control and DLB cases (P<0.0379, Mann-Whitney test). This significance was even higher when the number of objects detected per ROI was calculated (P<0.0058, Mann-Whitney test). Although, no significant differences were detected in PFC and MFC, the decrease of PV cells in MC suggests that a combination of numerical and functional deficits of PV+ cells may contribute to the impairments in the neuronal network of this region of the brain in DLB patients.

A

Con   **DLB**

B

PFC

MFC

MC

200μM   200μM

C

PFC
% Coverage
ns
Con   DLB
Groups

PFC
# of objects/image
ns
Con   DLB
Groups

MFC
% Coverage
ns
Con   DLB
Groups

MFC
# of objects/image
ns
Con   DLB
Groups

Motor cortex
% Coverage
*
Con   DLB
Groups

Motor cortex
# of objects/image
**
Con   DLB
Groups
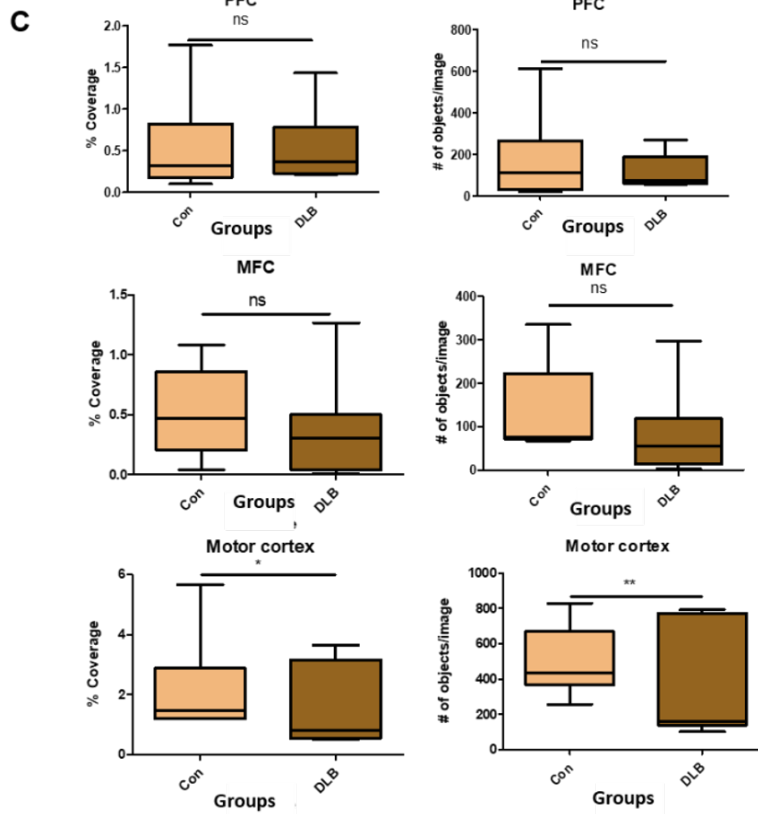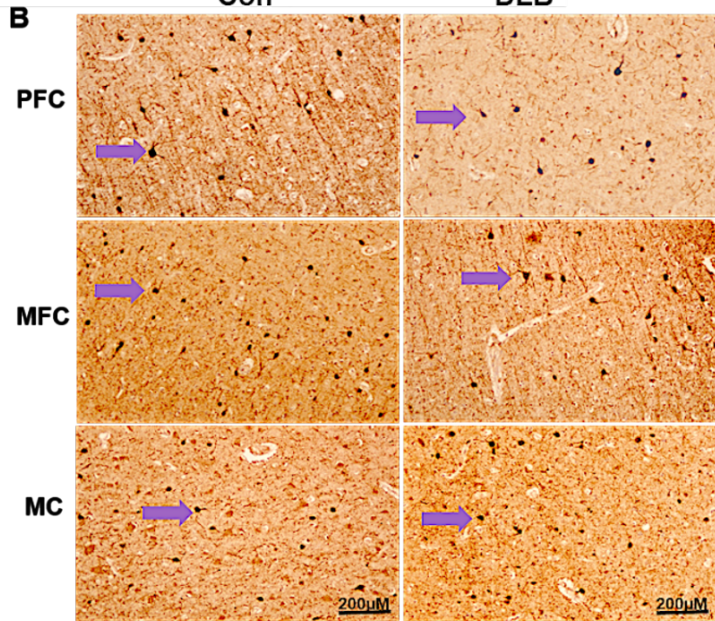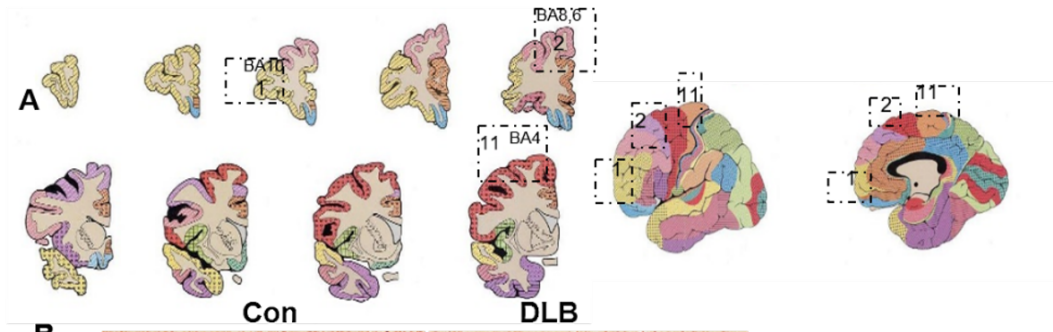
Figure 3. 7: Changes in PV+ interneuron population in the frontal lobe of human post-mortem brain tissues of DLB patients. (A) Representative images from Newcastle brain map of brain areas where PV+ fast spiking interneurons was analysed. 1= PFC (BA10), 2=MFC (BA8, 6), 11=MC (BA4). The regions were numbered according to their location in the TMA slides. **(B)** Representative images taken at 10X magnification of both control (left) and DLB (right), showing brain regions (PFC, MFC and MC), arrow indicating the immunopositivity of PV+ cells. **(C)** Box plot showing the comparison of percentage coverage of PV+ interneurons distribution in both DLB and non-diseased patients. Both percentage coverage and the number of objects per ROI of PV+ cells in PFC of control (n=7 cases) and DLB (n=7 cases) were not statistically significant (P>0.6991). Similarly, both measurements of PV+ cells in MFC of control (n=7 cases) and DLB (n=7 cases) were not statistically significant (P>0.4641). However, it was statistically significant in Motor cortex for both percentage change (P<0.0379) and number of objects (P<0.0058) per ROI.

3.3.2.2 Vulnerability of PV+ fast spiking interneurons in major sensory cortices of DLB patients

Given the observed results in the frontal lobe of DLB patients, I proceeded with the neuroanatomical quantifications of PV+ cells in the sensory cortices such as the parietal, temporal and occipital lobes. Following the staining with anti-PV antibody, PV+ cells with/ without neuronal processes were observed in parietal cortex from both control and DLB patients. Although, under simple observation, a higher density of the PV+ interneuron population in the control cases compared to the DLB cases is discernible, there were not statistically significant results in both percentage change and the number of objects per ROI (P>0.4314, Mann-Whitney test) (figure 3.8). Similar trend was observed in temporal cortex. Where the percentage coverage and the number of PV+ cells/ROI, is seemed to be reduced in DLB compared to the control case. Non-parametric analysis (Mann-Whitney test) shows that the results were not statistically significant (P>0.1807) (figure 3.8). Likewise, the percentage coverage of and the number of PV+ cells/ROI in the occipital OC, showed a trend in reduction in DLB compared to control case (figure 3.8). However, the results were not statistically significant (Mann-Whitney test; P>0.5338).

A

B

con   DLB

PC

TC

OC

200μM   200μM

C

Parietal cortex — ns

Parietal cortex — ns

Temporal — ns

Temporal — ns

Occipital cortex — ns

Occipital cortex — ns

Figure 3.8: Changes in PV+ interneurons population in sensory cortices of post-mortem brain tissues of DLB patients. (A) Representative images from Newcastle brain map of brain areas where PV+ fast spiking interneurons where analysed. 14= PC (BA7), 13=MFC (BA21, 22, 38, 42, 52), 15=MC (BA17). Regions numbered according to their location in the TMA slides. **(B)** Representative images taken at 10X magnification of both control (left) and DLB (right), showing brain regions (PC, TC and OC), arrow indicating the PV+ cells. **(C)** Box plot showing the comparison of percentage coverage (left) and the number of PV+ interneurons distribution (right) in both DLB and control cases. Both percentage coverage and the number of objects per ROI of PV+ cells in PC of control (n=7 cases) and DLB (n=7 cases) were not statistically significant (P>0.4314). Similarly, both measurements of PV+ cells in TC of control (n=7 cases) and DLB (n=7 cases) and OC control (n=7 cases) and DLB (n=7 cases) were not statistically significant (P>0.1807), (P>0.5338).

3.3.2.3 Changes in PV+ fast spiking interneurons in Insular, Cingulate and Entorhinal cortex of DLB patients.

Given the observed, changes in PV+ interneuron density in both, the frontal lobe and the major sensory cortices, PV+ cells with/without neuronal processes were also observed in the above-mentioned regions in both control (n=7 cases) and DLB (n=7 cases) patients (figure: 4.5.). Interestingly, a significant decrease in percentage coverage was observed EC (P>0.0452; Mann-Whitney test). These changes were highly significant when I analysed the results based on the quantification of the number of object/ROI (P<0.0070; Mann-Whitney test) (figure:3.9). Suggesting that interneurons in this region of DLB patients are severely affected. I then carried on analysing the IC. Interestingly, here I found that PV+ interneurons are markedly reduced in IC of DLB patients as well (n=7 cases) (figure: 3.9). The results were statistically significant for both percentage change/ ROI (non-parametric Mann-Whitney test; P<0.0140) and the number of object/ROI (non-parametric Mann-Whitney test; P<0.0371) compared to the control case (n=10 cases) (figure: 3.9). Nevertheless, PV+ interneurons were not significantly altered in the CC (DLB =7 and control=7 cases). Although, a slight reduction was observed in both the percentage coverage of PV+ interneurons (P>0.5887 Mann-Whitney test) and the number of objects per ROI (P>0.4704) Mann-Whitney test) and the results were not statistically significant (figure: 3.9).

A

B

	Con	DLB

EC

CC

IC

200μM

200μM

C

Entorhinal
*
% Coverage

Con   Group   DLB

Entorhinal
**
# of objects/image

Con   Group   DLB

Cingulate
ns
% Coverage

Con   Group   DLB

Cingulate
ns
# of objects/image

Con   Group   DLB

Insular Cortex
*
% Coverage

Con   Group   DLB

Insular Cortex
*
# of objects/image

Con   Group   DLB
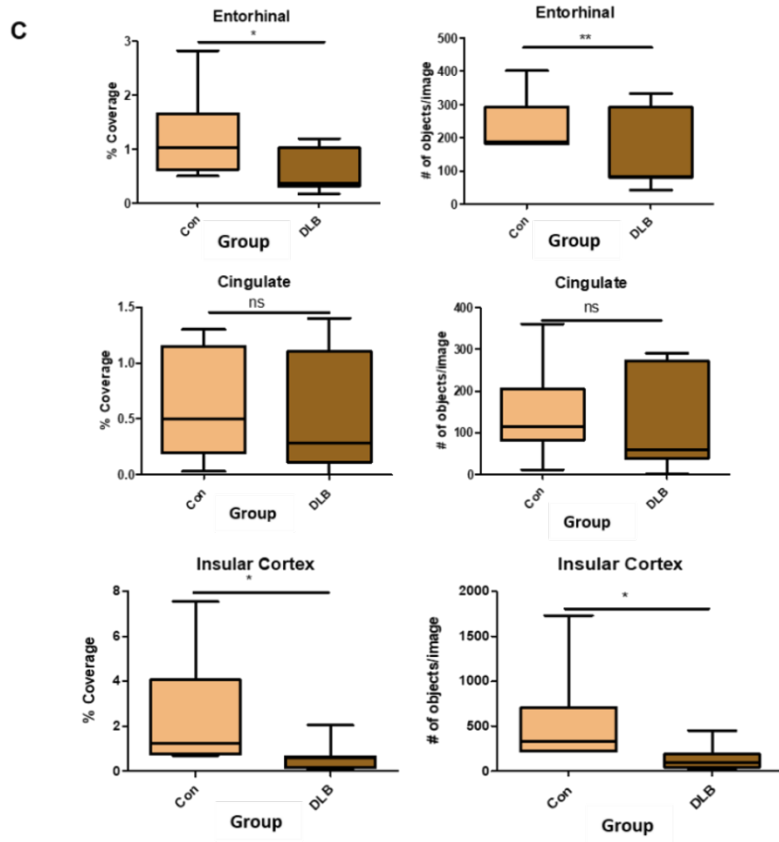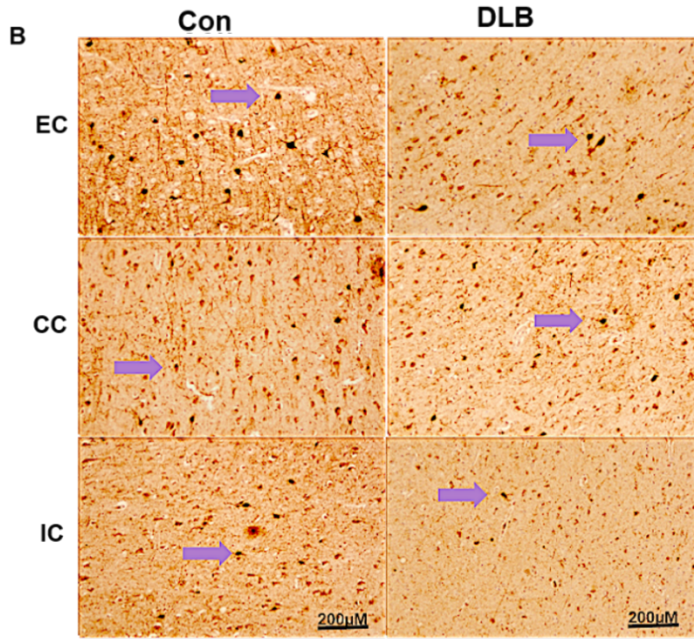
Figure 3. 9: Changes in PV+ fast spiking interneurons in Insular, cingulate and Entorhinal cortex of DLB patients. (A) Representative images from Newcastle brain map of brain areas where PV+ fast spiking interneurons where analysed. 10= EC (BA20), 4=CC (BA32), 8=IC (BA43). Regions numbered according to their location in the TMA slides. **(B)** Representative images taken at 10X magnification of both control (left) and DLB (right), showing brain regions (EC, CC and IC), arrow indicating the PV+ cells. **(C)** Box plot showing the comparison of percentage coverage (left) and the number of PV+ interneurons distribution/ROI (right) in both DLB and control cases. The percentage coverage was statistically significant (P<0.0452) and the significance was higher when compared the number of object per ROI (P<0.0070) of PV+ cells in EC of control (n=7 cases) and DLB (n=7 cases). Similarly, in IC control (n=7 cases) and DLB (n=7 cases), both percentage coverage (P<0.0140) and the number of object/ROI (P<0.0371). of PV+ cells were statistically significant. In the contrary in CC control (n=7 cases) and DLB (n=7 cases) the percentage coverage of PV+ interneurons (P>0.5887) and the number of objects per ROI (P>0.4704) were not statistically significant.

3.3.2.4 Vulnerability of PV+ fast spiking interneurons in the basal ganglia of DLB patients.

Given the observed reduction of PV+ interneurons across different brain regions, such as MC, IC and EC, I decided to proceed with the neuro-anatomical quantifications of these cells in the outer cortical layers beneath the cerebral hemispheres that are assembled in nuclear masses, collectively known as the basal ganglia, to corroborate whether similar changes could also be observed in this region. These areas include structures such as caudate nucleus (CN), putamen (PTm) (both also known as neostriatum) and Globus pallidum (GP). Indeed, PV+ cells with/without neuronal processes were visible in all BG (figure. 3.10), and a clear trend in reduction in the percentage coverage of PV+ cells (P<0.0132. Mann-Whitney test) was evident in GP. The results were highly significant with the quantification of the number/ROI of PV+ cells (P<0.0036. Mann-Whitney test). Similar results were observed in the CN, where both the percentage coverage (P<0.0017 Mann-Whitney test) and the number of objects/ ROI (P<0.2186. Mann-Whitney test) where statistically significant as well. Nevertheless, no clear change was observed in the density of PV+ interneuron

population in the PTm, and the results were not statistically significant in both percentage change and number of object/ROI (P>0.05 Mann-Whitney test) (figures. 3.10).

A

B

	Con	DLB
GP		
CN		
Ptm		

200µM   200µM

C

Globulus Palidum

Globulus Palidum

Caudate

Caudate

Putamen

Putamen
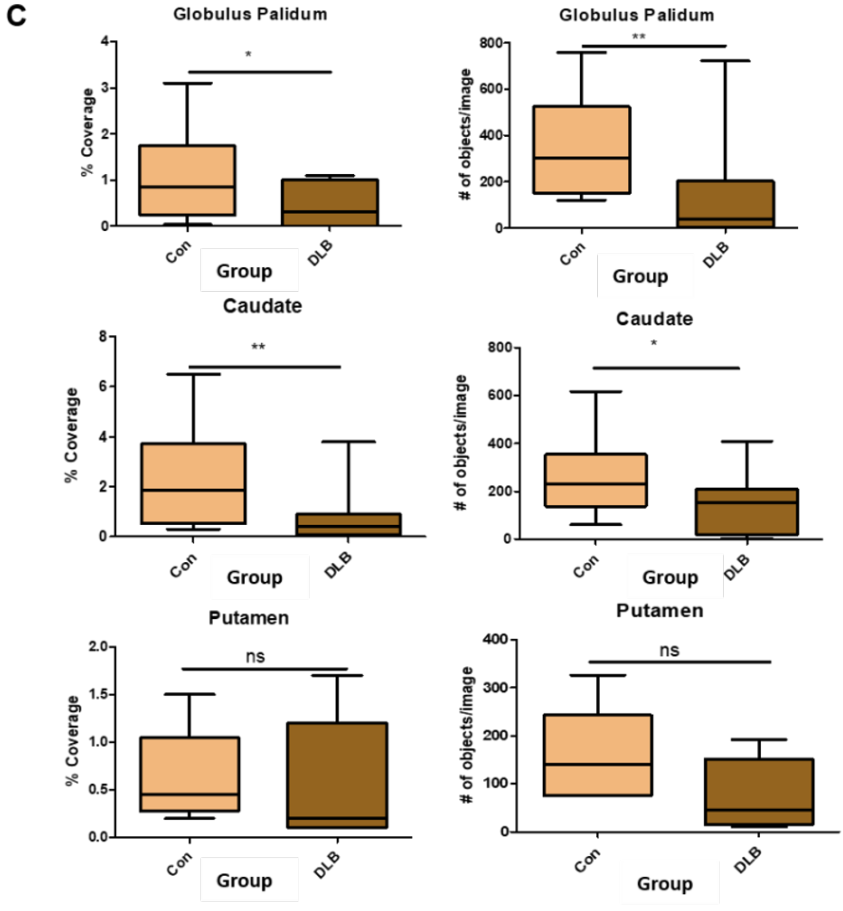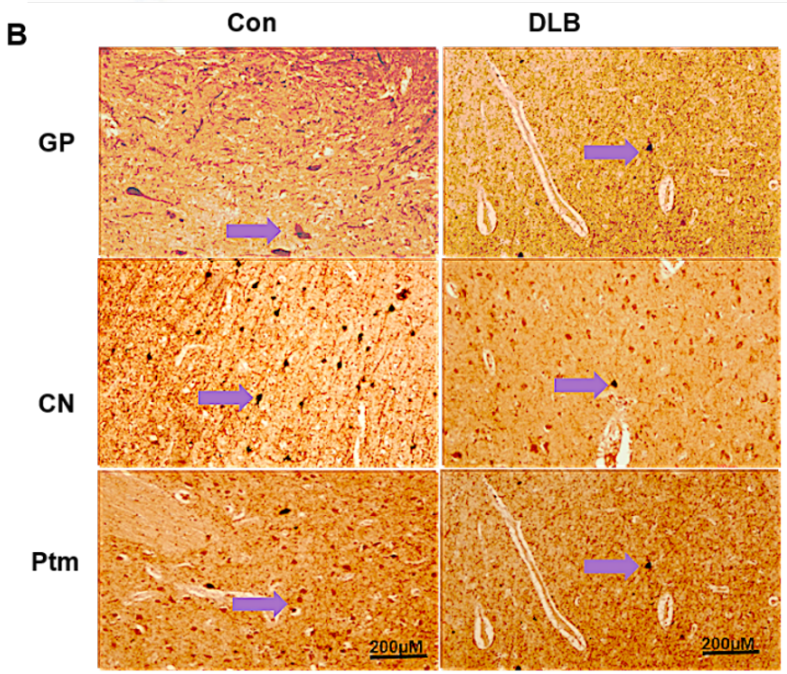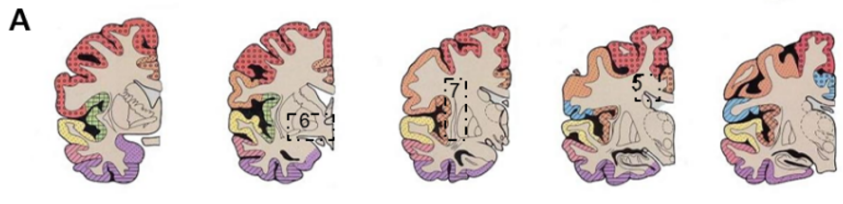
Figure 3. 10: Changes in PV+ fast spiking interneurons in Basal Ganglia of DLB patients. (A) Representative images from Newcastle brain map of brain areas where PV+ fast spiking interneurons where analysed. 6= GP, 5=CN, 7=PTm. Regions numbered according to their location in the TMA slides. **(B)** Representative images taken at 10X magnification of both control (left) and DLB (right), showing brain regions (GP, CN and PTm), arrow indicating the PV+ cells. **(C)** Box plot showing the comparison of percentage coverage (left) and the number of PV+ interneurons distribution (right) in both DLB and control cases. Both percentage coverage (P<0.0132) and the number of objects per ROI (P<0.0036) of PV+ cells in GP, (n=7 control DLB n=7 cases) were statistically significant. Similarly, in the CN, (control n=7, DLB n=7 cases) the percentage coverage (P<0.0017) and the number of objects/ ROI (P<0.2186) where statistically significant. In the contrary, no significant changes were observed in the PTm for both the percentage coverage (P>0.1807), and the number of PV+ cells/ ROI (P>0.5338). (control n=7 DLB (n=7 cases) and OC control (n=7 cases) and DLB (n=7 cases).

3.3.2.5 Vulnerability of PV+ fast spiking interneurons in the thalamus and the amygdala of human post-mortem brain tissues of DLB patients.

Considering that, the BG forms complex network connections with thalamus and the neocortex, I predicted that similar changes in PV+ cellular density would also be found in this area. Thus, I continued with the quantification of PV+ cells in the thalamus and the amygdala, Here I show that in the thalamic region, the number of PV+ cells are relatively preserved in the control patients, however, reduced in DLB patients, and the results were not statistically significant when compared to control cases (P>0.05. Mann-Whitney test). Notwithstanding, a significant reduction was observed in the amygdala in both the percentage coverage (P>0.0109. Mann-Whitney test) and number of PV+ cells /ROI (P>0.0078. Mann-Whitney test), which was highly significant. Suggesting that PV+ cells are targeted by αSyn pathogenicity in this area of the brain (Figure 3.11).

A

Con **DLB**

Thl

Agd

WM

200μM 200μM
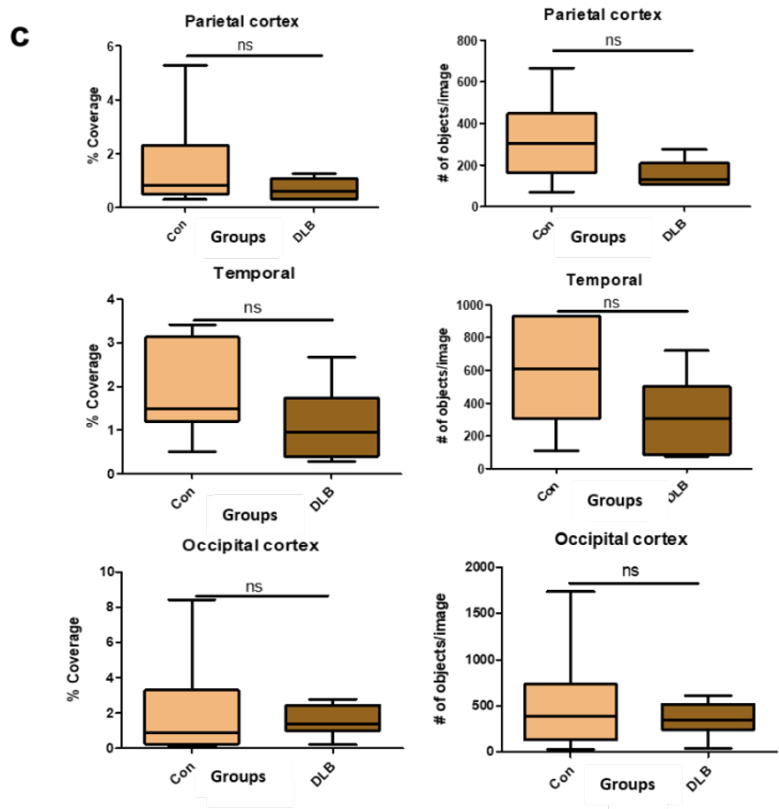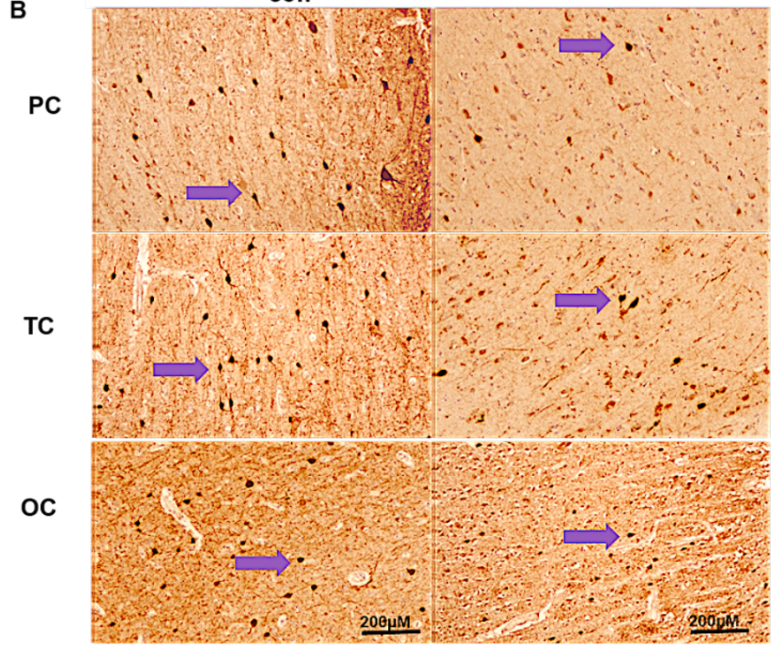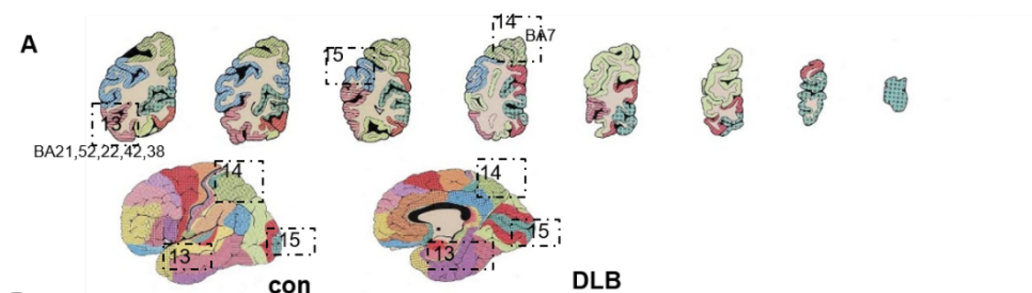
Thalamus

Thalamus

Amygdala

Amygdala
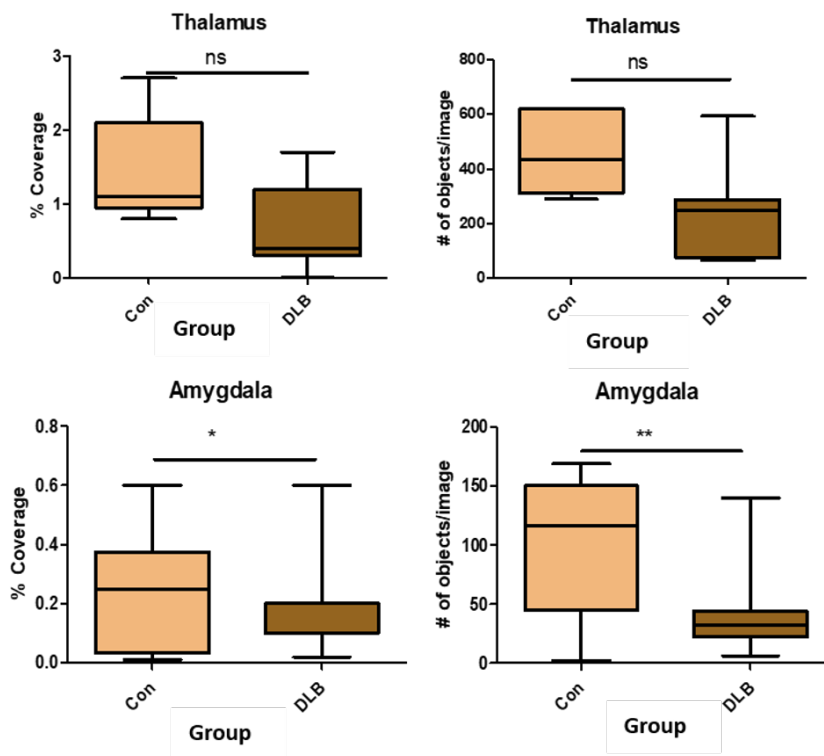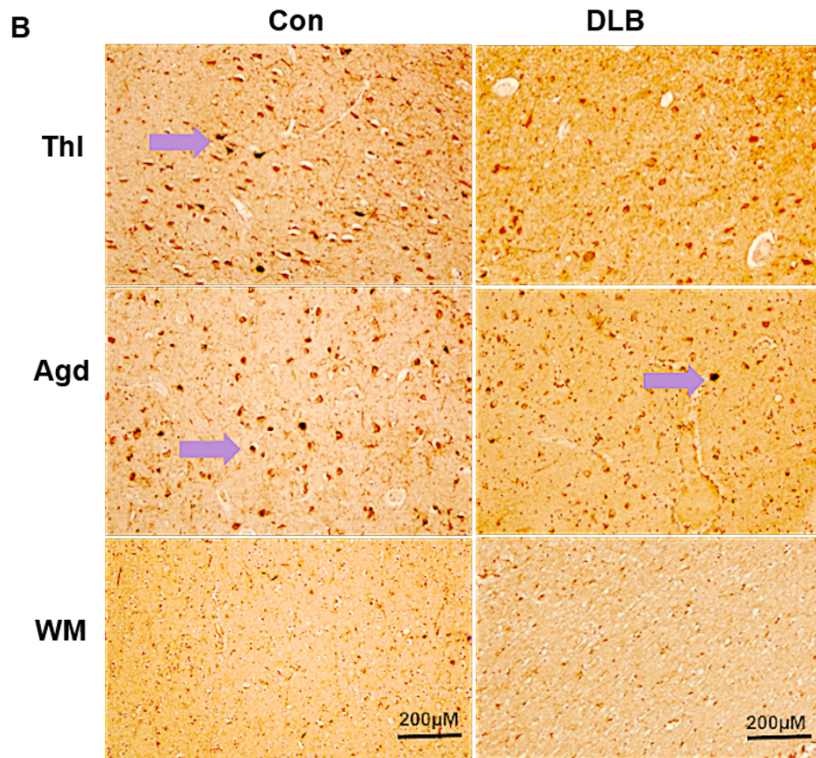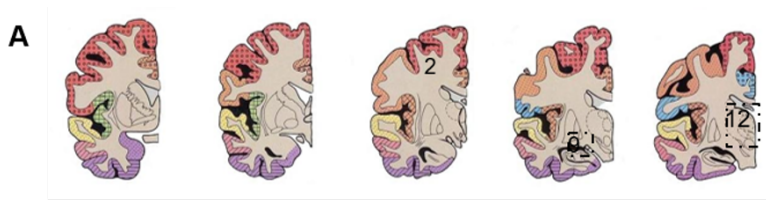
Figure 3. 11: Changes in PV+ interneurons population in frontal lobe of human post-mortem brain tissues of DLB patients. (A) Representative images from Newcastle brain map of brain areas where PV+ fast spiking interneurons where analysed. 12=Thl, 9=Amygdala. The regions where numbered according to their location in the TMA slides. **(B)** Representative images taken at 10X magnification of both control (left) and DLB (right), showing brain regions (thalamus and amygdala), arrow indicating the immunopositivity of PV+ cells. **(C)** Box plot showing the comparison of PV+ interneurons distribution in both DLB and non-diseased patients. Both percentage coverage and the number of objects per ROI of PV+ cells in thalamus of control (n=7 cases) and DLB (n=7 cases) were not statistically significant (P>0.6991). However, both the percentage coverage (P<0.0109) and the number of PV+ cells/ROI (P<0.0078) showed statistically significant change.

3.3.3 General comparison of PV+ interneurons density across brain regions in both control and DLB samples.

Following the observed changes in the density of PV+ interneurons in above-described brain regions, here I show in a heat map the changes in density per region studied from images taken from human post-mortem brain samples of both control and DLB patients (figure 3.12). The regions with higher loss of PV+ cells are represented in white and the areas with higher density are in purple. The higher density of PV+ cells is detected in the control cases, which presents more regions with purple colour. Whereas in DLB cases, more white regions are observed, compared to the purple regions. This suggests that the density of PV+ cells is reduced across different brain regions in DLB cases (figure 3.12). In addition, comparisons across cortical and subcortical brain regions were also performed, and I detected that the overall interaction between the disease and different cortical regions was statistically significant, thee immunoreactivity were particularly evident in the Parietal, insular and temporal cortices (Two-way repeated measures ANOVA, followed by Bonferroni multiple comparison test, $F_{(8,12)}$ =0.6887, ***P<0.0007) (figure 3.13). In the subcortical regions, the interactions between the disease and regions were statistically significant. These differences were more evident in the Caudate, Globus pallidum, and the thalamus were the most affected regions (Two-way RM ANOVA, followed by

Bonferroni multiple comparison test F $(5,12)$ =1.127, ***$P<0.0003$) (figure 3.14). Hence, I can conclude that, the density of PV+ cells may be severely reduced in some regions of the brain, during DLB pathogenesis.
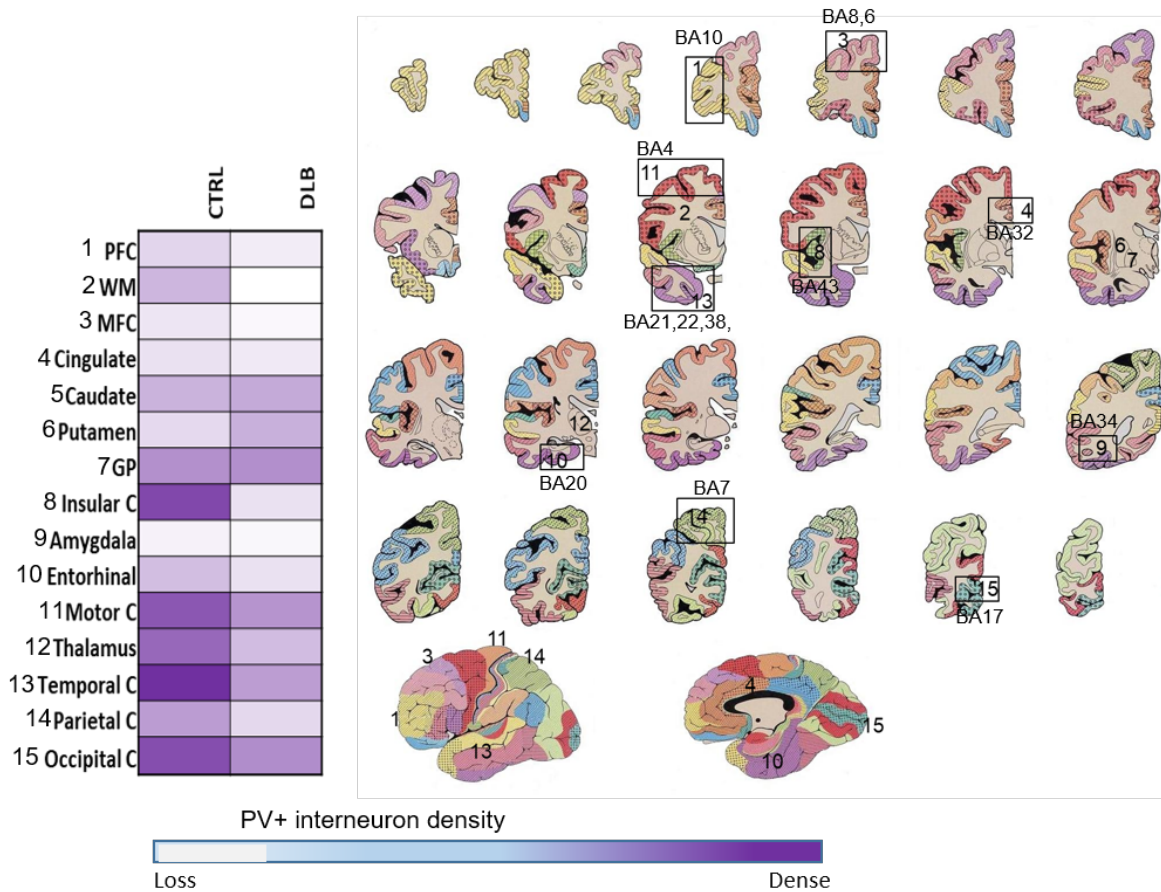
Figure 3. 12: Changes in PV+ interneuron number in human post-mortem brain tissues of DLB patients. Heat map showing the changes in density per region studied (left) Representative images of human post-mortem brain where slices were taken (right).
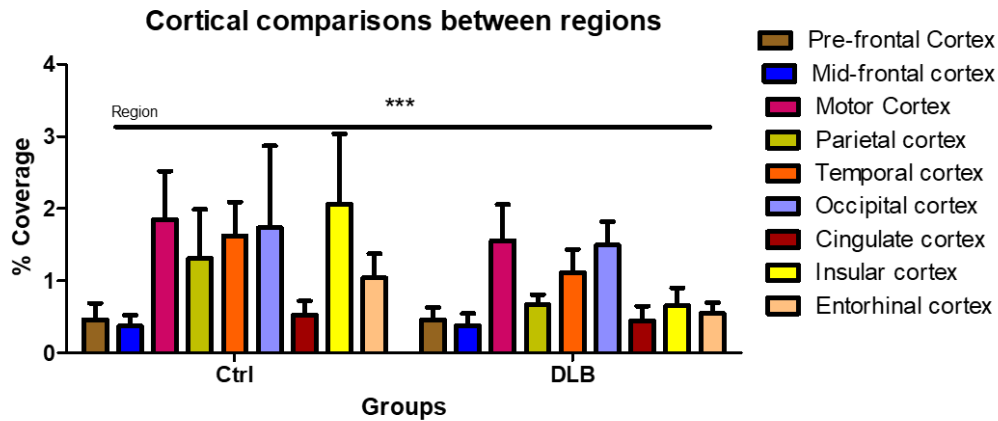
Figure 3.13: Changes in PV+ interneuron number in cortical regions of human post-mortem brain tissues of DLB patients. Bar chart showing changes in density of PV+ cells per region studied in the cortex. The interaction between disease and region with PV+ cells were significantly different in some regions of the DLB group, and among the regions, the Insular, Parietal and Temporal cortices showed the highest immunoreactivity (***$P < 0.0007$).
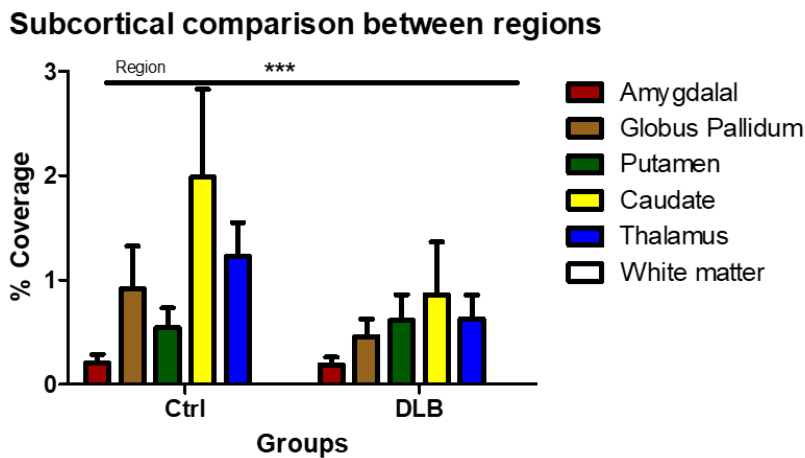
Figure 3. 14: Changes in PV+ interneuron number in subcortical regions of human post-mortem brain tissues of DLB patients. Bar chart showing changes in density of PV+ cells per region studied in the sub cortex. Higher interaction between the disease and region was observed, in relation to the density of PV+ cells. Among the subcortical regions, Caudate, GP, and the thalamus were the most affected regions (***$P < 0.0003$).

3.4 Discussion

The findings presented in this chapter, indicate that, while the density of PV+ interneurons remain relatively unchanged in some areas of the brain, such as (PFC, MFC, PC, TC, OC, CC, PTm and Thalamus). Significant reductions in the numbers of PV+ interneurons were clearly observed in regions such as the MC, EC, IC, CN, GP and the amygdala. In this work I have hypothesized that pre aggregated forms (fibrillary, mutated, and PTMs) of αSyn may accumulate in the PV+ cells, thus impairing their functions, with the subsequent neuronal cell death that leads to loss to the neuronal connectivity, impairments of the inhibitory synaptic inputs, resulting in abnormal neuronal network activity. Since, the neuronal network oscillations are impaired in DLB, as observed in the previous chapter (Robson et al., 2018b), I assume it could be a shadowing the impairments/reduction of PV+ interneurons, that results in loss of synapses of connecting neurons, thus impairing the rhythm of the neuronal oscillations which represents the cognitive and motor functions.

The significant reduction detected in the above-described regions, specifically the IC and EC, which are regions reported to be implicated with the development of prodromal stages of DLB (Roquet et al., 2017, Elder et al., 2017), may suggest a development of early pathogenic cascade that affect PV+ interneurons. This is supported by a study in young (2+A30P) mouse model of synucleinopathies, that shows that this group of mice tend to develop early hyperexcitability/ or interictal activity in the neuronal network oscillations (Tweedy, 2019). In the neuronal networks, hyperexcitability is a result of reduced IPSPs from inhibitory cells and increase of EPSPs from the pyramidal cells (Kann et al., 2014b). Meaning that, if the input from the pyramidal cells is not efficiently being suppressed due to the lack of inhibition input, which can be a result of dysfunctional /loss of inhibitory cells, the neuronal network oscillations, will be impaired. Thus, the observed changes in fast spiking interneurons (loss of action potential firing and the decrease of IPSPs amplitude) could be at the root of the impairments of gamma frequency oscillations in DLB as I demonstrated in the previous chapter.

Normal fast network oscillations (at beta and gamma frequency bands) are important for cognitive and motor functions in the brain (Bonanni et al., 2008, Bernstein et al., 2011a). In fact, Impairment of the oscillations specifically at the gamma band, underlie

the cognitive and motor dysfunctions observed in cognitive disorders (Mably and Colgin, 2018). This shows that PV+ cells may play an important role in the development of the synucleinopathies. This is a novel finding, as to my knowledge, no literature available have done a comprehensive study on the distribution of the PV+ cells across the human brain. However, besides the sample size, one reason that the result of some regions presented in this chapter were not statistically significant, could be due to the regional variability of PV+ interneurons, which adds complexity to the neuro-anatomical quantifications. Because some regions of the brain may have lower density of these cells in the first place or simply because of the variability of the control samples. Overall, the present study shows PV+ interneurons (and perhaps other neuronal types as well) are vulnerable in the mouse model and post-mortem brain tissue of DLB.

3.4.1 Parvalbumin expressing Interneurons in DLB

The brain neural circuitry demands a precise spatiotemporal coordination of the activity of pyramidal cells, organised by the inhibitory interneurons for the Information to be processed (Castejon and Nuñez, 2016, Cardin, 2018). The whole process is thought to rely heavily on the activity of the fast spiking interneurons, which are thought to generate PA at high frequency rate, reflecting the high-energy utilization demand from these neuronal population (Tremblay et al., 2016). The large diversity of interneurons in the cortex is represented by the GABAergic interneurons, in which PV expressing cells form the majority (Rudy et al., 2011). In fact, GABAergic interneurons are involved in pathogenesis of brain disorders including neurodevelopmental disorders, epilepsy and encephalopathies and neurodegeneration (Katsarou et al., 2017). A study using microarray analysis, showed that GABAergic neuronal function is altered in DLB and a possible dysfunction of the calcium binding protein GAD65/67 was shown in their immunohistochemistry studies (Khundakar et al., 2016). It is important to highlight that all interneurons secrete GABA as their neurotransmitter, except the stellate cells, which are thought to use glutamate instead, and are present in the fourth layer of the cortex (Sultan et al., 2013). Inhibitory/ GABAergic interneurons are classified into Retzius-Cajal cells, Martolini cells and Basket cells (Sultan et al., 2013). The later type has axonal branches that surround the soma of the pyramidal cells and is the focus of this chapter (figure 4.1). A subgroup of GABAergic

interneurons are PV expressing fast-spiking interneurons, representing 40% of all GABAergic interneurons (Rudy et al., 2011). However, little is known about their involvement in DLB pathogenesis. This chapter shows that PV+ cells are affected in regions associated with the heavy presence of DLB histopathological hallmarks. Indeed, the co-localisation of αSyn with PV+ expressing fast spiking interneurons was found to be linked to the decrease of this group of neuronal populations (Bernstein et al., 2011b). Although, a study suggests that PV+ interneurons are LB-free (Bernstein et al., 2011b), the loss PV+ expressing interneurons is worthy of note, given their involvement in the generation of neuronal gamma frequency oscillations which are essential for cognitive functions, as mentioned above (Bernstein et al., 2011b, Bonanni et al., 2008, Whittington and Traub, 2003). Moreover, the absence of LBs and LNs inside PV+ cells does not exclude the presence of pathological αSyn inside the cell, since αSyn constitute 1% of the total cytosolic proteins across the nervous system (Spillantini et al., 1998). I believe that pre-aggregated forms of the protein that are disordered or post-translationally modified may start to cause damage to the cell, before they form LBs/LNs inclusions. This may explain why in the work presented here PV+ interneurons, although devoid of LBs are found to be reduced in some areas of the brain of DLB patients.

Moreover, PV is a low molecular weight (12 kDa) calcium binding protein that is abundant in the cytosol of non-pyramidal cells (Tremblay et al., 2016, Plogmann and Celio, 1993). Although, little is known about the physiological significance of these proteins, as the understanding of their function is relatively vague, their involvement of calcium buffering and homeostasis and the consequent protection against excitotoxicity has been verified (Rintoul et al., 2001). Indeed, the efficient buffering of calcium by PV proteins and its significant expression in interneurons is thought to be fundamental for a proficient inhibition of the cortical neuronal network (Schwaller, 2010, Plogmann and Celio, 1993). In addition, in PV expressing cells, calcium is found to be normally bound to parvalbumin or calbindin buffering proteins in the endoplasmic reticulum and mitochondria (Schwaller, 2010, Schwaller, 2007). The excess entry of calcium, which is one of the causes of excitotoxicity, may impair these structures, with consequent cellular dysfunction and death (Celsi et al., 2009). Furthermore, the increased production of reactive oxygen species, such as, superoxide anion, hydroxyl radicals and hydrogen peroxide, which are generated when oxygen molecules are

reduced to water during oxygen and electron transport (Collin, 2019), causes damage of the cell by peroxidation of the cell lipid membrane. This is thought to increase membrane permeability in energy-depleted cells such as interneurons (Marambaud et al., 2009, Uttara et al., 2009). These are common pathogenic features of neuronal degeneration (see figure 1.6) Therefore, PV+ cells presents high vulnerability at the presence of metabolic stress, which one of the key pathogenic pathways in neurodegenerative diseases (Kann et al., 2014b).

In addition, cognitive decline, a core symptom of DLB (McKeith et al., 2017), is thought to reflect the impairments of gamma oscillations (Robson et al., 2018b, Kann et al., 2011, Kann et al., 2014b), which are dependent on the healthy function of the PV+ fast spiking interneurons (Kann, 2011, Kann et al., 2014a). Altered interneuron excitability, due to inability to buffer calcium critically contributes to the impairments of the neural oscillatory synchrony and rhythms (Morris et al., 2015, Verret et al., 2012). One study has shown that early treatment for PV+ interneurons by activity restoration is effective in preventing hyperexcitability and memory loss in the mouse model of AD (Hijazi et al., 2019). In fact, in AD optogenetic manipulation of PV+ cells was found to selectively restore gamma oscillations impaired by amyloid beta (AB) oligomers (Park et al., 2020). Thus, αSyn may impair the PV protein ability to buffer calcium causing the death of the interneurons, which leads to the dysfunction of the network oscillations, highlighting the crucial position of these cells for the maintenance of brain functions such as movements and the cognition, which are severely affected in DLB.

3.4.2 Density of Parvalbumin expressing interneurons in the frontal Lobe of DLB patients

Pyramidal cells and the interneurons compose the neural circuitry in the neocortex. Pyramidal cells represent the most abundant type and are present in higher density in the motor cortex (Baker et al., 2018a, Baker et al., 2018b), in contrast to the primary sensory areas where the presence of the pyramidal cells are lower (Baker et al., 2018a, Baker et al., 2018b). On the other hand, the population of inhibitory interneurons in the cortex is highly diverse, about 30% of neocortical neurons are GABAergic interneurons (Xu et al., 2010). Indeed, every layer of cortical pyramidal cells is under the specific control of a unique class of interneuron populations. However, some variability can be observed in regions such as thalamus, basal ganglia

and the cerebellum, where the degree of variability of the resident interneurons is relatively low, consisting with just few interneuron types (Pelkey et al., 2017, Buzsáki et al., 1983, Buzsáki and Wang, 2012). PV expressing interneurons represent the major group within the GABAergic interneurons in the cortex and they are found to be most abundant in the hippocampus and neocortex (Booker and Vida, 2018, Kann, 2016). Here I quantified PV+ interneurons in key areas of the brain affected in DLB, including frontal cortex (FC), which composes 25-33% of the brain, and is known to be the area responsible for the higher cognitive, executive functions and voluntary movements (Stuss and Craik, 2019). Due to the different functions performed in different areas of the frontal cortex, I divided this area in 3 main regions, i.e., PFC, MFC and MC, as discussed below.

The PFC establishes extensive connections with almost all regions of the brain, including the amygdala and mediodorsal thalamic nucleus (Ouhaz et al., 2018). It is responsible for gathering input information from all other areas of the brain, to produce complex cognitive functions, including thoughts, judgements, long-term plans, foresight and socially accepted behaviours, which are functions affected in DLB clinical profile (Hoffmann, 2013, Gross et al., 2013, McKeith et al., 2004, McKeith et al., 2017). Moreover, widespread histopathological hallmarks (LBs and LNs) of synucleinopathies are also observed here (Alafuzoff et al., 2009, Braak et al., 2003a, Braak et al., 1999). In the present work, I have not observed significant differences in the distribution of PV interneurons between DLB and control cases in PFC, which suggests a relative preservation of the density of the PV+ cells in DLB patients. Although changes in the structure and physiology of PV+ interneurons in the PFC has been reported as important factors in psychiatric disorders (Marín, 2012), no study to date reported changes in number of PV+ cells in the PFC in DLB, and the results presented here seems to show the same conclusion.

In parallel with the findings in PFC, although there was apparently less PV+ fast spiking interneurons in MFC from the DLB cases the difference was not significant compared to the control (figure 4.3). MFC, which is the association area responsible for the complex and flexible patterns of behaviour, also affected in DLB (Breukelaar et al., 2017, Peavy et al., 2013). The relative preservation of PV interneurons of the number of PV+ cells may/may not suggest that this group of cells are intact because dysfunction may occur without overt cell death. However, significant reduction in PV+

cells was observed in the MC, which is the area of the frontal lobe responsible for planning, control and initiating voluntary movements (Nardone et al., 2006, Takahashi et al., 2010). This is in agreement with a study by Nardone et al., that showed less pronounced dysregulation of inhibitory interneurons of the intracortical GABAergic interneurons in the MC of DLB patients (Nardone et al., 2006). In addition, pathogenic features such as hypoperfusion of MC is reported to be present in the development of parkinsonian symptoms in DLB (Nardone et al., 2006, Takahashi et al., 2010). Although, no significant changes were observed in the rostral and medial regions of the frontal lobe, the reductions in the number of PV+ cells in the MC may indeed influence the neuronal network of the supplementary and association areas, as they receive great amount of input from the primary motor area which resides in the motor cortex.

3.4.3 Parvalbumin interneurons in the cingulate cortex

Beneath the frontal lobe lies the CC, which is part of the limbic system, and is thought to be associated with emotions and pain related activation (Rolls, 2019). This region is found to be severely affected in DLB. In fact, αSyn levels are high in this region (Patterson et al., 2019). In addition this region is found to be hypoperfused in DLB, and is thought to be involved in the generation of visual hallucinations (Heitz et al., 2015). Although there was a trend in reduction of PV+ cells in the CC, the results presented in this work, however, show no significant changes, indicating a relative preservation of the PV+ interneurons in the CC of DLB patients. Because CC receives input from different brain areas, this prompted further analysis on other aspects that influences the neuronal network in this area. Since PV+ interneurons are embedded in a specialised form of extracellular matrix, commonly known as PNN, I thought they would be affected as well. Thus, using the A30P I further explored the viability of the PNN in CC. Nevertheless, similar results were also observed.

PNNs are essential for the regulation of the functions of GABAergic interneurons (Wen et al., 2018). In fact, the connectivity of PV+ interneurons is thought to be regulated by the PNN, an extracellular matrix that is frequently found surrounding PV+ cells (Alcaide et al., 2019). PNN selectively surrounds the PV+ interneurons, providing them protection against excitotoxicity (Cabungcal et al., 2013b, Cabungcal et al., 2013a, Morawski et al., 2004). The absence of significant numerical changes in this area,

revives the question about quality vs quantity, as it is possible that PV functions are impaired in this region before the numerical deficits of the cells are observed. Unfortunately, there is not currently available literature that explored the viability of PV+ cells and PNN in the CC, to compare with the results I present here. Another aspect of this study on the PNN is that the samples were underpowered, as the availability of 30P, mice were limited.

3.4.4 Parvalbumin interneurons in major sensory cortices

PC is the region responsible for processing sensory information, subdivided into two regions: the primary somatosensory and association cortex. It lies posterior to the central sulcus, and is believed to participate in the regulation of emotions as well (Kropf et al., 2019). This region forms anatomical connections with various subcortical regions including the basal ganglia, thalamus, and is involved in various cognitive functions such as attention and episodic memory (Metzger et al., 2013). PC processes sensory information such as space, perception, size, reading, writing and mathematical thinking (Bueti and Walsh, 2009, Sun and Wang, 2013). In DLB, this area is known to present loss of cortical tissue, associated with LBs related neuronal loss (Whitwell et al., 2007). Although, I observed a trend in numerical reduction of PV+ cells, no statistically significant reduction was observed in the PC. It has been reported that the density of PV+ interneurons is not changed in this region and in most of the cortical area. However, the PV protein levels inside the interneurons are known to decrease with age (Ueno et al., 2018). This is accompanied with the reduction of the size of the soma in the sensory cortices such as PC, in contrast, the density of the PNN is increased with ageing in PC (Ueno et al., 2018). Thus, the functional deficits in these cells may underlie the impairments in this region, which leads to the dysfunction of the neuronal networks.

In addition, temporal and occipital lobes are also reported to be affected in the DLB (Kenny et al., 2012). TC is known to house the primary auditory cortex and processes sensory information, converting it into meaningful information, language and emotions (Baker et al., 2018b). Neuropathological studies have shown atrophy of medial regions of the temporal cortex of DLB patients (Chavoix and Insausti, 2017). In my study no significant numerical changes in PV+ interneurons were found in this region. Similar results were also observed in the OC which is the visual centre of the brain, containing

the primary visual cortex and receiving stimulus from the lateral geniculate nucleus (Blumberg and Kreiman, 2010). Patients with DLB often experience a complex, well-formed and recurrent visual hallucination (RCVH), which is one of the core symptoms of the disease (McKeith et al., 2017, Outeiro et al., 2019). In MRI studies of DLB patients, reduction in functional activation and deficits in blood perfusion of this area were detected (Taylor et al., 2012). Indeed, abnormality in occipito-parietal region in DLB has been reported (Khundakar et al., 2016). Similarly, microarray analysis showed that GABAergic neuronal function is altered in DLB and a possible dysfunction of the calcium binding protein GAD65/67 was also shown in their immunohistochemistry studies (Khundakar et al., 2016). Here, the PV expressing cells in the occipital cortex remain unchanged, suggesting that another interneuron population may be affected instead. Overall, no significant reduction in the number PV expressing interneurons was observed in the major sensory cortices in DLB, however the observed trend toward reduction may suggest functional deficits of these cells.

3.4.5 Parvalbumin interneurons in the basal ganglia, amygdala and the thalamus

The BG is considered the largest subcortical collection of neurons located on both lateral sides of the thalamus and is implicated in tuning and the execution of the motor responses. It includes structures such as the caudate, the putamen (both known as neostriatum) and the Globus pallidum (Figures: 4.6.1; 4.6.2; 4.6.3) (Lanciego et al., 2012). It is important to highlight here that, the term BG "ganglia" is a misnomer, since the term ganglia refers to a group of neurons located in the peripheral nervous system. However, when the collection of neurons within intra-cortical structures of the SNC is usually called nucleus. Thus, I think the term basal nucleus would be anatomically more applicable. Nevertheless, the term BG is used in this thesis for consistency with the published literature. BG forms a complex feedback circuitry with the motor cortex, by providing important modulatory input to the cortex (Lanciego et al., 2012). Indeed, the importance of BG in movement control is highlighted by the devastating consequences in neurodegenerative diseases that progresses with basal ganglia dysfunction such as PD and DLB (Yanagisawa, 2018, Braak and Del Tredici, 2017, Braak et al., 2003a). Although it has been reported that PV+ interneurons in the BG are altered in neuropsychiatric disorders (Kalanithi et al., 2005), very little is known about their involvement in neurodegenerative diseases. In this work I observed no

significant changes in the density of PV+ interneuron population in the putamen in DLB. However, highly significant reduction in the number of PV+ cells was detected in the GP and CN of post-mortem brain tissue of DLB.

CN and PTm are known to be the input stage of the BG, as they receive glutamatergic excitation from the cortical neurons (Lanciego et al., 2012, Obeso et al., 2008). PTm receives mostly sensorimotor input, so it regulates motor activity, whereas CN receives its input from the frontal cortex, regulating mostly higher-order cognitive process (Leisman et al., 2014). This parallel adjustment explains the role of the BG in cognition and motor processing. GABAergic neurons from the neostriatum project their input to the GP thus inhibiting its activity. In turn, GABAergic neurons from GP project to and inhibit the thalamus (Leisman et al., 2014). On the other hand, thalamus (which is historically considered a part of the basal ganglia), is a major sensory relay and integrating centre of the cerebrum, as it receives all types of sensory input with the exception of smell (Hwang et al., 2017, Haber and Calzavara, 2009). Its inhibition by GP decreases the flow of excitation input from the thalamus to the cortex. The resulting increase of the excitation input from the cortex provides excitation input to the neostriatum, which then inhibits GP, thus resulting in disinhibition of the thalamus. Thus, the BG inhibits the thalamo-cortical pathway until instructed otherwise. The results presented in this chapter suggest that the density of PV+ cells are somewhat affected in the BG and thalamus and could thus compromise the normal functioning of this circuitry (Haber and Calzavara, 2009, Bhatia and Marsden, 1994). In fact, the importance of the BG in DLB is emphasized by the impairment in motor control presented as Parkinsonism, which is one of the core symptoms of the disease (McKeith et al., 2017). In addition, neurons from the SN project input to the neostriatum to elevate its activity. Thus, the loss of dopaminergic neurons may also contribute to the fall of the overall striatal activity, producing less inhibition to the GP. The resulting increase of GP activity produces excess inhibition to the thalamus decreasing the excitatory input to the cortex, resulting in hypokinesia (Alexander, 2004). The decrease in density or a functional impairment of the PV+ cells in these regions of the brain could perpetuate this vicious cycle of excitation inhibition imbalance, causing the development of DLB clinical profile.

The amygdala is considered a part of the limbic system and is involved in the regulation of the emotional response and plays a fundamental role in the acquisition

and storage of memories. In DLB, αSyn is predominant in the amygdala (Alexander, 2004, Sorrentino et al., 2019). Although the expression of αSyn varies across inhibitory synapses, the density of PV+ interneurons has been reported to be decreased in the amygdala and αSyn was found to be colocalized in PV+ cells as well (Flores-Cuadrado et al., 2017). This is in agreement with the results present here, as I show significant reduction in the number of PV+ cells in DLB. This highlights the importance of the amygdala in DLB pathogenesis

3.4.6 Decrease in PV+ interneurons in Hippocampus, entorhinal and Insular cortex of DLB

The temporal cortex is known to house the primary auditory cortex, and processes sensory information, converting it into meaningful information, language and emotions (Baker et al., 2018b). A neuropathological study of the region reported atrophy of medial regions of the temporal cortex of DLB patients (Chavoix and Insausti, 2017), which contains the primary auditory cortex (BA 41 and 42), located in the superior temporal gyrus. The language, visual perception and memory processing is located in the middle and inferior temporal gyri (Brugge et al., 2008, Reale et al., 2007). These are some of the most affected regions in neurodegenerative diseases including DLB and AD (Gómez-Isla et al., 1999). The temporal lobe also contains the entorhinal, hippocampal and parahipocampal cortices located in the infra-cortical layers of the medial temporal lobe (Eichenbaum and Lipton, 2008). In addition, declarative memories are also encoded in this area (Davachi and Dobbins, 2008).

The hippocampus and EC cortices are two of the earliest affected regions in DLB (Whitwell et al., 2007). Indeed, the EC is thought to be a key region for prodromal stages DLB, as it is shown to be atrophied in the early stages of the disease (Roquet et al., 2017). Here I observed a relative reduction of the PV+ cells in the hippocampus of A30P mice; however, the results were not statistically significant. Indeed, it has been reported that PV+ cells are partially reduced in the hippocampal cortex of DLB patients (Bernstein et al., 2011b), which may have consequences in the gamma oscillatory frequency as observed in the A30P mouse model of DLB (Robson et al., 2018b). Unfortunately, the data presented in the A30P were underpowered; therefore, it could influence the results, as their significance are sample size dependent. Thus, this study could have benefited with an increased sample size. Moreover, the

presence of PV+ fast spiking interneurons in other regions of the hippocampus such as, CA1 and CA2 were not quantified in this thesis, as they were not part of the investigations, considering the observed impaired gamma frequency oscillations, as previously reported (chapter 3). So that these gamma frequency impairments can be correlated with the quantification of the PV+ cells, it was fundamental to restrict the study in the same region where these oscillations were impaired. Additionally, the high variability of the sample data suggests, that a larger sample size could help determine whether the observed difference, although no significant, could correlate with the DLB. Likewise, feedforward inhibition mediated by PV+ interneurons is thought to control the output signals from the deep layers of the EC cortex (Willems et al., 2018) that are transferred to the hippocampus (Ye et al., 2018). Since here I demonstrate that PV+ cells are significantly reduced in this region, this suggests impairments in the output signals from the EC, resulting in excessive output from the EC with pathological relevance in the development of DLB.

Furthermore, αSyn pathology has been observed in the IC (Fathy et al., 2019), which subserves a variety of functions in human brain, such as, sensory processing, affection and cognition (Uddin et al., 2017). Interestingly, this region is thought to be key for prodromal stages DLB, as it is shown to be atrophied in the early stages of the disease (Roquet et al., 2017). In parallel with EC cortex, here I demonstrate that PV+ interneurons are markedly reduced IC of DLB cases. As in the other regions studied in this chapter, there is no currently available literature that studied PV+ cells in this region. Overall, the relative vulnerability of the PV+ cells in the hippocampus, together with its significant reduction in the EC and IC that I present in this chapter, suggests that pathological affectation of the αSyn burden in PV+ cells in these regions.

3.4.7 The significance of decreased density of PV+ interneurons in DLB

In DLB, neuronal cells respond to pathological stimuli by forming aggregates (LBs and LNs) of the cell constituents within the soma and axons that consequently leads to the death of the nerve cell (Hijaz and Volpicelli-Daley, 2020, Outeiro et al., 2019, Wales et al., 2013). Neurons are interdependent cells, therefore, damage to one nerve cell leads to the death of the others, and thus the subsequent tissue atrophy (Castelli et al., 2019). While the density of PV+ interneurons remain unchanged in some regions analysed in this chapter, showing non-significant trend towards reduction in PV+

interneuron density, the significant reduction detected in the IC, EC, MC, GP, CN thalamus and the amygdala, suggests impairments in the neuronal networks that are heavily dependent on and regulated by PV+ cells. For the reason that PV+ interneuron impairments, affects the synchronisation of the oscillatory rhythms, thus, impairing the generation of gamma oscillations in these regions of the brain. Because gamma frequency oscillations generated from the network circuits of these cells, forms complex of relationships between different brain regions, differentially affected, but act in synchrony with each other, to complement brain functions. The pertinent question that arises however, is whether the pathogenic effect of these interneurons relies on the reduction of their numbers or simply in the qualitative changes of the protein composition within their soma that influence their function such as their AP firing rate. As in pathological conditions such as epilepsy, alterations in PV+ fast spiking interneurons or the increase of high calcium permeability, due to the activation of the ionotropic glutamatergic receptors, is thought to cause the cytosolic calcium overload, that is believed to enhance ROS production (Moga et al., 2002, Rogawski, 2011). In parallel with the impairment of the antioxidant mechanisms, this may lead to higher levels of oxidative stress in PV+ fast spiking interneurons, compared to the other neuronal subpopulations, causing devastating consequences to the neuronal network activity. Peculiarly, most PV+ fast spiking interneurons seems to be surrounded with extracellular PNN polianionic matrix that provides them protection against the oxidative stress, which may then explain the vulnerability of these interneurons to the metabolic changes and oxidative stress (Cabungcal et al., 2013b, Steullet et al., 2017, Steullet et al., 2010). Thus, it may be possible that functional deficits play major role in disease pathogenesis over numerical deficits. Unfortunately, in this study, we did not have any data regarding cortical layers as the heterogeneity of the cytoarchitecture may contribute to the understanding of its functional organization, hence this is one of the limitations of this study.

3.4.8 Implication of PV+ cell loss for gamma frequency oscillations

Cognitive decline and motor impairments are core symptoms of DLB (McKeith et al., 2017), and gamma oscillations are thought to underlie these brain functions (Uehara et al., 2015, Robson et al., 2018b). The generation of these fast neuronal network oscillations relies heavily on the IPSPs from the interneurons where PV+ cells play an

essential role (Tremblay et al., 2016, Pelkey et al., 2017). Indeed, altered interneuron excitability is thought to critically contribute to impairments of the neural oscillatory synchrony and rhythms (Cardin, 2018, Gonzalez-Burgos et al., 2015, Gonzalez-Burgos and Lewis, 2008). In cortical networks, GABA neurotransmitter mediates inhibition signals form the interneurons, at the same time placing these interneurons in crucial position for the maintenance of the cognitive functions (Kann et al., 2014b).

PV+ interneurons display expanded mutual connections among themselves with strong inhibitory synapses, therefore, forming a fully functional network of interneurons, suited for the synchronization of the spiking activity with high temporal fidelity in cortical and subcortical regions (Tremblay et al., 2016, Pelkey et al., 2017, Krause et al., 2017). The PA depolarised from these interneurons form a subsequent synchronous IPSPs that inhibit multiple EPSPs and sometimes other IPSPs in the network (Kann et al., 2014b, Berger et al., 2010). This feature of connectivity facilitates the synchronous inhibition of multiple pyramidal cells in the network, therefore reflecting an intense GABAergic feedforward and feedback inhibition control over the pyramidal cells (Berger et al., 2010, Buzsáki and Wang, 2012, Tikidji-Hamburyan et al., 2015, Traub et al., 1996, Zheng et al., 2016). This GABAergic perisomatic and synchronous inhibition is thought to affect almost all pyramidal cells in the network, which will then reflect as the typical gamma frequency oscillations in the LFP recordings (Buzsáki and Wang, 2012, Tikidji-Hamburyan et al., 2015, Traub et al., 1996, Zheng et al., 2016). Thus, PV+ interneurons are thought to control the pattern and the timing of PA of the pyramidal cells. In fact, selective modification of glutamate receptors in PV+ interneurons affect the synchrony of gamma frequency oscillations, resulting in impairments of the cognitive functions (Mathalon and Sohal, 2015, Sohal, 2012b, Sohal et al., 2009). In contrast, pyramidal cells also contribute to the propagation of gamma frequency oscillations due to their specific activity patterns into downstream cortical and subcortical regions (Rotaru et al., 2012). Thus, it can be argued that gamma oscillations are the result of high PA, high synaptic efficacy and different local connectivity of the PV+ fast spiking interneurons, contrasting the lower spiking frequency and efficacy, but higher number of the pyramidal cells. In a coordinated manner the excitation and inhibition inputs are dynamically regulated and balanced by the interaction between PV+ and pyramidal cells (Kann et al., 2014b). The reduction of PV+ cells as observed here in this chapter in some regions of the

cortex, could hinder the gamma frequency rhythmogenesis, and thus affect the synchrony with other brain regions in DLB patients, resulting in the motor impairments and cognitive dysfunctions.

In addition, the changes in the glutamatergic excitatory activity or GABAergic inhibitory input to the excitatory cells, propels a sustained abnormal excessive discharge of synchronous activity of a large group of neurons that manifests as epileptic seizures (Aird and Gordon, 1993). Interneurons that contain GABA control the activity of the pyramidal cells, by restricting their excitatory input in both feedforward and feedback manner (Pelkey et al., 2017, Wendling et al., 2002). From the GABAergic interneuron subpopulations expressing calcium binding proteins calbindin D-28 (CB) and PV, specifically the PV+ chandelier cells are thought to play an essential role in controlling the excitability of the pyramidal cells (Woodruff et al., 2011, Berg et al., 2018, Rajkowska et al., 2007). In doing so, these neurons are thought to play important role in regulating and controlling the propagation of seizure activity (Sessolo et al., 2015).

Although there are no currently available studies that have reported impairments on gamma frequency oscillations in individual living with DLB, as most of the studies was carried out in animal models of synucleinopaties. Some studies have reported fast neuronal network abnormalities in individuals living with DLB. In fact, the changes in neuronal network oscillations are found to be pronounced in DLB in relation to other neurodegenerative dementias (van der Zande et al., 2018, Robson et al., 2018a). Alteration in the cortico-basal ganglia-thalamic loop in DLB has been reported to be associated with fast neuronal network impairments (Schumacher et al., 2019). This is in parallel with the finding presented in this chapter, as I demonstrate that PV+ cells, which plays essential role in gamma rhythmogenesis (Kann et al., 2014b), are reduced in the some brain regions of DLB patients, More specifically affecting the affecting the cortico-BG- thalamic loop. In fact, in the previous chapter I have shown that gamma oscillations are impaired in the DLB (A30P mouse model) due to mitochondrial dysfunction. Impairments of the interneuron functions or its consequent death, is thought to lead to neuronal network hyperexcitability (Kann et al., 2014b, Sun et al., 2012). This hyperexcitability underlie gamma network oscillations impairments (Tweedy et al., 2021). In fact, it is thought that altered interneuron excitability critically contributes to impairments of the neural synchrony and rhythm of the fast network oscillations (Cardin, 2018, Gonzalez-Burgos et al., 2015). Notwithstanding, the relative

preservation in PV+ cell numbers in some regions presented in this chapter, it is possible that interneuron function is significantly altered before neuronal cell death, due to the in ability of PV proteins to buffer calcium. This could lead to calcium overload in the neuron and the subsequent hyperexcitability, which underlie the impairments in the gamma frequency band, as demonstrated in the previous chapter, which parallels with the findings presented in this chapter. A limitation to this study is that it was not possible to quantify the amount of PV protein presented in a single PV+ cell in DLB and compare it with non-DLB cases. It is important to highlight as well, that the exclusive focus on gamma frequency oscillations in my research does not undermine the importance of other slower neuronal network oscillations for higher brain functions.

3.5 Conclusions

In this chapter, I predicted that the number of parvalbumin expressing interneurons would be reduced in regions that are affected with pathological burden of αSyn, and the results presented showed that the density of PNN and PV+ some regions of the brain of patients with DLB, as well as in the hippocampus and PFC of 9+ A30P mouse are altered. Parvalbumin expressing cells are significantly altered in areas such as the motor cortex, Globus pallidum, caudate nucleus thalamus and the amygdala, including the insular and entorhinal cortices, which are areas associated with the development of prodromal stages of the disease and are associated with higher LBs Burden. Despite some results presented no statistical significance, it is clear that in some cases there is trend to reduction in the PV interneurons. In fact, the loss of interneurons and the subsequent, impairments of gamma frequency oscillations have been reported in other neuropsychiatric disorders. The deficits presented in this chapter parallel those findings in the neuropsychiatric and other neurodegenerative diseases as the neural desynchrony observed in these studies are found to be associated with loss of PV+ cells (Uhlhaas and Singer, 2006, Uhlhaas and Singer, 2012). I believe these slight changes in the density of this interneuron populations can have negative impact in the normal functioning of these cells. The deficits may be functional either by protein dysfunction or cellular atrophy, not necessary translated in the reduction of cellular numbers. Moreover, in biological terms statistical insignificance of the results does not automatically reject the null hypothesis, as the quantification of the cells may not explain the αSyn-related damage into these highly sensitive and metabolism-dependent cells. Therefore, the results presented in this chapter are still biologically relevant, as there was clear differences and tendencies in the results above described. Moreover, no studies related to the neuroanatomical quantification of PV+ interneurons in most regions analysed in this chapter have been published so far. To my knowledge, this is the first study attempting to quantify the PV+ interneurons in different brain regions of individuals affected with DLB.

Chapter 4: Distribution of posttranslational modifications in Lewy body dementias

4.1 Introduction

As previously mentioned, LBs and LNs are intracytoplasmic deposits abundant with αSyn protein, which has become misfolded and aggregated, and is considered the main constituents of these inclusions (Nemani et al., 2010). Although, the precise mechanisms that trigger these aggregations are still unclear, it is known, that toxic forms of αSyn underlie the formation of these inclusions. Indeed, Normal αSyn is involved in synaptic vesicle trafficking and function (Lashuel et al., 2012). Nevertheless, pathological αSyn can form aggregates and trigger a series of pathogenic cascades typical of neurodegenerative proteinopathies (see chapter 1) (Obeso et al., 2010, Lin and Beal, 2006, Robson et al., 2018b). Whether the pathogenic consequences of DLB arise from the pre-aggregated forms of αSyn, i.e. before LBs/ LNs formations, or after, is still an object of an ongoing debate. To enlighten this, several literatures have reported that αSyn is subjected to monumental PTMs such as ubiquitination, nitration and phosphorylation. These changes are thought to modify the structure and function of the protein in pathological conditions (Junqueira et al., 2018, Barrett and Timothy Greenamyre, 2015, Omenn et al., 2016). In fact, Nitrated and phosphorylated αSyn have been found in brains of PD patients and phosphorylation at residue serine[129] was found to be the most prevalent form of PTMs in αSyn (Fujiwara et al., 2002, Neumann et al., 2002, Rocha et al., 2018). This is also supported by studies using transgenic mouse models that overexpress human mutant αSyn (A30P, A53T) and also those overexpressing wild-type human αSyn, showing phosphorylation of αSyn at serine[129] (Kahle et al., 2002, Wakamatsu et al., 2007). In addition, other studies have reported phosphorylation at amino acids tyrosine and threonine (Cozzone, 2005, Santos and Lindner, 2017, Rocha et al., 2018). Nevertheless, in regarding to phosphorylation, the results presented in this chapter focuses on αSyn phosphorylation at serine [129] (Pser [129]). Furthermore, nitration and ubiquitination are also found to be process of PTMs in αSyn. For instance, nitration may lead to fibrillogenesis by affecting αSyn solubility (Giasson et al., 2000). Indeed, high levels of nitrated αSyn contained in LBs were found to be linked to oligomer formation, mitochondrial dysfunction and neuronal apoptosis (Liu et al., 2011, Giasson et al., 2000). On the other hand, ubiquitination can affect protein degradation, therefore influencing protein localization, folding, concentration and aggregation. In a similar manner, the function of αSyn protein and its conformation may also be influenced by

phosphorylation, by inducing pathological conformational changes that potentiate the addition of other PTMs such as Ubiquitination and thus, impairing the subcellular localization of the protein (Reviewed in Tenreiro et al., 2014).

Despite the intensive studies to decipher how Phosphorylation, Ubiquitination and Nitration can influence αSyn toxicity, the exact mechanism that triggers its aggregation and pathogenicity is still to be unveiled. Assuming that, PTMs play an important role in the disease's pathogenesis, further study is needed, to unveil the impact of these PTMs on the synucleinopathies, in particular in LBDs, for better therapeutic strategy and intervention. The work presented here sheds some light in the involvement of these PTMs in αSyn dysfunction and aggregation. I hypothesized that αSyn PTMs are one of the early events that trigger the aggregation and/or dysfunction of the protein, possibly altering its physiological sub-cellular distribution (e.g., the nucleus or mitochondria), which in turn affect the normal function of neuronal cells. These changes may facilitate the formation of toxic forms of the protein that will then lead to neuronal cell death of a vital group of neurons such as those that plays key roles in the generation of the fast neuronal network oscillations, namely PV+ cells. Moreover, different PTMs may occur at different stages of the disease progression. Hence, identifying those most common and the ones that occur earliest may give us an insight of which PTMs, alter the function of the protein and their distribution. In LBDs, these PTMs may affect important cortical and subcortical structures, such as, locus coeruleus, the substantia nigra, the reticular formation, hippocampus, thalamus and the neocortex, commonly known to be affected in LBDs. Furthermore, early occurring PTMs may emerge in different brain regions at different stages of the diseases, depending on the relative vulnerability of each regions and the specificity of each diseases among the LBDs. Specifically, those regions, which are affected earliest in the disease according to Braak LB pathology / McKeith scale, I believe, they would present these PTMs earliest. Therefore, here I assessed the involvement of these PTMs of αSyn in post-mortem brain tissue of LBDs patient. This investigation is key to aid the comprehension and discernment of potential reasons for the pathological aggregation and the observed preference of distribution patterns seen in LBDs, in comparison with other synucleinopathies, as well as it provides an insight to achieve the efficacy in the therapeutic approach.

4.2 Methods

4.2.1 Human brain tissues

Tissue microarray (TMA) sections from different brain regions were examined for phosphorylated, nitrated and ubiquitinated αSyn using standard immunohistochemical staining. Two methods of antigen retrieval were first used (EDTA-based and Citrate-based) to determine the most appropriate for each experiment, although most sections reacted well to the EDTA. These methods were selected according to the manufacturer's recommendations, depending on the antibody specificity. To start with the experiments, slides were first pre-warmed in LEEC oven for 30 minutes, then dewaxed and rehydrated in alcohol gradient 99%(2x) 80% and 70% for 5 minutes each, before immunostaining. The slides were submerged into a boiling EDTA solution (2.86 mM, pH 8) within a pressure cooker for 8 minutes followed by a 2-minute heating at full pressure. After, the boiling procedure, all slides were washed 3 times for 5 minutes each with Tris buffered saline (TBS) pH 7.6 and Tris buffered saline with tween 20® (TBST) pH 7.6. Then Hydrogen peroxide (H_2O_2) 10% was added to block the action of endogenous peroxidases, and then the slides were demarcated with a pap pen. Next, nitrated αSyn antibody 1:200 (Thermofisher, UK) specific to nitration modification 1:50 (αSyn Tyr[133,125]), phosphorylated αSyn protein (αSyn Pser[129]) or anti-ubiquitin antibody 1:500 (Abcam, UK), were added as the primary antibody and incubated for 1h at room temperature. Next, the slides were washed with TBST 3 times for 5 minutes each, then yellow cap universal probe (Menapath, UK), was used as the secondary antibody and incubated for 30 minutes at room temperature. Once the sections were washed with TBST, avidin-biotinylated horseradish peroxidase (HRP)-Polymer (red) (Menapath HRP multipolymer), was added for 30 minutes at room temperature and sections were washed again with TBS 3 times for 5 minutes each and the chromogen DAB was added for approximately 3 minutes. Next, slides were washed in running water for 10 minutes and then submerged in Mayer's haematoxylin solution (Sigma Aldrich,UK) for 20 seconds. Slides were then washed in water, differentiated with 1% hydrochloric acid, in 70% ethanol for 2 seconds and then blued with 1% ammonia water for 2 seconds. Slides where washed again in normal flowing water for 2 seconds, to be then dehydrated in alcohol concentration 70% 80% and 99 % (2x) 5 minutes each. The sections were then transferred to clearing xylene 1 and 2, for 10 minutes each and then mounted with DePex destrene (DPX, Cellpath, Newton,

UK). For the negative controls, the primary antibodies were omitted but all other steps were followed as described above.

4.2.2 Data capture and analysis

TMA images were captured using an automated system consisting of a Nikon Eclipse 90i microscope, mounted with a DsFi1 camera (Nikon) and processed in NIS element software v 3.0 (Nikon). For the experiments here presented, I examined only freshly stained samples. First, position of the first of the cores on a TMA slide (figure 2.3) was mapped in the NIS element software, followed by a macro designed to take a map of the remaining 39 (figure 2.3). Image of each 40-tissue cores that contains in a single TMA tissue slide. The microscope was firstly positioned at the centre of the first tissue core at 10x magnification for guidance and brought into focus at 100x magnification, for background correction. After mapping all 40-tissue cores, the microscope was directed to the mapped co-ordinates of the first tissue core, and images of all the tissue cores were sequentially taken automatically. Following the completion of data capture, regions of interest (ROIs) were applied to each image manually to exclude any sample abnormalities such as folded tissues, tears, and regions consisting of white matter. A restriction threshold was then applied to capture all immuno-positive foci. In cases where the slides were missing a tissue core or simply one or some tissue cores were too damaged to be included in the analysis, the tissue core number and position were noted manually, and captured data was excluded.

The immuno-positive signal in each ROI was then calculated automatically after application of a pre-selected threshold. The red, green and blue (RGB) thresholds were set separately for each PTM-specific antibody signal, and the thresholds were set at a level that the immuno-positive pathological structures (LBs and LNs) were detected. The values of RGB intensity are measured on a scale between 0-255 (NIS elements user guide v 3.0, 2008, Nikon, Surrey UK) and were set as follows: p-αSyn[Ser129] (R25-170, G27-156, B11-126), n-αSyn[Tyr125,133] (R50-180, G20-168, B8-139) and ub-αSyn (R15-161, G7-139, B4-133) to minimize measurement of a non-specific background signal. The percentage area of the tissue covered by immuno-positive LBs and LNs were subsequently calculated and automatically exported into an excel spreadsheet. Mean values were then calculated for each brain region that was represented by more than one tissue core. All data graphs were generated and

exported from GraphPad prism (GraphPad Software, Inc., version7. USA) (Please see chapter 3).

The reported findings, are specific for aSyn PTMs at Pser129, because the recombinant Anti-alpha synuclein antibody (EP1536Y) used in this work was reported to have the highest specificity and sensitivity for detecting Pser129 αSyn in LBs (Delic et al., 2018). Similarly, the sensitivity and specificity of the Anti-Ubiquitin antibody was also reported (Meng et al., 2020). Although LBs are composed of more than 90 proteins, the detected signals for phosphorylation and Ubiquitination are specific for aSyn. Nevertheless, for the nitration Antibody, it seemed to pick non-specific signals, that fit the standard criteria of our Lab, selected for LBs and LNs.

4.2.3 Statistical Analyses

All data were statistically analysed using GraphPad Prism 9 (GraphPad Software, Inc., version 9.1.0. USA) and Sigma Plot (Systat software, USA). Statistical significance was defined as significant $*p < 0.05$, $**p < 0.01$ and $***p < 0.001$. To determine the normal distribution of the data and equal variance, the Shapiro-Wilk test and the Brown-Forsythe tests were used, respectively. The data were normally distributed and plotted as mean ± standard error of the mean (S.E.M.) as bar charts or box plots depicting the medians with interquartile range (IQR, Q1-Q3) or percentage change. When comparing multiple groups, I used Kruskal-Wallis one-way ANOVA. Pairwise multiple comparison (Dunn's or Tukey test) was used when p value (reported as significant, <0.05 and <0.001) in the ANOVA test showed significance, to determine which parameters were significantly different. For the analysis of the effects of two independent variables in the same sample, I used a two-way ANOVA with Bonferroni post hoc test, to determine which parameters where particularly different in the interaction between the disease groups and regions of the brain in study. Error bars represented standard deviation and the data were reported with F-value, degree of freedom an p value, which was reported as significant, $*<0.05$ and $**<0.001$. Sample sizes are shown in the respective figure legends.

4.3   Results

4.3.1   Regional comparison of phosphorylation of αSyn in post-mortem LBD cases.

Here I started with the analyses of the overall regional Interactions between disease groups and cerebral regions. The results presented, showed that cortical regions from LBDs were significantly different from the cortical regions in the control cases, with the cingulate cortex being the most affected region in DLB and the IC in PDD (Two-way ANOVA followed by Bonferroni Multiple Comparison post hoc test $F_{(3,24)}$ =2.053***P< 0.0001). Significant differences were also observed among the disease groups, with higher immunoreactivity circumscribed between DLB and PDD (Two-way ANOVA followed by Bonferroni Multiple Comparison post hoc multiple comparison test $F_{(3,24)}$ =4.642 *P< 0.0134). Nevertheless, in the subcortical regions, the interactions were even more markedly evident between regions from LBDs compared to control, particularly in the amygdala, where the highest immunoreactivity were observed in LBDs (Two-way ANOVA followed by Bonferroni Multiple Comparison post hoc test $F_{(3,15)}$ =1.844***P< 0.0001). Similarly, very significant differences were also observed between the disease groups, compared to control cases with higher immunoreactivity circumscribed in DLB (Two-way ANOVA followed by Bonferroni Multiple Comparison post hoc test $F_{(3,15)}$ =11.21***P< 0.0002). Thus, suggesting that the immunoreactivity of phosphorylated αSyn is high in LBD cases (Figure 4.6 and 4.7).
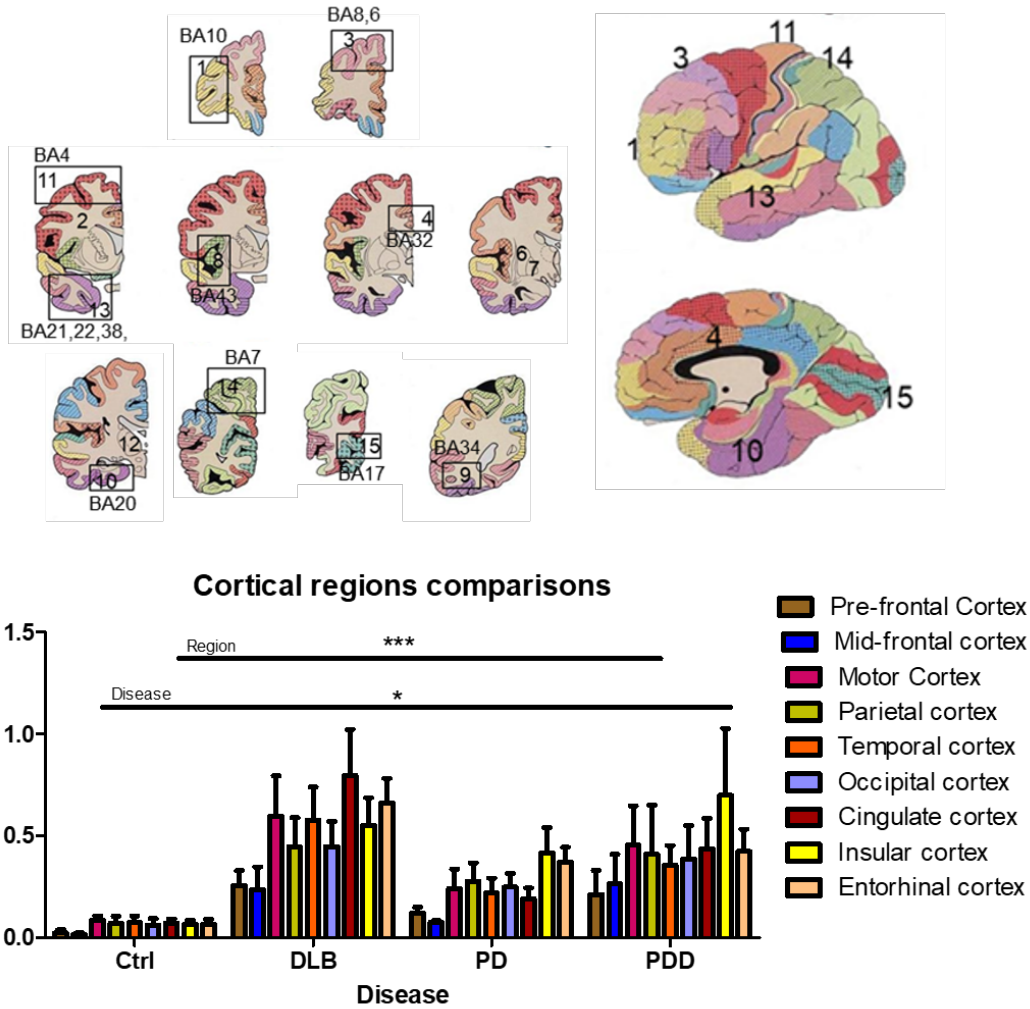
Figure 4. 1: Widespread phosphorylation is observed across cortical brain regions of LBD patients. A Representative image from Newcastle brain bank indicating the regions where the sections were extracted for this study. **B** Bar chart showing the comparison of percentage coverage of αSyn Pser[129] immunoreaction in cortical region. CC is the most affected region in DLB, whereas the IC is the most affected region in PD and PDD.
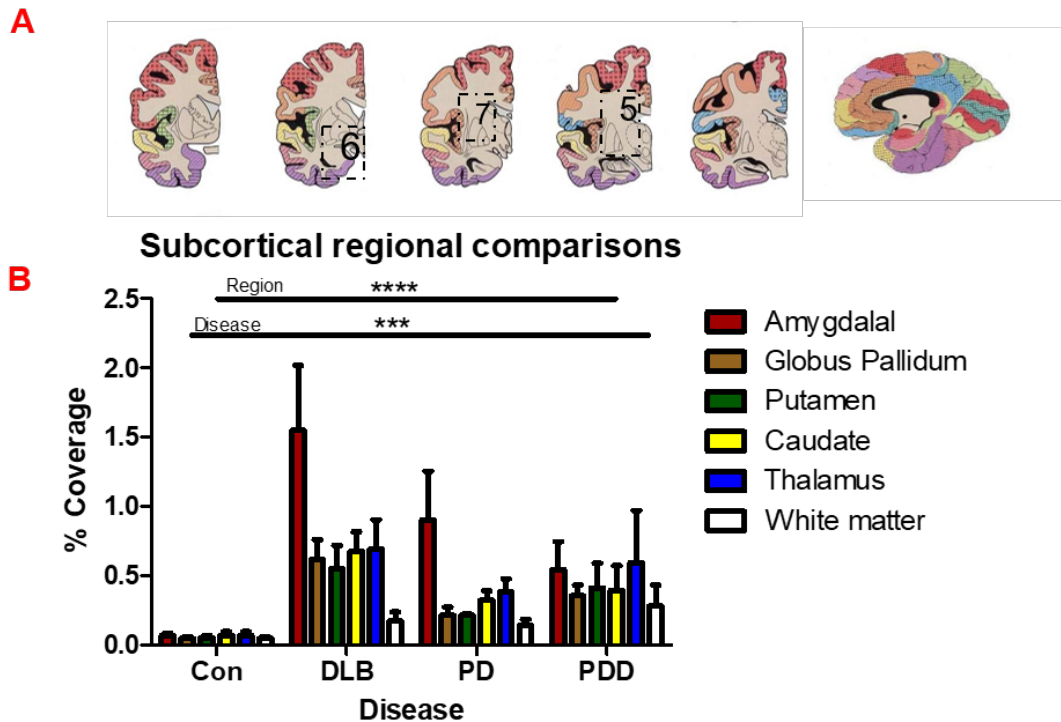
Figure 4. 2: Widespread phosphorylation is observed in subcortical regions of LBD patients. A Representative image from Newcastle brain bank indicating the regions where the sections were extracted for this study. **B** Bar chart showing the comparison of percentage coverage of αSyn Pser[129] immunoreaction in cortical region. The amygdala is the most phosphorylated region in LBDs.

4.3.2 αSyn is phosphorylated in prefrontal and midfrontal cortices but not in motor cortex of LBD patients.

Following the interaction analysis, I wanted to explore the specificity of these affectations per region of the brain. In similitude with the previous chapter, I started with the analysis of these pathological hallmarks in the frontal lobe of post-mortem brain tissue from healthy control and LBD cases. This region was divided into three areas (the PFC, MFC, MC) according to their organization in the TMA slide. Here, I predicted that the density of phosphorylated αSyn at serine[129] would be increased in these regions of post-mortem brain tissue of individuals that were clinicopathologically diagnosed with LBDs. Indeed, following the histochemical staining using the antibodies specific for αSyn phosphorylation (Pser[129]), intra-neuronal inclusions (LBs) with/without dystrophic neuronal processes (LNs) were observed brain tissues of DLB,

PD and PDD patients. A widespread phosphorylation of αSyn was observed within all LBDs in PFC, and the overall comparison between disease group showed statistically significant differences compared to control cases (Kruskal-Wallis test ANOVA followed by Dunn's Multiple Comparison test $*P<0.0108$). However, they were highly significant in DLB cases when compared to control and other disease groups ($**P<0.0051$), as no significant differences was observed in the number of LBs/LNs between PD and PDD cases (figure 4.1).

Considering the significant presence of phosphorylated αSyn observed in the rostral area of the frontal cortex. I assessed the neuroanatomical distribution of Pser[129], the MFC of LBD cases. Here I show that the distribution of phosphorylated αSyn is significantly increased in MFC tissues from LBD cases compared to control (Kruskal-Wallis test ANOVA followed by Dunn's Multiple Comparison test $**P<0.0078$). The changes were more evident in DLB and PDD compared to control and PD cases, where no statistically significant changes were observed in the number of LBs/LNs. Having found significant changes in PFC and MFC, of LBD patients, I extended the analysis to the MC. Here, the distribution of phosphorylated αSyn was not significantly increased in LBDs cases compared control (Kruskal-Wallis test ANOVA followed by Dunn's Multiple Comparison test $P>0.0709$), and no significant changes was observed in the number of LBs/LNs between the LBD group (Kruskal-Wallis test ANOVA followed by Dunn's Multiple Comparison test post $P>0.05$) (figure 4.1).
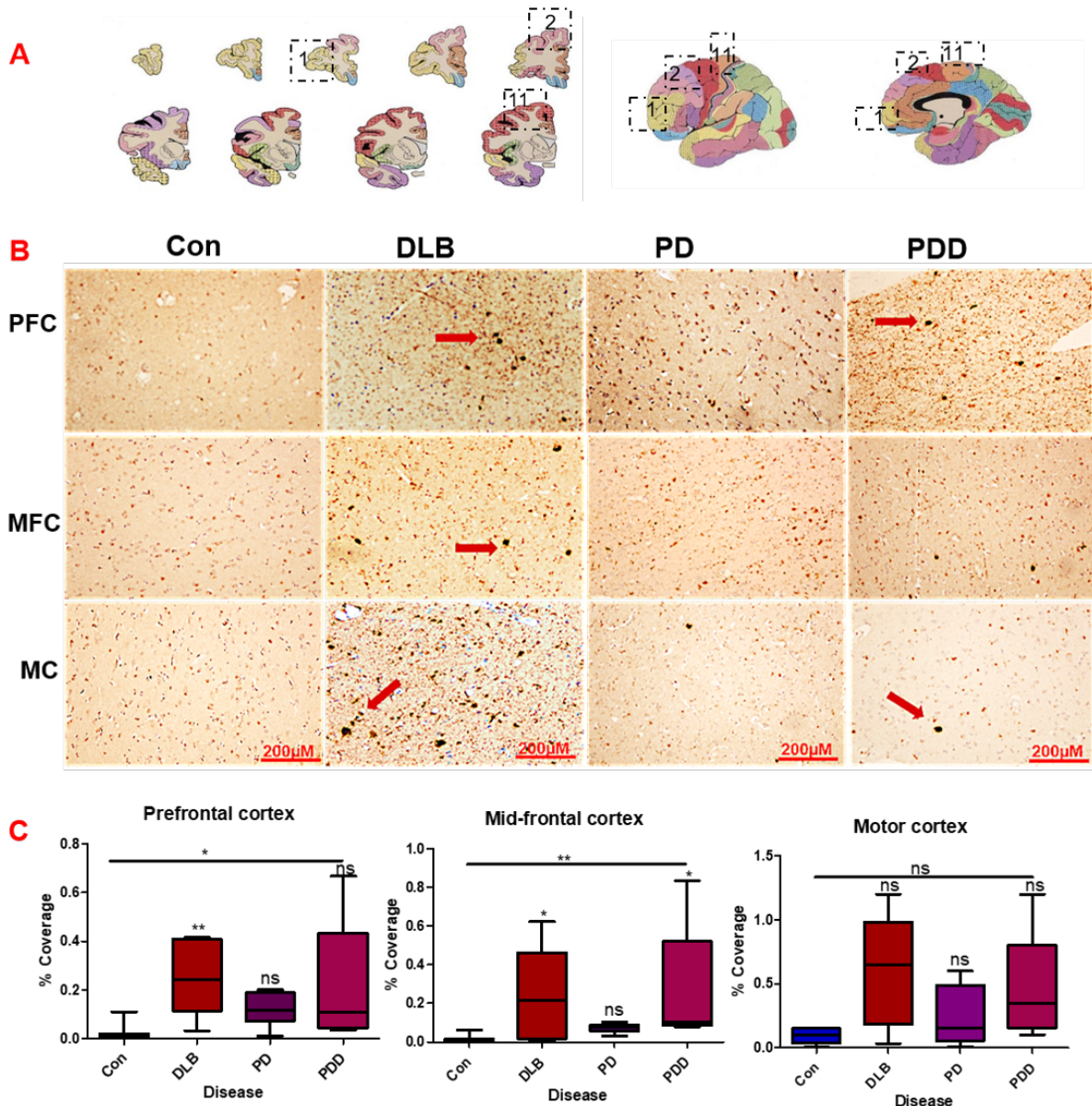
Figure 4. 3: Widespread phosphorylation is observed in frontal Lobe of DLB, but not in PD and PDD post-mortem cases. (A) Representative images from Newcastle brain Map, showing brain regions PFC=1, MFC=2 and MC=11 where the sections were taken for this study according to their organization in TMA slides. **(B)** Images showing phosphorylated LBs/LNs in from number of sections of PFC, MFC and MC of post-mortem brain tissue of LBD, at 10 X magnification. The arrows (in red) indicating the LBs. **(C)** Box plot showing the comparison of percentage coverage of LBs/LNs distribution in both LBD and control patients. The percentage coverage of LBs/LNs inclusions that are phosphorylated in PFC of control (n=7 cases), DLB (n=5 cases), PD (n=6 cases), PDD (5 cases), was statistically significant in LBD cases (*P<0.0108) compared to control. Similarly, the percentage coverage of LBs/LNs inclusions that

are phosphorylated in MFC of control (n=7 cases), DLB (n=5 cases), PD (n=6 cases), PDD (5 cases), was statistically significant in LBD cases compared to control (P>0.0078). However, the percentage coverage of LBs/LNs that are phosphorylated in MC of control (n=7 cases), DLB (n=5 cases), PD (n=6 cases), PDD (5 cases), was not statistically significant in LBD when compared to control cases.

4.3.3 Widespread phosphorylation of αSyn in major sensory cortices of LBD cases.

The quantification of Pser^{129} in sensory cortices including the PC, TC and OC is shown in figure 4.2. Under simple examination a higher density of phosphorylated LBs/LNs, inclusions were observed in PC of LBD patients. The changes in PC of LBD cases where statistically significant when compared to control (Kruskal-Wallis test ANOVA followed by Dunn's Multiple Comparison test *P<0.0402). However, the results were not statistically significant within the LBDs groups. Similar results were observed in TC. Here it was evident that Pser^{129} phosphorylated αSyn is significantly expressed in LBD cases, compared to control (Kruskal-Wallis test ANOVA followed by Dunn's Multiple Comparison test *P<0.0159). Statistically, significant results were evident In DLB when compared to other PD, PDD and control cases. Likewise, in the OC, I found that phosphorylated αSyn is significantly increased in LBD cases, compared to control (Kruskal-Wallis test ANOVA followed by Dunn's Multiple Comparison test *P<0.0196). However, the difference was evident in DLB cases when compared to PD, PDD and control (*P<0.0420). Overall, the number of αSyn Pser^{129} were significantly increased in major sensory areas of post-mortem brain tissue of LBD patients.
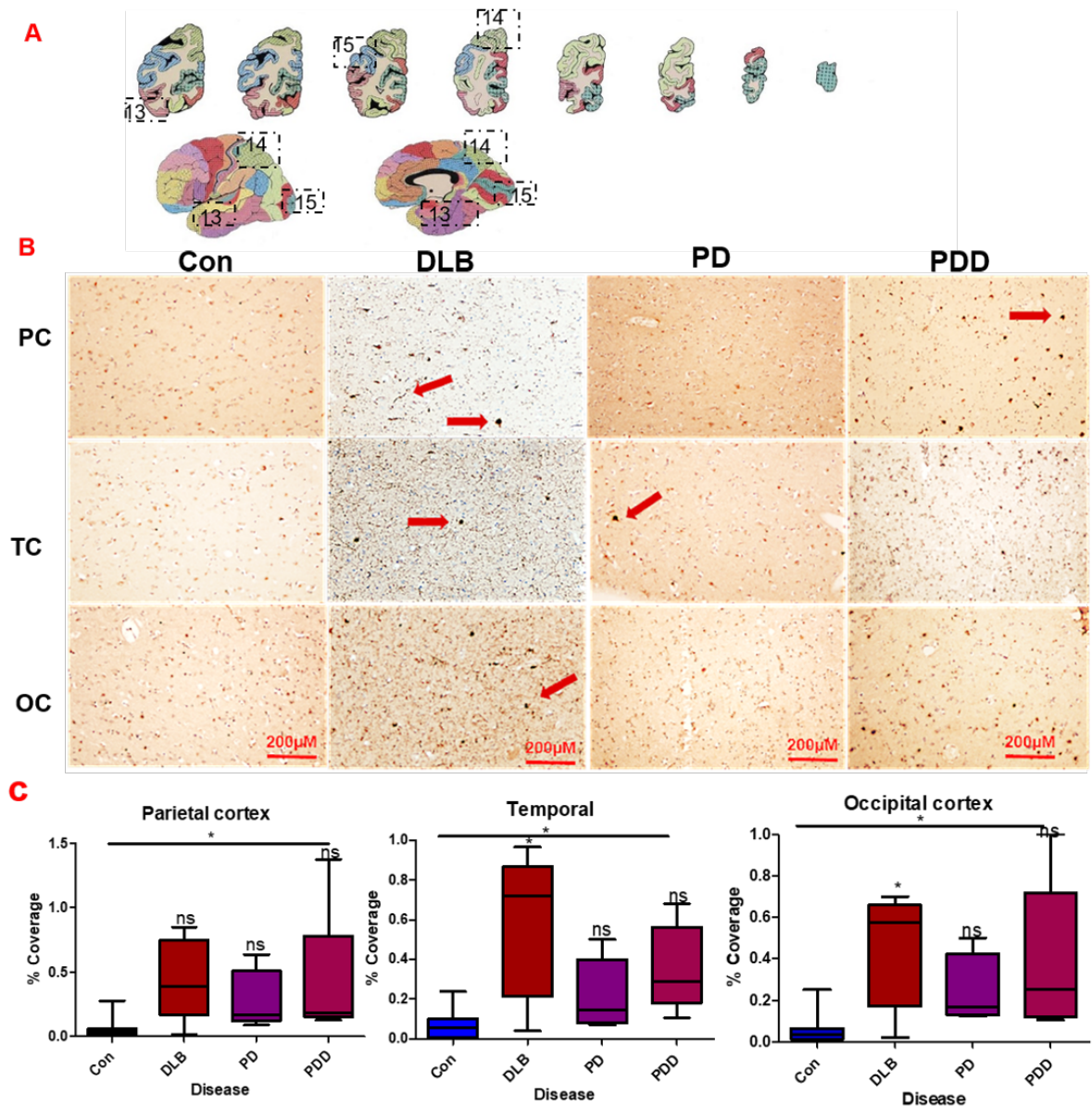
Figure 4. 4: Widespread phosphorylation in major sensory cortices of LBD cases. (A) Representative images from Newcastle brain Map, showing brain regions PC=14, TC=13 and OC=15 where the sections were taken for this study according to their organization in TMA slides. **(B)** Images showing phosphorylated LBs/LNs in from number of sections of PC, TC and OC of post-mortem brain tissue of LBD cases, at 10X magnification. The arrows (in red) indicating the LBs/LNs. **(C)** Box plot showing the comparison of percentage coverage of LBs/LNs distribution in control (n=7 cases), DLB (n=5 cases), PD (n=6 cases), PDD (5 cases), was statistically significant for LBD cases when compared to control in PC (*P<0.0402). However, in TC, the percentage coverage of LBs/LNs distribution in control (n=7 cases), DLB (n=5 cases), PD (n=6 cases), PDD (5 cases), although, was statistically significant for all LBD cases

(*P<0.0159), post-hoc test showed that this difference was more accentuated in DLB cases, but not for PD and PDD (ns). Similarly, the percentage coverage of LBs/LNs in control (n=7 cases), DLB (n=5 cases), PD (n=6 cases), PDD (5 cases) in the OC, was statistically significant in all LBD cases compared to control (P<0.0159), and post-hoc test showed that the significance was evident in DLB cases, but not for PD and PDD.

4.3.4 Phosphorylation of αSyn is increased in infracortical structures of LBD cases.

These regions include the EC, CC and IC. Here, I found that that, in the EC, immunoreaction to LBs/LNs by antibodies specific for αSyn Pser[129], were observed brain tissues of LBD cases. The widespread phosphorylation of αSyn was markedly observed within DLB and PD, with statistically significant results among the LBDs. This difference was highly significant when compared to control cases (Kruskal-Wallis test ANOVA followed by Dunn's Multiple Comparison test **P< 0.0016). Similarly, in the CC LBs/LNs immunoreactivity to αSyn Pser[129] within the LBDs were highly significant when compared to control cases (Kruskal-Wallis test ANOVA followed by Dunn's Multiple Comparison test **P< 0.0023). Within the disease group, statistically significant differences were observed in DLB and PDD, but not in PD cases. Identical results were observed in the IC, where highly significant differences were observed between the LBDs and the control cases. However, among the disease groups (within the LBDs) the differences where only statistically significant in DLB and PDD cases, similar to the observations in the CC (Kruskal-Wallis test ANOVA followed by Dunn's Multiple Comparison test **P< 0.0030). The high significance observed in these regions that are involved in the early development of DLB, sheds light on the temporal occurrence of these changes in the LBDs (Figure 4.3).
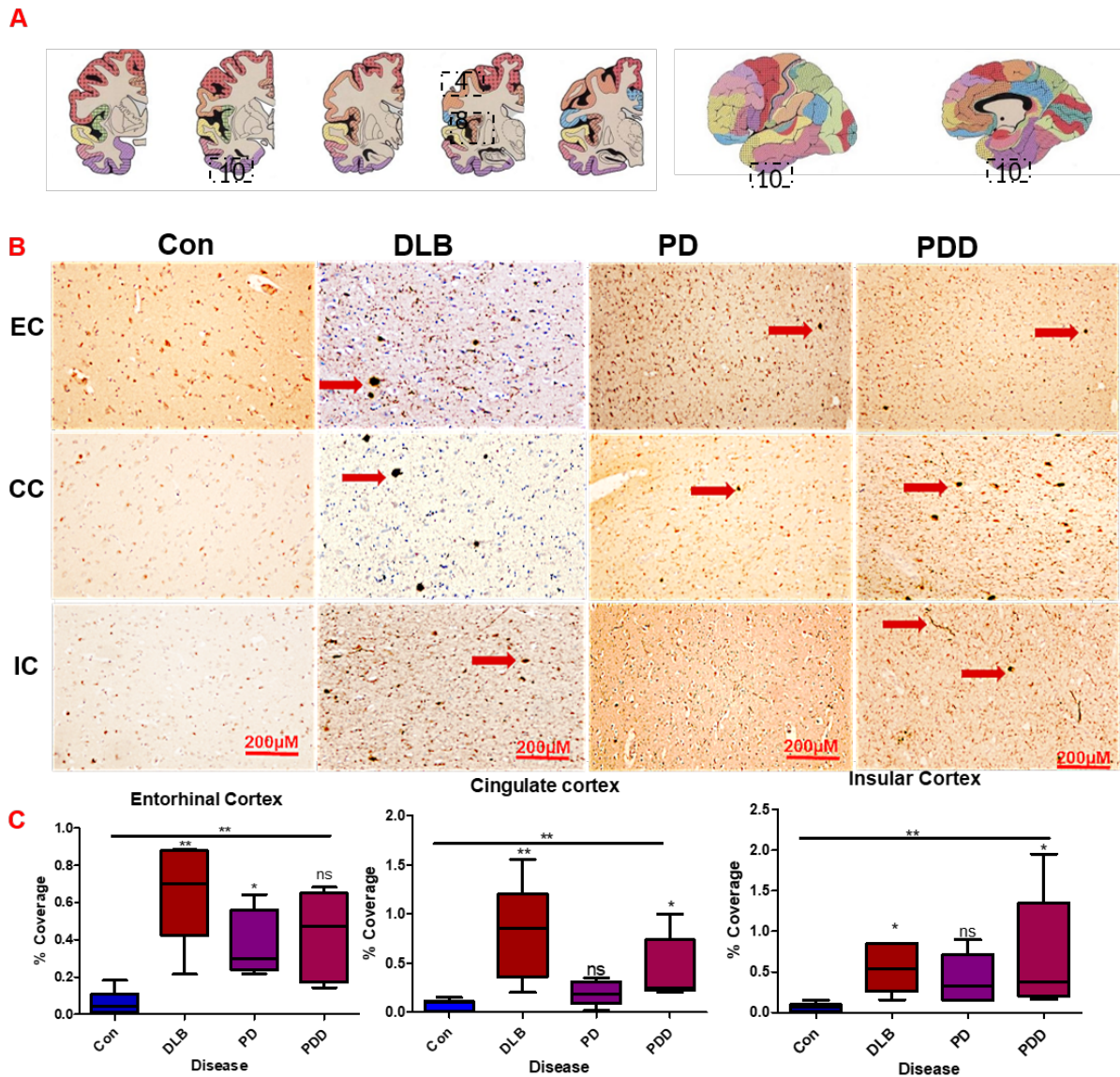
Figure 4. 5: Widespread phosphorylation of αSyn in EC, CC, and IC of LBD cases. (A) Representative images from Newcastle brain Map, showing brain regions EC=10, CC=4 and IC=8 where the sections were taken for this study according to their organization in TMA slides. **(B)** Images showing phosphorylated LBs/LNs in from number of sections of EC, CC and IC of post-mortem brain tissue of LBD, at 10 X magnification, the arrows (in red) indicating the LBs/LNs. **(C)** Box plot showing the comparison of percentage coverage of LBs/LNs distribution in EC, control (n=7 cases), DLB (n=5 cases), PD (n=6 cases), PDD (5 cases), the results were statistically significant for LBD cases when compared to control (**$P < 0.0016$). Post-hoc test showed that this was more accentuated in DLB cases and PD, but not for PDD. Similar results observed in CC, were the percentage coverage of LBs/LNs distribution in control (n=7 cases), DLB (n=5 cases), PD (n=6 cases), PDD (5 cases), was

statistically significant for all LBD cases, compared to control (**P<0.0023) post-hoc test showed that this was more accentuated in DLB cases and PDD, but not for PD. Similarly, the percentage coverage of LBs/LNs in control (n=7 cases), DLB (n=5 cases), PD (n=6 cases), PDD (5 cases) in the IC, was statistically significant in all LBD cases compared to control (**P<0.0030). Post-hoc test showed that the statistical significance was evident in DLB cases and PDD, but not for PD.

4.3.5 Extensive phosphorylation of αSyn in the basal ganglia of LBD patients.

Next, I analysed the subcortical structures included in the basal ganglia comprising the, CN, PTm and GP. Here I observed that immunoreaction to αSyn Pser[129] Antibody, was markedly evident in the whole BG. Areas such as GP, showed highly significant difference between the LBDs and control. However, post-hoc analysis showed that the difference among the disease groups was highly significant in DLB and PDD but not in PD. (Kruskal-Wallis test ANOVA followed by Dunn's Multiple Comparison test **P< 0.0012). Similar results were observed in CN, which also showed overall significant differences between LBDs and control cases. Nevertheless, the changes among LBDs were only significant in DLB (Kruskal-Wallis test ANOVA followed by Dunn's Multiple Comparison test **P< 0.0050). Identically, PTm, immunoreactivity to αSyn phosphorylation, was highly significant in LBDs when compared to control cases. The difference was also observed within the LBDs where highly significant results was observed in DLB and PDD but not in PD cases (Kruskal-Wallis test ANOVA followed by Dunn's Multiple Comparison test **P< 0.0020) (Figure 4.4).
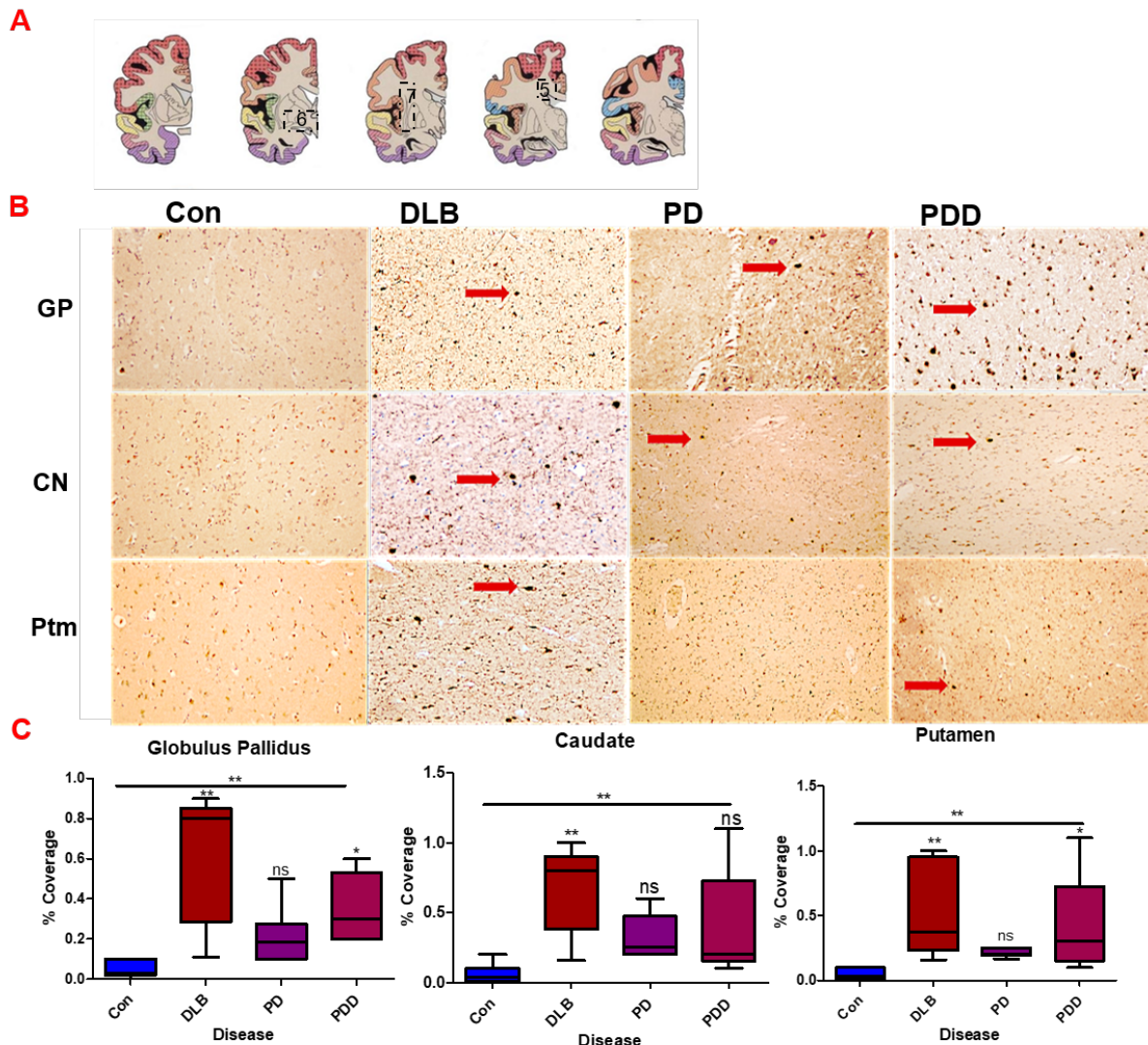
Figure 4. 6: Extensive phosphorylation of αSyn in the basal ganglia of LBD patients. (A) Representative images from Newcastle brain Map, showing brain regions GP=7, CN=5 and PTm=6 where the sections were taken for this study according to their organization in TMA slides. **(B)** Images showing phosphorylated LBs/LNs in from number of sections of GP, CN and PTm of post-mortem brain tissue of LBD, at 10 X magnification. The arrows (in red) indicating the LBs. **(C)** Box plot showing the comparison of percentage coverage of LBs/LNs distribution in control (n=7 cases), DLB (n=5 cases), PD (n=6 cases), PDD (5 cases), was statistically significant for LBDs cases when compared to control in GP (**P<0.0012), with highly significance in DLB cases. However, in CN, the percentage coverage of LBs/LNs distribution in control (n=7 cases), DLB (n=5 cases), PD (n=6 cases), PDD (5 cases), was statistically significant for all LBD cases (**P<0.0050), nevertheless, post-hoc test showed that this was more accentuated in DLB cases, but not for PD and PDD.

Similarly, the percentage coverage of LBs/LNs in control (n=7 cases), DLB (n=5 cases), PD (n=6 cases), PDD (5 cases) in PTm, were significant in all LBD cases compared to control (**P<0.0020), and post-hoc test also showed significance in DLB cases, but not for PD and PDD.

4.3.6 αSyn is phosphorylated in the amygdala and the thalamus of LBD patients.

In the thalamus, there were significant differences between the LBDs and control cases, and post-hoc analysis showed that the difference among the disease groups was highly significant in DLB, but not in PD and PDD cases. (Kruskal-Wallis test ANOVA followed by Dunn's Multiple Comparison test post hoc multiple comparison test *P< 0.0122). Identical results were observed in the amygdala, where significant differences were observed between LBDs and control, and αSyn Pser[129] immunoreactivity was markedly evident in the DLB cases (Kruskal-Wallis test ANOVA followed by Dunn's Multiple Comparison test *P<0.02082). I finally tested the immunoreactivity of Pser[129] antibody in the white mater, however, no evidence of LBs was observed, as these inclusions are usually found within the neuronal populations in the cortex (Figure 4.5).
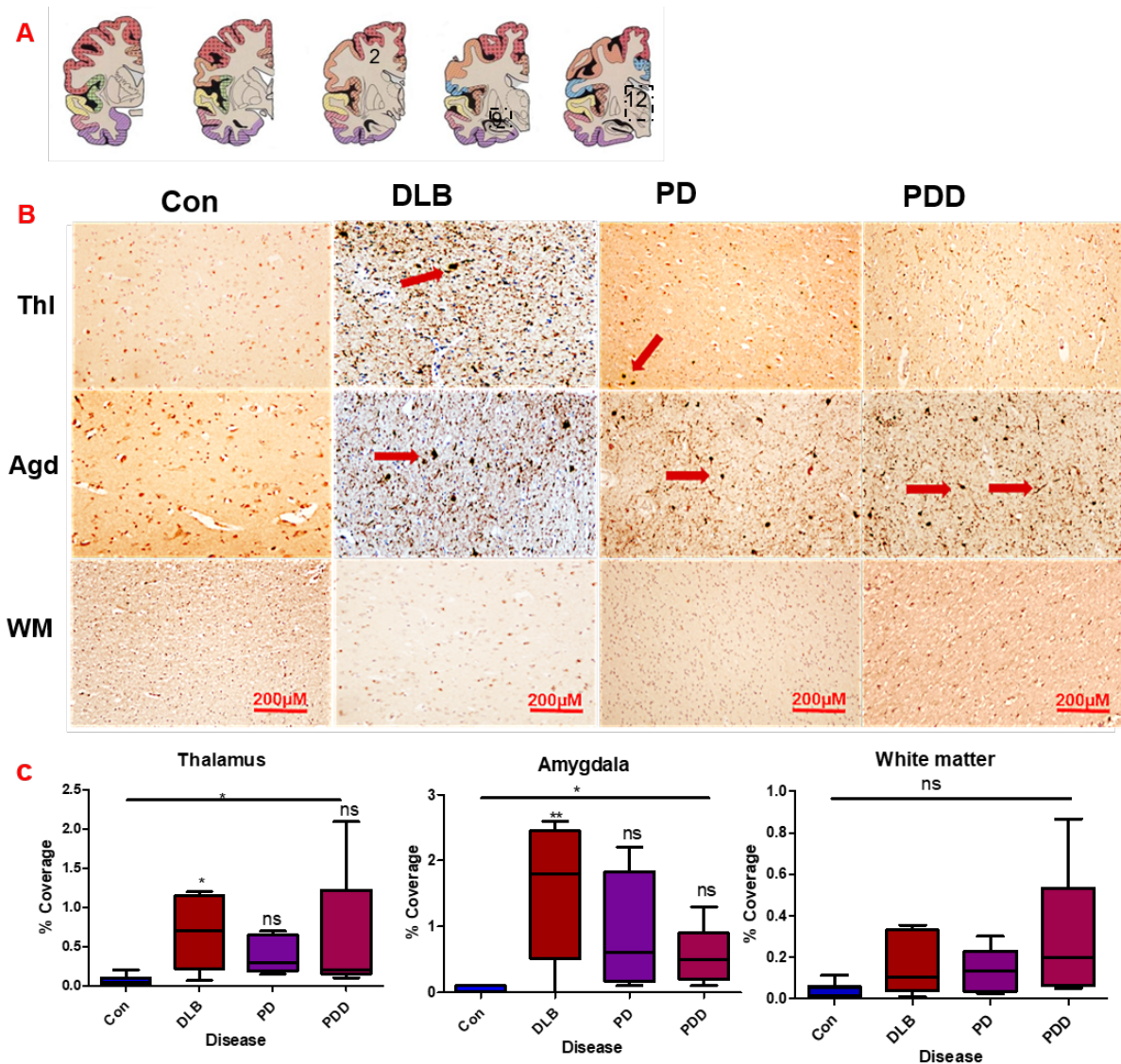
Figure 4. 7: αSyn is phosphorylated in the amygdala and the thalamus of LBD patients. (A) Representative images from Newcastle brain Map, showing brain regions Thalamus=12, Amygdala=9 and White matter=2 where the sections were taken for this study according to their organization in TMA slides. **(B)** Images showing phosphorylated LBs/LNs from number of sections of Thalamus and Amygdala of post-mortem brain tissue of LBD, at 10 X magnification. The arrows (in red) indicating the LBs/LNs. **(C)** Box plot showing the comparison of percentage coverage of LBs/LNs distribution in control (n=7 cases), DLB (n=5 cases), PD (n=6 cases), PDD (5 cases), was statistically significant for LBDs cases compared to control in Thalamus (*P<0.0012), with highly significance in DLB cases. Similarly, the percentage coverage of LBs/LNs in control (n=7 cases), DLB (n=5 cases), PD (n=6 cases), PDD (5 cases) in the amygdala, where the results were significant in all LBD cases compared to

control (*P<0.0159), and post-hoc test also showed significance in DLB cases, but not for PD and PDD. No sign of LBs immunoreactivity was observed within the white matter.

4.3.7 Regional comparison of ubiquitination of αSyn in LBD post-mortem cases.

Similar to phosphorylation analysis, the overall ubiquitination analysis for the interactions between the cortical regions in LBDs were significantly different from the controls, with the OC being the most affected region in DLB and the MC in PD and PDD (Two-way ANOVA followed by Bonferroni Multiple Comparison post hoc test $F_{(3,24)}$ =2.450**P< 0.0001). Significant differences were also observed among the disease groups, with higher immunoreactivity circumscribed between DLB (Two-way ANOVA followed by Bonferroni Multiple Comparison post hoc test $F_{(3,44)}$ =4.50*P< 0.0134). Nevertheless, in the subcortical areas, the regional interactions were even more evident between regions from LBDs compared to control. The GP was the region with the highest immunoreactivity in DLB and PD (Two-way ANOVA followed by Bonferroni Multiple Comparison post hoc test $F_{(3,15)}$ =2.117**P< 0.0034). Similarly, very significant differences were also observed between the disease groups, compared to control cases with higher immunoreactivity circumscribed in DLB (Two-way ANOVA followed by Bonferroni Multiple Comparison post hoc test $F_{(3,36)}$ =2.774**P< 0.0002).
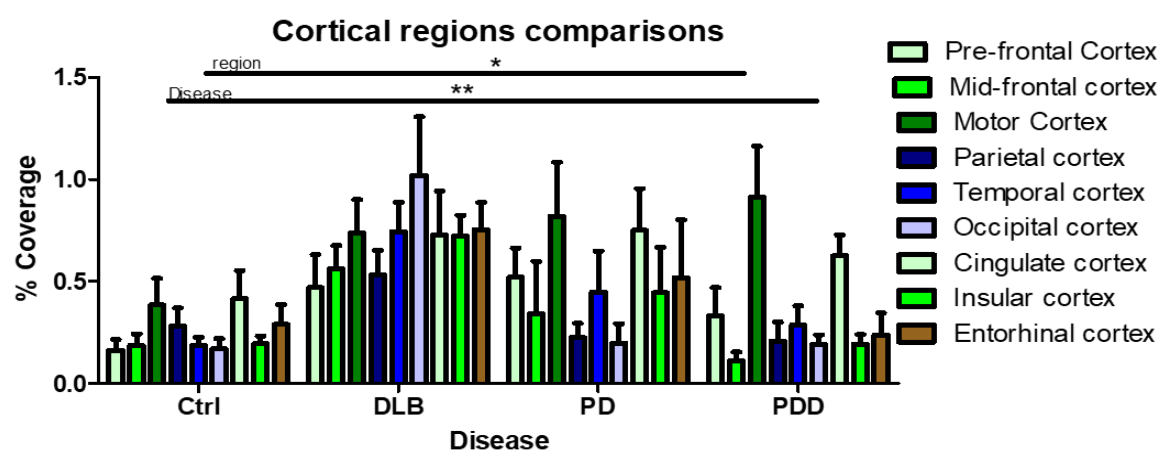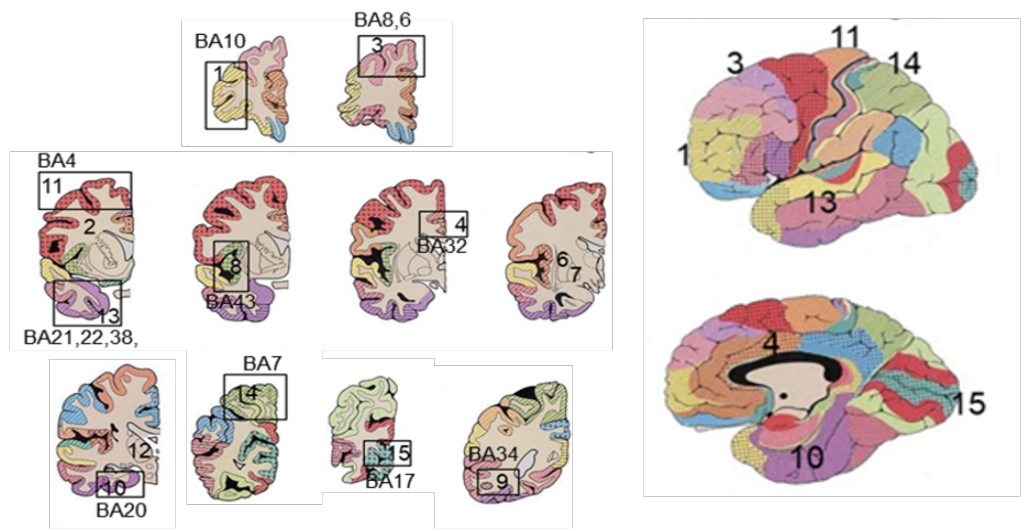
Figure 4. 8: Widespread Ubiquitination is observed across cortical brain regions of LBD patients. A Representative image from Newcastle brain bank indicating the regions where the sections were extracted for this study. **B** Bar chart showing the comparison of percentage coverage of αSyn Ubiquitination in cortical region. OC seems to be the most ubiquitinated region in DLB, whereas CC and MC are the most ubiquitinated regions in PD and PDD.
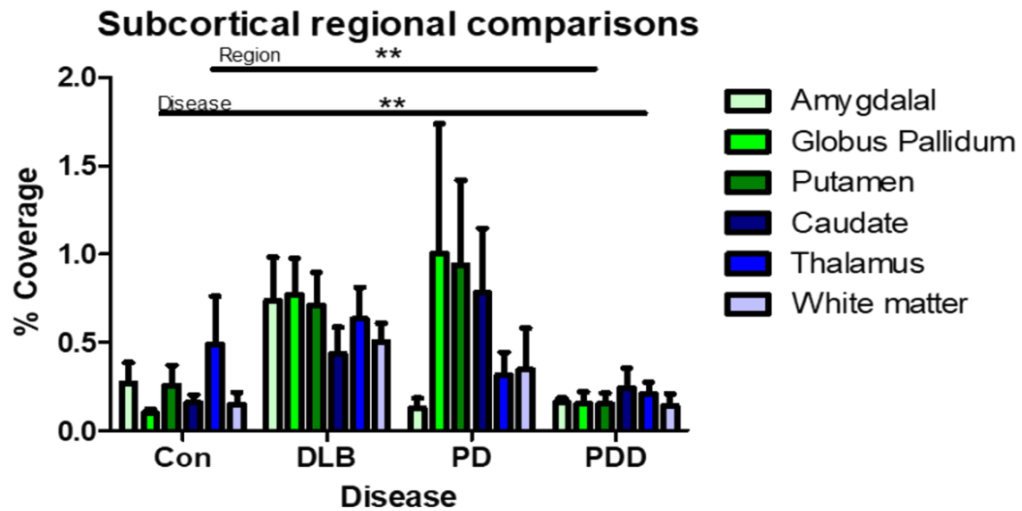
Figure 4. 9: Widespread Ubiquitination is observed in subcortical of LBD patients. A Representative image from Newcastle brain bank indicating the regions where the sections were extracted for this study. **B** Bar chart showing the comparison of percentage coverage of ubiquitination of αSyn. DLB and PD seems to be the diseases with the most ubiquitination and Putamen and Globulus pallidus the most affected subcortical regions.

4.3.8 αSyn ubiquitination is not pervasive in the cortical regions of LBD patients.

After the analysis of the overall interaction between disease and region, I assessed the specificity of ubiquitination per each region. The presence of ubiquitinated αSyn in the same regions where phosphorylation was assessed showed immunoreactivity to anti-ubiquitin antibody was not significantly different in PFC, MFC and MC of LBD cases compared to control (Kruskal-Wallis test ANOVA followed by Dunn's post hoc multiple comparison test P> 0.05). However, in MFC, DLB cases presented statistically significant results when compared to control cases (Kruskal-Wallis test ANOVA followed by Dunn's post hoc multiple comparison test *P<0.0446, Mann-Whitney test) (figure 5.8). Similar analysis was performed in the major sensory cortices. Although some immunoreactivity was observed, no statistically significant result in PC, TC, and OC in across LBD cases, compared to the control (Kruskal-Wallis test ANOVA followed by Dunn's post hoc multiple comparison test P> 0.05) (figure 4.8).
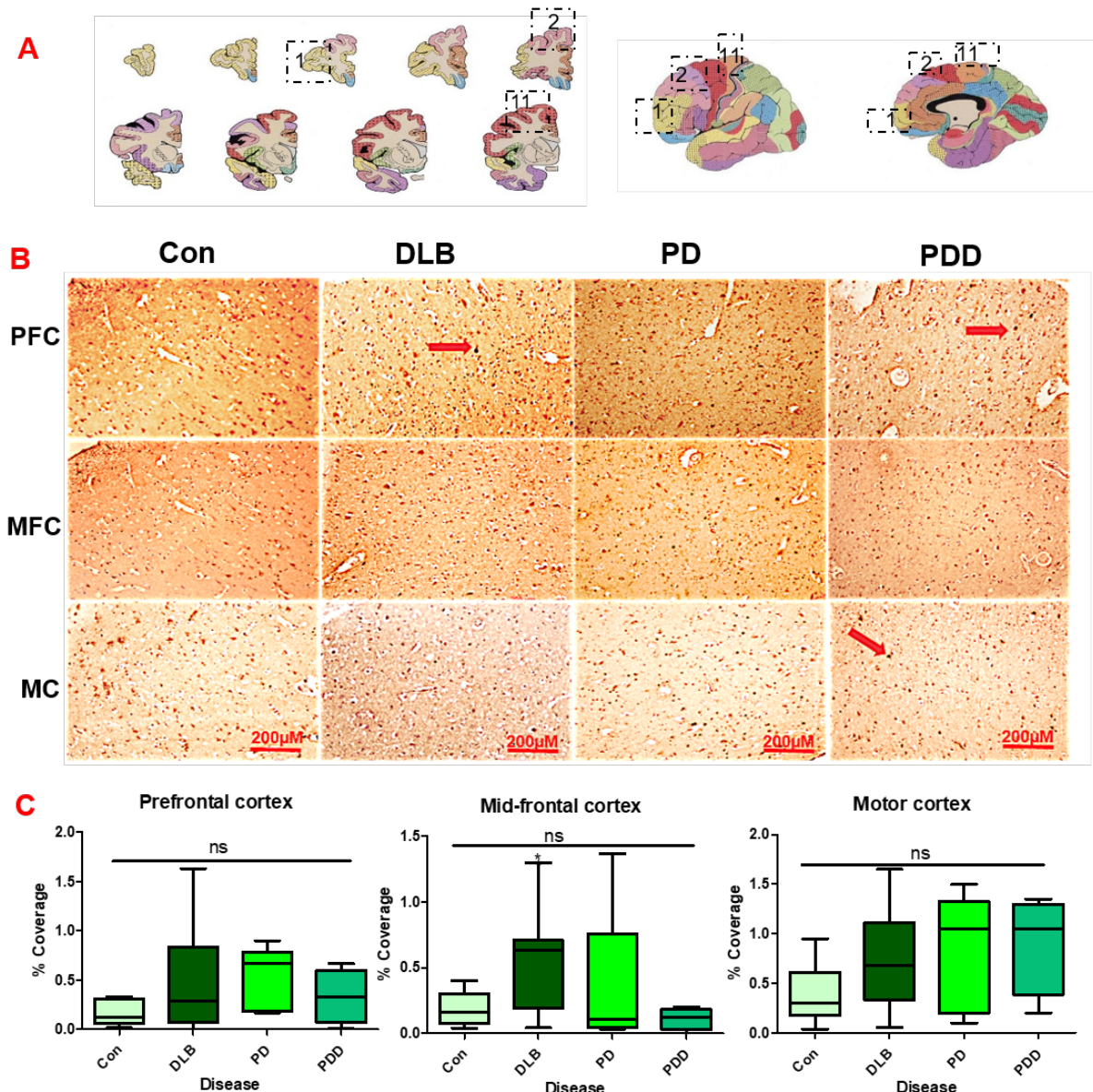
Figure 4. 10: αSyn ubiquitination is not pervasive in the frontal lobe of LBD cases. (A) Representative images from Newcastle brain Map, showing brain regions PFC=1, MFC=2 and MC=11 where the sections were taken for this study according to their organization in TMA slides. **(B)** Images showing ubiquitinated LBs from sections of PFC, MFC and MC of post-mortem brain tissue of LBD cases, at 10 X magnification. The arrows (in red) indicating the LBs. **(C)** Box plot showing the comparison of percentage coverage of LBs distribution in both LBD and control patients. The percentage coverage of LBs inclusions that are ubiquitinated in control (n=6 cases), DLB (n=10 cases), PD (n=5 cases), PDD (4 cases), were not significant among all cases and regions, except for the difference between the control and DLB case in MFC that was statistically significant (P>0.0446).
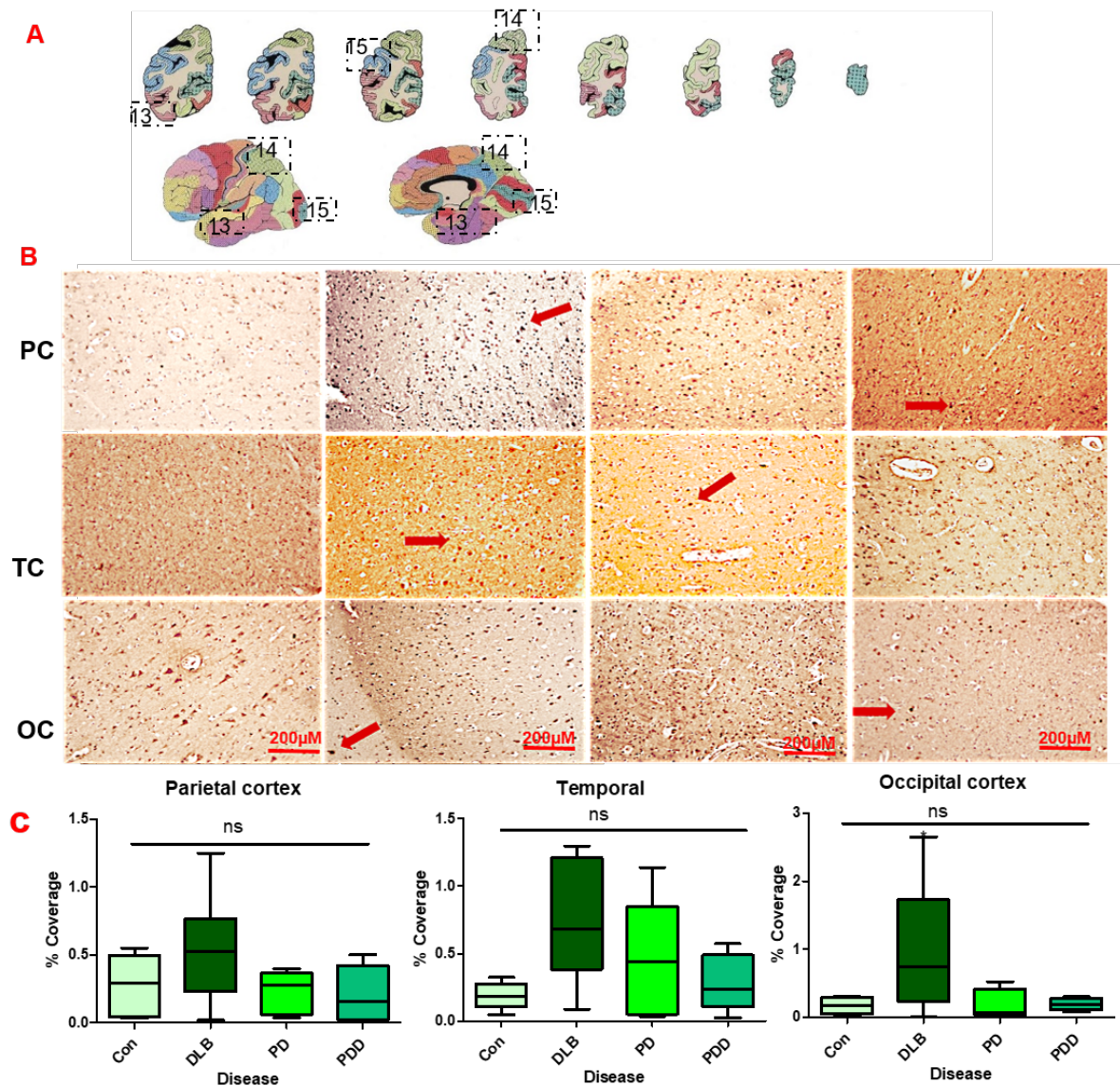
Figure 4. 11: αSyn ubiquitination is not pervasive in major sensory cortices of LBD cases. (A) Representative images from Newcastle brain Map, showing brain regions PC=14, TC=13 and OC=15 where the sections were taken for this study according to their organization in TMA slides. **(B)** Images showing ubiquitinated LBs from sections of PC, TC and OC of post-mortem brain tissue of LBD cases, at 10 X magnification. The arrows (in red) indicating the LBs. **(C)** Box plot showing the comparison of percentage coverage of LBs distribution in both LBD and control patients. The percentage coverage of LBs inclusions that are ubiquitinated in control

(n=6 cases), DLB (n=10 cases), PD (n=5 cases), PDD (4 cases), were not significantly different from the control cases among all cases and regions (P>0.05).

4.3.9 αSyn is ubiquitinated in the insular cortex, but not in the cingulate and entorhinal cortices of LBD patients.

Analysis of αSyn ubiquitination in the EC and CC showed that immunoreactivities were not statistically significant among LBD cases when compared to control cases in these regions (Kruskal-Wallis test ANOVA followed by Dunn's post hoc multiple comparison test P>0.05). However, immunoreactivity was greater in DLB compared to controls (P>0.0051, Mann-Whitney test). Interestingly, statistically significant results were observed in all LBDs when compared to the control cases in IC, (Kruskal-Wallis test ANOVA followed by Dunn's post hoc multiple comparison test **P<0.0098).
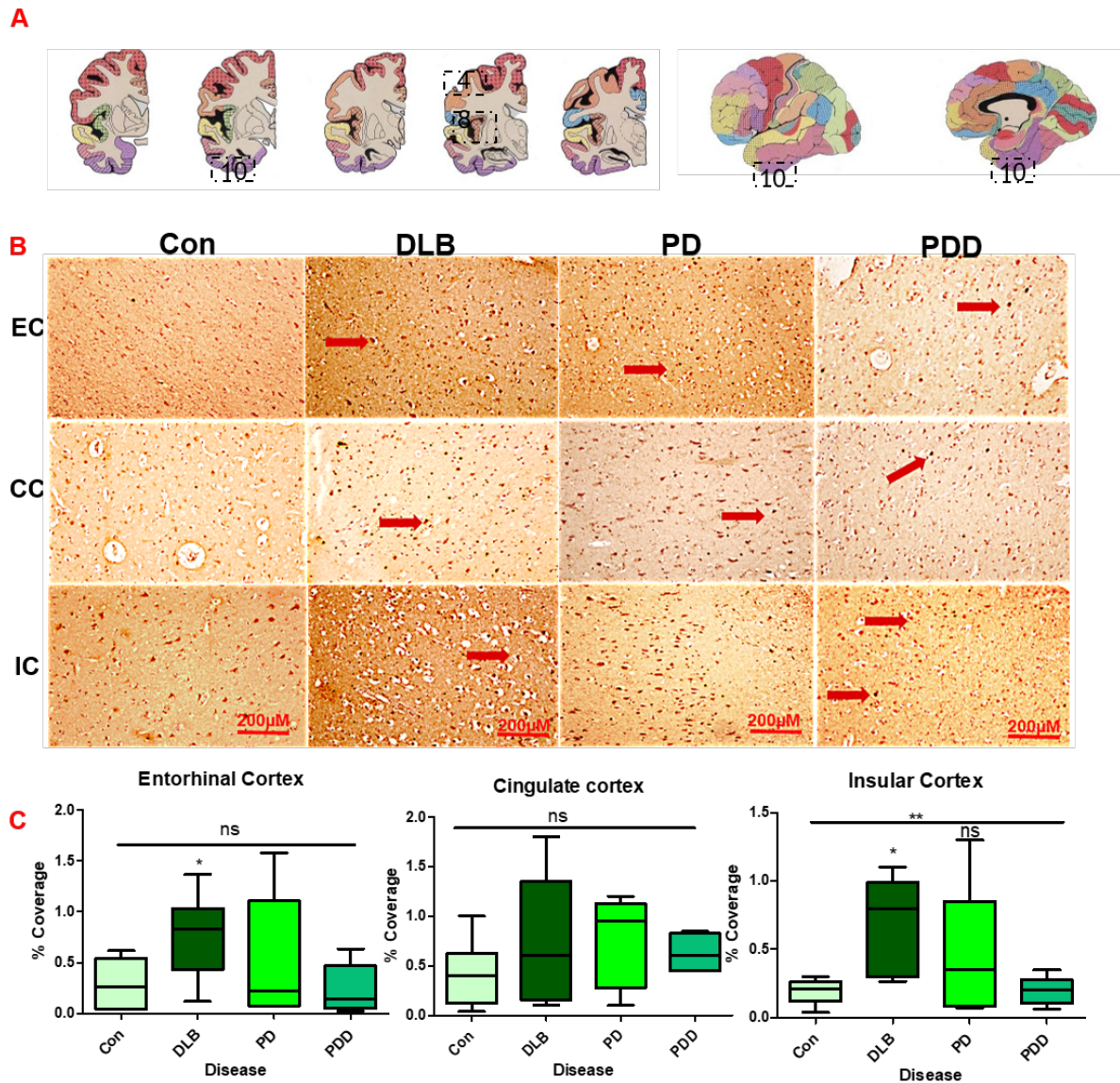
Figure 4. 12: Ubiquitination of αSyn in the insular cortex, but not in the cingulate and entorhinal cortices of LBD patients. (A) Images from Newcastle brain Map, showing brain regions EC=10, CC=4 and IC=8 were the sections were taken for this study according to their organization in TMA slides. **(B)** Images showing ubiquitinated LBs from sections of PC, TC and OC of post-mortem brain tissue of LBD cases, at 10 X magnification. The arrows (in red) indicating the LBs. **(C)** Box plot showing the comparison of percentage coverage of LBs distribution in both LBD and control patients. The percentage coverage of LBs inclusions that are ubiquitinated in control (n=6 cases), DLB (n=10 cases), PD (n=5 cases), PDD (4 cases), were not significant among all cases and regions (P>0.05), except in the insular cortex, where statistically significant differences were observed between LBD cases and control (**P<0.0098).

166

4.3.10 Ubiquitination of αSyn is not pervasive in the subcortical regions of LBD patients.

The analysis was then extended to the subcortical structures of the encephalon such as BG, thalamus, amygdala and the white mater. Here, I expected to find similar changes as observed in phosphorylation. However, the immunoreactivity to anti-ubiquitin-antibody was not statistically significant across these brain regions within the LBDs either when compared to control cases (Kruskal-Wallis test ANOVA followed by Dunn's post hoc multiple comparison test P>0.05).
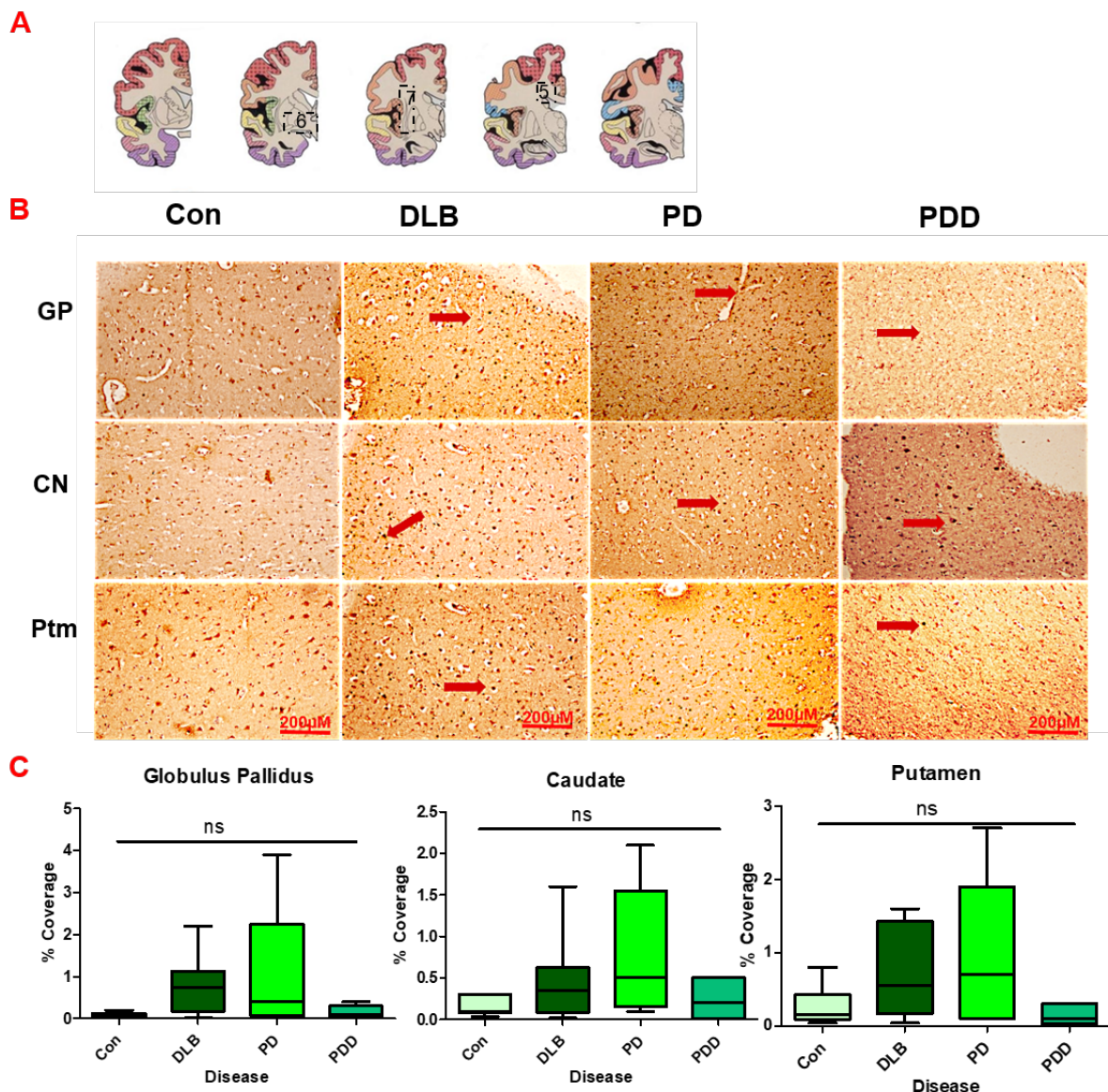
Figure 4. 13: Ubiquitination of αSyn is not pervasive in the basal ganglia of LBD patients. (A) Representative images from Newcastle brain Map, showing brain regions GP=7, CN=5 and PTm=6 where the sections were taken for this study

according to their organization in TMA slides. **(B)** Images showing ubiquitinated LBs in from number of sections of GP, CN and PTm of post-mortem brain tissue of LBD, at 10 X magnification. The arrows (in red) indicating the LBs. **(C)** Box plot showing the comparison of percentage coverage of LBs/LNs distribution in control (n=7 cases), DLB (n=5 cases), PD (n=6 cases), PDD (5 cases), was not statistically significant for LBDs cases when compared to control in GP (P>0.05).
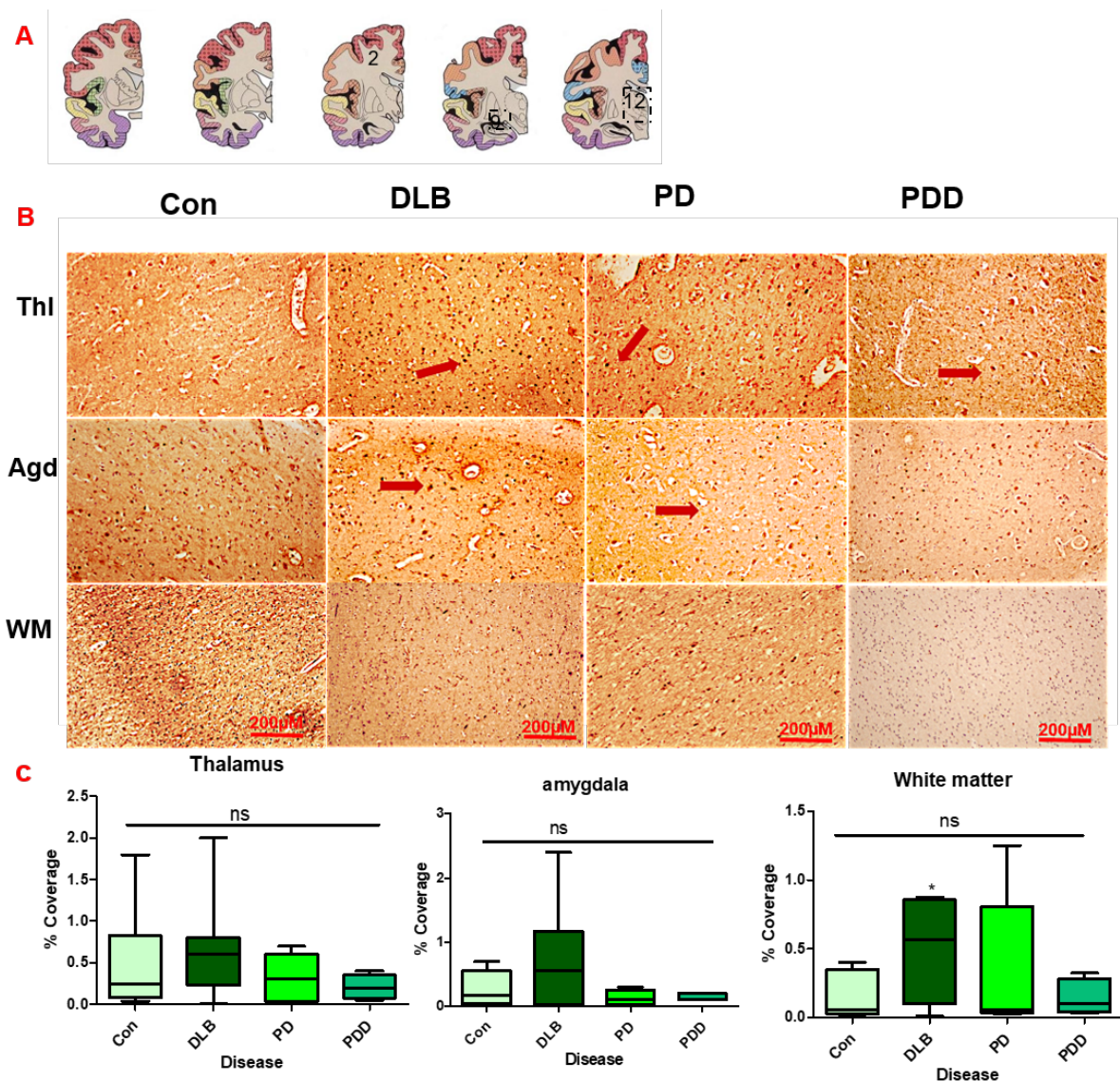
Figure 4. 14: Ubiquitination of αSyn is not pervasive in the amygdala and thalamus of LBD patients. (A) Representative images from Newcastle brain Map, showing brain regions Thl=12, Agd=9 and WM=2 where the sections were taken for this study according to their organization in TMA slides. **(B)** Images showing ubiquitinated LBs/LNs in from number of sections of Thl and Adg of post-mortem brain tissue of LBD, at 10 X magnification. The arrows (in red) indicating the LBs/LNs. **(C)**

Box plot showing the comparison of percentage coverage of LBs/LNs distribution in control (n=7 cases), DLB (n=5 cases), PD (n=6 cases), PDD (5 cases), was not statistically significant for LBDs cases when compared to control in Thl (P>0.05).

4.3.11 αSyn nitration across brain regions of LBD patients

I also assessed the extent of nitration in the same regions studied for phosphorylation and ubiquitination. However, Due to the lack of specificity of the nitration signals quantification of the results was difficult across all brain regions. In fact, nitration signals were similar in both control and the disease samples. Although I have attempted to determine the amount of LBs/LNs observed, the results for nitration were still unclear, as the antibody appeared to be over reactive even in the control cases (figures: 4.15; 4.16; 4.17). The figures bellow represents all the areas that were assessed, and it is clear that there was consistent pattern, and it is difficult to determine in any clear changes between disease groups and controls (Two-way ANOVA followed by Bonferroni Multiple Comparison post hoc test).

Con   DLB   AB Con

Nitration   Nitration   Nitration

Prefrontal cortex — ns

Mid-frontal cortex — ns

Motor cortex — ns

Parietal cortex — ns

Temporal — ns

Occipital cortex — ns

Entorhinal Cortex — ns

Insular Cortex — ns

Nitration

Cingulate cortex — *

Putamen — ns

Caudate — ns

Globulus Pallidus — ns

White matter — ns

Thalamus
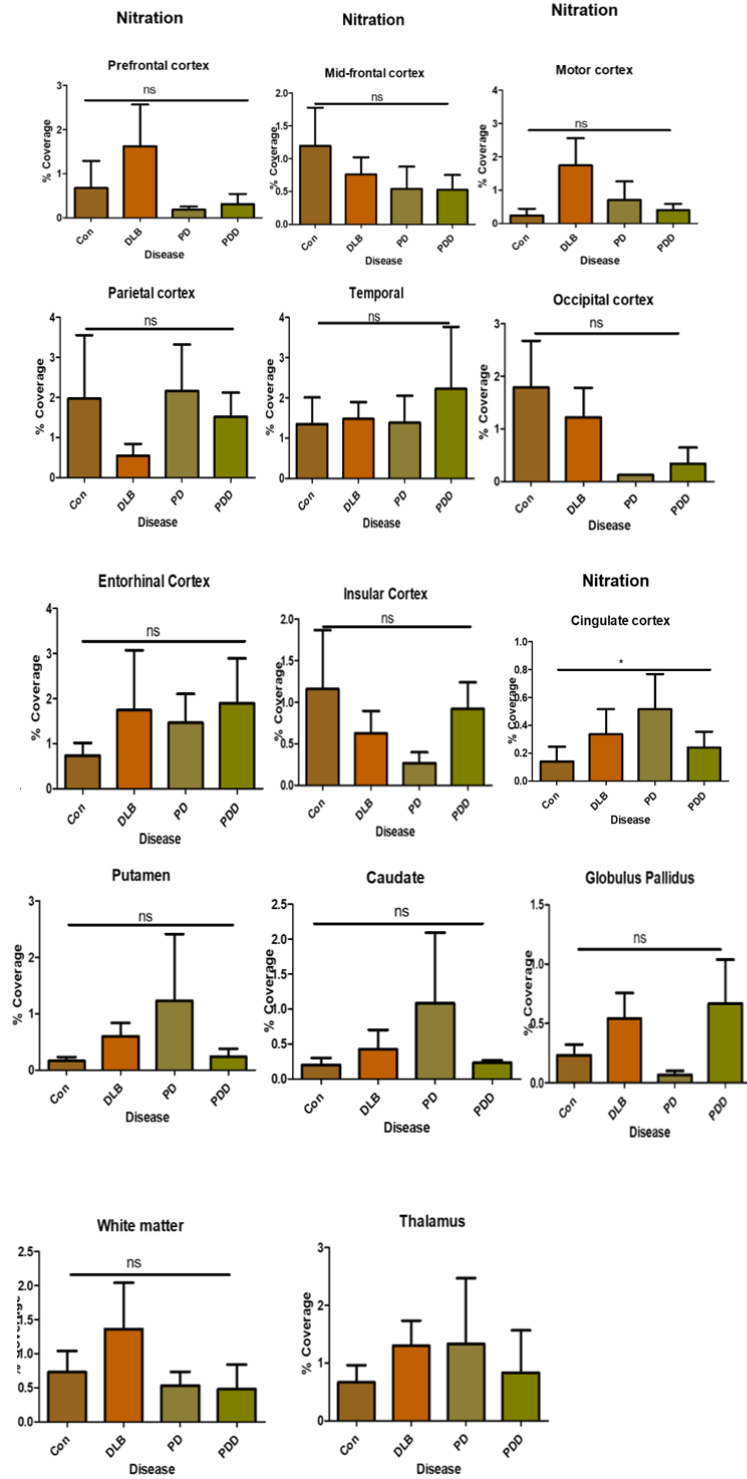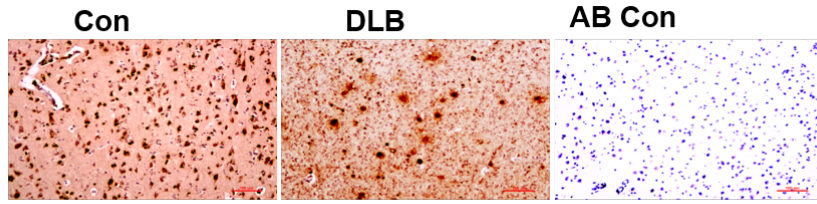
Figure 4. 15: Examples of Nitration images of LBD at 10X magnification showing unspecific signals due to the lack of specificity of the immunoreactivity. No significant changes were observed.
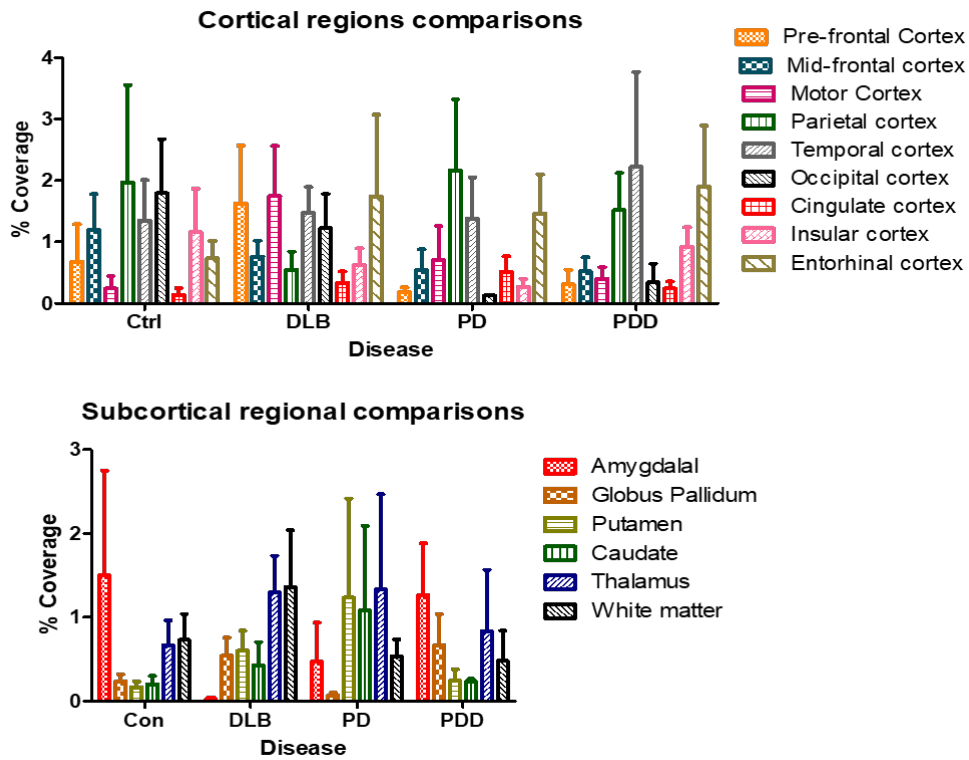
Figure 4. 16: Bar chart showing the comparison of percentage coverage of Nitrated αSyn immunoreaction in cortical region (Top) and subcortical regions (Bottom)

4.3.12 Summary comparison of different PTMs across brain regions in control and LBD cases.

The heat map shows the changes in different PTMs per region studied from images taken from human post-mortem brain samples of both control and LBD cases.
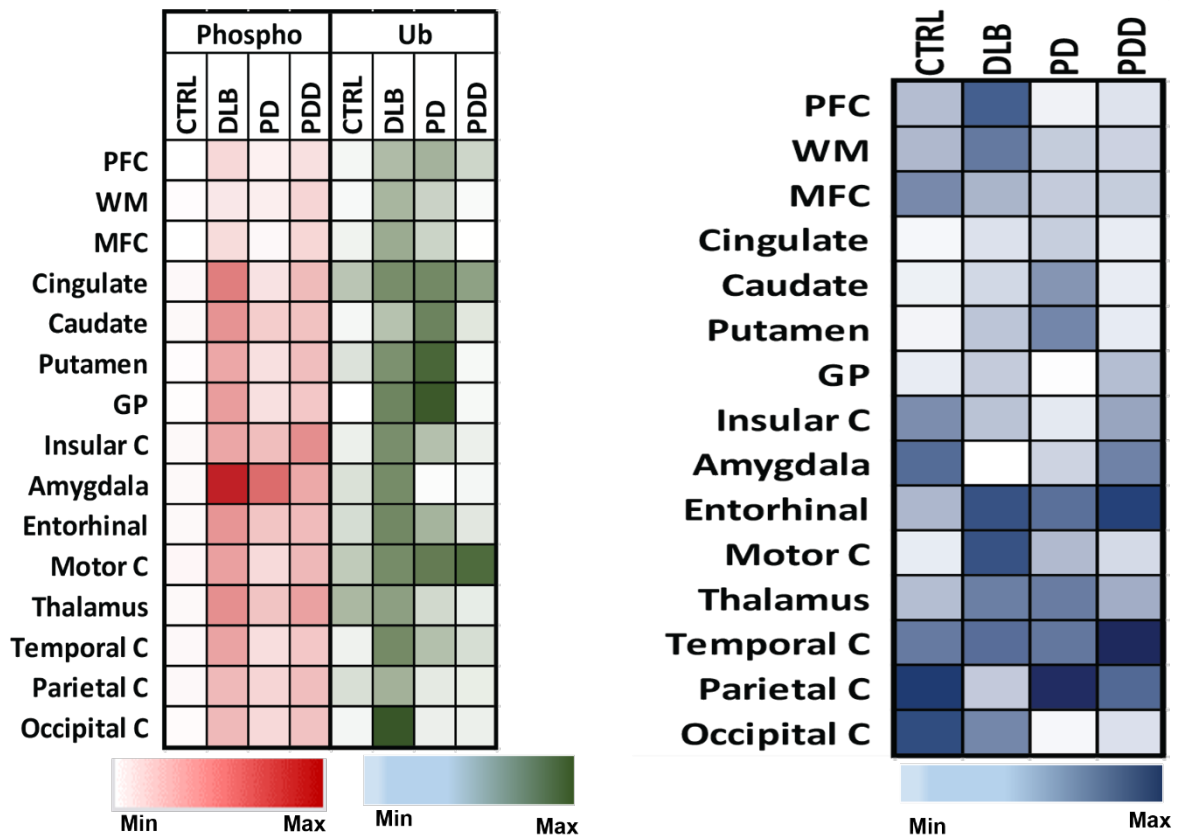
Figure 4. 17: Heat maps representing the distribution of phosphorylated, ubiquitinated and nitrated αSyn. Here we can observe that the area with the more colour intensity, represents the most affected areas, and for both Phosphorylation and Ubiquitination, DLB cases are the most affected. Nitration signals show a mosaic pattern of colorations, with no clear specificity of the immunoreactivity (see the appendix 3).

4.4 Discussion

Protein accumulation in the human brain is often associated with ageing. However, this age associated phenomena is yet to be elucidated, as the underlying pathogenic mechanisms have not been thoroughly studied (Mattson and Magnus, 2006, Mattson and Arumugam, 2018). LBDs are age related disorders that progress with pathologic aggregation of proteinaceous inclusions (LBs/LNs), mainly composed of aggregated toxic species αSyn, and they constitute the neuropathological basis for the classification of these diseases (Shults, 2006, Nemani et al., 2010, Spillantini et al., 1998). Whilst it is unclear if the end-stage products of aggregation (LBs/LNs) are the most relevant toxic forms of αSyn, it is widely assumed that the process of aggregation is critical and perhaps its intermediates (prefibrils and/or fibrillary oligomers), formed during such a process, may indeed be more relevant in the disease pathogenesis (Periquet et al., 2007, Hansen, 1997, Desplats et al., 2012). It has been confirmed that, under pathological conditions, αSyn can form aggregates and trigger a series of pathogenic cascades pathognomonic of LBDs and other neurodegenerative proteinopathies (Obeso et al., 2010, Lin and Beal, 2006, Robson et al., 2018b). Although, the very presence of LBs/LNs in patients with LBDs indicates their link with the disease, their exact role in developing LBDs clinical symptoms is still to be elucidated, as the question that remains to be answered is to whether the pathogenic consequences of LBDs arise from the pre-aggregated forms of αSyn (i.e., before LBs/LNs formation), or after. Because in some cases, patients with LBs/LNs, do not develop the clinical symptoms observed in LBDs (Outeiro et al., 2019, Dickson et al., 2008, DelleDonne et al., 2008).

Multiple lines of evidence have now indicated that pre-aggregated toxic species of αSyn, are responsible for the pathogenic cascades of LBDs, as they are known to cause mitochondrial dysfunction, oxidative stress, impairments in UPS, alteration in autophagy and triggers inflammatory response (Robson et al., 2018, Obeso et al., 2010, Lin and Beal, 2006). The sequence of events that proceeds this toxicity and the formation and distribution of LBs/LNs may be associated with αSyn PTMs, such as, phosphorylation, nitration and ubiquitination, in fact, alterations in these αSyn PTMs has been proposed to be among the major pathogenic features of LBDs (Fujiwara et al., 2002, Wakabayashi et al., 2003, Lowe et al., 1990). Indeed, recent studies have reported that αSyn is subjected to monumental PTMs such as ubiquitination, Nitration

and phosphorylation. These changes are thought to modify the protein structure and function, thus impairing the protein capacity to recognise and degrade damaged proteins through proteasome and lysosomal routes. This ultimately leads to the aggregation of abnormal proteins and the formation of LBs/LNs, as the neuropathological basis of LBDs (Junqueira et al., 2018, Barrett and Timothy Greenamyre, 2015, Omenn et al., 2016). In this chapter, the observed regional distribution of these PTMs of αSyn, may inform on the temporal sequence of PTMs occurring across different stages of the disease. That is to say PTMs appearing early in initial site of the CNS pathology e.g., infracortical structures, limbic system, and the amygdala, may develop prior to further spread into the neocortex. Thus, highlighting those PTMs of αSyn as potentially inducing the formation of toxic species of αSyn, which consequently facilitate the formation of LBs/LNs. The typical distribution of PTMs in affected regions of LBDs, and the significant differences between the disease groups and control cases as observed across almost all brain regions studied in this chapter, elucidate their functional implication in the LBDs pathogenesis. Since, the antibodies used for this study have been demonstrated to have high sensitivity and specificity for PTMs within a specific aminoacid sequence of αSyn protein (Meng et al., 2020, Delic et al., 2018), It is important to highlight that in this chapter, I have only analysed the PTMs of αSyn within the LBs and LNs inclusions. The non-aggregated αSyn were not analysed in this study, because it was not part of our laboratoy standard threshold settings for LBs and LNs detection. The function of the physiological and pathological differences of the brain regions outlined in this chapter was previously mentioned (see chapter 3).

4.4.1 αSyn phosphorylation in LBDs

αSyn phosphorylation is the most common PTMs studied in LBDs. it is known to be a reversible enzymatic addition of a negatively charged phosphate group from ATP to the amino-acids serine, threonine or tyrosine residues of αSyn. This causes conformational changes in the protein with consequent activation/inactivation of the protein function, increasing its tendency to misfold and aggregate or recruit other proteins (Manning et al., 2002a, Manning et al., 2002b). This is in accord with the fact that, LB/LNs are known to contain dysmorphic organelles, cellular membranes as well as other proteins (Shahmoradian et al., 2018), thus, it is plausible that αSyn phosphorylation may trigger this recruiting cascade to form the inclusions. Indeed, the

widespread phosphorylation observed in the regions analysed in this chapter provides clues about their involvement in LBs formations. Studies have shown that four serine residues (PSer[87] and Pser[129]) are the predominant phosphorylation sites, of which Pser[129], is the most commonly studied. Indeed, αSyn phosphorylation is largely limited at ser[129], although some evidence also supports a minor contribution of serine [87].

Under physiologic condition, Pser[129] is indeed very low; nevertheless, it is highly increased primarily at serine[129] in LBs/LNs containing fractions (Paleologou et al., 2010, Paleologou et al., 2008). Moreover, αSyn phosphorylation at ser[87] was also found to be low in controls but increased in LBs/LNs. Furthermore, αSyn phosphorylation is also observed in the related granular cytoplasmic inclusion of MSA (Paleologou et al., 2010, Invernizzi et al., 2012). This is in agreement with the findings here presented that showed, phosphorylation of αSyn within the LBs was widespread in the corresponding region of LBDs. Interestingly, here, the levels of phosphorylated αSyn were pervasively increased in the amygdala, in comparisons with other regions studied here. This is also in accord with studies that showed abnormal aggregation of αSyn in the amygdala as a primary pathogenic role in DLBs and is disease selective of the synucleinopathies, however, not restricted to them (Popescu et al., 2004). Because of this regional predominance in LBDs, it is suggested that the amygdala may indeed be prone to initiate the development of αSyn pathology (Sorrentino et al., 2019). In fact, the amygdala is shown to contain a unique strain like variation of pathologic αSyn which is thought to be determinant of the disease progression (Sorrentino et al., 2019). Thus, the results presented here support the important involvement of this region in the development of the disease.

Among the disease groups presented in this chapter, DLB and PDD seems to be the most affected with Pser[129] within the LBDs. However, within the cortical regions, the MC is more affected in DLB. Whereas IC is the most phosphorylated region in PD and PDD, confirming the hypothesis of widespread phosphorylation in these disease groups. Despite the evidence of prominence of Pser[129] in LBs/LNs, and the preferential phosphorylation of fibrillary αSyn at Ser[129], several studies suggested that this phosphorylation may be a late event in LBs formation, as Pser[129] phospho-mimetics reports slower/inhibited aggregation kinetics that wild type (WT) αSyn (Paleologou et al., 2010, Waxman and Giasson, 2011, Wales et al., 2013). Nevertheless, the evidence presented in this chapter suggests that, Phosphorylation of α-syn,

particularly at residue 129, may indeed be a key factor in LBs formation and LBD pathogenesis. This could be due to Pser[129] interfering with the functions of degradation enzymes as well as utilizing such proteins as co-aggregates (McFarland et al., 2009). Thus, the observed spectrum of distribution of these PTMs across affected regions in in LBDs, provides clues about their temporal occurrence in the disease progression, as it informs about αSyn toxicity in LBs. Furthermore, αSyn phosphorylation is dependent on the action of the kinases and phosphatases (Arawaka et al., 2017, Pronin et al., 2000). The temporo-spacial balance of these enzymes is key, as the concentration of these enzymes within the cell, determine the size of its phosphorylated protein. Thus, modulating these enzymes could be a potential next generation target for therapeutic of LBDs.

4.4.2 αSyn ubiquitination In LBDs

The molecular mechanism associated with the clearance of αSyn aggregates, are also key to understand αSyn related toxicity. Ubiquitin and its related enzymes are found in LBs/LNs (Engelender, 2008), and multiple lines of evidences have reported the presence of monoubituitinated α-syn as a predominant species in LBs (Wakabayashi et al., 2000, Lowe et al., 1990, Hasegawa et al., 2002, Tofaris et al., 2003, Anderson et al., 2006b). It is known that αSyn ubiquitination can affect the protein degradation system, therefore influencing the protein localization, folding, concentration and aggregation (Tenreiro et al., 2014). Despite, some studies have suggested that αSyn ubiquitination is not required for LBs/LNs formation. More recent studies suggest that αSyn ubiquitination, in association with other PTMs could represent an unsuccessful attempt in folding or depredating misfolded proteins, through a process that may not require polyubiquitination (Lopes da Silva, 2013). Because, αSyn ubiquitination dependent degradation may not be a major physiologic mechanism of αSyn, rather that this s process may only represent ubiquitination of toxic forms of αSyn (Zhang et al., 2019). Thus, the ubiquitination of αSyn may represent a disease specific pathway.

Although, some studies suggested that αSyn ubiquitination is not a prerequisite for LBs formation in synucleinopathies (Sampathu et al., 2003), in the work presented here, the ubiquitinated LBs were significantly increased within the regions of LBDs compared to the control cases. Among the disease group, DLB and PD were the most affected. The GP and Ptm in the subcortical regions were also highly affected.

However, in cortical regions, DLB registered high affectations in the OC. Nevertheless, in PD and PDD, the MC was the most ubiquitinated region. The observed widespread ubiquitination is in agreement with number of studies that shown that Ubiquitin including the enzymes system of ubiquitin are found in LBs inclusions and are disease specific of the synucleionpathies (Walden and Muqit, 2017, Betarbet et al., 2005, Mund et al., 2018, Bedford et al., 2008). Although, ubiquitinated α-syn is often present in the LBs inclusions. The mechanisms that underlie the ubiquitin modulation of α-syn aggregation are still unknown. In addition, multiple enzymes are, however, found to be associated with this process. A study of isolated LBs from PD patients detected the presence of the seven in absentia homologue (SIAH), an E3 ubiquitin ligase enzyme, previously reported to interact with and ubiquitinate α-syn (Liani et al., 2004, Engelender, 2008, Lee et al., 2008). De facto, lysine 12, 21 and 23 residues, the common targets of α-syn monoubiquitination, are also ubiquitinated by SIAH (Anderson et al., 2006a). This suggests that SIAH is involved in pathogenesis of the synucleinopathies. However, this remains to be unveiled, because some studies have found that only a small fraction of α-syn is ubiquitinated in LBs (Hasegawa et al., 2002). This may explain the fact that the size of the LBs observed in the ubiquitinated images presented here, are relatively small, compared to what was observed with phosphorylated LBs. Nevertheless, the widespread Ubiquitination of αSyn observed in LBDs group, sheds light about their involvement in the disease pathogenesis.

4.4.3 αSyn Nitration

Nitration is also found to be process of PTMs in LBDs. αSyn nitration is an oxidative protein modification that usually occurs in tyrosine residues of αSyn. In LBDs, oxidative stress is evidenced by the increased of oxidised proteins, lipids and DNA as a direct indication of failure of the compensatory antioxidant mechanism. The primary source of these nitrating reactions is the NOS, which modifies the biochemical properties of the amino acid residues, subsequently leading to significant changes in the structure and functions of αSyn. In LBDs, αSyn nitration is thought to cause αSyn fibrillogenesis by affecting the protein solubility (Giasson et al., 2000). Indeed, high levels of nitrated αSyn contained in LBs was found to be linked with the oligomer formation, mitochondrial dysfunction and neuronal apoptosis (Liu et al., 2011, Giasson et al., 2000).

LBDs is an age related disorder that course with decline in mitochondrial function and the antioxidant defences (Spano et al., 2015). This increases the chances of the oxidative injury to occur, leading to αSyn nitration (Spano et al., 2015, Yin et al., 2014b, Yin et al., 2014a). The question that arises is to whether αSyn nitration is an important early PTMs or simply a by-product that occurs later in LBDs pathogenesis and further worsens the disease. This I was not able to address with the experiments presented in this chapter, as incongruously, the nitration results were not consistent, because the control and diseased groups were unclear and possibly lacked specificity in detection of true positivity. Although most antibodies (monoclonal/polyclonal) can specifically recognise aminoacid residues within αSyn residue, the antibody used here, seems to lack specificity as it detected large number of non-specific signals in both LBDs and control groups. It is possible that specific sites or epitopes of nitration were obscured within the extracellular deposits, or simply the experimental design was not the appropriate.

4.4.4 The distribution of PTMs in LBDs

While the presence of LBs/LNs in brain stem and cortical regions has been widely identified, their biological significance for the development of the clinical signs and symptoms in LBDs still needs elucidation. Although, studies have suggested that oligomeric and protofibrillar αSyn are cytotoxic and underlie the formation of LBs/LNs inclusions (Ahmed et al., 2020), αSyn PTMs are typically observed in LBDs, may be the structural substrate of a failed cellular self-preservation mechanism designed to confine and eliminate toxic proteins (Zhang et al., 2019). Like other proteinaceous deposit, the PTMs of αSyn may induce a host response to a complex but mostly unknown upstream pathogenic cascade and distribution underlying these proteinopathies (Stefanis, 2012, Pajarillo et al., 2019).

Moreover, the existing Braak/Mckeith LBs staging used to classify the synucleinopathies is still incomplete, as it would benefit with the understanding of the underlying PTMs that progresses with LBs formation. In view of the findings discussed above, the PTMs distribution, may serve as a framework for current and future perspective of the clinico-pathologic studies, in trying to define the morphological substrates and the possible pathophysiologic correlates of LBDs. Although recent studies indicate that LBs/LNs are indeed progressive (Luk et al., 2012), I believe the

assessment of regional PTMs distribution patterns may help evaluated stage of their generation and toxicity. Furthermore, the topographic mapping of LBs/LNs as discussed in Braak/Mckeith scales, apparently have no relevance for cases with predominant dementia such as DLB and PDD (Braak et al., 1999, Braak and Del Tredici, 2017, Braak et al., 2003b, McKeith et al., 2017). Because it is unclear whether LBs/LNs inclusions are solidly relevant pathology in these diseases. Although their presence is pathognomonic of αSyn pathologic process, they are usually found in both symptomatic and asymptomatic patients with LBDs (van Duinen et al., 1999). Thus, LBs by itself may not represent reliable surrogate markers for LBDs, as they may be a late event in the disease. Conversely, LBDs may rather reflect one of several response patterns of the human brain due to dysregulated αSyn metabolism, influenced by PTMs, which would lead to synaptic and cellular dysfunction that would then translate into clinical symptoms even before the LBs aggregates are formed. Indeed, in previous chapter I demonstrated that a group of fast spiking interneurons (PV+cells) are reduced in DLB, and LBs are not present in this group of cells. This suggests that the direct impact of synaptic impairments that results from toxic forms of αSyn may result in neuronal cell death, and this in turns may translate into the clinical symptoms observed in LBDs.

The role of phosphorylated αSyn as a potential biomarker has been addressed in several studies. The quantification of total αSyn in the cerebrospinal fluid (CSF) in patients with synucleinopathies related disorders has been proposed as a potential biomarker (Hong et al., 2010, Mollenhauer et al., 2008). In fact, plasma αSyn is thought to be sensitive specific potential diagnostic biomarker for LBDs (Wang et al., 2019). Although, Pser129 αSyn was detected in human plasma, the same study reported that Pser 129 αSyn was not detected in CSF in LBDs (Cariulo et al., 2019). Similarly, Flouds et al. have shown that the total αSyn in the blood plasma of PD patients was similar to the findings in non-PD controls, in contrast, they found that the levels of αSyn Pser129 was undoubtedly higher in PD patients, in comparison to non-PD controls (Foulds et al., 2013). The detection of phosphorylated αSyn in the peripheral nervous system was also reported. Skin biopsies performed in PD subjects, revealed aggregation of phosphorylated αSyn in large and small fibbers (Stewart et al., 2015, Wang et al., 2012, Doppler et al., 2014a). In addition, aggregation of phosphorylated αSyn was found in the gastrointestinal tract of PD individuals (Pouclet et al., 2012,

Hilton et al., 2014). Furthermore, the total αSyn in the exosome has been suggested as a potential biomarker, as it is associated with the degree of severity of PD (Cerri et al., 2018). Thus, the studies presented in this chapter, adds to the existing literature by confirming a widespread phosphorylation of αSyn in LBs inclusions present in anatomically affected regions of individuals with LBDs.

4.5 Conclusion

αSyn posttranslational modifications are early events that trigger the pathogenic cascade of LBDs, by possibly altering the physiological function of αSyn and their distribution, which in turn affect the normal function of neuronal cells. These changes may facilitate the formation of toxic forms of the protein that will then cause neuronal cell death of important group of neurons such as those that play key roles in the generation of the fast neuronal network oscillations. Moreover, different PTMs may occur at different stages of the disease's progression. Their distributions across different brain regions may provide a clue about their temporal occurrence. Thus, the assessment of disease associated PTMs of αSyn is key to aid the comprehension and discernment of potential reasons for the pathological aggregation and the observed preference of distribution patterns seen in LBD, in comparison with other synucleinopathies. Although, the precise mechanisms that trigger αSyn aggregation are still unclear. Assuming that, alpha synuclein PTMs play an important role in the disease's pathogenesis, the studies presented in this chapter unveils the impact of phosphorylation and Ubiquitination in LBDs. Moreover, the assessment of the patterns of these PMTs in LBDs and most importantly how these PTMs are related to the disease progression may validate them as biomarkers for LBDs. In general, there is no correlation between the density of LBs and neuronal loss, which together with associated synaptic dysfunction could represent a more suitable surrogate indicator of the pathogenesis, caused by dysregulated αSyn metabolism that results in the formation of fibrillar and non-fibrillar forms or PTMs of the protein. At a more basic level, we need a better understanding of the pathologic significance of αSyn PTMs in LBs and its relations to neuronal loss most suitably in a prospective clinical pathological setting for better therapeutic strategy and intervention.

Chapter 5: Relationship between alpha synuclein Posttranslational modifications and parvalbumin cell loss
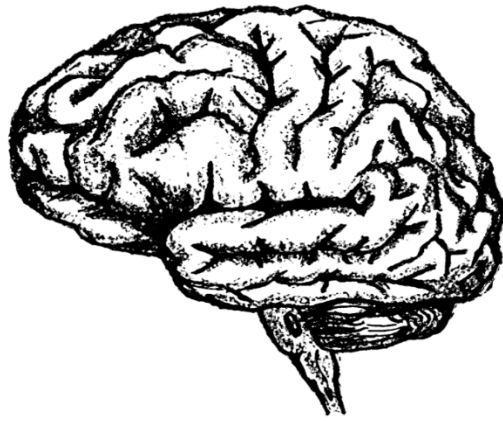
5.1 Introduction

The study of the physiologic and pathologic functions of aSyn continues to attract the attention of many researchers, as the exact mechanism by which aSyn aggregates to form the proteinaceous inclusion is still to be unveiled. In previous chapter, I proposed that, the protein's tendency to form aggregations, may be influenced by several post-translational modifications (PTMs), in a process that ends up destroying the native state of the protein, precipitating the protein to become toxic to the nerve cell as mentioned in the studies referenced here (Villar-Pique et al., 2016, Fujiwara et al., 2002, Hodara et al., 2004, Paleologou et al., 2008). These PTMs occur when an amino acid residue of the protein is modified by covalent bonds, leading to changes in protein properties, in conformity with the developmental or physiological requirements (Beck-Sickinger and Mörl, 2006, Prabakaran et al., 2012). Thus, PTMs such as phosphorylation, nitration and ubiquitination may be at the root of the toxic properties of aSyn that ultimately causes neuronal dysfunction and death (Chen and Feany, 2005, Oueslati et al., 2010). To date, the PTMs have been studied separately and mostly in PD cases (Oueslati et al., 2010, Paleologou et al., 2010). However, very little is known about their involvement in DLB. Here I compared and assessed the co-localization of the PTMs to address the question whether these changes interact with each other to increase aSyn toxicity, leading to synaptic dysfunction and neuronal cell death.

In addition, this chapter also presents the comparison of the different brain regions affected by phosphorylation and ubiquitination, in relation to the PV+ cell loss. This is important, as it may help to understand the degree of involvement of these PTMs in DLB when comparing to controls, including the affected stages of the diseases in relation to the PV+ interneuron loss. It may also help to create a clear topographic distribution of the PTMs. As previously hypothesised, although, LBs/LNs are pathognomonic of the synucleinopathies in general, these inclusions may probably be a late event in LBDs pathogenesis, as the presence of clinical symptoms may not be a direct consequence of LBs/LNs inclusions. In fact, aSyn may already be toxic to the neurons prior to inclusion formation, specifically, those neurons that have key roles in the neuronal network such as interneurons. Thus, the analysis presented in this chapter may shed light on the degree of involvement the PTMs in causing neuronal cell death in DLB and the synucleinopathies in general.

5.2 Methods

Since the results presented here are a continuation of the previous chapters, to assess how the methods were performed for the histochemical analysis for PD, PDD and DLB please see chapter 3 and 4. To avoid repetitions, here I have only the described the methods for the colocalization analysis for DLB alone which I performed independently, as these studies differ from the analysis performed in LBDs.

5.2.1 Immunohistochemistry statistical analysis

Although, in the chapter 3 and 4 I analysed the presence and interactions between the PTMs and PV+ cell loss. Here I analysed the correlations between the variables. Pearson's correlation test and Two-way MANOVA were used to test for presence of an interaction between PTMs and PV (I assessed whether they co-vary across brain regions and disease groups) with p-values and F-ratios obtained from Pilai's trace adjustment. All data were statistically analysed using Stata (StataCorp LLC). The data were reported with F-value, degree of freedom and p value, which was reported as significant, $*p < 0.05$, $**p < 0.01$ and $***p < 0.001$. Sample sizes are shown in the respective figure legends.

5.2.2 Immunofluorescence double-labelling

Post-mortem brain tissues from 16 neuropathological and clinically assessed non-diseased (control) and 19 clinically diagnosed DLB cases, were obtained from Newcastle brain tissue resource (NBTR) centre. For the Immunofluorescence experiments, I used samples from the Cingulate and Temporal cortex of Controls and DLB cases. In total 64 samples from DLB with Braak stage 5-6 and 58 control samples without LBs were used. They were immunostained for the presence of nitrated, ubiquitinated, phosphorylated and total αSyn protein. This was done using immunofluorescence double labelling techniques. Samples were warmed in LEEC oven for 60 minutes, and then dewaxed in xylene1-2, to be then rehydrated in alcohol gradient 99%-70%. Then sections underwent pressure cooker antigen retrieval with EDTA for approximately 10 minutes, after that, the slices were incubated in 10% Normal goat serum in TBS for 1h, prior the addition of the primary antibodies (see Table 6.1). Sections were then incubated overnight at 4°C. Next, the samples were washed with TBS and the secondary antibodies, Goat anti-mouse 488 and Goat anti-rabbit 594 (Table 6.1), were added and incubated for 1h. Slides were then washed

again with TBS, H2O and dipped in ethanol 70% and 1% Sudan black for 10 minutes, then dipped again ethanol 70% and washed in water, and mounted with DAPI. For the negative controls, the primary antibodies were omitted but all other steps were followed as it is described.

5.2.3 Data capture for colocalization, and statistical analysis

The images were taken using an automated system consisting of Nikon Eclipse 90i microscope, DsFi1 camera and NIS element software v 3.0. For these experiments, I examined only freshly stained samples. Once the slides were placed in the microscope and the correct position found, images were captured at different magnification. For statistical analysis, I selected 20x and 40x magnifications. For immunofluorescence, exposure time for each fluorophore was kept constant between slides to allow for comparison. Sample sizes are shown in the respective figure legends. For colocalization analysis, ImageJ software with JACoP plugin was used for quantification. Captured images were split into RGB colour channels and intensity selected via individual constant RGB thresholds for each channel was kept constant for the same experiment and magnification settings. Co-localisation was subsequently measured, using Pearson's, Mander's and overlapping coefficients, which are widely used to quantify the degree of colocalization between the fluorophores. In brief note, for the colocalization test (Pearson, Manders and overlap coefficients) in this immunofluorescence analysis, was used to confirm if the emission by the 2 fluorophores (red and green channel) occupies the same pixel of the same image. In this case I applied *Pearson's coefficient* which determines the correlation between the red and the green channel. Its values range between -1 and +1, where values equal to 1 would show a positive linear correlation, -1 negative linear correlation and 0 no correlation at all (Adler and Parmryd, 2010). *Mender's coefficient* determines the positional relation between the 2 biological objects or processes that are being analysed. In another words, it indicates an actual overlap of the signals, it represents the true degree of co-localization, its values goes from 0-1.0; where M1 and M2 of 1.0 and 0.3 for red and green channels suggests that red pixels co-localize with green but only 30% of green pixels co-localizes with red (MANDERS et al., 1993). Manders A is performed before threshold and Manders B after a threshold is applied. Finally, I performed the *overlap coefficients K1 and K2*, which splits the value of the co-localization into 2 parameters. This test allows to determine the contribution of each

antigen to the areas with co-localization. Nevertheless, Its value varies (Adler and Parmryd, 2010). *K1* is performed before threshold and K2 after a threshold is applied. The graph was generated using Microsoft excel and Graph Pad Prism.

Table 5. 1 List of the antibodies used for immunofluorescence studies

Antibody	Supplier	Dilution
Anti-nitration AB	Thermofisher	1:200/1:50
Anti-Ubiquitin	Abcam	1:500
Total aSyn AB	Abcam	1:500
aSyn PSer129	Abcam	1:200
Goat anti-mouse 488	Abcam	1:500
Goat anti-rabbit	Abcam	1:500

5.3 Results

5.3.1 Correlations between ubiquitinated, phosphorylated αSyn and PV+ interneurons in DLB.

Different from previous chapter where I analysed the correlations between PTMs and PV+ interneurons in different brain regions per disease groups separately. Because PV+ data is only available for DLB and control cases, I first compared whether PV+ interneurons, phosphorylation and Ubiquitination shows covariance in DLB and control cases across different brain regions. First, I performed Pearson correlation test, to analyse the presence of correlation between dependent variables PV+ cells, Pser[129] and ubiquitination. I observed negative correlation between the 3 variables in study (PV+ cells, Pser[129] and ubiquitination). This implies that when Pser[129] was highly expressed, PV+ cells were lower and vice-versa. However, the correlation was not significant (all p-values >0.05), as shown in the correlation matrix bellow (Table 5.2).

Table 5.2, Correlation matrix of PTMs and PV+ cell loss.

	PV	Pser129	Ubiqui~n
PV	1.0000		
Pser129	-0.0859	1.0000	
	0.2251		
Ubiquitina~n	-0.0819	-0.0369	1.0000
	0.2480	0.5952	

Note: Total number of observations, N (Sample size) = 201; Top value within each cell represents the correlation coefficient (-0.0859) and the value below is the p-value (0.2251)

Considering the results presented above, I proceeded to test for statistical differences between PV+ cells, Pser[129] and ubiquitination simultaneously. Thus, I used two-way MANOVA test, to test for the disease status and brain regions (i.e the substructures)

and the interaction effects of brain region and disease status. The interaction effect determines whether the effect of disease status is consistent across the different brain regions. The results I present in the table below, shows the results test for main effects and interaction effects for DLB. The overall model was significant, (MANOVA F $(29,171) =2.72$, $p<0.0001$). The results show a statistically significant interaction between disease status and brain region, (MANOVA F $(14,171) =1.53$, P-value=0.0197). This implies that the effect of the disease status on the dependent variables is not the same in the different regions of the brain. I further observed that PV, PSER and ubiquitination covary across the different brain regions (MANOVA F $(14,171) =2.08$, $P<0.0001$) and are differentially expressed between control and DLB (MANOVA, F $(1,171) =55.92$, $P=0.0001$) (Table 5.3).

Table 5.3 Interaction between the disease status and brain regions

Number of obs = 201

W = Wilks' lambda   L = Lawley-Hotelling trace
P = Pillai's trace   R = Roy's largest root

Source		Statistic	df	F(df1,	df2) =	F	Prob>F	
Model	W	0.2700	29	87.0	506.6	3.20	0.0000	a
	P	0.9466		87.0	513.0	2.72	0.0000	a
	L	1.9525		87.0	503.0	3.76	0.0000	a
	R	1.5107		29.0	171.0	8.91	0.0000	u
Residual			171					
Disease_s~s	W	0.5019	1	3.0	169.0	55.92	0.0000	e
	P	0.4981		3.0	169.0	55.92	0.0000	e
	L	0.9926		3.0	169.0	55.92	0.0000	e
	R	0.9926		3.0	169.0	55.92	0.0000	e
Substruct~e	W	0.6138	14	42.0	502.1	2.14	0.0001	a
	P	0.4373		42.0	513.0	2.08	0.0001	a
	L	0.5476		42.0	503.0	2.19	0.0000	a
	R	0.2872		14.0	171.0	3.51	0.0000	u
Disease_s~s#	W	0.6925	14	42.0	502.1	1.58	0.0140	a
Substruct~e	P	0.3345		42.0	513.0	1.53	0.0197	a
	L	0.4061		42.0	503.0	1.62	0.0097	a
	R	0.2898		14.0	171.0	3.54	0.0000	u
Residual			171					
Total			200					

e = exact, a = approximate, u = upper bound on F

I then proceeded to analyse the correlation between phosphorylation and ubiquitination in PD, PDD and control and across different brain regions. Similar to DLB, here I first performed Pearson correlation test, to analyse the presence of correlation between dependent variables, in this case Pser[129] and ubiquitination. Here I observed a positive correlation between the 2 variables in study, i.e., Pser[129] and ubiquitination (corr=0.1141, p-value=0.0196). This implies that when Pser[129] were high whenever ubiquitination was high, as shown in the correlation matrix bellow (Table 5.4).

Table 5.4, Correlation matrix of phosphorylation and ubiquitination.

	Pser129 Ubiqui~n
Pser129	1.0000
Ubiquitina~n	0.1141* 1.0000
	0.0196

Note: Total number of observations, N (Sample size) = 418; Top value within each cell represents the correlation coefficient (0.1141) and the value below is the p-value (0.1141); * shows significance at the 5% level.

Considering the results presented above, I proceeded to test for statistical differences between Pser[129] and ubiquitination simultaneously, using Two-way MANOVA with interaction, to test simultaneously for statistical differences between Pser[129] and Ubiquitination. I tested for main effects of disease status and brain region and interaction effects of brain region and disease status. The results for main effects and interaction effects for disease status (PD, PDD and Ctrl) and brain regions (substructures), shows that the overall model was significant, (MANOVA, $F_{(44,373)}$ =2.32, p<0.0001). The results show that interaction between disease status and brain region was not statistically significant (MANOVA, $F_{(28,373)}$ =1.13, P-value=0.2458). This implies that the effect of the disease status on the dependent variables was

similar in the different regions of the brain. I further observed that Pser[129] and ubiquitination covary across the different brain regions (MANOVA, $F_{(14,373)}$ =2.28, P=0.0002) and are differentially expressed between control and PD and PDD (MANOVA, $F_{(2,373)}$ =23.11, P<0.0001) (Table 5.5).

Table 5.5 Interaction between the disease status and brain regions

Source	Statistic		df	F(df1,	df2) =	F	Prob>F	
Model	W	0.6127	44	88.0	744.0	2.35	0.0000	e
	P	0.4299		88.0	746.0	2.32	0.0000	a
	L	0.5626		88.0	742.0	2.37	0.0000	a
	R	0.3792		44.0	373.0	3.21	0.0000	u
Residual			373					
Disease_s~s	W	0.7874	2	4.0	744.0	23.61	0.0000	e
	P	0.2205		4.0	746.0	23.11	0.0000	a
	L	0.2598		4.0	742.0	24.10	0.0000	a
	R	0.2120		2.0	373.0	39.54	0.0000	u
Substruct~e	W	0.8480	14	28.0	744.0	2.28	0.0002	e
	P	0.1578		28.0	746.0	2.28	0.0002	a
	L	0.1723		28.0	742.0	2.28	0.0002	a
	R	0.1096		14.0	373.0	2.92	0.0003	u
Disease_s~s#	W	0.8484	28	56.0	744.0	1.14	0.2336	e
Substruct~e	P	0.1563		56.0	746.0	1.13	0.2458	a
	L	0.1730		56.0	742.0	1.15	0.2219	a
	R	0.1298		28.0	373.0	1.73	0.0134	u
Residual			373					
Total			417					

e = exact, a = approximate, u = upper bound on F

5.3.2 Colocalization of different PTMs in Dementia with Lewy bodies.

5.3.2.1 Colocalization of Nitrated and phosphorylated aSyn in CC and TC of DLB patients.

Given the observed changes in αSyn phosphorylated at serine[129], so far described. I further performed colocalization analysis between the PTMs in the CC, from the immunofluorescent studies. This region was the focus because it is one of the most phosphorylated regions observed previously in DLB (see chapter 4). Moreover, the CC is within the limbic circuit loop, thus if there is a pathology in the amygdala, this

region is likely to be affected as well, I also assessed sections from the TC. The immunoreactivity of unmodified aSyn that contained detectable levels of nitrated protein was assessed immunofluorescence double labelling against phosphorylated aSyn. Here, I first used the same primary antibody concentration for anti-nitration antibody (1:200, figure 3). However, obtained result were not as clear as when we repeated the experiment at a higher concentration of the antibody (1:50), which was the final concentration for nitration antibody used for the rest of the experiments. The co-localization between nitrated and phosphorylated LBs/LNs was statistically significant in both Mander's and Pearson's test (*P<0.05,). However, this was not the case in all LBs, as some LBs that are phosphorylated, did not co-localise with the nitrated LBs. Furthermore, the degree of overlap for these two PTMs was not statistically significant when compared to controls (figure 5.3). It is important to highlight that in these experiments I assessed the colocalization of the two PTMs within the LBs, rather than regional or disease comparisons as it was performed in the histological studies. The co-localization coefficients and the sample size used for each these analyses are represented in the graphs and described in the figure legends as well.

A

TC
BA21
CC
BA32
TC
CC

B

	Nitration	Phosphorylation	Merged
DLB			
CTRL			
AB CTRL			

C

Nitration & Phosphorylation

Colocalization — Control / DLB
*
Pearson's coefficient

Nitration & Phosphorylation

distribution — Control / DLB
Pearson's coefficient

Nitration & Phosphorylation

Colocalization — CTRL / DLB
*
Mander's coefficient B

Nitration & Phosphorylation

Distribution — CTRL / DLB
Mander's coefficient B

Nitration & Phosphorylation

overlap — CTRL / DLB
NS
Overlap coefficient B

Nitration & Phosphorylation

Overlap — CTRL / DLB
Overlap coefficient B

Figure 5. 3: colocalization of nitrated and phosphorylated aSyn in DLB. (A) Representative images from Newcastle brain Map, showing the CC and TC where the slices were taken for the study **(B)** Images showing nitrated (green) and phosphorylated (red) and merged (orange) LBs in the CC of DLB cases, at 20 X magnification. The arrows (in black) indicating the LBs. **(C)** Bar chart (left) and corresponding scatter plot (right), showing the degree of colocalization under different colocalization tests (Pearson, Manders and the overlap coefficient) in control (n=10 cases) and DLB (n=10 cases).

5.3.2.2 Colocalization of Nitrated, ubiquitinated and Total αSyn in CC and TC of DLB patients

Further analysis was performed to corroborate whether the changes observed with phosphorylation would also be seen with the ubiquitination. Interestingly, the degree of colocalization between Ubiquitination and nitrated antibodies where not statistically significant in all three tests used (P>0.05,) (figure 5.4). Since the observed immunoreaction to anti ubiquitin antibody overlapping with the nitration antibody, was not statistically significant, I decided to correlate the nitration signal with another pan antibody that detects total cytosolic aSyn. Similarly, no significant differences were observed between the correlation of nitrated aSyn and total aSyn (P>0.05,) (figure 5.4).

A

TC
BA21
CC
BA32
TC
CC

B

| Nitration | Ubiquitin | Merged |

DLB

CTRL

AB CTRL

50 µm

50 µm

C

Nitration vs Ubiquitination

NS

Colocalization

Control
DLB

Control   DLB
Pearson's coefficient

Nitration vs Ubiquitination

Control
DLB

Control   DLB
Pearson's coefficient

Nitration vs Ubiquitination

NS

Colocalization

Control
DLB

Control   DLB
Mander's coefficient B

Nitration & Ubiquitination

Control
DLB

Control   DLB
Mander's coefficient B

Nitration vs Ubiquitination O

NS

Correlation

Control
DLB

Control   DLB
Overlap coefficient B

Nitration & Ubiquitination

Control
DLB

Control   DLB
Overlap coefficient B

193

Figure 5. 4: Colocalization of nitrated and ubiquitinated aSyn in DLB. (A) Representative images from Newcastle brain Map, showing the CC and TC where the slices were taken for the study **(B)** Images showing nitrated (green) and Ubiquitinated (red) and merged (orange) LBs from number of sections of CC of post-mortem brain tissue of DLB cases, at 20 X magnification. The arrows (in black) indicating the LBs. **(C)** Bar chart (left) and corresponding scatter plot (right), showing the degree of colocalization, using different colocalization tests (Pearson, Manders and the overlap coefficient) in control (n=10 cases) and DLB (n=10 cases).
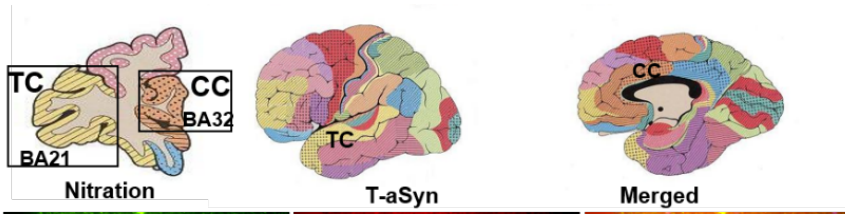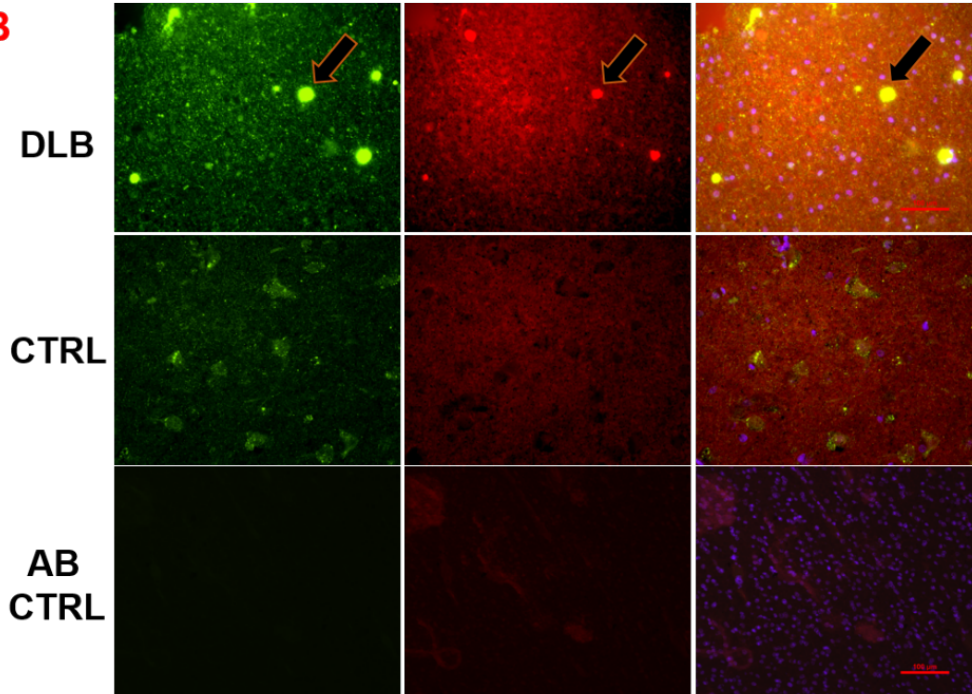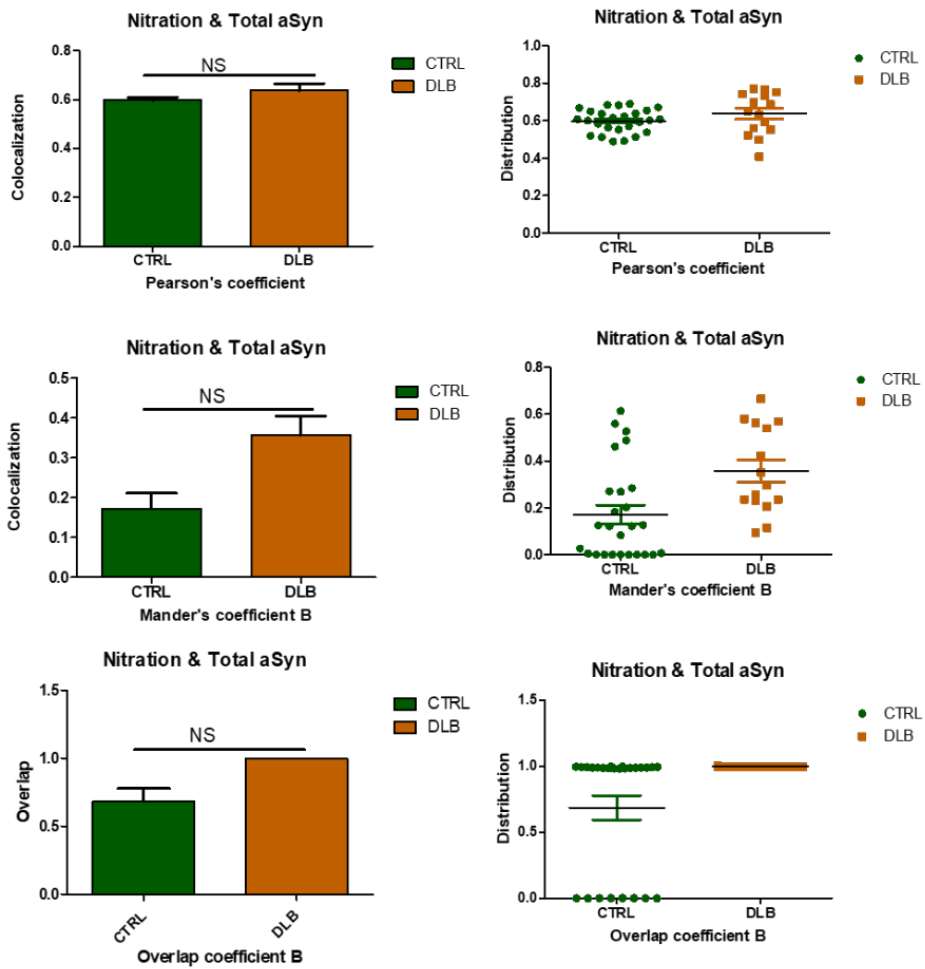
Figure 5. 5: Colocalization of nitrated and total aSyn in DLB. (A) Representative images from Newcastle brain Map, showing the CC and TC where the slices were taken for the study **(B)** Images showing nitrated (green) and Ubiquitinated (red) and merged (orange) LBs from number of sections of CC of post-mortem brain tissue of DLB cases, at 20 X magnification. The arrows (in black) indicating the LBs. **(C)** Bar chart (left) and corresponding scatter plot (right), showing the degree of colocalization, using different colocalization tests (Pearson, Manders and the overlap coefficient) in control (n=10 cases) and DLB (n=10 cases)

5.4 Discussion

5.4.1 Relationship between αSyn PTMs in LBDs

In this chapter, I have shown the correlations between ubiquitinated and phosphorylated αSyn in cortical and subcortical regions of LBDs cases. Since, in chapter 4 I have demonstrated that αSyn in LBs/LNs are widely phosphorylated and ubiquitinated in LBDs. Here, I tested correlations and colocalizations of the neuroanatomical distribution of the PTMs in LBDs, to corroborate their temporal occurrence to induce the formation of toxic forms of αSyn that leads to aggregations. Although, most research on αSyn PTMs is carried are studied individually (Zhang et al., 2019), phosphorylated αSyn have previously been shown to be targeted for ubiquitination in the synucleinopathies (Hasegawa et al., 2002). The results presented in this chapter supports this by showing positive correlation between phosphorylation and ubiquitination across brain regions affected with LBDs. To my knowledge, this is the first study that makes these comparisons of both PTMs in LBs/LNs involving different but neuroanatomically related brain structures reported to be affected in LBDs. Most studies that have analysed regional distribution of αSyn pathology used the conventional methods such as immunohistochemistry and haematoxylin eosin staining to detect αSyn aggregates in form of LBs/LNs inclusions (Del Tredici et al., 2002, Braak et al., 1999, Sandmann-Keil and Braak, 2005). Similar techniques were applied here, but using TMA slides (see chapter 3, 4 and 5). Here, the differences between the control and the disease status were highly significant. However, no significant differences were observed between the distinct regions within the disease and control groups. This lack of difference in the affected regions of DLB suggests that an association between phosphorylation and ubiquitination is occurring, as the impact within the region is quite similar for LBs detected in each region.

The analysis presented for this data is by no means exhaustive. As there are many more parameters to explore. For instance, it would be ideal to analyse how these associations affects each brain region per disease status. However, this would require a more complex and sophisticated analysis. I would argue that one way to do this, could be by analysing the interaction between the brain regions using some form of two-way ANOVA (which I tried before, I believe to be not adequate for the main question I am addressing in this thesis) or other forms of multiple regression analyses.

due to the time limitations, the complexity and extensiveness of my data, it was not possible to perform all the analysis I desired to do in this chapter, to answer all the possible questions, which is a limitation for this thesis. The analysis presented here are restricted to simply address the main questions of the thesis. Notwithstanding, I am still working on other analysis, which in the article for publication. Thus, for the purpose of the thesis, I have only shown this data.

5.4.2 Colocalization of Nitrated and phosphorylated αSyn in CC and TC of DLB patients.

Given the above described changes in PTMs and their degree of co-localization with Nitration, here Instead of examining all the regions, I focused on the CC and TC, as these regions are shown to be one of the cortical regions with high physiological levels of αSyn, in addition largely affected with Lewy body pathology (Erskine et al., 2018). In agreement with this, the results presented in this thesis shows that TC and CC is one of the regions where both phosphorylation and ubiquitination was observed in DLB (see chapter 5). The few sections from TC were used to corroborate the results obtained with CC; this was not the case with other brain regions, as there were not enough resources to acquire other samples from other brain regions, hence I have not included them in this study. To my knowledge, this is the first attempt to study the co-localisation of the three forms of PTMs of αSyn in DLB.

In the neocortex, MC and CC are the most affected regions for both ubiquitinated and phosphorylated αSyn, whereas within the subcortical regions the amygdala resulted to be the region with the highest affected for both ubiquitination and phosphorylation. Similar results were also found in PD and PDD cases. This is in accordance with a study that shows abnormal αSyn aggregation in MC CC and the amygdala of DLB patients (Popescu et al., 2004, Braak et al., 1999, Sandmann-Keil and Braak, 2005, Braak et al., 2004, Braak et al., 2003b). Saito et al., demonstrated that αSyn toxicity begins in the medulla oblongata or the amygdala specially when associated with AD to then extend to the cortical regions (Saito et al., 2003) In fact, amygdala involvement is thought to be selective in DLB. However, it is not restricted to this disease alone, as it is also found in DLB variant of AD (Popescu et al., 2004). Thus, the results presented here, suggests that αSyn immunoreactive inclusions that are phosphorylated and ubiquitinated have also predilection for specific cortical and subcortical regions (Braak

et al., 1999, Sandmann-Keil and Braak, 2005, Saito et al., 2003). Moreover, the strong relationship between ubiquitination and phosphorylation in LBs, implies that there is a possible interaction interrelation between phosphorylation and ubiquitination, leading to αSyn toxicity and aggregation. With this in mind, I may speculate that the PTMs of αSyn has strikingly higher expression in brain regions that are prone to Lewy pathology. Hence, the vulnerability of the Lewy body pathology may be the product of the neuro anatomical connections between these regions in associations with their regional autonomous factors.

The immunoreactivity of unmodified αSyn that contained detectable levels of nitrated protein was assessed immunofluorescence double labelling for phosphorylated, ubiquitinated and Total αSyn. I showed that the degree of co-localization between nitrated and phosphorylated LBs/LNs were significant. However, this was not the case in all LBs, as some LBs that are phosphorylated, do not co-localise with the nitrated LBs. Furthermore, overlap for these PTMs was not de same in the controls and patients. In agreement with the results presented here, a similar study using immunofluorescence double labelling antibodies against Pser[129] and nitrated αSyn have shown colocalization between these two forms of αSyn PTMs within the soma of DA neurons of a primate, as a result of a normal ageing. This co-immunoreaction was not observed in younger primates (McCormack et al., 2012).

Although, the reasons for the marked co immunoreaction between phosphorylation and nitration remains elusive, the results shown here does suggests that they may contribute in the αSyn toxicity, as almost no immunoreactivity was observed in control cases. On the other hand, the degree of co-localization between nitration and ubiquitination was not significant. Although, some degree of co-immunoreactivity can be found in some cases for these PTMs, the majority of the immunoreactivity were not co-localised with nitration. Since the observed immunoreaction to anti ubiquitin antibody overlapping with the nitration antibody, was not statistically significant, I decided to correlate the nitration signal with another pan antibody that detects total αSyn in the cytosol. Similarly, no significant differences were observed between the correlation of nitrated and total αSyn. One reason for the lack of significance may be

because they are pan antibodies as they are widely present even in normal cells, so they could be immunoreactive even to physiological αSyn and ubiquitin.

PTMs are known to compromise the biological activity of the proteins, with the potential to form toxic species of these proteins. For instance, αSyn phosphorylation is thought to bind with membrane phospholipids and other proteins, and αSyn nitration is thought to induce adaptive immune response and causing microglia activation (Paleologou et al., 2008, Pronin et al., 2000, Benner et al., 2008). Thus, the co-localization of these PTMs may likely be of pathological relevance in age related disorders such as DLB. Although, in this study, I cannot establish whether the co-localization of the PTMs have a direct causative role in the development of DLB. The widespread phosphorylation and the observed co-localization with nitration, together with other changes such as αSyn mutation, indicate that they are relevant in the disease pathogenesis. Furthermore, it was shown that phosphorylated and nitrated αSyn are less susceptible to be degraded by CMA, compared to the unmodified αSyn (Martinez-Vicente et al., 2008). Hence, the PTMs changes observed here may contribute to the αSyn accumulation.

In the histochemical studies (chapter 4) nitration experiment did not show signals that were indicative exclusively for LBs/LNs, as the antibody did not seem to be specific. However, this was not the case with the immunofluorescence, for the reasons that remains to be elucidated. After different adjustment in the antibody concentration, for the immunofluorescence studies, the results were somehow positive and immunopositive signals for LBs could be observed. Therefore, I decided to carry on with the investigations onto how they would correlate with the other PTMs. Another limitation for this study were that Nitration antibodies were uniquely made in mouse so the second antibodies that work with mouse were (Igg 488) which colour for green. The other antibodies would not work for this second antibody as they were made in different species. Thus, I had difficulties to find the right manufacturer that could provide Pser[129] and ubiquitinated antibodies that would work with this secondary antibody.

5.4.3 Parvalbumin cells and posttranslational modifications of αSyn.

The results obtained with αSyn PTMs and their colocalizations, prompted me to analyse them, to see whether they correlate with the observed changes in of PV+ cells

as observed in chapter 4. Multiple lines of evidence have been emerging, providing evidence of the involvement of PV+ interneurons to be a key for the development of dementia (Kann et al., 2014b, Raz et al., 2016, Verret et al., 2012, Fernández-Suárez et al., 2012, Uehara et al., 2015). Therefore, I believe that the biological relevance of PV+ interneuron should be analysed according to their relationship with αSyn toxicity. In fact, the co-localisation of αSyn with PV expressing fast spiking interneurons was found to be linked with the decrease of this group of neuronal populations in DLB (Bernstein et al., 2011b). In chapter 4, I reported that PV+ interneurons were significantly reduced in certain brain regions of DLB patients. The observed reduction in PV+ cells, led me to question whether the observed reduction were/were not associated with the so far observed phosphorylation and ubiquitination of αSyn (see chapter 5). Here I show that the degree of correlations between PV+ cells and αSyn ubiquitination in cortical and subcortical regions of DLB cases is statistically significant between disease and control groups. Interestingly, these differences were highly significant when compared between regions affected. Highly significant differences were observed when compare the subcortical regions, and PFC with the amygdala being the most affected region. Similar results were observed when I extended the analysis to compare the phosphorylation effects in PV+ cells in cortical regions of DLB patients. Significant differences were also observed between the different regions analysed, with higher increase of phosphorylation and reduction of PV+ cells in the PFC and the amygdala.

Synucleinopathies and other types of dementias are associated with neuronal loss across the cortical cortices and subcortical structures (Raz et al., 2016). In DLB, αSyn interacts to pathological stimuli by forming aggregates (LBs and LNs) of the cell constituents within the soma and axons that consequently leads to the death of the nerve cell (Hijaz and Volpicelli-Daley, 2020, Outeiro et al., 2019, Wales et al., 2013). Since, neurons are interdependent cells, the damage to one nerve cell leads to the death of the others, and thus the subsequent tissue atrophy (Castelli et al., 2019). The loss of these interneuron populations implies loss of neuronal connection across functional brain networks between cortical and subcortical structures. Thus, impairing the neuronal network oscillations such as, gamma oscillations that is thought to underlie important brain functions such as movement and cognition (Uehara et al., 2015, Robson et al., 2018b). Thus, the results presented here, provide an insight on

how the pathological burden of PTMs in αSyn affects this group of interneurons. Moreover, the loss/malfunction of PV cells is thought to affect negatively the function of the neuronal networks (Bernstein et al., 2011b). Therefore, this comparison of PTMs and the loss PV+ interneurons is worthy of note, given the importance of these cells in forming the neuronal networks and their involvement in the generation of gamma frequency oscillations which are essential for cognitive and motor functions (Bernstein et al., 2011b, Bonanni et al., 2008, Whittington and Traub, 2003)

5.5   Conclusion

In this chapter, I carried out a comparison analysis ubiquitinated and phosphorylated αSyn in LBs/LNs across different brain areas affected in DLB, according to the stages of the disease progression. I also analysed de degree of co-immunoreaction between phosphorylation, ubiquitination, nitration and total αSyn. Since αSyn PTMs are individually detected in regions that are affected with Lewy bodies pathology, I hypothesised that the degree of correlation between these PTMs would be increased in these regions of post-mortem brain tissue of LBD patients. Indeed, these correlations were evident in disease groups, with statistically significant differences when compared to control. The PFC, CC and the amygdala are the most affected regions observed in this study. Due to their presence and interrelation of these PTMs, regarding to the disease development. I can speculate that they may have contribute in the αSyn toxicity to develop the pathogenic cascade observed in LBDs. Thus, targeting these PTMs, may be used to develop novel therapeutic approaches for LBDs. Moreover, the observed association may not be exclusive to the PTMs studied in this chapter. I believe this may be a phenomenon that also occur with other posttranslational modifications that are known to occur in αSyn. Which will need further studies to corroborate.

Chapter 6: General Discussion
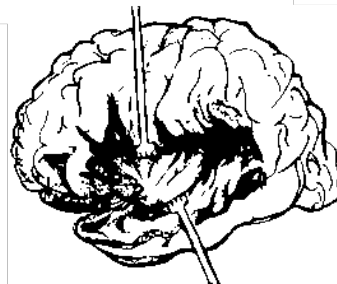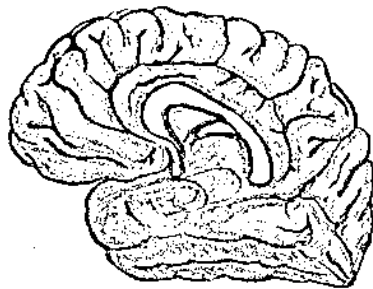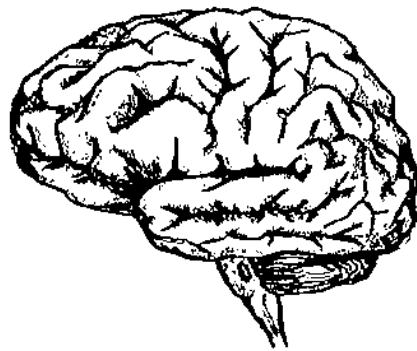
In this thesis, I have addressed the questions related to the distribution of PTMs in different areas of the brain in relation to LBD progression, their links with the reduction/dysfunction of PV+ interneurons and the subsequent impairment of gamma network oscillations in LBDs. I have chosen to focus my research on these topics, because they are implicated in the pathogenesis of age-related diseases aligned with the LBDs (Pajarillo et al., 2019, Beyer, 2006, Craig and McBain, 2015, Mably and Colgin, 2018, Robson et al., 2018b). Although, the exact role of PTMs, PV+ interneurons dysfunction and the impairments of fast neuronal network oscillations, has not been thoroughly investigated, the findings presented in this thesis shed light on these questions, as it unveils how PTMs and PV+ interneuron loss may be the basis of the pathogenic cascade that causes these synucleinopathies. The results presented in this thesis are summarised as follows:

- The mouse model (A30P) of synucleinopathy presents with mitochondrial dysfunction and exhibits greater impairment of fast neuronal network oscillations by showing reduction in the area power of gamma frequency band.

- Treatments aimed to restore the impairment of the oscillations such as, sodium pyruvate and Memantine, showed moderate positive effects in improving gamma frequency oscillations impaired in A30P mice.

- Significant reductions in the numbers of PV+ interneurons were evident in regions such as the MC, EC, IC, CN, GP and the amygdala. Although, the density of PV+ interneurons remained relatively unchanged in other areas of the brain, such as PFC, MFC, PC, TC, OC, CC, PTm and Thalamus. Moreover, the density of and PNN was not significantly changed in PFC of the A30P mice.

- αSyn PTMs such as ubiquitination and phosphorylation were detected in almost all regions of LBD patients, and phosphorylation of αSyn was widely present in LBs/LNs inclusions in almost all regions of LBD patients.

- Among the disease groups, DLB and PDD were the most affected by phosphorylation and within cortical regions, the CC was the most affected area

in DLB and the IC in PDD. In the subcortical regions, the amygdala was the region with the highest immunoreactivity in all LBDs.

- αSyn Ubiquitination showed higher immunoreactivity in the OC in DLB and in PD, and in PDD the MC was the most ubiquitinated region. However, In subcortical regions, GP is the region with the highest immunoreactivity in both DLB and PD. with higher immunoreactivity circumscribed in DLB.

- Positive correlations between phosphorylation and ubiquitination were observed across brain regions affected with LBDs.

- In the neocortex, MC and CC are the most affected regions for both ubiquitinated and phosphorylated αSyn, whereas within the subcortical regions, the amygdala was found to be the region with the highest rates of both ubiquitination and phosphorylation. Similar results were also found in PD and PDD cases.

- Negative correlations between PV+ cells and αSyn ubiquitination and phosphorylation were also present in cortical and subcortical regions of DLB cases. Highly significant interrrelation were observed in the PFC and the amygdala.

- The widespread phosphorylation and the observed co-localization with nitration, together with other changes such as αSyn mutation, indicate that they are relevant in the disease pathogenesis.

6.1   αSyn PTMs in LBDs

LBDs share the common pathological features of protein aggregation which forms LBs/LNs (Kosaka, 2014, McKeith et al., 1996, McKeith et al., 2004, Gurd et al., 2000, McKeith et al., 2017), where aSyn protein has been recognised as their main constituent (Baba et al., 1998, Kosaka et al., 1984, Kosaka, 2014, Dickson, 1999). Although, the role of aSyn in LBD pathogenesis has been a major area of focus since the discovery of point mutations in the aSyn gene of familial forms of PD (Nemani et

al., 2010, Polymeropoulos et al., 1997) and its rapid confirmation as the major component of LBs in 1997 (Spillantini et al., 1998, Spillantini et al., 1997) it is still unclear whether the disease, starts before or after the inclusion formation, thus, the exact cause that leads to the formation of LBs/LNs remains poorly understood. Nevertheless, more recent evidence has been emerging, suggesting that the pathogenic cascade of LBDs, starts before the proteins form LBs/LNs inclusions (Visanji et al., 2019). In fact, some studies have shown that, in some cases, a certain degree of LBs/LNs can also be detected in non-demented individuals, although the number and size of these aggregates is relatively lower compared to the disease-affected individuals. Likewise, in some individuals, these neuropathological inclusions (aggregate formation) correlate with frank dementia, while in others they appear to be inert with no impact on cognition and limited pathology (Kosaka, 2014, Kosaka et al., 1988). These observations have sparked questions such as why some aged individuals with LBs/LNs inclusions do not develop dementia, does the clinical disease phenotype start after the formation of LBs/LNs inclusions, and whether neurodegenerative diseases are a direct consequence of ageing or of a distinctive disease caused by an identifiable molecular pathology (Stern, 2012, Attems et al., 2005).

It is known that, during its lifetime, αSyn undergoes a series of PTMs in different regions of the protein, at different grades, leading to conformational changes that may trigger the aggregation process (Barrett and Timothy Greenamyre, 2015). Different regions of the protein containing different amino acid composition promotes different biochemical properties, that make them susceptible to PTMs such as phosphorylation, ubiquitination and nitration (Villar-Pique et al., 2016). When these modifications are irreversible, it modifies the physiological role, thus becoming prone to aggregate or alter toxicity. Although the connections between different mutations that occur in the αSyn gene and the different pathogenic pathways of the protein, that are attributed to different phenotypes within the synucleinopathies remains elusive. It is possible that the PTMs are facilitated by mutations that previously occur in the genes that codify the proteins, including the SNCA gene (see chapter 1). Although, in this thesis I have only investigated 3 PTMs of αSyn, it is important to highlight that other PTMs such as glycation, acetylation, nitration, glutathionylation, glycosylation, sumoylation, and truncation were also identified in αSyn (Fauvet et al., 2012, Theillet et al., 2016, Li et

al., 2005, Kunadt et al., 2015, Zhang et al., 2018, Spiro, 2002, Resh, 2016). For a relatively small molecule, this is a remarkable number of PTMs. Hence, I believe these PTMs may be at the base of αSyn toxicity that causes cellular dysfunction even before forming the inclusions, consequently leading to neuronal cell death. It is possible that these PTMs occur at the same time at different sites of the protein and colocalize, thus, potentiating αSyn toxicity and its propensity to aggregation. For instance, it was demonstrated that aSyn tendency to aggregate might be affected by the interrelation between phosphorylation and nitration (Fujiwara et al., 2002, Hodara et al., 2004, Paleologou et al., 2008).

Moreover, the observed co-localization of phosphorylation, ubiquitination and the nitration, together with other changes such as αSyn mutations, may indicate that they are relevant in the disease pathogenesis. Although, in this study, I cannot establish whether these co-localization and interrelationships of the PTMs have a direct causative role in the development of DLB, it is known that PTMs have the ability to induce monumental conformational changes in the physiologic properties of the protein (Beyer and Ariza, 2013). Signifying that the protein undergoes extensive PTMs before it becomes toxic. I suggest the protein toxicity may start before the aggregation, creating a series of neuronal dysfunctions within a specific set of neuronal population, thus inducing an idiopathic functional syndrome before structural changes becomes evident.

6.2 αSyn PTMs, PV+ interneurons dysfunction and abnormal neuronal network oscillations

PV+ cells are one of the main targets of toxic αSyn and play a key role on the neuronal network functions. The interrelationship between αSyn and PV+ cells is highlighted by the significant reductions in the numbers of these cells in DLB (Bernstein et al., 2011a, Inan et al., 2016, Kann et al., 2014b). Likewise, DLB, is found to progress with impairments of the abnormal network oscillations (Robson et al., 2018a). In fact, the reduction in density or loss of function of PV+ interneurons may be at the basis of the network connectivity impairment and the subsequent cognitive dysfunction, since they are shown to be affected in many neuropsychiatric disorders, including schizophrenia, and neurodegenerative disorders (Brady and Mufson, 1997, Nakazawa et al., 2012, Fuchs et al., 2007). Moreover, the loss of PV+ cells was reported in in animal model

of schizophrenia, and it's found to be associated with impairments of the neuronal network oscillations (Lodge et al., 2009)

Although αSyn is ubiquitous in the CNS (Goedert et al., 2013, Goedert, 2001, Ghiglieri et al., 2018), it has been suggested, that PV+ cells appear to be free of LBs/LNs inclusions. Notwithstanding, the same study demonstrated a partial loss of PV+ cells within the hippocampus of DLB patients (Bernstein et al., 2011b), suggesting that the reduction of these group pf cells may be associated with the increase of toxic species of αSyn, which is overexpressed in DLB. Thus, it is believed that hippocampal loss of PV+ cells might be due to the prolonged calcium overload in coadunation with the impaired mitochondrial function caused by αSyn (Bernstein et al., 2011a, Robson et al., 2018b). Mitochondrial dysfunction in mouse model synucleinopathies is one of the findings presented in this thesis; therefore, it would not be deviant to link the loss of PV+ cells due to mitochondrial impairment. This is also supported by a study demonstrating that, αSyn phosphorylated at Ser[129] , promoted mitochondrial dysfunction and the formation of ROS which are common pathogenic features of LBDs (Perfeito et al., 2014). In fact, a strong correlation between rotenone and Pser[129] αSyn in the formation of ROS, where the overexpression of αSyn triggered ROS release, as well as both the exposure of rotenone and the ROS release lead to greater phosphorylation of αSyn (Perfeito et al., 2014). Thus, αSyn Pser[129] could lead to biochemical changes (oxidative stress, mitochondrial complex I dysfunction and proteasome impairment) that are associated with LBD pathogenesis (see figure 1.6) (Lashuel et al., 2012, Lee and Trojanowski, 2006, Robson et al., 2018a).

One main consequence of αSyn associated numerical decrease of PV+ cells, is its negative impact in gamma rhythmogenesis in LBDs, as It has been demonstrated that PV+ fast spiking interneurons play a key role in the generation of the gamma frequency oscillations (Robson et al., 2018b). The involvement of PV cells in gamma rhythmogenesis was demonstrated in an *in vivo* optogenetic study in mice, where gamma oscillations were abolished when fast spiking PV+ interneurons were silenced (Sohal et al., 2009). In rodent *cornu ammonis* 3 (CA3) region of the hippocampus, gamma frequency oscillations are also found to be dependent on the PV+ cells (Traub et al., 2000, Ferando and Mody, 2015, Fuchs et al., 2007).

Gamma frequency oscillations are linked with learning, memory and information processing (Schneider et al., 2015b). They are generated by complex synaptic interactions between inhibitory GABAergic interneurons, (where PV+ basket cells play a major role) and excitatory pyramidal cells (Whittington and Traub, 2003, Kann, 2011). PV+ interneurons synchronize the firing of pyramidal cells by inhibiting the firing rate of the pyramidal cells. This process requires a high-energy consumption and an intact mitochondrial function (Kann et al., 2014b, Hu and Jonas, 2014). Thus, it is not unexpected that αSyn related mitochondrial dysfunction would be linked with the dysfunction/loss of these group of interneurons. In addition, PV+ cells are also impaired in other neuropsychiatric disorders such as schizophrenia, and these cells are affected when gamma oscillations are impaired (Kuki et al., 2015, Sohal, 2012a).

Furthermore, strong interrelationship between PV+ cells, αSyn ubiquitination and phosphorylation were present in cortical and subcortical regions of DLB cases, with highly significant correlations detected in the PFC and amygdala. These regions bear high burden of pathology (Flores-Cuadrado et al., 2017, Honkanen et al., 2014, Jellinger and Attems, 2013, Braak et al., 2003b). This signifies that the circuit that connects the two regions essential for cognitive functions are impaired in DLBs due to insufficient IPSP generated by the reduced numbers of PV+ cells. This interrelationship between increased phosphorylation, ubiquitination and the decrease in number of PV+ cells in brain regions that are heavily affected with the pathology, supports the hypothesis of early αSyn damage that occurs before the inclusion formation. This allows the establishment of an idiopathic functional impairment of the brain networks that leads to the development of the clinical phenotypes, even before the observed microscopic changes such as LBs/LNs inclusions and macroscopic modification such as atrophy of key regions becomes evident in LBDs.

6.3   Distribution of PTMs and their involvement in LBD pathogenesis

The distribution of PTMs across brain regions of individuals with LBDs, is an important aspect to analyse, as it provides an insight on how PTMs affects LBDs and may help to understand where the pathologic lesions starts and how it progresses. Since the accumulation of LBs and LNs is observed in different stages of pathological progression of these synucleinopathies, as proposed in Braak disease staging scale (Braak et al., 2003a), it is possible that PTMs follow the same pattern. Nevertheless,

no study has assessed the topographic distribution of these PTMs according to the disease stages progression as proposed in McKeith/Braak scales. I believe that the assessment of disease associated PTMs of aSyn is key to the comprehension and discernment of potential reasons for the pathological aggregation and the observed preference of distribution patterns as seen in these synucleinopathies.

Although different staging and classification systems have been used to classify the LBDs. the most widely known are Braak and Newcastle McKeith scales (Goedert et al., 2013, Braak et al., 2003b, Alafuzoff et al., 2009, McKeith et al., 2017). In this study, I was not able to compare the results of the distribution of PTMs with the existing Braak/McKeith scales, due to some limitations in the accessibility of the data, as the data was not available, and I was not granted the access to the archives where these datas were stored. Notwithstanding, it is possible to observe that the distribution of these PTMs observed here follow similar topographic spreading of LBs and LNs in anatomically related structures such as brainstem, mesocortex and neocortex as determines the pathological staging of LBDs as proposed by Braak et al (Braak et al., 2003a). For instance, in PD, the damage of DA neurons in the substantia nigra is the most important pathological Hallmark. Other extra nigral damages such as lesion of dorsal motor nucleus of IX/X cranial nerves have also been reported. Moreover, damage in caudal raphe nuclei, reticular nucleus, coeruleus and sub-coeruleus complex is also observed in PD. These regions were not studied in this thesis, because an adequate number of samples with complete LC and reticular formation were not available to anable a more thorough analysis. Nevertheless, lesions that progresses from the midbrain (Braak 1-3), and spread to the prosencephalic regions, with the involvement of the temporal mesocortex and allocortex and neocortex (braak 4-6) (Braak and Del Tredici, 2017, Braak et al., 2003a), were analysed. Thus, it was not possible to make a complete analysis of all the regions affected with LBDs as described in Braak/McKeith scales.

In addition, the involvement of the neocortical areas is important for the development of DLB and PDD and represents the clinic-pathologic severity of the disease, whereas PD is more restricted to the prosencephalic structures (Braak et al., 2003a, McKeith et al., 2017). One important aspect of disease progression described in these scales, is that it suggests that the characteristic pathological extension of the LBDs, follows a fixed topographic sequence of development in anatomically interconnected regions.

By observing, the regions with higher burden of PTMs similar trends can be observed on the distribution of phosphorylated αSyn where the amygdala represented the most affected region in the subcortical regions, followed by the PFC in cortical areas. Thus, these observations, provide a hint of the molecular mechanism that underlie this progression, which is crucial to understand the propagation of LBDs. On the other hand, In this thesis, I was unable to reliably demonstrate the distribution of nitrated αSyn. It is therefore unclear whether these PTMs follows the same anatomic distribution, as it is observed with phosphorylation and ubiquitination. Although the tools seemed not to work as well as desired, it was possible to see some specific immunoreactivity when used for fluorescence studies. In addition, I was not able to find other studies that have used nitration for histological studies, to try to follow their protocols or compare their results. Therefore, regarding to nitration experiments, in this thesis I presented a very preliminary results on the identification of nitrated aSyn in LBs.

6.4   The relevance of PTMs in the basal ganglia in LBDS pathogenesis

The basal ganglia (BG) are the most prominent subcortical telencephalic structure in mammals, it is a set of richly interconnected brain nucleus, which are involved in producing voluntary movements (Bhatia and Marsden, 1994, Mark et al., Lanciego et al., 2012). Moreover, its connections with sensory motor and cognitive apparatus of the brain, suggest that it may also be involved in more roles, such as, interpretation of sensory information (Lanciego et al., 2012). The major structures that compose this group of nucleus are the caudate nucleus (CN), putamen (Ptm), globus pallidum (GP) (Lanciego et al., 2012). The major sources of input to BG comes from the cortex and the thalamus (Leisman et al., 2014, Lanciego et al., 2012, Obeso et al., 2008). Most of the input stimuli arrive in the neostriatum (CN, Ptm, and the nucleus acumbens). The neostriatum receives input from the neocortex, thalamus (intralaminar nucleus) SN (from DA neurons) and the dorsal raphe nucleus. It also receives input from the limbic system and the hippocampus. The output signals from the neostriatum project to other BG nuclei, to then connect with the thalamus. The output signals are mostly inhibitory in their nature, thus inhibiting the cortico-thalamic-cortico pathways (figure 7.1) (Hwang et al., 2017, Haber and Calzavara, 2009, Leisman et al., 2014). In

addition, the neostriatum has also reciprocal connections with the SN (figure 7.1) (Haber and Calzavara, 2009, Haber, 2014).

Although most of the neurons in the BG are pyramidal neurons, the BG contain a vast amount of PV+ cells, which are characterized to have a medium sized round soma, varicose chapped dendrites that surrounds the soma of the pyramidal cells. These interneurons are similar to those observed in the hippocampus and the neocortex and they exert powerful GABAergic inhibition to the pyramidal cells excitatory signals (Contreras et al., 2019, Bhatia and Marsden, 1994, Mark et al.). Indeed, the inputs that arrive from cortex, amygdala and hippocampus propel inhibitory responses, attributed mostly to the PV+ cells from the neostriatum to the thalamus, which in turn inhibits the EPSP from the cortex. Thus creating a circuit of excitation-inhibition-excitation pattern in the BG-thalamus-cortical circuit (figure7.1) (Murata and Colonnese, 2019). Here I demonstrated a reduction in the density of PV+ cells that correlates with the increase of aSyn phosphorylation and ubiquitination, in the neostriatum (GP and CN), suggesting that the excitatory inputs that arrives from the cerebral cortex to the neostriatum, is not being effectively inhibited, due to the reduction in density of these cells. This conveys a reduction in the area of synapses of these cells, as their arborized dendritic shapes of their neuronal processes, establish multiple connections with various axons from pyramidal cells that descend from the cortex (Murata and Colonnese, 2019, Udakis et al., 2020). Thus, a loss of a single PV+ interneuron alone would be enough to initiate damage in the local neuronal circuit. Therefore, this affectation of the BG and thalamus and could thus compromise the normal functioning of this BG-thalamo-cortical circuitry.

In addition, the importance of the BG in LBDs is emphasized by the impairment in motor control, often presented as parkinsonism, which is one of the core symptoms of the disease (Obeso et al., 2008). The loss of dopaminergic neurons observed in PD may contribute to the fall in overall striatal activity, producing less inhibition to the GP. The resulting increase of GP activity produces excess inhibition to the thalamus thus decreasing the excitatory input to the cortex, resulting in hypokinesia (figure7.1) (Alexander, 2004). Although not studied here, another important structure involved in movement disorder is the SN, as it plays an important role in the BG-thalamo-cortical circuit (Damier et al., 1999). The SN is abundant in dopaminergic (DA) neurons, which forms projections that form the nigro-striatal pathways (Damier et al., 1999). The loss

of these neurons leads to the reduction of projection to the striatum, therefore to motor dysfunctions (Damier et al., 1999). The loss of the nigro-striatal connections subsequently leads to a loss of inhibition output from the SN par reticulate and the internal GP, to the sub-thalamic nucleus. On the other hand, this loss of inhibition leads to a relative hyperexcitability output from the sub-thalamic nucleus. Thus, inhibiting the thalamic regions to the motor cortex, resulting in akinetic rigidity, a core symptom of PD (Mark et al., Damier et al., 1999, Dickson, 2012, Alexander, 2004). The decrease in density or a functional impairment of the PV+ cells in these regions of the brain could perpetuate this vicious cycle of excitation inhibition imbalance observed in BG-thalamo-cortical circuit, due to the reduction of stimuli from SN to the neostriatum. This may occur due to the impairments of aSyn, as it is at the centre of the pathogenic consequences in LBDs. Because PV+ interneurons play Key roles in maintaining the neuronal networks in the brain (Ferguson and Gao, 2018). I believe toxic aSyn cause dysfunction/death in these neurons, which leads primarily to neuronal network dysfunctions, before the morphological changes become evident.

6.5 The relevance of PTMs in the Limbic system and the cortex in LBDS pathogenesis

The limbic system (LS) forms a connective loop around the mesencephalic and diencephalic structures. It comprises the cingulate cortex (CC), orbitofrontal cortex (OBFC), insular cortex (IC), parahipocampals gyrus, hippocampus and the amygdala. The LS is responsible for processing emotions, learning and memory (Rolls, 2019). The hippocampus receives its major inputs from the entorhinal cortex, which are mainly glutamatergic passing through all the four regions (CA1, CA2, CA3, CA4) targeting mainly the CA3 which is the pyramidal cell layer. In the hippocampal formation, there is a strict regulated interaction between the glutamatergic dentate granular cells, and pyramidal cells in the CA3 and CA1 regions, involved in excitatory transmission, and the GABAergic interneurons, responsible for inhibitory input (Leranth and Hajszan, 2007). Although in mice we observed no significant decreases in PV+ cells, it has been reported that PV+ cells are partially reduced in the hippocampal cortex of DLB patients (Bernstein et al., 2011b). The observed statistical insignificance of the results in the hippocampus does not obscure the fact that functional damage is occurring, as the quantification of these cells does not uniquely

explain the αSyn-related damage into these highly sensitive and metabolism-dependent cells. It is possible however, that functional deficits occur way before the numerical decrease. This explains the impairments of the gamma oscillatory frequency as observed in the A30P mouse model of DLB, Giving the role of PV+ in gamma rhythmogenesis (Kann, 2011, Robson et al., 2018b). This also means that, the feedforward inhibition mediated by PV+ interneurons, that is thought to control the output signals from the deep layers of the EC cortex is impaired, as it is considered to be the starting point of the hippocampal circuit, because it provides most of the excitatory input to the hippocampus (Willems et al., 2018, Ye et al., 2018). This may also explain the early hippocampal hyperexcitability observed in A30P mice (Tweedy, 2019) The observed αSyn-related loss of PV+ cells in the EC, suggests that impulses transferred to the hippocampus are impaired in these cases. Since the afferents from the hippocampus forms the postcomissural fibres of the fornix which part terminating in the mammillary body and others innervates the thalamus, hypothalamus (Mathiasen et al., 2019), indicates that these neuronal circuitry are impaired in LBDs as well.

In addition, other non-fornical fibres connect directly to the EC, the retroslenial cortices and the amygdala. The amygdala in turns connect to the PFC, CC, TC the hypothalamus and the association cortices (figure7.1) (Bubb et al., 2017). The amygdala also connects to the BG through the neostriatum, and these projections are relayed back to the thalamo-cortical circuit (Haber and Calzavara, 2009, Haber, 2016). It is important to highlight that the amygdala is involved in the regulation of the emotional response and plays a fundamental role in the acquisition and storage of memories (Haber and Calzavara, 2009, Haber, 2016). These faculties are impaired in LBDs (McKeith et al., 2017). In this thesis, I have demonstrated the amygdala is the subcortical region most affected with PTMs of αSyn, and higher correlations with the reduction of PV+ cells were also observed in this region. In fact, toxic forms of αSyn are found to be predominant in the amygdala (Alexander, 2004, Sorrentino et al., 2019). Moreover, the density of PV+ interneurons has been reported to be decreased in the amygdala and αSyn was found to be colocalized in PV+ cells (Flores-Cuadrado et al., 2017). Although the expression of αSyn varies across inhibitory synapses, the results presented here are indeed suggestive of αSyn-related dysfunction of the neurons in the amygdala, thus causing disruption within the circuit (figure 7.1). Thus, this limbic-cortical circuit disruption is key to elucidating the pathogenic cascade of

LBDs. There are no current studies, which attempted to quantify these group of PV+ cells in these regions in LBDs. Hence it is quite difficult to precise and compare the number of neurons present in these regions. Moreover, the regional variability of the PV+ interneuron populations across different brain regions makes the quantification process a bit difficult, as some regions of the brain may have lower density of these cells in the first place or simply because of the variability of the control samples.
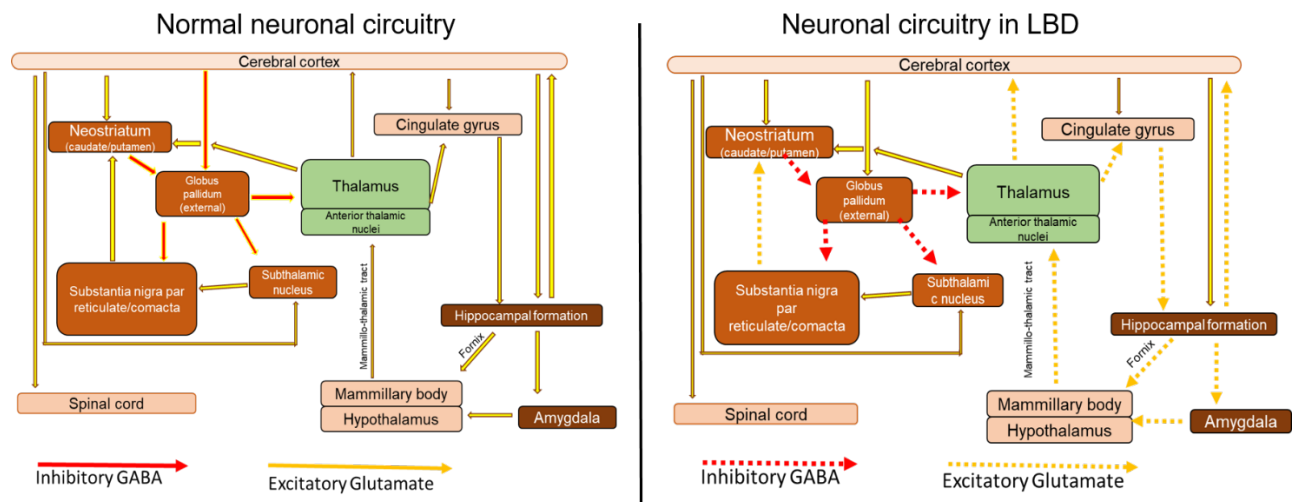
Figure 6. 1: Neuronal connections in normal individuals and patients with LBDs. this figure shows the major connections of the basal ganglia, limbic system, and the cortex. Excitatory connections are shown in yellow lines; inhibitory connections are shown in red lines. Many connections are omitted for clarity. Damage to the basal ganglia circuitry, reduces the inhibitory inputs to the thalamus thus disrupting the BG-thalamo-cortical circuit. This is heightened by damage into the amygdala and the cortex, causing a cascade of disruptions in the brain networks of LBDs.

Although, significant differences are observed at the macroscopic level in LBDs, as DLB shows different structural changes and atrophy patterns, when compared with PD and PDD, the pathophysiological and molecular mechanism that underlie them seems to share common pathways as well as common causative factor which is the abnormal aggregation of aSyn (Hansen et al., 2019, Braak and Del Tredici, 2017, Colloby et al., 2012, Patterson et al., 2019). In fact, the pathological aspects of aSyn are widely recognized as having a detrimental effect on tissues during the ageing process. In addition, the clinical constellations of DLB, PD and PDD show significant overlap among them(Hansen et al., 2019, Patterson et al., 2019). The results I present in this thesis, corroborate this by showing that, aSyn PTMs mitochondrial dysfunctions

and abnormal neuronal network oscillations. I determined that due to misfolded and aggregated alpha synuclein, the neuronal mitochondrial functions are impaired, leading to the death of a specific set of interneurons highly specialized in the generation of fast neuronal network oscillations in the brain. Using Electrophysiology local field potential, I observed that under the blockage of complex I and IV of the mitochondria electron transport chain, fast neuronal network oscillations are impaired. Subsequently, this observation was confirmed using both Histopathological, and immunofluorescence methods, that shown that this is affects primarily the fast-spiking interneuron population, due to the aggregation of alpha synuclein protein. Interestingly, following the above-described impairments, I also observed that the protein undergoes a series of monumental posttranslational modification that leads to the protein loss of primary structure and consequently increase its tendency to form aggregates (LBs and LN). The implications of this work are far reaching as I identified a potential novel strategy for alleviating neuronal degeneration.

6.6   Future directions

The results presented in this thesis could benefit from additional studies such as the analysis of the PNN density in the hippocampus including CA2, CA1of the A30P mice, as well as, in other regions human post-mortem brain tissue. This study could also be improved in the future by investigation with an increased sample size, due to the heterogeneity in controls, as changes in density of PNN and PV+ cells were marginal. A functional study in mice would also help to assess the impact of impairments in PV cess in movement's disorders. In addition, Changes in PV+ interneurons in frontal lobe are thought to be mediated polysialylated form of the neural adhesion molecule (PSANCAM). It would be important to quantify or to study this compound to corroborate the relative changes in PV cells as observed in this study.

Glutamate is the main neurotransmitter used for EPSP, by primarily acting on the NMDA receptors (Zhou and Danbolt, 2014), whereas GABA is the main inhibitory neurotransmitter used in this circuit (Wu and Sun, 2015). The results presented with memantime data, showed a trend towards improving the Gamma network oscillations, impaired in mouse model of synucleinopathies. Thus, more studies are necessary to study the effect of this compound, as modulating the NMDA receptors with memantine may be an ideal candidate for future therapeutic experiments. It would also be

beneficial to include some comparisons with other NMDA receptor agonists such as pregnelone sulphate, to aid in the comparison of the effects of these agonists. For this comparison, I believe pregnedolone may be fundamental and more reliable. In addition, KCN was shown to depolarize and abolish the activity of the fast-spiking interneurons, by reducing the inhibitory post synaptic potential (IPSP) on the pyramidal cells (Whittaker et al., 2011a). The same study also showed that a high concentration of KCN (100 µM) had no effect on the excitatory postsynaptic potential (EPSPs) in the pyramidal cells. This suggests that the changes in the neuronal network oscillations may not be associated with the diminution in glutamatergic neurotransmission. This would also be interesting to explore in the future.

This thesis would also be enhanced by the assessment of Sodium pyruvate in the improvement of the neuronal network oscillations. Some studies have shown that pyruvate, (which is the final product of glycolysis), can reverse the effect of oxidative stress in cardiac tissue (Knott et al., 2006, Donnelly and Finlay, 2015). In fact, sodium pyruvate was previously shown to have a therapeutic effect in myopathic mitochondrial DNA diseases and in patients with oxidative phosphorylation disorders by increasing the glycolytic pathways (Saito et al., 2012, Fujii et al., 2014). Moreover, the administration of pyruvate in human SK-N-SH neuroblastoma cells was shown to have protective effects to the mitochondria from oxidative stress (Wang et al., 2007b). Thus, further studies of this compound would aid in the elucidation of the mechanism to restore the impaired gamma oscillations.

Additionally, some of the mice used in this work presented EEG epileptiform activity during the experiments, which I believe to be occurring long before the impairments of gamma network oscillations and the subsequent cognitive dysfunction, which is present in the A30P mice at 12 months of age. these hyperexcitability were not further explored given the limited time and resources. Thus, it would be important to study them in the future as well.

Phosphorylated αSyn can be further investigated to be used as a potential biomarker, as the results presented in this thesis, highlights the importance of its investigation for the development of diagnostic and therapeutic strategies. Another important marker that could also be a good candidate for diagnostic and therapeutic strategies is the nitrated αSyn, given that efficient protocols are developed for their detections in

histological studies. Furthermore, if robust correlation between different PTMs and morphologic changes is confirmed by additional future pathological studies, the neuropathological staging classification system will also need to be revised accordingly, in accordance with a recent critical reappraisal of braak staging scheme.

6.7 Concluding remarks

This thesis has highlighted the involvement of different PTMs of αSyn such as phosphorylation, ubiquitination and nitration in the impairments of the neuronal network oscillations, as described in the synucleinopathies. I have hypothesized that PTMs are one of the early events that trigger the aggregation and/or dysfunction of αSyn, possibly altering its physiological sub-cellular distribution, causing the dysfunction of subcellular organelles such as the mitochondria. These changes in αSyn would then produce the pathogenic cascade of αSyn that culminates in neuronal dysfunction and death, affecting primarily the PV+ interneurons, causing the impairments of gamma network oscillations that underlie cognitive dysfunction and motor impairments, that characterize the LBDs. I confirmed my hypothesis by identifying an interrelationship between aSyn PTMs and reduction of PV+ interneurons in some regions of the brain of LBD patients, and impairments of gamma frequency oscillations in A30P mouse model of synucleinopathy, due to mitochondrial dysfunction. Thus, this study establishes that PTMs modifications are relevant to LBDs pathogenesis and progression. The PTMs interacts with αSyn to cause the observed pathological aggregation (LBs/LNs), leading to potential functional and pathogenic consequences so far detected, that describe the development of LBD. This suggests that the disease pathogenesis may in fact begin before the protein forms LBs/LNs aggregates. Hence, the accumulation of these PTMs in the protein could be a key step that links aSyn to neuronal dysfunction and death in the pathogenesis of human synucleinopathies. Furthermore, this is the first study that shows phosphorylated and ubiquitinated αSyn contained in LBs/LNs inclusions, are widely distributed cross-different brain regions affected with LBDs and they show correlations. These results may serve as a framework for future perspective clinicopathologic studies trying to define the morphologic and pathophysiologic substrate of disease progression in LBDs, and help elucidating the clinico-pathologic interconnectivity observed in the synucleinopathies. Moreover, the elucidation of this mechanism of disease-causing

PTMs on αSyn structure, function and localization may help to better aid the development of new treatments for LBDs.

References

AARSLAND, D., ANDERSEN, K., LARSEN, J. P., LOLK, A. & KRAGH-SORENSEN, P. 2003. Prevalence and characteristics of dementia in Parkinson disease: an 8-year prospective study. *Arch Neurol,* 60**,** 387-92.

AARSLAND, D., ANDERSEN, K., LARSEN, J. P., LOLK, A., NIELSEN, H. & KRAGH-SORENSEN, P. 2001. Risk of dementia in Parkinson's disease: a community-based, prospective study. *Neurology,* 56**,** 730-6.

ADAMS, N. E., SHERFEY, J. S., KOPELL, N. J., WHITTINGTON, M. A. & LEBEAU, F. E. 2017. Hetereogeneity in Neuronal Intrinsic Properties: A Possible Mechanism for Hub-Like Properties of the Rat Anterior Cingulate Cortex during Network Activity. *eNeuro,* 4.

ADLER, J. & PARMRYD, I. 2010. Quantifying colocalization by correlation: the Pearson correlation coefficient is superior to the Mander's overlap coefficient. *Cytometry A,* 77**,** 733-42.

AGHAJANIAN, G. K. & RASMUSSEN, K. 1989. Intracellular studies in the facial nucleus illustrating a simple new method for obtaining viable motoneurons in adult rat brain slices. *Synapse,* 3**,** 331-8.

AHMED, R., HUANG, J., WEBER, D. K., GOPINATH, T., VEGLIA, G., AKIMOTO, M., KHONDKER, A., RHEINSTÄDTER, M. C., HUYNH, V., WYLIE, R. G., BOZELLI, J. C., EPAND, R. M. & MELACINI, G. 2020. Molecular Mechanism for the Suppression of Alpha Synuclein Membrane Toxicity by an Unconventional Extracellular Chaperone. *Journal of the American Chemical Society,* 142**,** 9686-9699.

AIRD, R. B. & GORDON, N. S. 1993. Some excitatory and inhibitory factors involved in the epileptic state. *Brain Dev,* 15**,** 299-304.

AKAM, T., OREN, I., MANTOAN, L., FERENCZI, E. & KULLMANN, D. M. 2012. Oscillatory dynamics in the hippocampus support dentate gyrus–CA3 coupling. *Nature neuroscience,* 15**,** 763-768.

ALAFUZOFF, I., INCE, P. G., ARZBERGER, T., AL-SARRAJ, S., BELL, J., BODI, I., BOGDANOVIC, N., BUGIANI, O., FERRER, I., GELPI, E., GENTLEMAN, S., GIACCONE, G., IRONSIDE, J. W., KAVANTZAS, N., KING, A., KORKOLOPOULOU, P., KOVACS, G. G., MEYRONET, D., MONORANU, C., PARCHI, P., PARKKINEN, L., PATSOURIS, E., ROGGENDORF, W., ROZEMULLER, A., STADELMANN-NESSLER, C., STREICHENBERGER, N., THAL, D. R. & KRETZSCHMAR, H. 2009. Staging/typing of Lewy body related alpha-synuclein pathology: a study of the BrainNet Europe Consortium. *Acta Neuropathol,* 117**,** 635-52.

ALBIN, R. L., YOUNG, A. B. & PENNEY, J. B. 1989. The functional anatomy of basal ganglia disorders. *Trends Neurosci,* 12**,** 366-75.

ALCAIDE, J., GUIRADO, R., CRESPO, C., BLASCO-IBÁÑEZ, J. M., VAREA, E., SANJUAN, J. & NACHER, J. 2019. Alterations of perineuronal nets in the dorsolateral prefrontal cortex of neuropsychiatric patients. *International journal of bipolar disorders,* 7**,** 24-24.

ALEXANDER, G. E. 2004. Biology of Parkinson's disease: pathogenesis and pathophysiology of a multisystem neurodegenerative disorder. *Dialogues in clinical neuroscience,* 6**,** 259-280.

ALLEN REISH, H. E. & STANDAERT, D. G. 2015. Role of alpha-synuclein in inducing innate and adaptive immunity in Parkinson disease. *J Parkinsons Dis,* 5**,** 1-19.

AMIN, J., HOLMES, C., DOREY, R. B., TOMMASINO, E., CASAL, Y. R., WILLIAMS, D. M., DUPUY, C., NICOLL, J. A. R. & BOCHE, D. 2020. Neuroinflammation in dementia with Lewy bodies: a human post-mortem study. *Translational Psychiatry,* 10**,** 267.

ANDERSON, E. J., KATUNGA, L. A. & WILLIS, M. S. 2012. Mitochondria as a Source and Target of Lipid Peroxidation Products in Healthy and Diseased Heart. *Clinical and experimental pharmacology & physiology,* 39**,** 10.1111/j.1440-1681.2011.05641.x.

ANDERSON, J. P., WALKER, D. E., GOLDSTEIN, J. M., DE LAAT, R., BANDUCCI, K., CACCAVELLO, R. J., BARBOUR, R., HUANG, J., KLING, K., LEE, M., DIEP, L., KEIM, P. S., SHEN, X., CHATAWAY, T., SCHLOSSMACHER, M. G., SEUBERT, P., SCHENK, D., SINHA, S., GAI, W. P. & CHILCOTE, T. J.

2006a. Phosphorylation of Ser-129 is the dominant pathological modification of alpha-synuclein in familial and sporadic Lewy body disease. *J Biol Chem,* 281**,** 29739-52.

ANDERSON, J. P., WALKER, D. E., GOLDSTEIN, J. M., DE LAAT, R., BANDUCCI, K., CACCAVELLO, R. J., BARBOUR, R., HUANG, J., KLING, K., LEE, M., DIEP, L., KEIM, P. S., SHEN, X., CHATAWAY, T., SCHLOSSMACHER, M. G., SEUBERT, P., SCHENK, D., SINHA, S., GAI, W. P. & CHILCOTE, T. J. 2006b. Phosphorylation of Ser-129 Is the Dominant Pathological Modification of α-Synuclein in Familial and Sporadic Lewy Body Disease. *Journal of Biological Chemistry,* 281**,** 29739-29752.

ANDERSSON, R., LINDSKOG, M. & FISAHN, A. 2010. Histamine H3 receptor activation decreases kainate-induced hippocampal gamma oscillations in vitro by action potential desynchronization in pyramidal neurons. *The Journal of physiology,* 588**,** 1241-1249.

ANGELOVA, P. R., LUDTMANN, M. H., HORROCKS, M. H., NEGODA, A., CREMADES, N., KLENERMAN, D., DOBSON, C. M., WOOD, N. W., PAVLOV, E. V., GANDHI, S. & ABRAMOV, A. Y. 2016. Ca2+ is a key factor in alpha-synuclein-induced neurotoxicity. *J Cell Sci,* 129**,** 1792-801.

ARAWAKA, S., SATO, H., SASAKI, A., KOYAMA, S. & KATO, T. 2017. Mechanisms underlying extensive Ser129-phosphorylation in alpha-synuclein aggregates. *Acta Neuropathol Commun,* 5**,** 48.

ARMSTRONG, C. & SOLTESZ, I. 2012. Basket cell dichotomy in microcircuit function. *The Journal of physiology,* 590**,** 683-694.

ASCOLI, G. A., ALONSO-NANCLARES, L., ANDERSON, S. A., BARRIONUEVO, G., BENAVIDES-PICCIONE, R., BURKHALTER, A., BUZSÁKI, G., CAULI, B., DEFELIPE, J., FAIRÉN, A., FELDMEYER, D., FISHELL, G., FREGNAC, Y., FREUND, T. F., GARDNER, D., GARDNER, E. P., GOLDBERG, J. H., HELMSTAEDTER, M., HESTRIN, S., KARUBE, F., KISVÁRDAY, Z. F., LAMBOLEZ, B., LEWIS, D. A., MARIN, O., MARKRAM, H., MUÑOZ, A., PACKER, A., PETERSEN, C. C. H., ROCKLAND, K. S., ROSSIER, J., RUDY, B., SOMOGYI, P., STAIGER, J. F., TAMAS, G., THOMSON, A. M., TOLEDO-RODRIGUEZ, M., WANG, Y., WEST, D. C., YUSTE, R. & THE PETILLA INTERNEURON NOMENCLATURE, G. 2008. Petilla terminology: nomenclature of features of GABAergic interneurons of the cerebral cortex. *Nature Reviews Neuroscience,* 9**,** 557-568.

ASSAYAG, K., YAKUNIN, E., LOEB, V., SELKOE, D. J. & SHARON, R. 2007. Polyunsaturated fatty acids induce alpha-synuclein-related pathogenic changes in neuronal cells. *The American journal of pathology,* 171**,** 2000-2011.

ATTEMS, J., KONIG, C., HUBER, M., LINTNER, F. & JELLINGER, K. A. 2005. Cause of death in demented and non-demented elderly inpatients; an autopsy study of 308 cases. *J Alzheimers Dis,* 8**,** 57-62.

ATTEMS, J., WALKER, L. & JELLINGER, K. A. 2014. Olfactory bulb involvement in neurodegenerative diseases. *Acta Neuropathol,* 127**,** 459-75.

BABA, M., NAKAJO, S., TU, P. H., TOMITA, T., NAKAYA, K., LEE, V. M., TROJANOWSKI, J. Q. & IWATSUBO, T. 1998. Aggregation of alpha-synuclein in Lewy bodies of sporadic Parkinson's disease and dementia with Lewy bodies. *The American journal of pathology,* 152**,** 879-884.

BAKER, A., KALMBACH, B., MORISHIMA, M., KIM, J., JUAVINETT, A., LI, N. & DEMBROW, N. 2018a. Specialized Subpopulations of Deep-Layer Pyramidal Neurons in the Neocortex: Bridging Cellular Properties to Functional Consequences. *The Journal of Neuroscience,* 38**,** 5441.

BAKER, C. M., BURKS, J. D., BRIGGS, R. G., MILTON, C. K., CONNER, A. K., GLENN, C. A., SALI, G., MCCOY, T. M., BATTISTE, J. D., O'DONOGHUE, D. L. & SUGHRUE, M. E. 2018b. A Connectomic Atlas of the Human Cerebrum-Chapter 6: The Temporal Lobe. *Oper Neurosurg (Hagerstown),* 15**,** S245-s294.

BARADARAN, R., BERRISFORD, J. M., MINHAS, G. S. & SAZANOV, L. A. 2013. Crystal structure of the entire respiratory complex I. *Nature,* 494**,** 443-448.

BARRETT, P. J. & TIMOTHY GREENAMYRE, J. 2015. Post-translational modification of α-synuclein in Parkinson's disease. *Brain Research,* 1628**,** 247-253.

BARTESAGHI, S. & RADI, R. 2018. Fundamentals on the biochemistry of peroxynitrite and protein tyrosine nitration. *Redox Biology,* 14**,** 618-625.

BASAR, E. 2013. Brain oscillations in neuropsychiatric disease. *Dialogues Clin Neurosci,* 15**,** 291-300.

BASAR, E., EMEK-SAVAS, D. D., GUNTEKIN, B. & YENER, G. G. 2016. Delay of cognitive gamma responses in Alzheimer's disease. *Neuroimage Clin,* 11**,** 106-15.

BECK-SICKINGER, A. G. & MÖRL, K. 2006. Posttranslational Modification of Proteins. Expanding Nature's Inventory. By Christopher T. Walsh. *Angewandte Chemie International Edition,* 45**,** 1020-1020.

BEDFORD, L., HAY, D., PAINE, S., REZVANI, N., MEE, M., LOWE, J. & MAYER, R. J. 2008. Is malfunction of the ubiquitin proteasome system the primary cause of α-synucleinopathies and other chronic human neurodegenerative disease? *Biochimica et Biophysica Acta (BBA) - Molecular Basis of Disease,* 1782**,** 683-690.

BENNER, E. J., BANERJEE, R., REYNOLDS, A. D., SHERMAN, S., PISAREV, V. M., TSIPERSON, V., NEMACHEK, C., CIBOROWSKI, P., PRZEDBORSKI, S., MOSLEY, R. L. & GENDELMAN, H. E. 2008. Nitrated alpha-synuclein immunity accelerates degeneration of nigral dopaminergic neurons. *PLoS One,* 3**,** e1376.

BENNETT, M. C., BISHOP, J. F., LENG, Y., CHOCK, P. B., CHASE, T. N. & MOURADIAN, M. M. 1999. Degradation of alpha-synuclein by proteasome. *J Biol Chem,* 274**,** 33855-8.

BENTEA, E., VERBRUGGEN, L. & MASSIE, A. 2017. The Proteasome Inhibition Model of Parkinson's Disease. *Journal of Parkinson's disease,* 7**,** 31-63.

BERG, E. M., BERTUZZI, M. & AMPATZIS, K. 2018. Complementary expression of calcium binding proteins delineates the functional organization of the locomotor network. *Brain structure & function,* 223**,** 2181-2196.

BERGER, T. K., SILBERBERG, G., PERIN, R. & MARKRAM, H. 2010. Brief bursts self-inhibit and correlate the pyramidal network. *PLoS biology,* 8**,** e1000473.

BERNSTEIN, H.-G., JOHNSON, M., PERRY, R. H., LEBEAU, F. E. N., DOBROWOLNY, H., BOGERTS, B. & PERRY, E. K. 2011a. Partial loss of parvalbumin-containing hippocampal interneurons in dementia with Lewy bodies. *Neuropathology,* 31**,** 1-10.

BERNSTEIN, H. G., JOHNSON, M., PERRY, R. H., LEBEAU, F. E., DOBROWOLNY, H., BOGERTS, B. & PERRY, E. K. 2011b. Partial loss of parvalbumin-containing hippocampal interneurons in dementia with Lewy bodies. *Neuropathology,* 31**,** 1-10.

BETARBET, R., SHERER, T. B. & GREENAMYRE, J. T. 2005. Ubiquitin-proteasome system and Parkinson's diseases. *Exp Neurol,* 191 Suppl 1**,** S17-27.

BETTERTON, R. T., BROAD, L. M., TSANEVA-ATANASOVA, K. & MELLOR, J. R. 2017. Acetylcholine modulates gamma frequency oscillations in the hippocampus by activation of muscarinic M1 receptors. *The European journal of neuroscience,* 45**,** 1570-1585.

BEYER, K. 2006. α-Synuclein structure, posttranslational modification and alternative splicing as aggregation enhancers. *Acta Neuropathologica,* 112**,** 237-251.

BEYER, K. & ARIZA, A. 2013. alpha-Synuclein posttranslational modification and alternative splicing as a trigger for neurodegeneration. *Mol Neurobiol,* 47**,** 509-24.

BHATIA, K. P. & MARSDEN, C. D. 1994. The behavioural and motor consequences of focal lesions of the basal ganglia in man. *Brain,* 117 (Pt 4)**,** 859-76.

BIAN, S. Z., ZHANG, J., LIU, W. L., SUN, Z. H., GU, Z. L. & JIANG, X. G. 2009. [Receptor antagonist of NMDA and animal models of schizophrenia]. *Fa Yi Xue Za Zhi,* 25**,** 443-6.

BIRBEN, E., SAHINER, U. M., SACKESEN, C., ERZURUM, S. & KALAYCI, O. 2012. Oxidative Stress and Antioxidant Defense. *The World Allergy Organization journal,* 5**,** 9-19.

BLASIAK, J., PAWLOWSKA, E., SZCZEPANSKA, J. & KAARNIRANTA, K. 2019. Interplay between Autophagy and the Ubiquitin-Proteasome System and Its Role in the Pathogenesis of Age-Related Macular Degeneration. *International journal of molecular sciences,* 20**,** 210.

BLUMBERG, J. & KREIMAN, G. 2010. How cortical neurons help us see: visual recognition in the human brain. *The Journal of clinical investigation,* 120**,** 3054-3063.

BODNER, C. R., DOBSON, C. M. & BAX, A. 2009. Multiple tight phospholipid-binding modes of alpha-synuclein revealed by solution NMR spectroscopy. *J Mol Biol,* 390**,** 775-90.

BOESVELDT, S., VERBAAN, D., KNOL, D. L., VISSER, M., VAN ROODEN, S. M., VAN HILTEN, J. J. & BERENDSE, H. W. 2008. A comparative study of odor identification and odor discrimination deficits in Parkinson's disease. *Mov Disord,* 23**,** 1984-90.

BONANNI, L., FRANCIOTTI, R., NOBILI, F., KRAMBERGER, M. G., TAYLOR, J. P., GARCIA-PTACEK, S., FALASCA, N. W., FAMA, F., CROMARTY, R., ONOFRJ, M. & AARSLAND, D. 2016. EEG Markers of Dementia with Lewy Bodies: A Multicenter Cohort Study. *J Alzheimers Dis,* 54**,** 1649-1657.

BONANNI, L., THOMAS, A., TIRABOSCHI, P., PERFETTI, B., VARANESE, S. & ONOFRJ, M. 2008. EEG comparisons in early Alzheimer's disease, dementia with Lewy bodies and Parkinson's disease with dementia patients with a 2-year follow-up. *Brain,* 131**,** 690-705.

BOOKER, S. A. & VIDA, I. 2018. Morphological diversity and connectivity of hippocampal interneurons. *Cell and Tissue Research,* 373**,** 619-641.

BÖRGERS, C. & KOPELL, N. 2005. Effects of noisy drive on rhythms in networks of excitatory and inhibitory neurons. *Neural Comput,* 17**,** 557-608.

BOZZALI, M., FALINI, A., CERCIGNANI, M., BAGLIO, F., FARINA, E., ALBERONI, M., VEZZULLI, P., OLIVOTTO, F., MANTOVANI, F., SHALLICE, T., SCOTTI, G., CANAL, N. & NEMNI, R. 2005. Brain tissue damage in dementia with Lewy bodies: an in vivo diffusion tensor MRI study. *Brain,* 128**,** 1595-1604.

BRAAK, H., ALAFUZOFF, I., ARZBERGER, T., KRETZSCHMAR, H. & DEL TREDICI, K. 2006. Staging of Alzheimer disease-associated neurofibrillary pathology using paraffin sections and immunocytochemistry. *Acta Neuropathol,* 112**,** 389-404.

BRAAK, H. & DEL TREDICI, K. 2017. Neuropathological Staging of Brain Pathology in Sporadic Parkinson's disease: Separating the Wheat from the Chaff. *J Parkinsons Dis,* 7**,** S71-s85.

BRAAK, H., DEL TREDICI, K., RUB, U., DE VOS, R. A., JANSEN STEUR, E. N. & BRAAK, E. 2003a. Staging of brain pathology related to sporadic Parkinson's disease. *Neurobiol Aging,* 24**,** 197-211.

BRAAK, H., GHEBREMEDHIN, E., RÜB, U., BRATZKE, H. & DEL TREDICI, K. 2004. Stages in the development of Parkinson's disease-related pathology. *Cell Tissue Res,* 318**,** 121-34.

BRAAK, H., SANDMANN-KEIL, D., GAI, W. & BRAAK, E. 1999. Extensive axonal Lewy neurites in Parkinson's disease: a novel pathological feature revealed by alpha-synuclein immunocytochemistry. *Neurosci Lett,* 265**,** 67-9.

BRAAK, H., TREDICI, K. D., RÜB, U., DE VOS, R. A. I., JANSEN STEUR, E. N. H. & BRAAK, E. 2003b. Staging of brain pathology related to sporadic Parkinson's disease. *Neurobiology of Aging,* 24**,** 197-211.

BRADY, D. R. & MUFSON, E. J. 1997. Parvalbumin-immunoreactive neurons in the hippocampal formation of Alzheimer's diseased brain. *Neuroscience,* 80**,** 1113-25.

BRAS, I. C., DOMINGUEZ-MEIJIDE, A., GERHARDT, E., KOSS, D., LAZARO, D. F., SANTOS, P. I., VASILI, E., XYLAKI, M. & OUTEIRO, T. F. 2020. Synucleinopathies: Where we are and where we need to go. *J Neurochem*.

BREUKELAAR, I. A., ANTEES, C., GRIEVE, S. M., FOSTER, S. L., GOMES, L., WILLIAMS, L. M. & KORGAONKAR, M. S. 2017. Cognitive control network anatomy correlates with neurocognitive behavior: A longitudinal study. *Human brain mapping,* 38**,** 631-643.

BROWN, D. R. 2007. Interactions between metals and alpha-synuclein--function or artefact? *Febs j,* 274**,** 3766-74.

BRUGGE, J. F., VOLKOV, I. O., OYA, H., KAWASAKI, H., REALE, R. A., FENOY, A., STEINSCHNEIDER, M. & HOWARD, M. A., 3RD 2008. Functional localization of auditory cortical fields of human: click-train stimulation. *Hear Res,* 238**,** 12-24.

BUBB, E. J., KINNAVANE, L. & AGGLETON, J. P. 2017. Hippocampal - diencephalic - cingulate networks for memory and emotion: An anatomical guide. *Brain and neuroscience advances,* 1**,** 2398212817723443.

BUELL, A. K., GALVAGNION, C., GASPAR, R., SPARR, E., VENDRUSCOLO, M., KNOWLES, T. P. J., LINSE, S. & DOBSON, C. M. 2014. Solution conditions determine the relative importance of

nucleation and growth processes in α-synuclein aggregation. *Proceedings of the National Academy of Sciences,* 111**,** 7671-7676.

BUETI, D. & WALSH, V. 2009. The parietal cortex and the representation of time, space, number and other magnitudes. *Philosophical transactions of the Royal Society of London. Series B, Biological sciences,* 364**,** 1831-1840.

BURKE, W. J. 2003. 3,4-dihydroxyphenylacetaldehyde: a potential target for neuroprotective therapy in Parkinson's disease. *Curr Drug Targets CNS Neurol Disord,* 2**,** 143-8.

BURRE, J. 2015. The Synaptic Function of alpha-Synuclein. *J Parkinsons Dis,* 5**,** 699-713.

BURRE, J., SHARMA, M., TSETSENIS, T., BUCHMAN, V., ETHERTON, M. R. & SUDHOF, T. C. 2010. Alpha-synuclein promotes SNARE-complex assembly in vivo and in vitro. *Science,* 329**,** 1663-7.

BURRE, J., VIVONA, S., DIAO, J., SHARMA, M., BRUNGER, A. T. & SUDHOF, T. C. 2013. Properties of native brain alpha-synuclein. *Nature,* 498**,** E4-6; discussion E6-7.

BURTON, E. J., BARBER, R., MUKAETOVA-LADINSKA, E. B., ROBSON, J., PERRY, R. H., JAROS, E., KALARIA, R. N. & O'BRIEN, J. T. 2009. Medial temporal lobe atrophy on MRI differentiates Alzheimer's disease from dementia with Lewy bodies and vascular cognitive impairment: a prospective study with pathological verification of diagnosis. *Brain,* 132**,** 195-203.

BUSSELL, R., JR. & ELIEZER, D. 2001. Residual structure and dynamics in Parkinson's disease-associated mutants of alpha-synuclein. *J Biol Chem,* 276**,** 45996-6003.

BUSSELL, R., JR. & ELIEZER, D. 2003. A structural and functional role for 11-mer repeats in alpha-synuclein and other exchangeable lipid binding proteins. *J Mol Biol,* 329**,** 763-78.

BUSSELL, R., JR. & ELIEZER, D. 2004. Effects of Parkinson's disease-linked mutations on the structure of lipid-associated alpha-synuclein. *Biochemistry,* 43**,** 4810-8.

BUSTAMANTE, H. A., GONZÁLEZ, A. E., CERDA-TRONCOSO, C., SHAUGHNESSY, R., OTTH, C., SOZA, A. & BURGOS, P. V. 2018. Interplay Between the Autophagy-Lysosomal Pathway and the Ubiquitin-Proteasome System: A Target for Therapeutic Development in Alzheimer's Disease. *Frontiers in cellular neuroscience,* 12**,** 126-126.

BUZSÁKI, G. 2005. Theta rhythm of navigation: link between path integration and landmark navigation, episodic and semantic memory. *Hippocampus,* 15**,** 827-40.

BUZSÁKI, G., ANASTASSIOU, C. A. & KOCH, C. 2012. The origin of extracellular fields and currents--EEG, ECoG, LFP and spikes. *Nature reviews. Neuroscience,* 13**,** 407-420.

BUZSÁKI, G., LEUNG, L. W. & VANDERWOLF, C. H. 1983. Cellular bases of hippocampal EEG in the behaving rat. *Brain Res,* 287**,** 139-71.

BUZSÁKI, G. & WANG, X.-J. 2012. Mechanisms of gamma oscillations. *Annual review of neuroscience,* 35**,** 203-225.

CABUNGCAL, J. H., STEULLET, P., KRAFTSIK, R., CUENOD, M. & DO, K. Q. 2013a. Early-life insults impair parvalbumin interneurons via oxidative stress: reversal by N-acetylcysteine. *Biol Psychiatry,* 73**,** 574-82.

CABUNGCAL, J. H., STEULLET, P., MORISHITA, H., KRAFTSIK, R., CUENOD, M., HENSCH, T. K. & DO, K. Q. 2013b. Perineuronal nets protect fast-spiking interneurons against oxidative stress. *Proc Natl Acad Sci U S A,* 110**,** 9130-5.

CARDIN, J. A. 2018. Inhibitory Interneurons Regulate Temporal Precision and Correlations in Cortical Circuits. *Trends in neurosciences,* 41**,** 689-700.

CARIULO, C., MARTUFI, P., VERANI, M., AZZOLLINI, L., BRUNI, G., WEISS, A., DEGUIRE, S. M., LASHUEL, H. A., SCARICAMAZZA, E., SANCESARIO, G. M., SCHIRINZI, T., MERCURI, N. B., SANCESARIO, G., CARICASOLE, A. & PETRICCA, L. 2019. Phospho-S129 Alpha-Synuclein Is Present in Human Plasma but Not in Cerebrospinal Fluid as Determined by an Ultrasensitive Immunoassay. *Frontiers in Neuroscience,* 13.

CARRELL, R. W. & LOMAS, D. A. 1997. Conformational disease. *Lancet,* 350**,** 134-8.

CASTEJON, C. & NUÑEZ, A. 2016. Cortical Neural Computation by Discrete Results Hypothesis. *Frontiers in Neural Circuits,* 10.

CASTELLI, V., BENEDETTI, E., ANTONOSANTE, A., CATANESI, M., PITARI, G., IPPOLITI, R., CIMINI, A. & D'ANGELO, M. 2019. Neuronal Cells Rearrangement During Aging and Neurodegenerative Disease: Metabolism, Oxidative Stress and Organelles Dynamic. *Frontiers in molecular neuroscience,* 12**,** 132-132.

CASTILLO-CARRANZA, D. L., ZHANG, Y., GUERRERO-MUNOZ, M. J., KAYED, R., RINCON-LIMAS, D. E. & FERNANDEZ-FUNEZ, P. 2012. Differential activation of the ER stress factor XBP1 by oligomeric assemblies. *Neurochem Res,* 37**,** 1707-17.

CELSI, F., PIZZO, P., BRINI, M., LEO, S., FOTINO, C., PINTON, P. & RIZZUTO, R. 2009. Mitochondria, calcium and cell death: a deadly triad in neurodegeneration. *Biochimica et biophysica acta,* 1787**,** 335-344.

CERRI, S., GHEZZI, C., SAMPIERI, M., SIANI, F., AVENALI, M., DORNINI, G., ZANGAGLIA, R., MINAFRA, B. & BLANDINI, F. 2018. The Exosomal/Total α-Synuclein Ratio in Plasma Is Associated With Glucocerebrosidase Activity and Correlates With Measures of Disease Severity in PD Patients. *Frontiers in Cellular Neuroscience,* 12.

CHAU, K. Y., CHING, H. L., SCHAPIRA, A. H. & COOPER, J. M. 2009. Relationship between alpha synuclein phosphorylation, proteasomal inhibition and cell death: relevance to Parkinson's disease pathogenesis. *J Neurochem,* 110**,** 1005-13.

CHAVARRIA, C. & SOUZA, J. M. 2013. Oxidation and nitration of alpha-synuclein and their implications in neurodegenerative diseases. *Arch Biochem Biophys,* 533**,** 25-32.

CHAVOIX, C. & INSAUSTI, R. 2017. Self-awareness and the medial temporal lobe in neurodegenerative diseases. *Neurosci Biobehav Rev,* 78**,** 1-12.

CHEN, L. & FEANY, M. B. 2005. Alpha-synuclein phosphorylation controls neurotoxicity and inclusion formation in a Drosophila model of Parkinson disease. *Nat Neurosci,* 8**,** 657-63.

CHEN, L., PERIQUET, M., WANG, X., NEGRO, A., MCLEAN, P. J., HYMAN, B. T. & FEANY, M. B. 2009. Tyrosine and serine phosphorylation of alpha-synuclein have opposing effects on neurotoxicity and soluble oligomer formation. *The Journal of clinical investigation,* 119**,** 3257-3265.

CHEN, L., XIE, Z., TURKSON, S. & ZHUANG, X. 2015. A53T human alpha-synuclein overexpression in transgenic mice induces pervasive mitochondria macroautophagy defects preceding dopamine neuron degeneration. *J Neurosci,* 35**,** 890-905.

CHEN, R.-H., CHEN, Y.-H. & HUANG, T.-Y. 2019. Ubiquitin-mediated regulation of autophagy. *Journal of Biomedical Science,* 26**,** 80.

CHEN, S. C.-C., CHEN, F.-C. & LI, W.-H. 2010. Phosphorylated and Nonphosphorylated Serine and Threonine Residues Evolve at Different Rates in Mammals. *Molecular Biology and Evolution,* 27**,** 2548-2554.

CHOI, B. K., CHOI, M. G., KIM, J. Y., YANG, Y., LAI, Y., KWEON, D. H., LEE, N. K. & SHIN, Y. K. 2013. Large alpha-synuclein oligomers inhibit neuronal SNARE-mediated vesicle docking. *Proc Natl Acad Sci U S A,* 110**,** 4087-92.

CHOU, A. P., LI, S., FITZMAURICE, A. G. & BRONSTEIN, J. M. 2010. Mechanisms of Rotenone-induced Proteasome Inhibition. *Neurotoxicology,* 31**,** 367-372.

CHOUBEY, V., SAFIULINA, D., VAARMANN, A., CAGALINEC, M., WARESKI, P., KUUM, M., ZHARKOVSKY, A. & KAASIK, A. 2011. Mutant A53T alpha-synuclein induces neuronal death by increasing mitochondrial autophagy. *J Biol Chem,* 286**,** 10814-24.

CHUNG, C. Y., KOPRICH, J. B., SIDDIQI, H. & ISACSON, O. 2009. Dynamic changes in presynaptic and axonal transport proteins combined with striatal neuroinflammation precede dopaminergic neuronal loss in a rat model of AAV alpha-synucleinopathy. *J Neurosci,* 29**,** 3365-73.

CIECHANOVER, A. & KWON, Y. T. 2015. Degradation of misfolded proteins in neurodegenerative diseases: therapeutic targets and strategies. *Experimental & Molecular Medicine,* 47**,** e147-e147.

CLAYTON, M. S., YEUNG, N. & COHEN KADOSH, R. 2015. The roles of cortical oscillations in sustained attention. *Trends Cogn Sci,* 19**,** 188-95.

COLLA, E. 2019. Linking the Endoplasmic Reticulum to Parkinson's Disease and Alpha-Synucleinopathy. *Front Neurosci,* 13**,** 560.

COLLA, E., COUNE, P., LIU, Y., PLETNIKOVA, O., TRONCOSO, J. C., IWATSUBO, T., SCHNEIDER, B. L. & LEE, M. K. 2012. Endoplasmic reticulum stress is important for the manifestations of alpha-synucleinopathy in vivo. *J Neurosci,* 32**,** 3306-20.

COLLIN, F. 2019. Chemical Basis of Reactive Oxygen Species Reactivity and Involvement in Neurodegenerative Diseases. *International journal of molecular sciences,* 20**,** 2407.

COLLOBY, S. J., MCPARLAND, S., O'BRIEN, J. T. & ATTEMS, J. 2012. Neuropathological correlates of dopaminergic imaging in Alzheimer's disease and Lewy body dementias. *Brain,* 135**,** 2798-808.

CONTRERAS, A., HINES, D. J. & HINES, R. M. 2019. Molecular Specialization of GABAergic Synapses on the Soma and Axon in Cortical and Hippocampal Circuit Function and Dysfunction. *Frontiers in Molecular Neuroscience,* 12.

COOPER, A. A., GITLER, A. D., CASHIKAR, A., HAYNES, C. M., HILL, K. J., BHULLAR, B., LIU, K., XU, K., STRATHEARN, K. E., LIU, F., CAO, S., CALDWELL, K. A., CALDWELL, G. A., MARSISCHKY, G., KOLODNER, R. D., LABAER, J., ROCHET, J. C., BONINI, N. M. & LINDQUIST, S. 2006. Alpha-synuclein blocks ER-Golgi traffic and Rab1 rescues neuron loss in Parkinson's models. *Science,* 313**,** 324-8.

CRABTREE, D. M. & ZHANG, J. 2012. Genetically engineered mouse models of Parkinson's disease. *Brain research bulletin,* 88**,** 13-32.

CRAIG, M. T. & MCBAIN, C. J. 2015. Fast gamma oscillations are generated intrinsically in CA1 without the involvement of fast-spiking basket cells. *The Journal of neuroscience : the official journal of the Society for Neuroscience,* 35**,** 3616-3624.

CROMARTY, R. A., ELDER, G. J., GRAZIADIO, S., BAKER, M., BONANNI, L., ONOFRJ, M., O'BRIEN, J. T. & TAYLOR, J.-P. 2016. Neurophysiological biomarkers for Lewy body dementias. *Clinical neurophysiology : official journal of the International Federation of Clinical Neurophysiology,* 127**,** 349-359.

CROWTHER, R. A., JAKES, R., SPILLANTINI, M. G. & GOEDERT, M. 1998. Synthetic filaments assembled from C-terminally truncated alpha-synuclein. *FEBS Lett,* 436**,** 309-12.

CRYSTAL, H. A., DICKSON, D. W., LIZARDI, J. E., DAVIES, P. & WOLFSON, L. I. 1990. Antemortem diagnosis of diffuse Lewy body disease. *Neurology,* 40**,** 1523-8.

DAAR, A. S., SINGER, P. A., LEAH PERSAD, D., PRAMMING, S. K., MATTHEWS, D. R., BEAGLEHOLE, R., BERNSTEIN, A., BORYSIEWICZ, L. K., COLAGIURI, S., GANGULY, N., GLASS, R. I., FINEGOOD, D. T., KOPLAN, J., NABEL, E. G., SARNA, G., SARRAFZADEGAN, N., SMITH, R., YACH, D. & BELL, J. 2007. Grand challenges in chronic non-communicable diseases. *Nature,* 450**,** 494-496.

DALFÓ, E., GÓMEZ-ISLA, T., ROSA, J. L., NIETO BODELÓN, M., CUADRADO TEJEDOR, M., BARRACHINA, M., AMBROSIO, S. & FERRER, I. 2004. Abnormal alpha-synuclein interactions with Rab proteins in alpha-synuclein A30P transgenic mice. *J Neuropathol Exp Neurol,* 63**,** 302-13.

DAMIER, P., HIRSCH, E. C., AGID, Y. & GRAYBIEL, A. M. 1999. The substantia nigra of the human brain. II. Patterns of loss of dopamine-containing neurons in Parkinson's disease. *Brain,* 122 (Pt 8)**,** 1437-48.

DANIELSON, S. R., HELD, J. M., OO, M., RILEY, R., GIBSON, B. W. & ANDERSEN, J. K. 2011. Quantitative mapping of reversible mitochondrial Complex I cysteine oxidation in a Parkinson disease mouse model. *The Journal of biological chemistry,* 286**,** 7601-7608.

DANZER, K. M., HAASEN, D., KAROW, A. R., MOUSSAUD, S., HABECK, M., GIESE, A., KRETZSCHMAR, H., HENGERER, B. & KOSTKA, M. 2007. Different species of alpha-synuclein oligomers induce calcium influx and seeding. *J Neurosci,* 27**,** 9220-32.

DAVACHI, L. & DOBBINS, I. G. 2008. Declarative Memory. *Current directions in psychological science,* 17**,** 112-118.

DAVIDSON, W. S., JONAS, A., CLAYTON, D. F. & GEORGE, J. M. 1998. Stabilization of alpha-synuclein secondary structure upon binding to synthetic membranes. *J Biol Chem,* 273**,** 9443-9.

DAW, M. I., TRICOIRE, L., ERDELYI, F., SZABO, G. & MCBAIN, C. J. 2009. Asynchronous transmitter release from cholecystokinin-containing inhibitory interneurons is widespread and target-cell independent. *J Neurosci,* 29**,** 11112-22.

DE RIJK, M. C., TZOURIO, C., BRETELER, M. M., DARTIGUES, J. F., AMADUCCI, L., LOPEZ-POUSA, S., MANUBENS-BERTRAN, J. M., ALPEROVITCH, A. & ROCCA, W. A. 1997. Prevalence of parkinsonism and Parkinson's disease in Europe: the EUROPARKINSON Collaborative Study. European Community Concerted Action on the Epidemiology of Parkinson's disease. *J Neurol Neurosurg Psychiatry,* 62**,** 10-5.

DEFELIPE, J., LÓPEZ-CRUZ, P. L., BENAVIDES-PICCIONE, R., BIELZA, C., LARRAÑAGA, P., ANDERSON, S., BURKHALTER, A., CAULI, B., FAIRÉN, A., FELDMEYER, D., FISHELL, G., FITZPATRICK, D., FREUND, T. F., GONZÁLEZ-BURGOS, G., HESTRIN, S., HILL, S., HOF, P. R., HUANG, J., JONES, E. G., KAWAGUCHI, Y., KISVÁRDAY, Z., KUBOTA, Y., LEWIS, D. A., MARÍN, O., MARKRAM, H., MCBAIN, C. J., MEYER, H. S., MONYER, H., NELSON, S. B., ROCKLAND, K., ROSSIER, J., RUBENSTEIN, J. L., RUDY, B., SCANZIANI, M., SHEPHERD, G. M., SHERWOOD, C. C., STAIGER, J. F., TAMÁS, G., THOMSON, A., WANG, Y., YUSTE, R. & ASCOLI, G. A. 2013. New insights into the classification and nomenclature of cortical GABAergic interneurons. *Nat Rev Neurosci,* 14**,** 202-16.

DEL TREDICI, K., RÜB, U., DE VOS, R. A., BOHL, J. R. & BRAAK, H. 2002. Where does parkinson disease pathology begin in the brain? *J Neuropathol Exp Neurol,* 61**,** 413-26.

DELIC, V., CHANDRA, S., ABDELMOTILIB, H., MALTBIE, T., WANG, S., KEM, D., SCOTT, H. J., UNDERWOOD, R. N., LIU, Z., VOLPICELLI-DALEY, L. A. & WEST, A. B. 2018. Sensitivity and specificity of phospho-Ser129 α-synuclein monoclonal antibodies. *J Comp Neurol,* 526**,** 1978-1990.

DELLEDONNE, A., KLOS, K. J., FUJISHIRO, H., AHMED, Z., PARISI, J. E., JOSEPHS, K. A., FRIGERIO, R., BURNETT, M., WSZOLEK, Z. K., UITTI, R. J., AHLSKOG, J. E. & DICKSON, D. W. 2008. Incidental Lewy body disease and preclinical Parkinson disease. *Arch Neurol,* 65**,** 1074-80.

DELLI PIZZI, S., FRANCIOTTI, R., TAYLOR, J.-P., THOMAS, A., TARTARO, A., ONOFRJ, M. & BONANNI, L. 2015. Thalamic Involvement in Fluctuating Cognition in Dementia with Lewy Bodies: Magnetic Resonance Evidences. *Cerebral cortex (New York, N.Y. : 1991),* 25**,** 3682-3689.

DESHAIES, R. J. & JOAZEIRO, C. A. 2009. RING domain E3 ubiquitin ligases. *Annu Rev Biochem,* 78**,** 399-434.

DESPLATS, P., LEE, H. J., BAE, E. J., PATRICK, C., ROCKENSTEIN, E., CREWS, L., SPENCER, B., MASLIAH, E. & LEE, S. J. 2009. Inclusion formation and neuronal cell death through neuron-to-neuron transmission of alpha-synuclein. *Proc Natl Acad Sci U S A,* 106**,** 13010-5.

DESPLATS, P., SPENCER, B., CREWS, L., PATHEL, P., MORVINSKI-FRIEDMANN, D., KOSBERG, K., ROBERTS, S., PATRICK, C., WINNER, B., WINKLER, J. & MASLIAH, E. 2012. alpha-Synuclein induces alterations in adult neurogenesis in Parkinson disease models via p53-mediated repression of Notch1. *J Biol Chem,* 287**,** 31691-702.

DEVI, L., RAGHAVENDRAN, V., PRABHU, B. M., AVADHANI, N. G. & ANANDATHEERTHAVARADA, H. K. 2008. Mitochondrial import and accumulation of alpha-synuclein impair complex I in human dopaminergic neuronal cultures and Parkinson disease brain. *J Biol Chem,* 283**,** 9089-100.

DHEERENDRA, P., LYNCH, N. M., CRUTWELL, J., CUNNINGHAM, M. O. & SMULDERS, T. V. 2018. In vitro characterization of gamma oscillations in the hippocampal formation of the domestic chick. *The European journal of neuroscience,* 48**,** 2807-2815.

DI MAIO, R., BARRETT, P. J., HOFFMAN, E. K., BARRETT, C. W., ZHARIKOV, A., BORAH, A., HU, X., MCCOY, J., CHU, C. T., BURTON, E. A., HASTINGS, T. G. & GREENAMYRE, J. T. 2016. alpha-Synuclein binds to TOM20 and inhibits mitochondrial protein import in Parkinson's disease. *Sci Transl Med,* 8**,** 342ra78.

DIAS, V., JUNN, E. & MOURADIAN, M. M. 2013. The role of oxidative stress in Parkinson's disease. *Journal of Parkinson's disease,* 3**,** 461-491.

DICKINSON, R., AWAIZ, S., WHITTINGTON, M. A., LIEB, W. R. & FRANKS, N. P. 2003. The effects of general anaesthetics on carbachol-evoked gamma oscillations in the rat hippocampus in vitro. *Neuropharmacology,* 44**,** 864-72.

DICKSON, D. W. 1999. Tau and synuclein and their role in neuropathology. *Brain Pathol,* 9**,** 657-61.

DICKSON, D. W. 2012. Parkinson's disease and parkinsonism: neuropathology. *Cold Spring Harbor perspectives in medicine,* 2**,** a009258.

DICKSON, D. W., FUJISHIRO, H., DELLEDONNE, A., MENKE, J., AHMED, Z., KLOS, K. J., JOSEPHS, K. A., FRIGERIO, R., BURNETT, M., PARISI, J. E. & AHLSKOG, J. E. 2008. Evidence that incidental Lewy body disease is pre-symptomatic Parkinson's disease. *Acta Neuropathol,* 115**,** 437-44.

DIÓGENES, M. J., DIAS, R. B., ROMBO, D. M., VICENTE MIRANDA, H., MAIOLINO, F., GUERREIRO, P., NÄSSTRÖM, T., FRANQUELIM, H. G., OLIVEIRA, L. M. A., CASTANHO, M. A. R. B., LANNFELT, L., BERGSTRÖM, J., INGELSSON, M., QUINTAS, A., SEBASTIÃO, A. M., LOPES, L. V. & OUTEIRO, T. F. 2012. Extracellular Alpha-Synuclein Oligomers Modulate Synaptic Transmission and Impair LTP Via NMDA-Receptor Activation. *The Journal of Neuroscience,* 32**,** 11750.

DOBSON, C. M. 1999. Protein misfolding, evolution and disease. *Trends Biochem Sci,* 24**,** 329-32.

DOCHERTY, M. J. & BURN, D. J. 2010. Parkinson's disease dementia. *Curr Neurol Neurosci Rep,* 10**,** 292-8.

DONNELLY, R. P. & FINLAY, D. K. 2015. Glucose, glycolysis and lymphocyte responses. *Molecular Immunology,* 68**,** 513-519.

DOPPLER, K., EBERT, S., UCEYLER, N., TRENKWALDER, C., EBENTHEUER, J., VOLKMANN, J. & SOMMER, C. 2014a. Cutaneous neuropathy in Parkinson's disease: a window into brain pathology. *Acta Neuropathol,* 128**,** 99-109.

DOPPLER, K., EBERT, S., UÇEYLER, N., TRENKWALDER, C., EBENTHEUER, J., VOLKMANN, J. & SOMMER, C. 2014b. Cutaneous neuropathy in Parkinson's disease: a window into brain pathology. *Acta neuropathologica,* 128**,** 99-109.

DORVAL, V. & FRASER, P. E. 2006. Small ubiquitin-like modifier (SUMO) modification of natively unfolded proteins tau and alpha-synuclein. *J Biol Chem,* 281**,** 9919-24.

DOTY, R. L., BROMLEY, S. M. & STERN, M. B. 1995. Olfactory testing as an aid in the diagnosis of Parkinson's disease: development of optimal discrimination criteria. *Neurodegeneration,* 4**,** 93-7.

DREYER, E. B., ZHANG, D. & LIPTON, S. A. 1995. Transcriptional or translational inhibition blocks low dose NMDA-mediated cell death. *Neuroreport,* 6**,** 942-4.

DRIVER, J. E., RACCA, C., CUNNINGHAM, M. O., TOWERS, S. K., DAVIES, C. H., WHITTINGTON, M. A. & LEBEAU, F. E. 2007. Impairment of hippocampal gamma-frequency oscillations in vitro in mice overexpressing human amyloid precursor protein (APP). *Eur J Neurosci,* 26**,** 1280-8.

DUGGER, B. N. & DICKSON, D. W. 2017. Pathology of Neurodegenerative Diseases. *Cold Spring Harbor perspectives in biology,* 9**,** a028035.

EICHENBAUM, H. & LIPTON, P. A. 2008. Towards a functional organization of the medial temporal lobe memory system: role of the parahippocampal and medial entorhinal cortical areas. *Hippocampus,* 18**,** 1314-1324.

EKMARK-LEWÉN, S., LINDSTRÖM, V., GUMUCIO, A., IHSE, E., BEHERE, A., KAHLE, P. J., NORDSTRÖM, E., ERIKSSON, M., ERLANDSSON, A., BERGSTRÖM, J. & INGELSSON, M. 2018a. Early fine motor impairment and behavioral dysfunction in (Thy-1)-h[A30P] alpha-synuclein mice. *Brain and behavior,* 8**,** e00915-e00915.

EKMARK-LEWÉN, S., LINDSTRÖM, V., GUMUCIO, A., IHSE, E., BEHERE, A., KAHLE, P. J., NORDSTRÖM, E., ERIKSSON, M., ERLANDSSON, A., BERGSTRÖM, J. & INGELSSON, M. 2018b. Early fine motor impairment and behavioral dysfunction in (Thy-1)-h[A30P] alpha-synuclein mice. *Brain Behav,* 8**,** e00915.

ELBAZ, A., DUFOUIL, C. & ALPEROVITCH, A. 2007. Interaction between genes and environment in neurodegenerative diseases. *C R Biol,* 330**,** 318-28.

ELDER, G. J., MACTIER, K., COLLOBY, S. J., WATSON, R., BLAMIRE, A. M., O'BRIEN, J. T. & TAYLOR, J.-P. 2017. The influence of hippocampal atrophy on the cognitive phenotype of dementia with Lewy bodies. *International journal of geriatric psychiatry,* 32**,** 1182-1189.

ELKON, H., DON, J., MELAMED, E., ZIV, I., SHIRVAN, A. & OFFEN, D. 2002. Mutant and wild-type α-synuclein interact with mitochondrial cytochrome C oxidase. *Journal of Molecular Neuroscience,* 18**,** 229-238.

EMMANOUILIDOU, E., STEFANIS, L. & VEKRELLIS, K. 2010. Cell-produced alpha-synuclein oligomers are targeted to, and impair, the 26S proteasome. *Neurobiol Aging,* 31**,** 953-68.

EMRE, M., AARSLAND, D., BROWN, R., BURN, D. J., DUYCKAERTS, C., MIZUNO, Y., BROE, G. A., CUMMINGS, J., DICKSON, D. W., GAUTHIER, S., GOLDMAN, J., GOETZ, C., KORCZYN, A., LEES, A., LEVY, R., LITVAN, I., MCKEITH, I., OLANOW, W., POEWE, W., QUINN, N., SAMPAIO, C., TOLOSA, E. & DUBOIS, B. 2007. Clinical diagnostic criteria for dementia associated with Parkinson's disease. *Mov Disord,* 22**,** 1689-707; quiz 1837.

ENGELENDER, S. 2008. Ubiquitination of α-synuclein and autophagy in Parkinson's disease. *Autophagy,* 4**,** 372-374.

ERSKINE, D., PATTERSON, L., ALEXANDRIS, A., HANSON, P. S., MCKEITH, I. G., ATTEMS, J. & MORRIS, C. M. 2018. Regional levels of physiological α-synuclein are directly associated with Lewy body pathology. *Acta Neuropathol,* 135**,** 153-154.

ESPOSITO, A., DOHM, C. P., KERMER, P., BÄHR, M. & WOUTERS, F. S. 2007. alpha-Synuclein and its disease-related mutants interact differentially with the microtubule protein tau and associate with the actin cytoskeleton. *Neurobiol Dis,* 26**,** 521-31.

FAHN, S. 2011. Classification of movement disorders. *Mov Disord,* 26**,** 947-57.

FATHY, Y. Y., JONKER, A. J., OUDEJANS, E., DE JONG, F. J. J., VAN DAM, A. W., ROZEMULLER, A. J. M. & VAN DE BERG, W. D. J. 2019. Differential insular cortex subregional vulnerability to α-synuclein pathology in Parkinson's disease and dementia with Lewy bodies. *Neuropathol Appl Neurobiol,* 45**,** 262-277.

FAUVET, B., MBEFO, M. K., FARES, M. B., DESOBRY, C., MICHAEL, S., ARDAH, M. T., TSIKA, E., COUNE, P., PRUDENT, M., LION, N., ELIEZER, D., MOORE, D. J., SCHNEIDER, B., AEBISCHER, P., EL-AGNAF, O. M., MASLIAH, E. & LASHUEL, H. A. 2012. alpha-Synuclein in central nervous system and from erythrocytes, mammalian cells, and Escherichia coli exists predominantly as disordered monomer. *J Biol Chem,* 287**,** 15345-64.

FERANDO, I. & MODY, I. 2015. In vitro gamma oscillations following partial and complete ablation of δ subunit-containing GABAA receptors from parvalbumin interneurons. *Neuropharmacology,* 88**,** 91-98.

FERGUSON, B. R. & GAO, W.-J. 2018. PV Interneurons: Critical Regulators of E/I Balance for Prefrontal Cortex-Dependent Behavior and Psychiatric Disorders. *Frontiers in neural circuits,* 12**,** 37-37.

FERMAN, T. J., SMITH, G. E., BOEVE, B. F., GRAFF-RADFORD, N. R., LUCAS, J. A., KNOPMAN, D. S., PETERSEN, R. C., IVNIK, R. J., WSZOLEK, Z., UITTI, R. & DICKSON, D. W. 2006. Neuropsychological differentiation of dementia with Lewy bodies from normal aging and Alzheimer's disease. *Clin Neuropsychol,* 20**,** 623-36.

FERNANDEZ, C. O., HOYER, W., ZWECKSTETTER, M., JARES-ERIJMAN, E. A., SUBRAMANIAM, V., GRIESINGER, C. & JOVIN, T. M. 2004. NMR of alpha-synuclein-polyamine complexes elucidates the mechanism and kinetics of induced aggregation. *Embo j,* 23**,** 2039-46.

FERNÁNDEZ-SUÁREZ, D., CELORRIO, M., LANCIEGO, J. L., FRANCO, R. & AYMERICH, M. S. 2012. Loss of Parvalbumin-Positive Neurons From the Globus Pallidus in Animal Models of Parkinson Disease. *Journal of Neuropathology & Experimental Neurology,* 71**,** 973-982.

FERREIRA, S. A. & ROMERO-RAMOS, M. 2018. Microglia Response During Parkinson's Disease: Alpha-Synuclein Intervention. *Frontiers in cellular neuroscience,* 12**,** 247-247.

FINLEY, D. 2009. Recognition and processing of ubiquitin-protein conjugates by the proteasome. *Annual review of biochemistry,* 78**,** 477-513.

FISAHN, A., PIKE, F. G., BUHL, E. H. & PAULSEN, O. 1998. Cholinergic induction of network oscillations at 40 Hz in the hippocampus in vitro. *Nature,* 394**,** 186-9.

FISAHN, A., YAMADA, M., DUTTAROY, A., GAN, J.-W., DENG, C.-X., MCBAIN, C. J. & WESS, J. 2002. Muscarinic Induction of Hippocampal Gamma Oscillations Requires Coupling of the M1 Receptor to Two Mixed Cation Currents. *Neuron,* 33**,** 615-624.

FLORES-CUADRADO, A., UBEDA-BAÑON, I., SAIZ-SANCHEZ, D. & MARTINEZ-MARCOS, A. 2017. α-Synucleinopathy in the Human Amygdala in Parkinson Disease: Differential Vulnerability of Somatostatin- and Parvalbumin-Expressing Neurons. *Journal of Neuropathology & Experimental Neurology,* 76**,** 754-758.

FOLCH, J., BUSQUETS, O., ETTCHETO, M., SÁNCHEZ-LÓPEZ, E., CASTRO-TORRES, R. D., VERDAGUER, E., GARCIA, M. L., OLLOQUEQUI, J., CASADESÚS, G., BEAS-ZARATE, C., PELEGRI, C., VILAPLANA, J., AULADELL, C. & CAMINS, A. 2018. Memantine for the Treatment of Dementia: A Review on its Current and Future Applications. *Journal of Alzheimer's disease : JAD,* 62**,** 1223-1240.

FOLSTEIN, M. F., FOLSTEIN, S. E. & MCHUGH, P. R. 1975. "Mini-mental state". A practical method for grading the cognitive state of patients for the clinician. *J Psychiatr Res,* 12**,** 189-98.

FOULDS, P. G., DIGGLE, P., MITCHELL, J. D., PARKER, A., HASEGAWA, M., MASUDA-SUZUKAKE, M., MANN, D. M. & ALLSOP, D. 2013. A longitudinal study on alpha-synuclein in blood plasma as a biomarker for Parkinson's disease. *Sci Rep,* 3**,** 2540.

FRANKLIN, K. B. J. & PAXINOS, G. 2013. *Paxinos and Franklin's The mouse brain in stereotaxic coordinates*.

FREICHEL, C., NEUMANN, M., BALLARD, T., MULLER, V., WOOLLEY, M., OZMEN, L., BORRONI, E., KRETZSCHMAR, H. A., HAASS, C., SPOOREN, W. & KAHLE, P. J. 2007. Age-dependent cognitive decline and amygdala pathology in alpha-synuclein transgenic mice. *Neurobiol Aging,* 28**,** 1421-35.

FREUND, T. F. & KATONA, I. 2007. Perisomatic inhibition. *Neuron,* 56**,** 33-42.

FUCHS, E. C., ZIVKOVIC, A. R., CUNNINGHAM, M. O., MIDDLETON, S., LEBEAU, F. E., BANNERMAN, D. M., ROZOV, A., WHITTINGTON, M. A., TRAUB, R. D., RAWLINS, J. N. & MONYER, H. 2007. Recruitment of parvalbumin-positive interneurons determines hippocampal function and associated behavior. *Neuron,* 53**,** 591-604.

FUJII, T., NOZAKI, F., SAITO, K., HAYASHI, A., NISHIGAKI, Y., MURAYAMA, K., TANAKA, M., KOGA, Y., HIEJIMA, I. & KUMADA, T. 2014. Efficacy of pyruvate therapy in patients with mitochondrial disease: a semi-quantitative clinical evaluation study. *Mol Genet Metab,* 112**,** 133-8.

FUJIWARA, H., HASEGAWA, M., DOHMAE, N., KAWASHIMA, A., MASLIAH, E., GOLDBERG, M. S., SHEN, J., TAKIO, K. & IWATSUBO, T. 2002. alpha-Synuclein is phosphorylated in synucleinopathy lesions. *Nat Cell Biol,* 4**,** 160-4.

FUKUDA, A., CZURKO, A., HIDA, H., MURAMATSU, K., LENARD, L. & NISHINO, H. 1995. Appearance of deteriorated neurons on regionally different time tables in rat brain thin slices maintained in physiological condition. *Neurosci Lett,* 184**,** 13-6.

GANAPATHY, K., DATTA, I., SOWMITHRA, S., JOSHI, P. & BHONDE, R. 2016. Influence of 6-Hydroxydopamine Toxicity on alpha-Synuclein Phosphorylation, Resting Vesicle Expression, and Vesicular Dopamine Release. *J Cell Biochem,* 117**,** 2719-2736.

GARCIA-REITBOCK, P., ANICHTCHIK, O., BELLUCCI, A., IOVINO, M., BALLINI, C., FINEBERG, E., GHETTI, B., DELLA CORTE, L., SPANO, P., TOFARIS, G. K., GOEDERT, M. & SPILLANTINI, M. G. 2010. SNARE protein redistribution and synaptic failure in a transgenic mouse model of Parkinson's disease. *Brain,* 133**,** 2032-44.

GATT, A. P., DUNCAN, O. F., ATTEMS, J., FRANCIS, P. T., BALLARD, C. G. & BATEMAN, J. M. 2016. Dementia in Parkinson's disease is associated with enhanced mitochondrial complex I deficiency. *Mov Disord,* 31**,** 352-9.

GAUGLER, M. N., GENC, O., BOBELA, W., MOHANNA, S., ARDAH, M. T., EL-AGNAF, O. M., CANTONI, M., BENSADOUN, J. C., SCHNEGGENBURGER, R., KNOTT, G. W., AEBISCHER, P. & SCHNEIDER, B. L. 2012. Nigrostriatal overabundance of α-synuclein leads to decreased vesicle density and deficits in dopamine release that correlate with reduced motor activity. *Acta Neuropathol,* 123**,** 653-69.

GELDER, M., GATH, D. & MAYOU, R. 1989. *Oxford textbook of psychiatry, 2nd ed,* New York, NY, US, Oxford University Press.

GERST, J. E. 1999. SNAREs and SNARE regulators in membrane fusion and exocytosis. *Cell Mol Life Sci,* 55**,** 707-34.

GHIGLIERI, V., CALABRESE, V. & CALABRESI, P. 2018. Alpha-Synuclein: From Early Synaptic Dysfunction to Neurodegeneration. *Frontiers in Neurology,* 9.

GIASSON, B. I., DUDA, J. E., MURRAY, I. V., CHEN, Q., SOUZA, J. M., HURTIG, H. I., ISCHIROPOULOS, H., TROJANOWSKI, J. Q. & LEE, V. M. 2000. Oxidative damage linked to neurodegeneration by selective alpha-synuclein nitration in synucleinopathy lesions. *Science,* 290**,** 985-9.

GODA, Y. 1997. SNAREs and regulated vesicle exocytosis. *Proceedings of the National Academy of Sciences,* 94**,** 769-772.

GOEDERT, M. 2001. Alpha-synuclein and neurodegenerative diseases. *Nature Reviews Neuroscience,* 2**,** 492.

GOEDERT, M., SPILLANTINI, M. G., DEL TREDICI, K. & BRAAK, H. 2013. 100 years of Lewy pathology. *Nat Rev Neurol,* 9**,** 13-24.

GOLDSTEIN, A. Y., WANG, X. & SCHWARZ, T. L. 2008. Axonal transport and the delivery of pre-synaptic components. *Curr Opin Neurobiol,* 18**,** 495-503.

GÓMEZ-ISLA, T., GROWDON, W. B., MCNAMARA, M., NEWELL, K., GÓMEZ-TORTOSA, E., HEDLEY-WHYTE, E. T. & HYMAN, B. T. 1999. Clinicopathologic correlates in temporal cortex in dementia with Lewy bodies. *Neurology,* 53**,** 2003-9.

GONZALEZ-BURGOS, G., CHO, R. Y. & LEWIS, D. A. 2015. Alterations in cortical network oscillations and parvalbumin neurons in schizophrenia. *Biological psychiatry,* 77**,** 1031-1040.

GONZALEZ-BURGOS, G. & LEWIS, D. A. 2008. GABA neurons and the mechanisms of network oscillations: implications for understanding cortical dysfunction in schizophrenia. *Schizophrenia bulletin,* 34**,** 944-961.

GOSAVI, N., LEE, H.-J., LEE, J. S., PATEL, S. & LEE, S.-J. 2002. Golgi Fragmentation Occurs in the Cells with Prefibrillar α-Synuclein Aggregates and Precedes the Formation of Fibrillar Inclusion. *Journal of Biological Chemistry,* 277**,** 48984-48992.

GREY, M., LINSE, S., NILSSON, H., BRUNDIN, P. & SPARR, E. 2011. Membrane interaction of alpha-synuclein in different aggregation states. *J Parkinsons Dis,* 1**,** 359-71.

GROSS, R. G., CAMP, E., MCMILLAN, C. T., DREYFUSS, M., GUNAWARDENA, D., COOK, P. A., MORGAN, B., SIDEROWF, A., HURTIG, H. I., STERN, M. B. & GROSSMAN, M. 2013. Impairment of script comprehension in Lewy body spectrum disorders. *Brain and language,* 125**,** 330-343.

GURD, J. M., HERZBERG, L., JOACHIM, C., MARSHALL, J. C., JOBST, K., MCSHANE, R. H., HINDLEY, N. J. & KING, E. E. 2000. Dementia with Lewy bodies: a pure case. *Brain Cogn,* 44**,** 307-23.

HABER, S. N. 2014. The place of dopamine in the cortico-basal ganglia circuit. *Neuroscience,* 282**,** 248-257.

HABER, S. N. 2016. Corticostriatal Circuitry. *In:* PFAFF, D. W. & VOLKOW, N. D. (eds.) *Neuroscience in the 21st Century.* New York, NY: Springer New York.

HABER, S. N. & CALZAVARA, R. 2009. The cortico-basal ganglia integrative network: the role of the thalamus. *Brain Res Bull,* 78**,** 69-74.

HAGGERTY, T., CREDLE, J., RODRIGUEZ, O., WILLS, J., OAKS, A. W., MASLIAH, E. & SIDHU, A. 2011. Hyperphosphorylated Tau in an α-synuclein-overexpressing transgenic model of Parkinson's disease. *The European journal of neuroscience,* 33**,** 1598-1610.

HÁJOS, N., KATONA, I., NAIEM, S. S., MACKIE, K., LEDENT, C., MODY, I. & FREUND, T. F. 2000. Cannabinoids inhibit hippocampal GABAergic transmission and network oscillations. *Eur J Neurosci,* 12**,** 3239-49.

HAJOS, N., PALHALMI, J., MANN, E. O., NEMETH, B., PAULSEN, O. & FREUND, T. F. 2004. Spike timing of distinct types of GABAergic interneuron during hippocampal gamma oscillations in vitro. *J Neurosci,* 24**,** 9127-37.

HAMPTON, R. Y. 2000. ER stress response: Getting the UPR hand on misfolded proteins. *Current Biology,* 10**,** R518-R521.

HANSEN, C., ANGOT, E., BERGSTROM, A. L., STEINER, J. A., PIERI, L., PAUL, G., OUTEIRO, T. F., MELKI, R., KALLUNKI, P., FOG, K., LI, J. Y. & BRUNDIN, P. 2011. alpha-Synuclein propagates from mouse brain to grafted dopaminergic neurons and seeds aggregation in cultured human cells. *J Clin Invest,* 121**,** 715-25.

HANSEN, D., LING, H., LASHLEY, T., HOLTON, J. L. & WARNER, T. T. 2019. Review: Clinical, neuropathological and genetic features of Lewy body dementias. *Neuropathology and Applied Neurobiology,* 45**,** 635-654.

HANSEN, L. A. 1997. The Lewy body variant of Alzheimer disease. *J Neural Transm Suppl,* 51**,** 83-93.

HAQUE, F., PANDEY, A. P., CAMBREA, L. R., ROCHET, J.-C. & HOVIS, J. S. 2010. Adsorption of alpha-synuclein on lipid bilayers: modulating the structure and stability of protein assemblies. *The journal of physical chemistry. B,* 114**,** 4070-4081.

HARPER, J. D., LIEBER, C. M. & LANSBURY, P. T., JR. 1997. Atomic force microscopic imaging of seeded fibril formation and fibril branching by the Alzheimer's disease amyloid-beta protein. *Chem Biol,* 4**,** 951-9.

HASEGAWA, M., FUJIWARA, H., NONAKA, T., WAKABAYASHI, K., TAKAHASHI, H., LEE, V. M., TROJANOWSKI, J. Q., MANN, D. & IWATSUBO, T. 2002. Phosphorylated alpha-synuclein is ubiquitinated in alpha-synucleinopathy lesions. *J Biol Chem,* 277**,** 49071-6.

HEINZ, S., FREYBERGER, A., LAWRENZ, B., SCHLADT, L., SCHMUCK, G. & ELLINGER-ZIEGELBAUER, H. 2017. Mechanistic Investigations of the Mitochondrial Complex I Inhibitor Rotenone in the Context of Pharmacological and Safety Evaluation. *Scientific Reports,* 7**,** 45465.

HEISTEK, T., TIMMERMAN, J., SPIJKER, S., BRUSSAARD, A. & MANSVELDER, H. 2010. GABAergic synapse properties may explain genetic variation in hippocampal network oscillations in mice. *Frontiers in Cellular Neuroscience,* 4.

HEITZ, C., NOBLET, V., CRETIN, B., PHILIPPI, N., KREMER, L., STACKFLETH, M., HUBELE, F., ARMSPACH, J. P., NAMER, I. & BLANC, F. 2015. Neural correlates of visual hallucinations in dementia with Lewy bodies. *Alzheimer's Research & Therapy,* 7**,** 6.

HELY, M. A., REID, W. G., ADENA, M. A., HALLIDAY, G. M. & MORRIS, J. G. 2008. The Sydney multicenter study of Parkinson's disease: the inevitability of dementia at 20 years. *Mov Disord,* 23**,** 837-44.

HERRERO, M. T. & MORELLI, M. 2017. Multiple mechanisms of neurodegeneration and progression. *Prog Neurobiol,* 155**,** 1.

HERRMANN, C. S. & DEMIRALP, T. 2005. Human EEG gamma oscillations in neuropsychiatric disorders. *Clin Neurophysiol,* 116**,** 2719-33.

HERSHKO, A. & CIECHANOVER, A. 1998. The ubiquitin system. *Annu Rev Biochem,* 67**,** 425-79.

HIJAZ, B. A. & VOLPICELLI-DALEY, L. A. 2020. Initiation and propagation of α-synuclein aggregation in the nervous system. *Molecular Neurodegeneration,* 15**,** 19.

HIJAZI, S., HEISTEK, T. S., SCHELTENS, P., NEUMANN, U., SHIMSHEK, D. R., MANSVELDER, H. D., SMIT, A. B. & VAN KESTEREN, R. E. 2019. Early restoration of parvalbumin interneuron activity prevents memory loss and network hyperexcitability in a mouse model of Alzheimer's disease. *Molecular Psychiatry.*

HILTON, D., STEPHENS, M., KIRK, L., EDWARDS, P., POTTER, R., ZAJICEK, J., BROUGHTON, E., HAGAN, H. & CARROLL, C. 2014. Accumulation of alpha-synuclein in the bowel of patients in the pre-clinical phase of Parkinson's disease. *Acta Neuropathol,* 127**,** 235-41.

HOCHSTRASSER, M. 2006. Lingering mysteries of ubiquitin-chain assembly. *Cell,* 124**,** 27-34.

HODARA, R., NORRIS, E. H., GIASSON, B. I., MISHIZEN-EBERZ, A. J., LYNCH, D. R., LEE, V. M. & ISCHIROPOULOS, H. 2004. Functional consequences of alpha-synuclein tyrosine nitration: diminished binding to lipid vesicles and increased fibril formation. *J Biol Chem,* 279**,** 47746-53.

HOFFMANN, M. 2013. The human frontal lobes and frontal network systems: an evolutionary, clinical, and treatment perspective. *ISRN neurology,* 2013**,** 892459-892459.

HONG, Z., SHI, M., CHUNG, K. A., QUINN, J. F., PESKIND, E. R., GALASKO, D., JANKOVIC, J., ZABETIAN, C. P., LEVERENZ, J. B., BAIRD, G., MONTINE, T. J., HANCOCK, A. M., HWANG, H., PAN, C., BRADNER, J., KANG, U. J., JENSEN, P. H. & ZHANG, J. 2010. DJ-1 and alpha-synuclein in human cerebrospinal fluid as biomarkers of Parkinson's disease. *Brain,* 133**,** 713-26.

HONKANEN, R., ROUHINEN, S., WANG, S. H., PALVA, J. M. & PALVA, S. 2014. Gamma Oscillations Underlie the Maintenance of Feature-Specific Information and the Contents of Visual Working Memory. *Cerebral Cortex,* 25**,** 3788-3801.

HORMUZDI, S. G., PAIS, I., LEBEAU, F. E., TOWERS, S. K., ROZOV, A., BUHL, E. H., WHITTINGTON, M. A. & MONYER, H. 2001. Impaired electrical signaling disrupts gamma frequency oscillations in connexin 36-deficient mice. *Neuron,* 31**,** 487-95.

HSU, L. J., SAGARA, Y., ARROYO, A., ROCKENSTEIN, E., SISK, A., MALLORY, M., WONG, J., TAKENOUCHI, T., HASHIMOTO, M. & MASLIAH, E. 2000. alpha-synuclein promotes mitochondrial deficit and oxidative stress. *Am J Pathol,* 157**,** 401-10.

HU, H. & JONAS, P. 2014. A supercritical density of Na(+) channels ensures fast signaling in GABAergic interneuron axons. *Nat Neurosci,* 17**,** 686-93.

HWANG, K., BERTOLERO, M. A., LIU, W. B. & D'ESPOSITO, M. 2017. The Human Thalamus Is an Integrative Hub for Functional Brain Networks. *The Journal of neuroscience : the official journal of the Society for Neuroscience,* 37**,** 5594-5607.

INAN, M., ZHAO, M., MANUSZAK, M., KARAKAYA, C., RAJADHYAKSHA, A. M., PICKEL, V. M., SCHWARTZ, T. H., GOLDSTEIN, P. A. & MANFREDI, G. 2016. Energy deficit in parvalbumin neurons leads to circuit dysfunction, impaired sensory gating and social disability. *Neurobiology of Disease,* 93**,** 35-46.

INVERNIZZI, G., PAPALEO, E., SABATE, R. & VENTURA, S. 2012. Protein aggregation: mechanisms and functional consequences. *Int J Biochem Cell Biol,* 44**,** 1541-54.

JACKSON, G. A. 2012. Oxford Textbook of Old Age Psychiatry. Editors Robin Jacoby, Catherine Oppenheimer, Tom Dening and Alan Thomas. *Dementia,* 11**,** 765-765.

JANKOVIC, J. 2010. Camptocormia, head drop and other bent spine syndromes: heterogeneous etiology and pathogenesis of Parkinsonian deformities. *Mov Disord,* 25**,** 527-8.

JELLINGER, K. A. & ATTEMS, J. 2013. Neuropathological approaches to cerebral aging and neuroplasticity. *Dialogues in clinical neuroscience,* 15**,** 29-43.

JELLINGER, K. A. & KORCZYN, A. D. 2018. Are dementia with Lewy bodies and Parkinson's disease dementia the same disease? *BMC Medicine,* 16**,** 34.

JENSEN, P. H., NIELSEN, M. S., JAKES, R., DOTTI, C. G. & GOEDERT, M. 1998. Binding of alpha-synuclein to brain vesicles is abolished by familial Parkinson's disease mutation. *J Biol Chem,* 273**,** 26292-4.

JUNQUEIRA, S. C., CENTENO, E. G. Z., WILKINSON, K. A. & CIMAROSTI, H. 2018. Post-translational modifications of Parkinson's disease-related proteins: Phosphorylation, SUMOylation and Ubiquitination. *Biochimica et Biophysica Acta (BBA) - Molecular Basis of Disease*.

KAHLE, P. J. 2008. alpha-Synucleinopathy models and human neuropathology: similarities and differences. *Acta Neuropathol,* 115**,** 87-95.

KAHLE, P. J., NEUMANN, M., OZMEN, L. & HAASS, C. 2000a. Physiology and pathophysiology of alpha-synuclein. Cell culture and transgenic animal models based on a Parkinson's disease-associated protein. *Ann N Y Acad Sci,* 920**,** 33-41.

KAHLE, P. J., NEUMANN, M., OZMEN, L., MÜLLER, V., JACOBSEN, H., SCHINDZIELORZ, A., OKOCHI, M., LEIMER, U., VAN DER PUTTEN, H., PROBST, A., KREMMER, E., KRETZSCHMAR, H. A. & HAASS, C. 2000b. Subcellular localization of wild-type and Parkinson's disease-associated mutant α-synuclein in human and transgenic mouse brain. *Journal of Neuroscience,* 20**,** 6365-6373.

KALAITZAKIS, M. E., GRAEBER, M. B., GENTLEMAN, S. M. & PEARCE, R. K. 2008. The dorsal motor nucleus of the vagus is not an obligatory trigger site of Parkinson's disease: a critical analysis of alpha-synuclein staging. *Neuropathol Appl Neurobiol,* 34**,** 284-95.

KALANITHI, P. S. A., ZHENG, W., KATAOKA, Y., DIFIGLIA, M., GRANTZ, H., SAPER, C. B., SCHWARTZ, M. L., LECKMAN, J. F. & VACCARINO, F. M. 2005. Altered parvalbumin-positive neuron distribution in basal ganglia of individuals with Tourette syndrome. *Proceedings of the National Academy of Sciences of the United States of America,* 102**,** 13307.

KAMPF, C., OLSSON, I., RYBERG, U., SJÖSTEDT, E. & PONTÉN, F. 2012. Production of tissue microarrays, immunohistochemistry staining and digitalization within the human protein atlas. *Journal of visualized experiments : JoVE***,** 3620.

KANN, O. 2011. The energy demand of fast neuronal network oscillations: insights from brain slice preparations. *Front Pharmacol,* 2**,** 90.

KANN, O. 2016. The interneuron energy hypothesis: Implications for brain disease. *Neurobiol Dis,* 90**,** 75-85.

KANN, O., HUCHZERMEYER, C., KOVACS, R., WIRTZ, S. & SCHUELKE, M. 2011. Gamma oscillations in the hippocampus require high complex I gene expression and strong functional performance of mitochondria. *Brain,* 134**,** 345-58.

KANN, O., PAPAGEORGIOU, I. E. & DRAGUHN, A. 2014a. Highly energized inhibitory interneurons are a central element for information processing in cortical networks. *J Cereb Blood Flow Metab,* 34**,** 1270-82.

KANN, O., PAPAGEORGIOU, I. E. & DRAGUHN, A. 2014b. Highly energized inhibitory interneurons are a central element for information processing in cortical networks. *Journal of Cerebral Blood Flow & Metabolism,* 34**,** 1270-1282.

KATSAROU, A.-M., MOSHÉ, S. L. & GALANOPOULOU, A. S. 2017. INTERNEURONOPATHIES AND THEIR ROLE IN EARLY LIFE EPILEPSIES AND NEURODEVELOPMENTAL DISORDERS. *Epilepsia open,* 2**,** 284-306.

KATZENSCHLAGER, R., ZIJLMANS, J., EVANS, A., WATT, H. & LEES, A. J. 2004. Olfactory function distinguishes vascular parkinsonism from Parkinson's disease. *J Neurol Neurosurg Psychiatry,* 75**,** 1749-52.

KAWAGUCHI, Y. & KUBOTA, Y. 1997. GABAergic cell subtypes and their synaptic connections in rat frontal cortex. *Cereb Cortex,* 7**,** 476-86.

KEENEY, P. M., XIE, J., CAPALDI, R. A. & BENNETT, J. P., JR. 2006. Parkinson's disease brain mitochondrial complex I has oxidatively damaged subunits and is functionally impaired and misassembled. *J Neurosci,* 26**,** 5256-64.

KENNY, E. R., BLAMIRE, A. M., FIRBANK, M. J. & O'BRIEN, J. T. 2012. Functional connectivity in cortical regions in dementia with Lewy bodies and Alzheimer's disease. *Brain : a journal of neurology,* 135**,** 569-581.

KHUNDAKAR, A. A., HANSON, P. S., ERSKINE, D., LAX, N. Z., ROSCAMP, J., KARYKA, E., TSEFOU, E., SINGH, P., COCKELL, S. J., GRIBBEN, A., RAMSAY, L., BLAIN, P. G., MOSIMANN, U. P., LETT, D. J., ELSTNER, M., TURNBULL, D. M., XIANG, C. C., BROWNSTEIN, M. J., O'BRIEN, J. T., TAYLOR, J.-P., ATTEMS, J., THOMAS, A. J., MCKEITH, I. G. & MORRIS, C. M. 2016. Analysis of primary visual cortex in dementia with Lewy bodies indicates GABAergic involvement associated with recurrent complex visual hallucinations. *Acta neuropathologica communications,* 4**,** 66-66.

KILPELÄINEN, T., JULKU, U. H., SVARCBAHS, R. & MYÖHÄNEN, T. T. 2019. Behavioural and dopaminergic changes in double mutated human A30P*A53T alpha-synuclein transgenic mouse model of Parkinson´s disease. *Scientific Reports,* 9**,** 17382.

KIM, C., HO, D. H., SUK, J. E., YOU, S., MICHAEL, S., KANG, J., JOONG LEE, S., MASLIAH, E., HWANG, D., LEE, H. J. & LEE, S. J. 2013. Neuron-released oligomeric alpha-synuclein is an endogenous agonist of TLR2 for paracrine activation of microglia. *Nat Commun,* 4**,** 1562.

KIM, K., KIM, S. H., KIM, J., KIM, H. & YIM, J. 2012. Glutathione s-transferase omega 1 activity is sufficient to suppress neurodegeneration in a Drosophila model of Parkinson disease. *J Biol Chem,* 287**,** 6628-41.

KNOTT, E. M., SUN, J., LEI, Y., RYOU, M.-G., OLIVENCIA-YURVATI, A. H. & MALLET, R. T. 2006. Pyruvate Mitigates Oxidative Stress During Reperfusion of Cardioplegia-Arrested Myocardium. *The Annals of Thoracic Surgery,* 81**,** 928-934.

KOIVISTO, H., LEINONEN, H., PUURULA, M., HAFEZ, H. S., BARRERA, G. A., STRIDH, M. H., WAAGEPETERSEN, H. S., TIAINEN, M., SOININEN, P., ZILBERTER, Y. & TANILA, H. 2016. Chronic Pyruvate Supplementation Increases Exploratory Activity and Brain Energy Reserves in Young and Middle-Aged Mice. *Frontiers in aging neuroscience,* 8**,** 41-41.

KOSAKA, K. 2014. Lewy body disease and dementia with Lewy bodies. *Proceedings of the Japan Academy. Series B, Physical and biological sciences,* 90**,** 301-306.

KOSAKA, K., TSUCHIYA, K. & YOSHIMURA, M. 1988. Lewy body disease with and without dementia: a clinicopathological study of 35 cases. *Clin Neuropathol,* 7**,** 299-305.

KOSAKA, K., YOSHIMURA, M., IKEDA, K. & BUDKA, H. 1984. Diffuse type of Lewy body disease: progressive dementia with abundant cortical Lewy bodies and senile changes of varying degree--a new disease? *Clinical neuropathology,* 3**,** 185-192.

KRAUSE, B. M., MURPHY, C. A., UHLRICH, D. J. & BANKS, M. I. 2017. PV+ Cells Enhance Temporal Population Codes but not Stimulus-Related Timing in Auditory Cortex. *Cerebral Cortex,* 29**,** 627-647.

KROPF, E., SYAN, S. K., MINUZZI, L. & FREY, B. N. 2019. From anatomy to function: the role of the somatosensory cortex in emotional regulation. *Revista brasileira de psiquiatria (Sao Paulo, Brazil : 1999),* 41**,** 261-269.

KRUGER, R., KUHN, W., LEENDERS, K. L., SPRENGELMEYER, R., MULLER, T., WOITALLA, D., PORTMAN, A. T., MAGUIRE, R. P., VEENMA, L., SCHRODER, U., SCHOLS, L., EPPLEN, J. T., RIESS, O. & PRZUNTEK, H. 2001. Familial parkinsonism with synuclein pathology: clinical and PET studies of A30P mutation carriers. *Neurology,* 56**,** 1355-62.

KRUMOVA, P., MEULMEESTER, E., GARRIDO, M., TIRARD, M., HSIAO, H. H., BOSSIS, G., URLAUB, H., ZWECKSTETTER, M., KUGLER, S., MELCHIOR, F., BAHR, M. & WEISHAUPT, J. H. 2011. Sumoylation inhibits alpha-synuclein aggregation and toxicity. *J Cell Biol,* 194**,** 49-60.

KUHLMAN, S. J., OLIVAS, N. D., TRING, E., IKRAR, T., XU, X. & TRACHTENBERG, J. T. 2013. A disinhibitory microcircuit initiates critical-period plasticity in the visual cortex. *Nature,* 501**,** 543-546.

KUKI, T., FUJIHARA, K., MIWA, H., TAMAMAKI, N., YANAGAWA, Y. & MUSHIAKE, H. 2015. Contribution of parvalbumin and somatostatin-expressing GABAergic neurons to slow oscillations and the balance in beta-gamma oscillations across cortical layers. *Front Neural Circuits,* 9**,** 6.

KUMAR, K. R., LOHMANN, K. & KLEIN, C. 2012. Genetics of Parkinson disease and other movement disorders. *Curr Opin Neurol,* 25**,** 466-74.

KUNADT, M., ECKERMANN, K., STUENDL, A., GONG, J., RUSSO, B., STRAUSS, K., RAI, S., KUGLER, S., FALOMIR LOCKHART, L., SCHWALBE, M., KRUMOVA, P., OLIVEIRA, L. M., BAHR, M., MOBIUS, W., LEVIN, J., GIESE, A., KRUSE, N., MOLLENHAUER, B., GEISS-FRIEDLANDER, R., LUDOLPH, A. C., FREISCHMIDT, A., FEILER, M. S., DANZER, K. M., ZWECKSTETTER, M., JOVIN, T. M., SIMONS, M., WEISHAUPT, J. H. & SCHNEIDER, A. 2015. Extracellular vesicle sorting of alpha-Synuclein is regulated by sumoylation. *Acta Neuropathol,* 129**,** 695-713.

KUZUHARA, S., MORI, H., IZUMIYAMA, N., YOSHIMURA, M. & IHARA, Y. 1988. Lewy bodies are ubiquitinated. A light and electron microscopic immunocytochemical study. *Acta Neuropathol,* 75**,** 345-53.

LAIRD, M. D., CLERC, P., POLSTER, B. M. & FISKUM, G. 2013. Augmentation of normal and glutamate-impaired neuronal respiratory capacity by exogenous alternative biofuels. *Transl Stroke Res,* 4**,** 643-51.

LAKEY, L. 2012. Making a name for dementia: a national challenge. *Ment Health Today***,** 18-9.

LAMBERT, M. P., BARLOW, A. K., CHROMY, B. A., EDWARDS, C., FREED, R., LIOSATOS, M., MORGAN, T. E., ROZOVSKY, I., TROMMER, B., VIOLA, K. L., WALS, P., ZHANG, C., FINCH, C. E., KRAFFT, G. A. & KLEIN, W. L. 1998. Diffusible, nonfibrillar ligands derived from Abeta1-42 are potent central nervous system neurotoxins. *Proc Natl Acad Sci U S A,* 95**,** 6448-53.

LANCIEGO, J. L., LUQUIN, N. & OBESO, J. A. 2012. Functional neuroanatomy of the basal ganglia. *Cold Spring Harbor perspectives in medicine,* 2**,** a009621-a009621.

LANGMOEN, I. A. & ANDERSEN, P. 1983. Summation of excitatory postsynaptic potentials in hippocampal pyramidal cells. *J Neurophysiol,* 50**,** 1320-9.

LASHUEL, H. A., OVERK, C. R., OUESLATI, A. & MASLIAH, E. 2012. The many faces of α-synuclein: from structure and toxicity to therapeutic target. *Nature Reviews Neuroscience,* 14**,** 38.

LASHUEL, H. A., PETRE, B. M., WALL, J., SIMON, M., NOWAK, R. J., WALZ, T. & LANSBURY, P. T., JR. 2002. Alpha-synuclein, especially the Parkinson's disease-associated mutants, forms pore-like annular and tubular protofibrils. *J Mol Biol,* 322**,** 1089-102.

LEE, J. T., WHEELER, T. C., LI, L. & CHIN, L. S. 2008. Ubiquitination of alpha-synuclein by Siah-1 promotes alpha-synuclein aggregation and apoptotic cell death. *Hum Mol Genet,* 17**,** 906-17.

LEE, S. & JONES, S. R. 2013. Distinguishing mechanisms of gamma frequency oscillations in human current source signals using a computational model of a laminar neocortical network. *Frontiers in human neuroscience,* 7**,** 869-869.

LEE, V. M. & TROJANOWSKI, J. Q. 2006. Mechanisms of Parkinson's disease linked to pathological alpha-synuclein: new targets for drug discovery. *Neuron,* 52**,** 33-8.

LEHTONEN, Š., SONNINEN, T.-M., WOJCIECHOWSKI, S., GOLDSTEINS, G. & KOISTINAHO, J. 2019. Dysfunction of Cellular Proteostasis in Parkinson's Disease. *Frontiers in Neuroscience,* 13.

LEISMAN, G., BRAUN-BENJAMIN, O. & MELILLO, R. 2014. Cognitive-motor interactions of the basal ganglia in development. *Frontiers in systems neuroscience,* 8**,** 16-16.

LERANTH, C. & HAJSZAN, T. 2007. Extrinsic afferent systems to the dentate gyrus. *Progress in brain research,* 163**,** 63-84.

LESAGE, S., ANHEIM, M., LETOURNEL, F., BOUSSET, L., HONORE, A., ROZAS, N., PIERI, L., MADIONA, K., DURR, A., MELKI, R., VERNY, C. & BRICE, A. 2013. G51D alpha-synuclein mutation causes a novel parkinsonian-pyramidal syndrome. *Ann Neurol,* 73**,** 459-71.

LEVY, G., SCHUPF, N., TANG, M. X., COTE, L. J., LOUIS, E. D., MEJIA, H., STERN, Y. & MARDER, K. 2002. Combined effect of age and severity on the risk of dementia in Parkinson's disease. *Ann Neurol,* 51**,** 722-9.

LI, L., NADANACIVA, S., BERGER, Z., SHEN, W., PAUMIER, K., SCHWARTZ, J., MOU, K., LOOS, P., MILICI, A. J., DUNLOP, J. & HIRST, W. D. 2014. Human A53T α-Synuclein Causes Reversible Deficits in Mitochondrial Function and Dynamics in Primary Mouse Cortical Neurons. *PLOS ONE,* 8**,** e85815.

LI, W., TU, D., BRUNGER, A. T. & YE, Y. 2007a. A ubiquitin ligase transfers preformed polyubiquitin chains from a conjugating enzyme to a substrate. *Nature,* 446**,** 333-7.

LI, W., WEST, N., COLLA, E., PLETNIKOVA, O., TRONCOSO, J. C., MARSH, L., DAWSON, T. M., JAKALA, P., HARTMANN, T., PRICE, D. L. & LEE, M. K. 2005. Aggregation promoting C-terminal truncation of alpha-synuclein is a normal cellular process and is enhanced by the familial Parkinson's disease-linked mutations. *Proc Natl Acad Sci U S A,* 102**,** 2162-7.

LI, W. W., YANG, R., GUO, J. C., REN, H. M., ZHA, X. L., CHENG, J. S. & CAI, D. F. 2007b. Localization of alpha-synuclein to mitochondria within midbrain of mice. *Neuroreport,* 18**,** 1543-6.

LI, Y., XIE, X. E., XING, H., YUAN, X., WANG, Y., JIN, Y., WANG, J., VREUGDENHIL, M., ZHAO, Y., ZHANG, R. & LU, C. 2019. The Modulation of Gamma Oscillations by Methamphetamine in Rat Hippocampal Slices. *Frontiers in Cellular Neuroscience,* 13.

LIANI, E., EYAL, A., AVRAHAM, E., SHEMER, R., SZARGEL, R., BERG, D., BORNEMANN, A., RIESS, O., ROSS, C. A., ROTT, R. & ENGELENDER, S. 2004. Ubiquitylation of synphilin-1 and alpha-synuclein by SIAH and its presence in cellular inclusions and Lewy bodies imply a role in Parkinson's disease. *Proc Natl Acad Sci U S A,* 101**,** 5500-5.

LIGHT, G. A., WILLIAMS, L. E., MINOW, F., SPROCK, J., RISSLING, A., SHARP, R., SWERDLOW, N. R. & BRAFF, D. L. 2010. Electroencephalography (EEG) and event-related potentials (ERPs) with human participants. *Current protocols in neuroscience,* Chapter 6**,** Unit-6.25.24.

LIMA, V. A., DO NASCIMENTO, L. A., ELIEZER, D. & FOLLMER, C. 2019. Role of Parkinson's Disease-Linked Mutations and N-Terminal Acetylation on the Oligomerization of alpha-Synuclein Induced by 3,4-Dihydroxyphenylacetaldehyde. *ACS Chem Neurosci,* 10**,** 690-703.

LIN, M. T. & BEAL, M. F. 2006. Mitochondrial dysfunction and oxidative stress in neurodegenerative diseases. *Nature,* 443**,** 787.

LINDERSSON, E., BEEDHOLM, R., HOJRUP, P., MOOS, T., GAI, W., HENDIL, K. B. & JENSEN, P. H. 2004. Proteasomal inhibition by alpha-synuclein filaments and oligomers. *J Biol Chem,* 279**,** 12924-34.

LISMAN, J., BUZSÁKI, G., EICHENBAUM, H., NADEL, L., RANGANATH, C. & REDISH, A. D. 2017. Viewpoints: how the hippocampus contributes to memory, navigation and cognition. *Nature neuroscience,* 20**,** 1434-1447.

LITVINENKO, I. V., ODINAK, M. M., MOGIL'NAYA, V. I. & PERSTNEV, S. V. 2010. Use of memantine (akatinol) for the correction of cognitive impairments in Parkinson's disease complicated by dementia. *Neurosci Behav Physiol,* 40**,** 149-55.

LIU, G., ZHANG, C., YIN, J., LI, X., CHENG, F., LI, Y., YANG, H., UEDA, K., CHAN, P. & YU, S. 2009. alpha-Synuclein is differentially expressed in mitochondria from different rat brain regions and dose-dependently down-regulates complex I activity. *Neurosci Lett,* 454**,** 187-92.

LIU, J., CHANG, L., SONG, Y., LI, H. & WU, Y. 2019. The Role of NMDA Receptors in Alzheimer's Disease. *Frontiers in Neuroscience,* 13.

LIU, Y., QIANG, M., WEI, Y. & HE, R. 2011. A novel molecular mechanism for nitrated {alpha}-synuclein-induced cell death. *J Mol Cell Biol,* 3**,** 239-49.

LO, D. & GROSSBERG, G. T. 2011. Use of memantine for the treatment of dementia. *Expert Rev Neurother,* 11**,** 1359-70.

LODGE, D. J., BEHRENS, M. M. & GRACE, A. A. 2009. A loss of parvalbumin-containing interneurons is associated with diminished oscillatory activity in an animal model of schizophrenia. *The Journal of neuroscience : the official journal of the Society for Neuroscience,* 29**,** 2344-2354.

LOEB, V., YAKUNIN, E., SAADA, A. & SHARON, R. 2010. The transgenic overexpression of alpha-synuclein and not its related pathology associates with complex I inhibition. *J Biol Chem,* 285**,** 7334-43.

LOPES DA SILVA, F. 2013. EEG and MEG: Relevance to Neuroscience. *Neuron,* 80**,** 1112-1128.

LOWE, J., MCDERMOTT, H., LANDON, M., MAYER, R. J. & WILKINSON, K. D. 1990. Ubiquitin carboxyl-terminal hydrolase (PGP 9.5) is selectively present in ubiquitinated inclusion bodies characteristic of human neurodegenerative diseases. *J Pathol,* 161**,** 153-60.

LU, C. B., VREUGDENHIL, M. & TOESCU, E. C. 2012. The effect of aging-associated impaired mitochondrial status on kainate-evoked hippocampal gamma oscillations. *Neurobiology of aging,* 33**,** 2692-2703.

LUK, K. C., KEHM, V. M., ZHANG, B., O'BRIEN, P., TROJANOWSKI, J. Q. & LEE, V. M. Y. 2012. Intracerebral inoculation of pathological α-synuclein initiates a rapidly progressive neurodegenerative α-synucleinopathy in mice. *The Journal of experimental medicine,* 209**,** 975-986.

LUTH, E. S., STAVROVSKAYA, I. G., BARTELS, T., KRISTAL, B. S. & SELKOE, D. J. 2014. Soluble, prefibrillar alpha-synuclein oligomers promote complex I-dependent, Ca2+-induced mitochondrial dysfunction. *J Biol Chem,* 289**,** 21490-507.

MA, S. Y., RINNE, J. O., COLLAN, Y., ROYTTA, M. & RINNE, U. K. 1996. A quantitative morphometrical study of neuron degeneration in the substantia nigra in Parkinson's disease. *J Neurol Sci,* 140**,** 40-5.

MABLY, A. J. & COLGIN, L. L. 2018. Gamma oscillations in cognitive disorders. *Current Opinion in Neurobiology,* 52**,** 182-187.

MAHUL-MELLIER, A. L., FAUVET, B., GYSBERS, A., DIKIY, I., OUESLATI, A., GEORGEON, S., LAMONTANARA, A. J., BISQUERTT, A., ELIEZER, D., MASLIAH, E., HALLIDAY, G., HANTSCHEL, O. & LASHUEL, H. A. 2014. c-Abl phosphorylates alpha-synuclein and regulates its degradation: implication for alpha-synuclein clearance and contribution to the pathogenesis of Parkinson's disease. *Hum Mol Genet,* 23**,** 2858-79.

MAITI, P., MANNA, J. & DUNBAR, G. L. 2017. Current understanding of the molecular mechanisms in Parkinson's disease: Targets for potential treatments. *Translational Neurodegeneration,* 6**,** 28.

MAK, E., SU, L., WILLIAMS, G. B. & O'BRIEN, J. T. 2014. Neuroimaging characteristics of dementia with Lewy bodies. *Alzheimer's research & therapy,* 6**,** 18-18.

MALTSEV, A. S., YING, J. & BAX, A. 2012. Impact of N-terminal acetylation of alpha-synuclein on its random coil and lipid binding properties. *Biochemistry,* 51**,** 5004-13.

MANDERS, E. M. M., VERBEEK, F. J. & ATEN, J. A. 1993. Measurement of co-localization of objects in dual-colour confocal images. *Journal of Microscopy,* 169**,** 375-382.

MANNING, G., PLOWMAN, G. D., HUNTER, T. & SUDARSANAM, S. 2002a. Evolution of protein kinase signaling from yeast to man. *Trends Biochem Sci,* 27**,** 514-20.

MANNING, G., WHYTE, D. B., MARTINEZ, R., HUNTER, T. & SUDARSANAM, S. 2002b. The protein kinase complement of the human genome. *Science,* 298**,** 1912-34.

MARAMBAUD, P., DRESES-WERRINGLOER, U. & VINGTDEUX, V. 2009. Calcium signaling in neurodegeneration. *Molecular Neurodegeneration,* 4**,** 20.

MARÍN, O. 2012. Interneuron dysfunction in psychiatric disorders. *Nat Rev Neurosci,* 13**,** 107-20.

MARK, E., NIALL, Q. & KAILASH, B. *Parkinson's Disease and Other Movement Disorders (Oxford Specialist Handbooks in Neurology),* Oxford, UK, Oxford University Press.

MARKRAM, H., TOLEDO-RODRIGUEZ, M., WANG, Y., GUPTA, A., SILBERBERG, G. & WU, C. 2004. Interneurons of the neocortical inhibitory system. *Nature Reviews Neuroscience,* 5**,** 793-807.

MAROTEAUX, L., CAMPANELLI, J. T. & SCHELLER, R. H. 1988. Synuclein: a neuron-specific protein localized to the nucleus and presynaptic nerve terminal. *J Neurosci,* 8**,** 2804-15.

MARQUES, O. & OUTEIRO, T. F. 2012. Alpha-synuclein: from secretion to dysfunction and death. *Cell Death & Disease,* 3**,** e350-e350.

MARTI, M. J., TOLOSA, E. & CAMPDELACREU, J. 2003. Clinical overview of the synucleinopathies. *Mov Disord,* 18 Suppl 6**,** S21-7.

MARTIN, L. J., SEMENKOW, S., HANAFORD, A. & WONG, M. 2014. Mitochondrial permeability transition pore regulates Parkinson's disease development in mutant alpha-synuclein transgenic mice. *Neurobiol Aging,* 35**,** 1132-52.

MARTINEZ-VICENTE, M., TALLOCZY, Z., KAUSHIK, S., MASSEY, A. C., MAZZULLI, J., MOSHAROV, E. V., HODARA, R., FREDENBURG, R., WU, D. C., FOLLENZI, A., DAUER, W., PRZEDBORSKI, S., ISCHIROPOULOS, H., LANSBURY, P. T., SULZER, D. & CUERVO, A. M. 2008. Dopamine-modified alpha-synuclein blocks chaperone-mediated autophagy. *J Clin Invest,* 118**,** 777-88.

MARUI, W., ISEKI, E., KATO, M., AKATSU, H. & KOSAKA, K. 2004. Pathological entity of dementia with Lewy bodies and its differentiation from Alzheimer's disease. *Acta Neuropathol,* 108**,** 121-8.

MASPERO, E., MARI, S., VALENTINI, E., MUSACCHIO, A., FISH, A., PASQUALATO, S. & POLO, S. 2011. Structure of the HECT:ubiquitin complex and its role in ubiquitin chain elongation. *EMBO Rep,* 12**,** 342-9.

MATHALON, D. H. & SOHAL, V. S. 2015. Neural Oscillations and Synchrony in Brain Dysfunction and Neuropsychiatric Disorders: It's About Time. *JAMA Psychiatry,* 72**,** 840-4.

MATHIASEN, M. L., LOUCH, R. C., NELSON, A. D., DILLINGHAM, C. M. & AGGLETON, J. P. 2019. Trajectory of hippocampal fibres to the contralateral anterior thalamus and mammillary bodies in rats, mice, and macaque monkeys. *Brain and neuroscience advances,* 3**,** 2398212819871205-2398212819871205.

MATTILA, P. M., RINNE, J. O., HELENIUS, H., DICKSON, D. W. & ROYTTA, M. 2000. Alpha-synuclein-immunoreactive cortical Lewy bodies are associated with cognitive impairment in Parkinson's disease. *Acta Neuropathol,* 100**,** 285-90.

MATTSON, M. P. & ARUMUGAM, T. V. 2018. Hallmarks of Brain Aging: Adaptive and Pathological Modification by Metabolic States. *Cell metabolism,* 27**,** 1176-1199.

MATTSON, M. P. & MAGNUS, T. 2006. Aging and Neuronal Vulnerability. *Nature reviews. Neuroscience,* 7**,** 278-294.

MCCORMACK, A. L., MAK, S. K. & DI MONTE, D. A. 2012. Increased α-synuclein phosphorylation and nitration in the aging primate substantia nigra. *Cell Death &Amp; Disease,* 3**,** e315.

MCFARLAND, N. R., FAN, Z., XU, K., SCHWARZSCHILD, M. A., FEANY, M. B., HYMAN, B. T. & MCLEAN, P. J. 2009. Alpha-synuclein S129 phosphorylation mutants do not alter nigrostriatal toxicity in a rat model of Parkinson disease. *J Neuropathol Exp Neurol,* 68**,** 515-24.

MCKEITH, I., MINTZER, J., AARSLAND, D., BURN, D., CHIU, H., COHEN-MANSFIELD, J., DICKSON, D., DUBOIS, B., DUDA, J. E., FELDMAN, H., GAUTHIER, S., HALLIDAY, G., LAWLOR, B., LIPPA, C., LOPEZ, O. L., CARLOS MACHADO, J., O'BRIEN, J., PLAYFER, J. & REID, W. 2004. Dementia with Lewy bodies. *Lancet Neurol,* 3**,** 19-28.

MCKEITH, I. G. 2006. Consensus guidelines for the clinical and pathologic diagnosis of dementia with Lewy bodies (DLB): report of the Consortium on DLB International Workshop. *J Alzheimers Dis,* 9**,** 417-23.

MCKEITH, I. G., BOEVE, B. F., DICKSON, D. W., HALLIDAY, G., TAYLOR, J.-P., WEINTRAUB, D., AARSLAND, D., GALVIN, J., ATTEMS, J., BALLARD, C. G., BAYSTON, A., BEACH, T. G., BLANC, F., BOHNEN, N., BONANNI, L., BRAS, J., BRUNDIN, P., BURN, D., CHEN-PLOTKIN, A., DUDA, J. E., EL-AGNAF, O., FELDMAN, H., FERMAN, T. J., FFYTCHE, D., FUJISHIRO, H., GALASKO, D., GOLDMAN, J. G., GOMPERTS, S. N., GRAFF-RADFORD, N. R., HONIG, L. S., IRANZO, A., KANTARCI, K., KAUFER, D., KUKULL, W., LEE, V. M. Y., LEVERENZ, J. B., LEWIS, S., LIPPA, C., LUNDE, A., MASELLIS, M., MASLIAH, E., MCLEAN, P., MOLLENHAUER, B., MONTINE, T. J., MORENO, E., MORI, E., MURRAY, M., O'BRIEN, J. T., ORIMO, S., POSTUMA, R. B., RAMASWAMY, S., ROSS, O. A., SALMON, D. P., SINGLETON, A., TAYLOR, A., THOMAS, A., TIRABOSCHI, P., TOLEDO, J. B., TROJANOWSKI, J. Q., TSUANG, D., WALKER, Z., YAMADA, M. & KOSAKA, K. 2017. Diagnosis and management of dementia with Lewy bodies: Fourth consensus report of the DLB Consortium. *Neurology,* 89**,** 88-100.

MCKEITH, I. G., BURN, D. J., BALLARD, C. G., COLLERTON, D., JAROS, E., MORRIS, C. M., MCLAREN, A., PERRY, E. K., PERRY, R., PIGGOTT, M. A. & O'BRIEN, J. T. 2003. Dementia with Lewy bodies. *Semin Clin Neuropsychiatry,* 8**,** 46-57.

MCKEITH, I. G., DICKSON, D. W., LOWE, J., EMRE, M., O'BRIEN, J. T., FELDMAN, H., CUMMINGS, J., DUDA, J. E., LIPPA, C., PERRY, E. K., AARSLAND, D., ARAI, H., BALLARD, C. G., BOEVE, B., BURN, D. J., COSTA, D., DEL SER, T., DUBOIS, B., GALASKO, D., GAUTHIER, S., GOETZ, C. G., GOMEZ-TORTOSA, E., HALLIDAY, G., HANSEN, L. A., HARDY, J., IWATSUBO, T., KALARIA, R. N., KAUFER, D., KENNY, R. A., KORCZYN, A., KOSAKA, K., LEE, V. M., LEES, A., LITVAN, I., LONDOS, E., LOPEZ, O. L., MINOSHIMA, S., MIZUNO, Y., MOLINA, J. A., MUKAETOVA-LADINSKA, E. B., PASQUIER, F., PERRY, R. H., SCHULZ, J. B., TROJANOWSKI, J. Q. & YAMADA, M. 2005. Diagnosis and management of dementia with Lewy bodies: third report of the DLB Consortium. *Neurology,* 65**,** 1863-72.

MCKEITH, I. G., GALASKO, D., KOSAKA, K., PERRY, E. K., DICKSON, D. W., HANSEN, L. A., SALMON, D. P., LOWE, J., MIRRA, S. S., BYRNE, E. J., LENNOX, G., QUINN, N. P., EDWARDSON, J. A., INCE, P. G., BERGERON, C., BURNS, A., MILLER, B. L., LOVESTONE, S., COLLERTON, D., JANSEN, E. N., BALLARD, C., DE VOS, R. A., WILCOCK, G. K., JELLINGER, K. A. & PERRY, R. H. 1996.

Consensus guidelines for the clinical and pathologic diagnosis of dementia with Lewy bodies (DLB): report of the consortium on DLB international workshop. *Neurology,* 47**,** 1113-24.

MCNAUGHT, K. S. & JENNER, P. 2001. Proteasomal function is impaired in substantia nigra in Parkinson's disease. *Neurosci Lett,* 297**,** 191-4.

MCNAUGHT, K. S., OLANOW, C. W., HALLIWELL, B., ISACSON, O. & JENNER, P. 2001. Failure of the ubiquitin-proteasome system in Parkinson's disease. *Nat Rev Neurosci,* 2**,** 589-94.

MEDLER, K. & GLEASON, E. L. 2002. Mitochondrial Ca(2+) buffering regulates synaptic transmission between retinal amacrine cells. *J Neurophysiol,* 87**,** 1426-39.

MENG, Y., QIAO, H., DING, J., HE, Y., FAN, H., LI, C. & QIU, P. 2020. Effect of Parkin on methamphetamine-induced α-synuclein degradation dysfunction in vitro and in vivo. *Brain Behav,* 10**,** e01574.

METZGER, C., VAN DER WERF, Y. & WALTER, M. 2013. Functional mapping of thalamic nuclei and their integration into cortico-striatal-thalamo-cortical loops via ultra-high resolution imaging—from animal anatomy to in vivo imaging in humans. *Frontiers in Neuroscience,* 7.

MIAKE, H., MIZUSAWA, H., IWATSUBO, T. & HASEGAWA, M. 2002. Biochemical characterization of the core structure of alpha-synuclein filaments. *J Biol Chem,* 277**,** 19213-9.

MIKI, Y., TOMIYAMA, M., UENO, T., HAGA, R., NISHIJIMA, H., SUZUKI, C., MORI, F., KAIMORI, M., BABA, M. & WAKABAYASHI, K. 2010. Clinical availability of skin biopsy in the diagnosis of Parkinson's disease. *Neurosci Lett,* 469**,** 357-9.

MIRRA, S. S., HEYMAN, A., MCKEEL, D., SUMI, S. M., CRAIN, B. J., BROWNLEE, L. M., VOGEL, F. S., HUGHES, J. P., BELLE, G. V. & BERG, L. 1991. The Consortium to Establish a Registry for Alzheimer's Disease (CERAD). *Part II. Standardization of the neuropathologic assessment of Alzheimer's disease,* 41**,** 479-479.

MOGA, D., HOF, P. R., VISSAVAJJHALA, P., MORAN, T. M. & MORRISON, J. H. 2002. Parvalbumin-containing interneurons in rat hippocampus have an AMPA receptor profile suggestive of vulnerability to excitotoxicity. *Journal of Chemical Neuroanatomy,* 23**,** 249-253.

MOLLENHAUER, B., CULLEN, V., KAHN, I., KRASTINS, B., OUTEIRO, T. F., PEPIVANI, I., NG, J., SCHULZ-SCHAEFFER, W., KRETZSCHMAR, H. A., MCLEAN, P. J., TRENKWALDER, C., SARRACINO, D. A., VONSATTEL, J. P., LOCASCIO, J. J., EL-AGNAF, O. M. & SCHLOSSMACHER, M. G. 2008. Direct quantification of CSF alpha-synuclein by ELISA and first cross-sectional study in patients with neurodegeneration. *Exp Neurol,* 213**,** 315-25.

MONTINE, T. J., PHELPS, C. H., BEACH, T. G., BIGIO, E. H., CAIRNS, N. J., DICKSON, D. W., DUYCKAERTS, C., FROSCH, M. P., MASLIAH, E., MIRRA, S. S., NELSON, P. T., SCHNEIDER, J. A., THAL, D. R., TROJANOWSKI, J. Q., VINTERS, H. V., HYMAN, B. T., NATIONAL INSTITUTE ON, A. & ALZHEIMER'S, A. 2012. National Institute on Aging-Alzheimer's Association guidelines for the neuropathologic assessment of Alzheimer's disease: a practical approach. *Acta neuropathologica,* 123**,** 1-11.

MOORS, T. E., MAAT, C. A., NIEDIEKER, D., MONA, D., PETERSEN, D., TIMMERMANS-HUISMAN, E., KOLE, J., EL-MASHTOLY, S. F., ZAGO, W., BARBOUR, R., MUNDIGL, O., KALUZA, K., HUBER, S., HUG, M. N., KREMER, T., RITTER, M., DZIADEK, S., GEURTS, J. J. G., GERWERT, K., BRITSCHGI, M. & VAN DE BERG, W. D. J. 2018. Detailed structural orchestration of Lewy pathology in Parkinson's disease as revealed by 3D multicolor STED microscopy. *bioRxiv***,** 470476.

MORAWSKI, M., BRÜCKNER, M. K., RIEDERER, P., BRÜCKNER, G. & ARENDT, T. 2004. Perineuronal nets potentially protect against oxidative stress. *Exp Neurol,* 188**,** 309-15.

MORRIS, M., SANCHEZ, P. E., VERRET, L., BEAGLE, A. J., GUO, W., DUBAL, D., RANASINGHE, K. G., KOYAMA, A., HO, K., YU, G. Q., VOSSEL, K. A. & MUCKE, L. 2015. Network dysfunction in α-synuclein transgenic mice and human Lewy body dementia. *Annals of Clinical and Translational Neurology,* 2**,** 1012-1028.

MUND, T., MASUDA-SUZUKAKE, M., GOEDERT, M. & PELHAM, H. R. 2018. Ubiquitination of alpha-synuclein filaments by Nedd4 ligases. *PloS one,* 13**,** e0200763-e0200763.

MURATA, Y. & COLONNESE, M. T. 2019. Thalamic inhibitory circuits and network activity development. *Brain research,* 1706**,** 13-23.

NAKAMURA, K., NEMANI, V. M., AZARBAL, F., SKIBINSKI, G., LEVY, J. M., EGAMI, K., MUNISHKINA, L., ZHANG, J., GARDNER, B., WAKABAYASHI, J., SESAKI, H., CHENG, Y., FINKBEINER, S., NUSSBAUM, R. L., MASLIAH, E. & EDWARDS, R. H. 2011. Direct membrane association drives mitochondrial fission by the Parkinson disease-associated protein alpha-synuclein. *J Biol Chem,* 286**,** 20710-26.

NAKAMURA, K., NEMANI, V. M., WALLENDER, E. K., KAEHLCKE, K., OTT, M. & EDWARDS, R. H. 2008. Optical reporters for the conformation of alpha-synuclein reveal a specific interaction with mitochondria. *J Neurosci,* 28**,** 12305-17.

NAKAZAWA, K., ZSIROS, V., JIANG, Z., NAKAO, K., KOLATA, S., ZHANG, S. & BELFORTE, J. E. 2012. GABAergic interneuron origin of schizophrenia pathophysiology. *Neuropharmacology,* 62**,** 1574-83.

NARDONE, R., BRATTI, A. & TEZZON, F. 2006. Motor cortex inhibitory circuits in dementia with Lewy bodies and in Alzheimer's disease. *Journal of Neural Transmission,* 113**,** 1679-1684.

NEMANI, V. M., LU, W., BERGE, V., NAKAMURA, K., ONOA, B., LEE, M. K., CHAUDHRY, F. A., NICOLL, R. A. & EDWARDS, R. H. 2010. Increased expression of alpha-synuclein reduces neurotransmitter release by inhibiting synaptic vesicle reclustering after endocytosis. *Neuron,* 65**,** 66-79.

NEUMANN, M., KAHLE, P. J., GIASSON, B. I., OZMEN, L., BORRONI, E., SPOOREN, W., MÜLLER, V., ODOY, S., FUJIWARA, H., HASEGAWA, M., IWATSUBO, T., TROJANOWSKI, J. Q., KRETZSCHMAR, H. A. & HAASS, C. 2002. Misfolded proteinase K-resistant hyperphosphorylated α-synuclein in aged transgenic mice with locomotor deterioration and in human α-synucleinopathies. *Journal of Clinical Investigation,* 110**,** 1429-1439.

NEUNER, J., FILSER, S., MICHALAKIS, S., BIEL, M. & HERMS, J. 2014. A30P α-Synuclein interferes with the stable integration of adult-born neurons into the olfactory network. *Scientific Reports,* 4**,** 3931.

NICHOLLS, D. G., BRAND, M. D. & GERENCSER, A. A. 2015. Mitochondrial bioenergetics and neuronal survival modelled in primary neuronal culture and isolated nerve terminals. *J Bioenerg Biomembr,* 47**,** 63-74.

NIELSEN, M. S., VORUM, H., LINDERSSON, E. & JENSEN, P. H. 2001. Ca2+ binding to alpha-synuclein regulates ligand binding and oligomerization. *J Biol Chem,* 276**,** 22680-4.

NIMMRICH, V., DRAGUHN, A. & AXMACHER, N. 2015. Neuronal Network Oscillations in Neurodegenerative Diseases. *Neuromolecular Med,* 17**,** 270-84.

O'BRIEN, J. T., PALING, S., BARBER, R., WILLIAMS, E. D., BALLARD, C., MCKEITH, I. G., GHOLKAR, A., CRUM, W. R., ROSSOR, M. N. & FOX, N. C. 2001. Progressive brain atrophy on serial MRI in dementia with Lewy bodies, AD, and vascular dementia. *Neurology,* 56**,** 1386-8.

OBESO, J. A., RODRÍGUEZ-OROZ, M. C., BENITEZ-TEMINO, B., BLESA, F. J., GURIDI, J., MARIN, C. & RODRIGUEZ, M. 2008. Functional organization of the basal ganglia: therapeutic implications for Parkinson's disease. *Mov Disord,* 23 Suppl 3**,** S548-59.

OBESO, J. A., RODRIGUEZ-OROZ, M. C., GOETZ, C. G., MARIN, C., KORDOWER, J. H., RODRIGUEZ, M., HIRSCH, E. C., FARRER, M., SCHAPIRA, A. H. V. & HALLIDAY, G. 2010. Missing pieces in the Parkinson's disease puzzle. *Nature Medicine,* 16**,** 653.

OKAMOTO, S.-I., LI, Z., JU, C., SCHÖLZKE, M. N., MATHEWS, E., CUI, J., SALVESEN, G. S., BOSSY-WETZEL, E. & LIPTON, S. A. 2002. Dominant-interfering forms of MEF2 generated by caspase cleavage contribute to NMDA-induced neuronal apoptosis. *Proceedings of the National Academy of Sciences of the United States of America,* 99**,** 3974-3979.

OKOCHI, M., WALTER, J., KOYAMA, A., NAKAJO, S., BABA, M., IWATSUBO, T., MEIJER, L., KAHLE, P. J. & HAASS, C. 2000. Constitutive phosphorylation of the Parkinson's disease associated alpha-synuclein. *J Biol Chem,* 275**,** 390-7.

OLANOW, C. W. & MCNAUGHT, K. S. 2006. Ubiquitin-proteasome system and Parkinson's disease. *Mov Disord,* 21**,** 1806-23.

OLICHNEY, J. M., GALASKO, D., SALMON, D. P., HOFSTETTER, C. R., HANSEN, L. A., KATZMAN, R. & THAL, L. J. 1998. Cognitive decline is faster in Lewy body variant than in Alzheimer's disease. *Neurology,* 51**,** 351-7.

OLSHANSKY, S. J. 1985. Pursuing longevity: delay vs elimination of degenerative diseases. *American journal of public health,* 75**,** 754-757.

OLTEANU, A. & PIELAK, G. J. 2004. Peroxidative aggregation of alpha-synuclein requires tyrosines. *Protein science : a publication of the Protein Society,* 13**,** 2852-2856.

OMENN, G. S., LANE, L., LUNDBERG, E. K., BEAVIS, R. C., OVERALL, C. M. & DEUTSCH, E. W. 2016. Metrics for the Human Proteome Project 2016: Progress on Identifying and Characterizing the Human Proteome, Including Post-Translational Modifications. *J Proteome Res,* 15**,** 3951-3960.

OTIS, T. S. & MODY, I. 1992. Modulation of decay kinetics and frequency of GABAA receptor-mediated spontaneous inhibitory postsynaptic currents in hippocampal neurons. *Neuroscience,* 49**,** 13-32.

OUESLATI, A., FOURNIER, M. & LASHUEL, H. A. 2010. Chapter 7 - Role of post-translational modifications in modulating the structure, function and toxicity of α-synuclein: Implications for Parkinson's disease pathogenesis and therapies. *In:* BJÖRKLUND, A. & CENCI, M. A. (eds.) *Progress in Brain Research.* Elsevier.

OUESLATI, A., SCHNEIDER, B. L., AEBISCHER, P. & LASHUEL, H. A. 2013. Polo-like kinase 2 regulates selective autophagic alpha-synuclein clearance and suppresses its toxicity in vivo. *Proc Natl Acad Sci U S A,* 110**,** E3945-54.

OUHAZ, Z., FLEMING, H. & MITCHELL, A. S. 2018. Cognitive Functions and Neurodevelopmental Disorders Involving the Prefrontal Cortex and Mediodorsal Thalamus. *Frontiers in Neuroscience,* 12.

OUTEIRO, T. F., KOSS, D. J., ERSKINE, D., WALKER, L., KURZAWA-AKANBI, M., BURN, D., DONAGHY, P., MORRIS, C., TAYLOR, J.-P., THOMAS, A., ATTEMS, J. & MCKEITH, I. 2019. Dementia with Lewy bodies: an update and outlook. *Molecular neurodegeneration,* 14**,** 5-5.

PAJARILLO, E., RIZOR, A., LEE, J., ASCHNER, M. & LEE, E. 2019. The role of posttranslational modifications of α-synuclein and LRRK2 in Parkinson's disease: Potential contributions of environmental factors. *Biochimica et biophysica acta. Molecular basis of disease,* 1865**,** 1992-2000.

PALEOLOGOU, K. E., OUESLATI, A., SHAKKED, G., ROSPIGLIOSI, C. C., KIM, H. Y., LAMBERTO, G. R., FERNANDEZ, C. O., SCHMID, A., CHEGINI, F., GAI, W. P., CHIAPPE, D., MONIATTE, M., SCHNEIDER, B. L., AEBISCHER, P., ELIEZER, D., ZWECKSTETTER, M., MASLIAH, E. & LASHUEL, H. A. 2010. Phosphorylation at S87 is enhanced in synucleinopathies, inhibits alpha-synuclein oligomerization, and influences synuclein-membrane interactions. *J Neurosci,* 30**,** 3184-98.

PALEOLOGOU, K. E., SCHMID, A. W., ROSPIGLIOSI, C. C., KIM, H. Y., LAMBERTO, G. R., FREDENBURG, R. A., LANSBURY, P. T., JR., FERNANDEZ, C. O., ELIEZER, D., ZWECKSTETTER, M. & LASHUEL, H. A. 2008. Phosphorylation at Ser-129 but not the phosphomimics S129E/D inhibits the fibrillation of alpha-synuclein. *J Biol Chem,* 283**,** 16895-905.

PÁLHALMI, J., PAULSEN, O., FREUND, T. F. & HÁJOS, N. 2004. Distinct properties of carbachol- and DHPG-induced network oscillations in hippocampal slices. *Neuropharmacology,* 47**,** 381-389.

PARK, J. Y., PAIK, S. R., JOU, I. & PARK, S. M. 2008. Microglial phagocytosis is enhanced by monomeric alpha-synuclein, not aggregated alpha-synuclein: implications for Parkinson's disease. *Glia,* 56**,** 1215-23.

PARK, K., LEE, J., JANG, H. J., RICHARDS, B. A., KOHL, M. M. & KWAG, J. 2020. Optogenetic activation of parvalbumin and somatostatin interneurons selectively restores theta-nested gamma oscillations and oscillation-induced spike timing-dependent long-term potentiation impaired by amyloid β oligomers. *BMC Biology,* 18**,** 7.

PARK, S. M., JUNG, H. Y., KIM, T. D., PARK, J. H., YANG, C. H. & KIM, J. 2002. Distinct roles of the N-terminal-binding domain and the C-terminal-solubilizing domain of alpha-synuclein, a molecular chaperone. *J Biol Chem,* 277**,** 28512-20.

PASANEN, P., MYLLYKANGAS, L., SIITONEN, M., RAUNIO, A., KAAKKOLA, S., LYYTINEN, J., TIENARI, P. J., POYHONEN, M. & PAETAU, A. 2014. Novel alpha-synuclein mutation A53E associated with atypical multiple system atrophy and Parkinson's disease-type pathology. *Neurobiol Aging,* 35**,** 2180.e1-5.

PATTERSON, L., FIRBANK, M. J., COLLOBY, S. J., ATTEMS, J., THOMAS, A. J. & MORRIS, C. M. 2019. Neuropathological Changes in Dementia With Lewy Bodies and the Cingulate Island Sign. *Journal of neuropathology and experimental neurology,* 78**,** 717-724.

PAUMIER, K. L., SUKOFF RIZZO, S. J., BERGER, Z., CHEN, Y., GONZALES, C., KAFTAN, E., LI, L., LOTARSKI, S., MONAGHAN, M., SHEN, W., STOLYAR, P., VASILYEV, D., ZALESKA, M., D. HIRST, W. & DUNLOP, J. 2013. Behavioral Characterization of A53T Mice Reveals Early and Late Stage Deficits Related to Parkinson's Disease. *PLOS ONE,* 8**,** e70274.

PAXINOU, E., CHEN, Q., WEISSE, M., GIASSON, B. I., NORRIS, E. H., RUETER, S. M., TROJANOWSKI, J. Q., LEE, V. M. & ISCHIROPOULOS, H. 2001. Induction of alpha-synuclein aggregation by intracellular nitrative insult. *J Neurosci,* 21**,** 8053-61.

PEAVY, G. M., SALMON, D. P., EDLAND, S. D., TAM, S., HANSEN, L. A., MASLIAH, E., GALASKO, D. & HAMILTON, J. M. 2013. Neuropsychiatric features of frontal lobe dysfunction in autopsy-confirmed patients with lewy bodies and "pure" Alzheimer disease. *The American journal of geriatric psychiatry : official journal of the American Association for Geriatric Psychiatry,* 21**,** 509-519.

PELKEY, K. A., CHITTAJALLU, R., CRAIG, M. T., TRICOIRE, L., WESTER, J. C. & MCBAIN, C. J. 2017. Hippocampal GABAergic Inhibitory Interneurons. *Physiological reviews,* 97**,** 1619-1747.

PERAZA, L. R., CROMARTY, R., KOBELEVA, X., FIRBANK, M. J., KILLEN, A., GRAZIADIO, S., THOMAS, A. J., O'BRIEN, J. T. & TAYLOR, J.-P. 2018. Electroencephalographic derived network differences in Lewy body dementia compared to Alzheimer's disease patients. *Scientific Reports,* 8**,** 4637.

PERFEITO, R., LÁZARO, D. F., OUTEIRO, T. F. & REGO, A. C. 2014. Linking alpha-synuclein phosphorylation to reactive oxygen species formation and mitochondrial dysfunction in SH-SY5Y cells. *Molecular and Cellular Neuroscience,* 62**,** 51-59.

PERIQUET, M., FULGA, T., MYLLYKANGAS, L., SCHLOSSMACHER, M. G. & FEANY, M. B. 2007. Aggregated alpha-synuclein mediates dopaminergic neurotoxicity in vivo. *J Neurosci,* 27**,** 3338-46.

PERRIN, R. J., WOODS, W. S., CLAYTON, D. F. & GEORGE, J. M. 2001. Exposure to long chain polyunsaturated fatty acids triggers rapid multimerization of synucleins. *J Biol Chem,* 276**,** 41958-62.

PIETERSEN, A. N., PATEL, N., JEFFERYS, J. G. & VREUGDENHIL, M. 2009. Comparison between spontaneous and kainate-induced gamma oscillations in the mouse hippocampus in vitro. *Eur J Neurosci,* 29**,** 2145-56.

PINAULT, D. 2008. N-methyl d-aspartate receptor antagonists ketamine and MK-801 induce wake-related aberrant gamma oscillations in the rat neocortex. *Biol Psychiatry,* 63**,** 730-5.

PLOGMANN, D. & CELIO, M. R. 1993. Intracellular concentration of parvalbumin in nerve cells. *Brain Res,* 600**,** 273-9.

PLOTEGHER, N., BERTI, G., FERRARI, E., TESSARI, I., ZANETTI, M., LUNELLI, L., GREGGIO, E., BISAGLIA, M., VERONESI, M., GIROTTO, S., DALLA SERRA, M., PEREGO, C., CASELLA, L. & BUBACCO, L. 2017. DOPAL derived alpha-synuclein oligomers impair synaptic vesicles physiological function. *Sci Rep,* 7**,** 40699.

PLOTEGHER, N., GRATTON, E. & BUBACCO, L. 2014. Number and Brightness analysis of alpha-synuclein oligomerization and the associated mitochondrial morphology alterations in live cells. *Biochim Biophys Acta,* 1840**,** 2014-24.

POLYMEROPOULOS, M. H., LAVEDAN, C., LEROY, E., IDE, S. E., DEHEJIA, A., DUTRA, A., PIKE, B., ROOT, H., RUBENSTEIN, J., BOYER, R., STENROOS, E. S., CHANDRASEKHARAPPA, S., ATHANASSIADOU, A., PAPAPETROPOULOS, T., JOHNSON, W. G., LAZZARINI, A. M., DUVOISIN, R. C., DI IORIO, G., GOLBE, L. I. & NUSSBAUM, R. L. 1997. Mutation in the alpha-synuclein gene identified in families with Parkinson's disease. *Science,* 276**,** 2045-7.

POPESCU, A., LIPPA, C. F., LEE, V. M.-Y. & TROJANOWSKI, J. Q. 2004. Lewy Bodies in the Amygdala: Increase of α-Synuclein Aggregates in Neurodegenerative Diseases With Tau-Based Inclusions. *Archives of Neurology,* 61**,** 1915-1919.

POUCLET, H., LEBOUVIER, T., CORON, E., NEUNLIST, M. & DERKINDEREN, P. 2012. Lewy pathology in gastric and duodenal biopsies in Parkinson's Disease. *Mov Disord,* 27**,** 708.

POZO DEVOTO, V. M., DIMOPOULOS, N., ALLOATTI, M., PARDI, M. B., SAEZ, T. M., OTERO, M. G., CROMBERG, L. E., MARÍN-BURGIN, A., SCASSA, M. E., STOKIN, G. B., SCHINDER, A. F., SEVLEVER, G. & FALZONE, T. L. 2017. αSynuclein control of mitochondrial homeostasis in human-derived neurons is disrupted by mutations associated with Parkinson's disease. *Scientific Reports,* 7**,** 5042.

PRABAKARAN, S., LIPPENS, G., STEEN, H. & GUNAWARDENA, J. 2012. Post-translational modification: nature's escape from genetic imprisonment and the basis for dynamic information encoding. *Wiley interdisciplinary reviews. Systems biology and medicine,* 4**,** 565-583.

PRESTON, A. R. & EICHENBAUM, H. 2013. Interplay of hippocampus and prefrontal cortex in memory. *Curr Biol,* 23**,** R764-73.

PRINCE, M., BRYCE, R., ALBANESE, E., WIMO, A., RIBEIRO, W. & FERRI, C. P. 2013. The global prevalence of dementia: a systematic review and metaanalysis. *Alzheimers Dement,* 9**,** 63-75.e2.

PRONIN, A. N., MORRIS, A. J., SURGUCHOV, A. & BENOVIC, J. L. 2000. Synucleins are a novel class of substrates for G protein-coupled receptor kinases. *J Biol Chem,* 275**,** 26515-22.

PROTS, I., VEBER, V., BREY, S., CAMPIONI, S., BUDER, K., RIEK, R., BOHM, K. J. & WINNER, B. 2013. alpha-Synuclein oligomers impair neuronal microtubule-kinesin interplay. *J Biol Chem,* 288**,** 21742-54.

PROUKAKIS, C., DUDZIK, C. G., BRIER, T., MACKAY, D. S., COOPER, J. M., MILLHAUSER, G. L., HOULDEN, H. & SCHAPIRA, A. H. 2013. A novel alpha-synuclein missense mutation in Parkinson disease. *Neurology,* 80**,** 1062-4.

PRZEDBORSKI, S., VILA, M. & JACKSON-LEWIS, V. 2003. Neurodegeneration: what is it and where are we? *The Journal of clinical investigation,* 111**,** 3-10.

PUSCHMANN, A., ROSS, O. A., VILARINO-GUELL, C., LINCOLN, S. J., KACHERGUS, J. M., COBB, S. A., LINDQUIST, S. G., NIELSEN, J. E., WSZOLEK, Z. K., FARRER, M., WIDNER, H., VAN WESTEN, D., HAGERSTROM, D., MARKOPOULOU, K., CHASE, B. A., NILSSON, K., REIMER, J. & NILSSON, C. 2009. A Swedish family with de novo alpha-synuclein A53T mutation: evidence for early cortical dysfunction. *Parkinsonism Relat Disord,* 15**,** 627-32.

QIAO, S., LUO, J. H. & JIN, J. H. 2012. [Role of microglial activation induced by alpha-synuclein in pathogenesis of Parkinson's disease]. *Zhejiang Da Xue Xue Bao Yi Xue Ban,* 41**,** 210-4.

QIN, Z., HU, D., HAN, S., REANEY, S. H., DI MONTE, D. A. & FINK, A. L. 2007. Effect of 4-Hydroxy-2-nonenal Modification on α-Synuclein Aggregation. *Journal of Biological Chemistry,* 282**,** 5862-5870.

QUIROGA, R. Q. 2013. Gnostic cells in the 21st century. *Acta Neurobiol Exp (Wars),* 73**,** 463-71.

RADI, R. 2004. Nitric oxide, oxidants, and protein tyrosine nitration. *Proceedings of the National Academy of Sciences,* 101**,** 4003-4008.

RADI, R., CASSINA, A., HODARA, R., QUIJANO, C. & CASTRO, L. 2002. Peroxynitrite reactions and formation in mitochondria. *Free Radic Biol Med,* 33**,** 1451-64.

RAJKOWSKA, G., O'DWYER, G., TELEKI, Z., STOCKMEIER, C. A. & MIGUEL-HIDALGO, J. J. 2007. GABAergic Neurons Immunoreactive for Calcium Binding Proteins are Reduced in the Prefrontal Cortex in Major Depression. *Neuropsychopharmacology,* 32**,** 471-482.

RAKSHI, J. S., UEMA, T., ITO, K., BAILEY, D. L., MORRISH, P. K., ASHBURNER, J., DAGHER, A., JENKINS, I. H., FRISTON, K. J. & BROOKS, D. J. 1999. Frontal, midbrain and striatal dopaminergic function in early and advanced Parkinson's disease A 3D [(18)F]dopa-PET study. *Brain,* 122 (Pt 9)**,** 1637-50.

RAVINA, B., MARDER, K., FERNANDEZ, H. H., FRIEDMAN, J. H., MCDONALD, W., MURPHY, D., AARSLAND, D., BABCOCK, D., CUMMINGS, J., ENDICOTT, J., FACTOR, S., GALPERN, W., LEES, A., MARSH, L., STACY, M., GWINN-HARDY, K., VOON, V. & GOETZ, C. 2007. Diagnostic criteria for psychosis in Parkinson's disease: report of an NINDS, NIMH work group. *Mov Disord,* 22**,** 1061-8.

RAZ, L., KNOEFEL, J. & BHASKAR, K. 2016. The neuropathology and cerebrovascular mechanisms of dementia. *Journal of cerebral blood flow and metabolism : official journal of the International Society of Cerebral Blood Flow and Metabolism,* 36**,** 172-186.

REALE, R. A., CALVERT, G. A., THESEN, T., JENISON, R. L., KAWASAKI, H., OYA, H., HOWARD, M. A. & BRUGGE, J. F. 2007. Auditory-visual processing represented in the human superior temporal gyrus. *Neuroscience,* 145**,** 162-84.

REEVE, A. K., LUDTMANN, M. H., ANGELOVA, P. R., SIMCOX, E. M., HORROCKS, M. H., KLENERMAN, D., GANDHI, S., TURNBULL, D. M. & ABRAMOV, A. Y. 2015. Aggregated alpha-synuclein and complex I deficiency: exploration of their relationship in differentiated neurons. *Cell Death Dis,* 6**,** e1820.

RESH, M. D. 2016. Fatty acylation of proteins: The long and the short of it. *Prog Lipid Res,* 63**,** 120-31.

REZAIE, P., CAIRNS, N. J., CHADWICK, A. & LANTOS, P. L. 1996. Lewy bodies are located preferentially in limbic areas in diffuse Lewy body disease. *Neurosci Lett,* 212**,** 111-4.

RICHARD, I. H., PAPKA, M., RUBIO, A. & KURLAN, R. 2002. Parkinson's disease and dementia with Lewy bodies: One disease or two? *Movement Disorders,* 17**,** 1161-1165.

RIEKER, C., DEV, K. K., LEHNHOFF, K., BARBIERI, S., KSIAZEK, I., KAUFFMANN, S., DANNER, S., SCHELL, H., BODEN, C., RUEGG, M. A., KAHLE, P. J., VAN DER PUTTEN, H. & SHIMSHEK, D. R. 2011. Neuropathology in Mice Expressing Mouse Alpha-Synuclein. *PLOS ONE,* 6**,** e24834.

RINTOUL, G. L., RAYMOND, L. A. & BAIMBRIDGE, K. G. 2001. Calcium buffering and protection from excitotoxic cell death by exogenous calbindin-D28k in HEK 293 cells. *Cell Calcium,* 29**,** 277-87.

ROBINSON, A. B., MCKERROW, J. H. & CARY, P. 1970. Controlled deamidation of peptides and proteins: an experimental hazard and a possible biological timer. *Proceedings of the National Academy of Sciences of the United States of America,* 66**,** 753-757.

ROBSON, E., TWEEDY, C., MANZANZA, N., TAYLOR, J.-P., ATKINSON, P., RANDALL, F., REEVE, A., CLOWRY, G. J. & LEBEAU, F. E. N. 2018a. Impaired Fast Network Oscillations and Mitochondrial Dysfunction in a Mouse Model of Alpha-synucleinopathy (A30P). *Neuroscience,* 377**,** 161-173.

ROBSON, E., TWEEDY, C., MANZANZA, N., TAYLOR, J. P., ATKINSON, P., RANDALL, F., REEVE, A., CLOWRY, G. J. & LEBEAU, F. E. N. 2018b. Impaired Fast Network Oscillations and Mitochondrial Dysfunction in a Mouse Model of Alpha-synucleinopathy (A30P). *Neuroscience,* 377**,** 161-173.

ROGAWSKI, M. A. 2011. Revisiting AMPA receptors as an antiepileptic drug target. *Epilepsy currents,* 11**,** 56-63.

ROLLS, E. T. 2019. The cingulate cortex and limbic systems for emotion, action, and memory. *Brain Structure and Function,* 224**,** 3001-3018.

ROQUET, D., NOBLET, V., ANTHONY, P., PHILIPPI, N., DEMUYNCK, C., CRETIN, B., MARTIN-HUNYADI, C., LOUREIRO DE SOUSA, P. & BLANC, F. 2017. Insular atrophy at the prodromal stage of dementia with Lewy bodies: a VBM DARTEL study. *Scientific reports,* 7**,** 9437-9437.

ROSTOVTSEVA, T. K., GURNEV, P. A., PROTCHENKO, O., HOOGERHEIDE, D. P., YAP, T. L., PHILPOTT, C. C., LEE, J. C. & BEZRUKOV, S. M. 2015. alpha-Synuclein Shows High Affinity Interaction with

Voltage-dependent Anion Channel, Suggesting Mechanisms of Mitochondrial Regulation and Toxicity in Parkinson Disease. *J Biol Chem,* 290**,** 18467-77.

ROTARU, D. C., LEWIS, D. A. & GONZALEZ-BURGOS, G. 2012. The role of glutamatergic inputs onto parvalbumin-positive interneurons: relevance for schizophrenia. *Reviews in the neurosciences,* 23**,** 97-109.

ROTHMAN, S. M., GRIFFIOEN, K. J., FISHBEIN, K. W., SPENCER, R. G., MAKROGIANNIS, S., CONG, W. N., MARTIN, B. & MATTSON, M. P. 2014. Metabolic abnormalities and hypoleptinemia in alpha-synuclein A53T mutant mice. *Neurobiol Aging,* 35**,** 1153-61.

RUDY, B., FISHELL, G., LEE, S. & HJERLING-LEFFLER, J. 2011. Three groups of interneurons account for nearly 100% of neocortical GABAergic neurons. *Developmental neurobiology,* 71**,** 45-61.

RYAN, B. J., HOEK, S., FON, E. A. & WADE-MARTINS, R. 2015. Mitochondrial dysfunction and mitophagy in Parkinson's: from familial to sporadic disease. *Trends Biochem Sci,* 40**,** 200-10.

SAITO, K., KIMURA, N., ODA, N., SHIMOMURA, H., KUMADA, T., MIYAJIMA, T., MURAYAMA, K., TANAKA, M. & FUJII, T. 2012. Pyruvate therapy for mitochondrial DNA depletion syndrome. *Biochim Biophys Acta,* 1820**,** 632-6.

SAITO, Y., KAWASHIMA, A., RUBERU, N. N., FUJIWARA, H., KOYAMA, S., SAWABE, M., ARAI, T., NAGURA, H., YAMANOUCHI, H., HASEGAWA, M., IWATSUBO, T. & MURAYAMA, S. 2003. Accumulation of Phosphorylated α-Synuclein in Aging Human Brain. *Journal of Neuropathology & Experimental Neurology,* 62**,** 644-654.

SAMPATHU, D. M., GIASSON, B. I., PAWLYK, A. C., TROJANOWSKI, J. Q. & LEE, V. M. Y. 2003. Ubiquitination of alpha-synuclein is not required for formation of pathological inclusions in alpha-synucleinopathies. *The American journal of pathology,* 163**,** 91-100.

SANDMANN-KEIL, D. & BRAAK, H. 2005. [Postmortal diagnosis of Parkinson's disease]. *Pathologe,* 26**,** 214-20.

SCHMID, A. W., FAUVET, B., MONIATTE, M. & LASHUEL, H. A. 2013. Alpha-synuclein post-translational modifications as potential biomarkers for Parkinson disease and other synucleinopathies. *Molecular & cellular proteomics : MCP,* 12**,** 3543-3558.

SCHNEIDER, J., LEWEN, A., TA, T.-T., GALOW, L. V., ISOLA, R., PAPAGEORGIOU, I. E. & KANN, O. 2015a. A reliable model for gamma oscillations in hippocampal tissue. *Journal of Neuroscience Research,* 93**,** 1067-1078.

SCHNEIDER, J., LEWEN, A., TA, T. T., GALOW, L. V., ISOLA, R., PAPAGEORGIOU, I. E. & KANN, O. 2015b. A reliable model for gamma oscillations in hippocampal tissue. *J Neurosci Res,* 93**,** 1067-78.

SCHULZ-SCHAEFFER, W. J. 2010. The synaptic pathology of alpha-synuclein aggregation in dementia with Lewy bodies, Parkinson's disease and Parkinson's disease dementia. *Acta neuropathologica,* 120**,** 131-143.

SCHUMACHER, J., PERAZA, L. R., FIRBANK, M., THOMAS, A. J., KAISER, M., GALLAGHER, P., O'BRIEN, J. T., BLAMIRE, A. M. & TAYLOR, J.-P. 2019. Dysfunctional brain dynamics and their origin in Lewy body dementia. *Brain,* 142**,** 1767-1782.

SCHWALLER, B. 2007. Emerging Functions of the "Ca2+ Buffers" Parvalbumin, Calbindin D-28k and Calretinin in the Brain. *In:* LAJTHA, A. & BANIK, N. (eds.) *Handbook of Neurochemistry and Molecular Neurobiology: Neural Protein Metabolism and Function.* Boston, MA: Springer US.

SCHWALLER, B. 2010. Cytosolic Ca2+ buffers. *Cold Spring Harbor perspectives in biology,* 2**,** a004051-a004051.

SEGLEN, P. O., BERG, T. O., BLANKSON, H., FENGSRUD, M., HOLEN, I. & STRØMHAUG, P. E. 1996. Structural Aspects of Autophagy. *In:* SUZUKI, K. & BOND, J. S. (eds.) *Intracellular Protein Catabolism.* Boston, MA: Springer US.

SESSOLO, M., MARCON, I., BOVETTI, S., LOSI, G., CAMMAROTA, M., RATTO, G. M., FELLIN, T. & CARMIGNOTO, G. 2015. Parvalbumin-Positive Inhibitory Interneurons Oppose Propagation But Favor Generation of Focal Epileptiform Activity. *The Journal of Neuroscience,* 35**,** 9544.

SEVCSIK, E., TREXLER, A. J., DUNN, J. M. & RHOADES, E. 2011. Allostery in a disordered protein: oxidative modifications to alpha-synuclein act distally to regulate membrane binding. *J Am Chem Soc,* 133**,** 7152-8.

SHAHMORADIAN, S. H., LEWIS, A. J., GENOUD, C., GRAFF-MEYER, A., HENCH, J., MOORS, T., SCHWEIGHAUSER, G., WANG, J., GOLDIE, K. N., SUETTERLIN, R., CASTANO-DIEZ, D., PEREZ-NAVARRO, P., HUISMAN, E., IPSEN, S., INGRASSIA, A., DE GIER, Y., ROZEMULLER, A. J. M., DA PAEPE, A., ERNY, J., STAEMPFLI, A., HOERNSCHEMEYER, J., GROSSERUESCHKAMP, F., NIEDIEKER, D., EL-MASHTOLY, S. F., QUADRI, M., VAN IJCKEN, W. F. J., BONIFATI, V., GERWERT, K., BOHRMANN, B., FRANK, S., BRITSCHGI, M., STAHLBERG, H., VAN DE BERG, W. & LAUER, M. E. 2018. Lewy pathology in Parkinson's disease consists of a crowded organellar, membranous medley. *bioRxiv***,** 137976.

SHENG, Z. H. 2014. Mitochondrial trafficking and anchoring in neurons: New insight and implications. *J Cell Biol,* 204**,** 1087-98.

SHEPHERD, C. E., THIEL, E., MCCANN, H., HARDING, A. J. & HALLIDAY, G. M. 2000. Cortical Inflammation in Alzheimer Disease but Not Dementia With Lewy Bodies. *Archives of Neurology,* 57**,** 817-822.

SHULTS, C. W. 2006. Lewy bodies. *Proceedings of the National Academy of Sciences of the United States of America,* 103**,** 1661.

SIGURDSSON, T. & DUVARCI, S. 2015. Hippocampal-Prefrontal Interactions in Cognition, Behavior and Psychiatric Disease. *Front Syst Neurosci,* 9**,** 190.

SKINNER, F. K., KOPELL, N. & MARDER, E. 1994. Mechanisms for oscillation and frequency control in reciprocally inhibitory model neural networks. *Journal of Computational Neuroscience,* 1**,** 69-87.

SKOVRONSKY, D. M., LEE, V. M. & TROJANOWSKI, J. Q. 2006. Neurodegenerative diseases: new concepts of pathogenesis and their therapeutic implications. *Annu Rev Pathol,* 1**,** 151-70.

SMITH, W. W., JIANG, H., PEI, Z., TANAKA, Y., MORITA, H., SAWA, A., DAWSON, V. L., DAWSON, T. M. & ROSS, C. A. 2005. Endoplasmic reticulum stress and mitochondrial cell death pathways mediate A53T mutant alpha-synuclein-induced toxicity. *Hum Mol Genet,* 14**,** 3801-11.

SOHAL, V. S. 2012a. Insights into cortical oscillations arising from optogenetic studies. *Biological psychiatry,* 71**,** 1039-1045.

SOHAL, V. S. 2012b. Insights into cortical oscillations arising from optogenetic studies. *Biol Psychiatry,* 71**,** 1039-45.

SOHAL, V. S., ZHANG, F., YIZHAR, O. & DEISSEROTH, K. 2009. Parvalbumin neurons and gamma rhythms enhance cortical circuit performance. *Nature,* 459**,** 698-702.

SORRENTINO, Z. A., GOODWIN, M. S., RIFFE, C. J., DHILLON, J.-K. S., XIA, Y., GORION, K.-M., VIJAYARAGHAVAN, N., MCFARLAND, K. N., GOLBE, L. I., YACHNIS, A. T. & GIASSON, B. I. 2019. Unique α-synuclein pathology within the amygdala in Lewy body dementia: implications for disease initiation and progression. *Acta Neuropathologica Communications,* 7**,** 142.

SOSA-ORTIZ, A. L., ACOSTA-CASTILLO, I. & PRINCE, M. J. 2012. Epidemiology of dementias and Alzheimer's disease. *Arch Med Res,* 43**,** 600-8.

SOUSA, V. L., BELLANI, S., GIANNANDREA, M., YOUSUF, M., VALTORTA, F., MELDOLESI, J. & CHIEREGATTI, E. 2009. {alpha}-synuclein and its A30P mutant affect actin cytoskeletal structure and dynamics. *Molecular biology of the cell,* 20**,** 3725-3739.

SOUZA, J. M., GIASSON, B. I., CHEN, Q., LEE, V. M. & ISCHIROPOULOS, H. 2000. Dityrosine cross-linking promotes formation of stable alpha -synuclein polymers. Implication of nitrative and oxidative stress in the pathogenesis of neurodegenerative synucleinopathies. *J Biol Chem,* 275**,** 18344-9.

SPANO, M., SIGNORELLI, M., VITALIANI, R., AGUGLIA, E. & GIOMETTO, B. 2015. The possible involvement of mitochondrial dysfunctions in Lewy body dementia: a systematic review. *Functional neurology,* 30**,** 151-158.

SPILLANTINI, M. G., CROWTHER, R. A., JAKES, R., HASEGAWA, M. & GOEDERT, M. 1998. alpha-Synuclein in filamentous inclusions of Lewy bodies from Parkinson's disease and dementia with lewy bodies. *Proc Natl Acad Sci U S A,* 95**,** 6469-73.

SPILLANTINI, M. G., SCHMIDT, M. L., LEE, V. M., TROJANOWSKI, J. Q., JAKES, R. & GOEDERT, M. 1997. Alpha-synuclein in Lewy bodies. *Nature,* 388**,** 839-40.

SPIRO, R. G. 2002. Protein glycosylation: nature, distribution, enzymatic formation, and disease implications of glycopeptide bonds. *Glycobiology,* 12**,** 43R-56R.

STEFANIS, L. 2012. α-Synuclein in Parkinson's disease. *Cold Spring Harbor perspectives in medicine,* 2**,** a009399-a009399.

STERN, Y. 2012. Cognitive reserve in ageing and Alzheimer's disease. *The Lancet. Neurology,* 11**,** 1006-1012.

STEULLET, P., CABUNGCAL, J. H., COYLE, J., DIDRIKSEN, M., GILL, K., GRACE, A. A., HENSCH, T. K., LAMANTIA, A. S., LINDEMANN, L., MAYNARD, T. M., MEYER, U., MORISHITA, H., O'DONNELL, P., PUHL, M., CUENOD, M. & DO, K. Q. 2017. Oxidative stress-driven parvalbumin interneuron impairment as a common mechanism in models of schizophrenia. *Mol Psychiatry,* 22**,** 936-943.

STEULLET, P., CABUNGCAL, J. H., KULAK, A., KRAFTSIK, R., CHEN, Y., DALTON, T. P., CUENOD, M. & DO, K. Q. 2010. Redox dysregulation affects the ventral but not dorsal hippocampus: impairment of parvalbumin neurons, gamma oscillations, and related behaviors. *J Neurosci,* 30**,** 2547-58.

STEWART, T., SOSSI, V., AASLY, J. O., WSZOLEK, Z. K., UITTI, R. J., HASEGAWA, K., YOKOYAMA, T., ZABETIAN, C. P., LEVERENZ, J. B., STOESSL, A. J., WANG, Y., GINGHINA, C., LIU, C., CAIN, K. C., AUINGER, P., KANG, U. J., JENSEN, P. H., SHI, M. & ZHANG, J. 2015. Phosphorylated α-synuclein in Parkinson's disease: correlation depends on disease severity. *Acta neuropathologica communications,* 3**,** 7-7.

STIVERS, N. S., PELISCH, N., OREM, B. C., WILLIAMS, J., NALLY, J. M. & STIRLING, D. P. 2017. The toll-like receptor 2 agonist Pam3CSK4 is neuroprotective after spinal cord injury. *Exp Neurol,* 294**,** 1-11.

STONE, S. L. 2016. Chapter 26 - Ubiquitination of Plant Transcription Factors. *In:* GONZALEZ, D. H. (ed.) *Plant Transcription Factors.* Boston: Academic Press.

STREIT, W. J. & XUE, Q. S. 2016. Microglia in dementia with Lewy bodies. *Brain Behav Immun,* 55**,** 191-201.

STUSS, D. T. & CRAIK, F. I. M. 2019. Alterations in Executive Functions with Aging. *In:* HEILMAN, K. M. & NADEAU, S. E. (eds.) *Cognitive Changes and the Aging Brain.* Cambridge: Cambridge University Press.

SUGENO, N., TAKEDA, A., HASEGAWA, T., KOBAYASHI, M., KIKUCHI, A., MORI, F., WAKABAYASHI, K. & ITOYAMA, Y. 2008. Serine 129 phosphorylation of alpha-synuclein induces unfolded protein response-mediated cell death. *J Biol Chem,* 283**,** 23179-88.

SULTAN, K., BROWN, K. & SHI, S.-H. 2013. Production and organization of neocortical interneurons. *Frontiers in Cellular Neuroscience,* 7.

SUN, L., GRÜTZNER, C., BÖLTE, S., WIBRAL, M., TOZMAN, T., SCHLITT, S., POUSTKA, F., SINGER, W., FREITAG, C. & J UHLHAAS, P. 2012. *Impaired Gamma-Band Activity during Perceptual Organization in Adults with Autism Spectrum Disorders: Evidence for Dysfunctional Network Activity in Frontal-Posterior Cortices.*

SUN, Y. & WANG, H. 2013. The parietal cortex in sensemaking: the dissociation of multiple types of spatial information. *Comput Intell Neurosci,* 2013**,** 152073.

SURENDRANATHAN, A., SU, L., MAK, E., PASSAMONTI, L., HONG, Y. T., ARNOLD, R., VÁZQUEZ RODRÍGUEZ, P., BEVAN-JONES, W. R., BRAIN, S. A. E., FRYER, T. D., AIGBIRHIO, F. I., ROWE, J. B. & O'BRIEN, J. T. 2018. Early microglial activation and peripheral inflammation in dementia with Lewy bodies. *Brain,* 141**,** 3415-3427.

SWIRSKI, M., MINERS, J. S., DE SILVA, R., LASHLEY, T., LING, H., HOLTON, J., REVESZ, T. & LOVE, S. 2014. Evaluating the relationship between amyloid-β and α-synuclein phosphorylated at Ser129 in dementia with Lewy bodies and Parkinson's disease. *Alzheimer's Research & Therapy,* 6**,** 77.

TAKAHASHI, M., KANUKA, H., FUJIWARA, H., KOYAMA, A., HASEGAWA, M., MIURA, M. & IWATSUBO, T. 2003. Phosphorylation of alpha-synuclein characteristic of synucleinopathy lesions is recapitulated in alpha-synuclein transgenic Drosophila. *Neurosci Lett,* 336**,** 155-8.

TAKAHASHI, R., ISHII, K., SHIMADA, K., OHKAWA, S. & NISHIMURA, Y. 2010. Hypoperfusion of the motor cortex associated with parkinsonism in dementia with Lewy bodies. *J Neurol Sci,* 288**,** 88-91.

TAKAHASHI, T., YAMASHITA, H., NAKAMURA, T., NAGANO, Y. & NAKAMURA, S. 2002. Tyrosine 125 of alpha-synuclein plays a critical role for dimerization following nitrative stress. *Brain Res,* 938**,** 73-80.

TANAKA, K. 2009. The proteasome: overview of structure and functions. *Proceedings of the Japan Academy. Series B, Physical and biological sciences,* 85**,** 12-36.

TANAKA, K. & CHIBA, T. 1998. The proteasome: a protein-destroying machine. *Genes Cells,* 3**,** 499-510.

TAYLOR, J.-P., FIRBANK, M. J., HE, J., BARNETT, N., PEARCE, S., LIVINGSTONE, A., VUONG, Q., MCKEITH, I. G. & O'BRIEN, J. T. 2012. Visual cortex in dementia with Lewy bodies: magnetic resonance imaging study. *The British journal of psychiatry : the journal of mental science,* 200**,** 491-498.

TENNETI, L., D'EMILIA, D. M., TROY, C. M. & LIPTON, S. A. 1998. Role of caspases in N-methyl-D-aspartate-induced apoptosis in cerebrocortical neurons. *J Neurochem,* 71**,** 946-59.

TENREIRO, S., ECKERMANN, K. & OUTEIRO, T. F. 2014. Protein phosphorylation in neurodegeneration: friend or foe? *Front Mol Neurosci,* 7**,** 42.

THAL, D. R., GHEBREMEDHIN, E., RUB, U., YAMAGUCHI, H., DEL TREDICI, K. & BRAAK, H. 2002a. Two types of sporadic cerebral amyloid angiopathy. *J Neuropathol Exp Neurol,* 61**,** 282-93.

THAL, D. R., RUB, U., ORANTES, M. & BRAAK, H. 2002b. Phases of A beta-deposition in the human brain and its relevance for the development of AD. *Neurology,* 58**,** 1791-800.

THEILLET, F. X., BINOLFI, A., BEKEI, B., MARTORANA, A., ROSE, H. M., STUIVER, M., VERZINI, S., LORENZ, D., VAN ROSSUM, M., GOLDFARB, D. & SELENKO, P. 2016. Structural disorder of monomeric alpha-synuclein persists in mammalian cells. *Nature,* 530**,** 45-50.

THOMAS, A., PERFETTI, B., BONANNI, L., ONOFRJ, M., TIRABOSCHI, P. & VARANESE, S. 2008. EEG comparisons in early Alzheimer's disease, dementia with Lewy bodies and Parkinson's disease with dementia patients with a 2-year follow-up. *Brain,* 131**,** 690-705.

TIKIDJI-HAMBURYAN, R. A., MARTÍNEZ, J. J., WHITE, J. A. & CANAVIER, C. C. 2015. Resonant Interneurons Can Increase Robustness of Gamma Oscillations. *The Journal of Neuroscience,* 35**,** 15682.

TOFARIS, G. K., RAZZAQ, A., GHETTI, B., LILLEY, K. S. & SPILLANTINI, M. G. 2003. Ubiquitination of alpha-synuclein in Lewy bodies is a pathological event not associated with impairment of proteasome function. *J Biol Chem,* 278**,** 44405-11.

TRAUB, R. D., BIBBIG, A., FISAHN, A., LEBEAU, F. E., WHITTINGTON, M. A. & BUHL, E. H. 2000. A model of gamma-frequency network oscillations induced in the rat CA3 region by carbachol in vitro. *Eur J Neurosci,* 12**,** 4093-106.

TRAUB, R. D., MILES, R. & BUZSÁKI, G. 1992. Computer simulation of carbachol-driven rhythmic population oscillations in the CA3 region of the in vitro rat hippocampus. *The Journal of physiology,* 451**,** 653-672.

TRAUB, R. D., WHITTINGTON, M. A., BUHL, E. H., JEFFERYS, J. G. & FAULKNER, H. J. 1999. On the mechanism of the gamma --> beta frequency shift in neuronal oscillations induced in rat hippocampal slices by tetanic stimulation. *J Neurosci,* 19**,** 1088-105.

TRAUB, R. D., WHITTINGTON, M. A., COLLING, S. B., BUZSAKI, G. & JEFFERYS, J. G. 1996. Analysis of gamma rhythms in the rat hippocampus in vitro and in vivo. *J Physiol,* 493 (Pt 2)**,** 471-84.

TREMBLAY, R., LEE, S. & RUDY, B. 2016. GABAergic Interneurons in the Neocortex: From Cellular Properties to Circuits. *Neuron,* 91**,** 260-292.

TROJSI, F., CHRISTIDI, F., MIGLIACCIO, R., SANTAMARÍA-GARCÍA, H. & SANTANGELO, G. 2018. Behavioural and Cognitive Changes in Neurodegenerative Diseases and Brain Injury. *Behavioural neurology,* 2018**,** 4935915-4935915.

TROSTCHANSKY, A., LIND, S., HODARA, R., OE, T., BLAIR, I. A., ISCHIROPOULOS, H., RUBBO, H. & SOUZA, J. M. 2006. Interaction with phospholipids modulates alpha-synuclein nitration and lipid-protein adduct formation. *The Biochemical journal,* 393**,** 343-349.

TWEEDY, C. 2019. *Age-dependent hippocampal network dysfuntion in a mouse model of alpha-synucleinopathy.* Thesis (Ph. D.)--Newcastle University, 2019.

TWEEDY, C., KINDRED, N., CURRY, J., WILLIAMS, C., TAYLOR, J.-P., ATKINSON, P., RANDALL, F., ERSKINE, D., MORRIS, C. M., REEVE, A. K., CLOWRY, G. J. & LEBEAU, F. E. N. 2021. Hippocampal network hyperexcitability in young transgenic mice expressing human mutant alpha-synuclein. *Neurobiology of Disease,* 149**,** 105226.

UDAKIS, M., PEDROSA, V., CHAMBERLAIN, S. E. L., CLOPATH, C. & MELLOR, J. R. 2020. Interneuron-specific plasticity at parvalbumin and somatostatin inhibitory synapses onto CA1 pyramidal neurons shapes hippocampal output. *Nature Communications,* 11**,** 4395.

UDDIN, L. Q., NOMI, J. S., HÉBERT-SEROPIAN, B., GHAZIRI, J. & BOUCHER, O. 2017. Structure and Function of the Human Insula. *Journal of clinical neurophysiology : official publication of the American Electroencephalographic Society,* 34**,** 300-306.

UEDA, K., FUKUSHIMA, H., MASLIAH, E., XIA, Y., IWAI, A., YOSHIMOTO, M., OTERO, D. A., KONDO, J., IHARA, Y. & SAITOH, T. 1993. Molecular cloning of cDNA encoding an unrecognized component of amyloid in Alzheimer disease. *Proc Natl Acad Sci U S A,* 90**,** 11282-6.

UEHARA, T., SUMIYOSHI, T. & KURACHI, M. 2015. New Pharmacotherapy Targeting Cognitive Dysfunction of Schizophrenia via Modulation of GABA Neuronal Function. *Current neuropharmacology,* 13**,** 793-801.

UENO, H., TAKAO, K., SUEMITSU, S., MURAKAMI, S., KITAMURA, N., WANI, K., OKAMOTO, M., AOKI, S. & ISHIHARA, T. 2018. Age-dependent and region-specific alteration of parvalbumin neurons and perineuronal nets in the mouse cerebral cortex. *Neurochemistry International,* 112**,** 59-70.

UHLHAAS, P. J. & SINGER, W. 2006. Neural synchrony in brain disorders: relevance for cognitive dysfunctions and pathophysiology. *Neuron,* 52**,** 155-68.

UHLHAAS, P. J. & SINGER, W. 2012. Neuronal dynamics and neuropsychiatric disorders: toward a translational paradigm for dysfunctional large-scale networks. *Neuron,* 75**,** 963-80.

UTTARA, B., SINGH, A. V., ZAMBONI, P. & MAHAJAN, R. T. 2009. Oxidative stress and neurodegenerative diseases: a review of upstream and downstream antioxidant therapeutic options. *Current neuropharmacology,* 7**,** 65-74.

VAN DER ZANDE, J. J., GOUW, A. A., VAN STEENOVEN, I., SCHELTENS, P., STAM, C. J. & LEMSTRA, A. W. 2018. EEG Characteristics of Dementia With Lewy Bodies, Alzheimer's Disease and Mixed Pathology. *Frontiers in aging neuroscience,* 10**,** 190-190.

VAN DUINEN, S. G., LAMMERS, G.-J., MAAT-SCHIEMAN, M. L. C. & ROOS, R. A. C. 1999. Numerous and widespread α-synuclein-negative Lewy bodies in an asymptomatic patient. *Acta Neuropathologica,* 97**,** 533-539.

VANN JONES, S. A. & O'BRIEN, J. T. 2014. The prevalence and incidence of dementia with Lewy bodies: a systematic review of population and clinical studies. *Psychol Med,* 44**,** 673-83.

VARSHAVSKY, A. 2001. Ubiquitin. *In:* BRENNER, S. & MILLER, J. H. (eds.) *Encyclopedia of Genetics.* New York: Academic Press.

VENDA, L. L., CRAGG, S. J., BUCHMAN, V. L. & WADE-MARTINS, R. 2010. alpha-Synuclein and dopamine at the crossroads of Parkinson's disease. *Trends Neurosci,* 33**,** 559-68.

VERRET, L., MANN, E. O., HANG, G. B., BARTH, A. M. I., COBOS, I., HO, K., DEVIDZE, N., MASLIAH, E., KREITZER, A. C., MODY, I., MUCKE, L. & PALOP, J. J. 2012. Inhibitory interneuron deficit links altered network activity and cognitive dysfunction in Alzheimer model. *Cell,* 149**,** 708-721.

VILLAR-PIQUE, A., LOPES DA FONSECA, T. & OUTEIRO, T. F. 2016. Structure, function and toxicity of alpha-synuclein: the Bermuda triangle in synucleinopathies. *J Neurochem,* 139 Suppl 1**,** 240-255.

VISANJI, N. P., LANG, A. E. & KOVACS, G. G. 2019. Beyond the synucleinopathies: alpha synuclein as a driving force in neurodegenerative comorbidities. *Translational neurodegeneration,* 8**,** 28-28.

VOS, M., LAUWERS, E. & VERSTREKEN, P. 2010. Synaptic Mitochondria in Synaptic Transmission and Organization of Vesicle Pools in Health and Disease. *Frontiers in Synaptic Neuroscience,* 2.

VOSPER, J. M. D., MCDOWELL, G. S., HINDLEY, C. J., FIORE-HERICHE, C. S., KUCEROVA, R., HORAN, I. & PHILPOTT, A. 2009. Ubiquitylation on canonical and non-canonical sites targets the transcription factor neurogenin for ubiquitin-mediated proteolysis. *The Journal of biological chemistry,* 284**,** 15458-15468.

VREUGDENHIL, M. & TOESCU, E. C. 2005. Age-dependent reduction of gamma oscillations in the mouse hippocampus in vitro. *Neuroscience,* 132**,** 1151-7.

WAKABAYASHI, K., ENGELENDER, S., YOSHIMOTO, M., TSUJI, S., ROSS, C. A. & TAKAHASHI, H. 2000. Synphilin-1 is present in Lewy bodies in Parkinson's disease. *Ann Neurol,* 47**,** 521-3.

WAKABAYASHI, K., MORI, F., OYAMA, Y., KURIHARA, A., KAMADA, M., YOSHIMOTO, M. & TAKAHASHI, H. 2003. Lewy bodies in Betz cells of the motor cortex in a patient with Parkinson's disease. *Acta Neuropathol,* 105**,** 189-92.

WALDEN, H. & MUQIT, M. M. K. 2017. Ubiquitin and Parkinson's disease through the looking glass of genetics. *The Biochemical journal,* 474**,** 1439-1451.

WALES, P., PINHO, R., LAZARO, D. F. & OUTEIRO, T. F. 2013. Limelight on alpha-synuclein: pathological and mechanistic implications in neurodegeneration. *J Parkinsons Dis,* 3**,** 415-59.

WALKER, D. G., LUE, L. F., ADLER, C. H., SHILL, H. A., CAVINESS, J. N., SABBAGH, M. N., AKIYAMA, H., SERRANO, G. E., SUE, L. I. & BEACH, T. G. 2013. Changes in properties of serine 129 phosphorylated alpha-synuclein with progression of Lewy-type histopathology in human brains. *Exp Neurol,* 240**,** 190-204.

WALSH, D. M., LOMAKIN, A., BENEDEK, G. B., CONDRON, M. M. & TEPLOW, D. B. 1997. Amyloid beta-protein fibrillogenesis. Detection of a protofibrillar intermediate. *J Biol Chem,* 272**,** 22364-72.

WANG, L., WANG, G., DUAN, Y., WANG, F., LIN, S., ZHANG, F., LI, H., LI, A. & LI, H. 2019. A Comparative Study of the Diagnostic Potential of Plasma and Erythrocytic α-Synuclein in Parkinson's Disease. *Neurodegenerative Diseases,* 19**,** 204-210.

WANG, M. & PICKART, C. M. 2005. Different HECT domain ubiquitin ligases employ distinct mechanisms of polyubiquitin chain synthesis. *Embo j,* 24**,** 4324-33.

WANG, X., HERR, R. A., CHUA, W. J., LYBARGER, L., WIERTZ, E. J. & HANSEN, T. H. 2007a. Ubiquitination of serine, threonine, or lysine residues on the cytoplasmic tail can induce ERAD of MHC-I by viral E3 ligase mK3. *J Cell Biol,* 177**,** 613-24.

WANG, X., PEREZ, E., LIU, R., YAN, L. J., MALLET, R. T. & YANG, S. H. 2007b. Pyruvate protects mitochondria from oxidative stress in human neuroblastoma SK-N-SH cells. *Brain Res,* 1132**,** 1-9.

WANG, Y., SHI, M., CHUNG, K. A., ZABETIAN, C. P., LEVERENZ, J. B., BERG, D., SRULIJES, K., TROJANOWSKI, J. Q., LEE, V. M.-Y., SIDEROWF, A. D., HURTIG, H., LITVAN, I., SCHIESS, M. C., PESKIND, E. R., MASUDA, M., HASEGAWA, M., LIN, X., PAN, C., GALASKO, D., GOLDSTEIN, D. S., JENSEN, P. H., YANG, H., CAIN, K. C. & ZHANG, J. 2012. Phosphorylated α-Synuclein in Parkinson's Disease. *Science Translational Medicine,* 4**,** 121ra20-121ra20.

WATROUS, A. J., FELL, J., EKSTROM, A. D. & AXMACHER, N. 2015. More than spikes: Common oscillatory mechanisms for content specific neural representations during perception and memory. *Current Opinion in Neurobiology,* 31**,** 33-39.

WATSON, R., BLAMIRE, A. M. & O'BRIEN, J. T. 2009. Magnetic resonance imaging in lewy body dementias. *Dement Geriatr Cogn Disord,* 28**,** 493-506.

WATSON, R., COLLOBY, S. J., BLAMIRE, A. M. & O'BRIEN, J. T. 2015. Assessment of regional gray matter loss in dementia with Lewy bodies: a surface-based MRI analysis. *Am J Geriatr Psychiatry,* 23**,** 38-46.

WAXMAN, E. A. & GIASSON, B. I. 2011. Characterization of kinases involved in the phosphorylation of aggregated alpha-synuclein. *J Neurosci Res,* 89**,** 231-47.

WEBB, J. L., RAVIKUMAR, B., ATKINS, J., SKEPPER, J. N. & RUBINSZTEIN, D. C. 2003. Alpha-Synuclein is degraded by both autophagy and the proteasome. *J Biol Chem,* 278**,** 25009-13.

WEN, T. H., BINDER, D. K., ETHELL, I. M. & RAZAK, K. A. 2018. The Perineuronal 'Safety' Net? Perineuronal Net Abnormalities in Neurological Disorders. *Frontiers in Molecular Neuroscience,* 11.

WENDLING, F., BARTOLOMEI, F., BELLANGER, J. J. & CHAUVEL, P. 2002. Epileptic fast activity can be explained by a model of impaired GABAergic dendritic inhibition. *Eur J Neurosci,* 15**,** 1499-508.

WHITFIELD, D. R., VALLORTIGARA, J., ALGHAMDI, A., HOWLETT, D., HORTOBAGYI, T., JOHNSON, M., ATTEMS, J., NEWHOUSE, S., BALLARD, C., THOMAS, A. J., O'BRIEN, J. T., AARSLAND, D. & FRANCIS, P. T. 2014. Assessment of ZnT3 and PSD95 protein levels in Lewy body dementias and Alzheimer's disease: association with cognitive impairment. *Neurobiol Aging,* 35**,** 2836-2844.

WHITTAKER, R. G., TURNBULL, D. M., WHITTINGTON, M. A. & CUNNINGHAM, M. O. 2011a. Impaired mitochondrial function abolishes gamma oscillations in the hippocampus through an effect on fast-spiking interneurons. *Brain,* 134**,** e180; author reply e181.

WHITTAKER, R. G., TURNBULL, D. M., WHITTINGTON, M. A. & CUNNINGHAM, M. O. 2011b. Impaired mitochondrial function abolishes gamma oscillations in the hippocampus through an effect on fast-spiking interneurons. *Brain,* 134**,** e180-e180.

WHITTINGTON, M. A. & TRAUB, R. D. 2003. Interneuron diversity series: inhibitory interneurons and network oscillations in vitro. *Trends Neurosci,* 26**,** 676-82.

WHITTINGTON, M. A., TRAUB, R. D. & JEFFERYS, J. G. 1995. Synchronized oscillations in interneuron networks driven by metabotropic glutamate receptor activation. *Nature,* 373**,** 612-5.

WHITWELL, J. L., WEIGAND, S. D., SHIUNG, M. M., BOEVE, B. F., FERMAN, T. J., SMITH, G. E., KNOPMAN, D. S., PETERSEN, R. C., BENARROCH, E. E., JOSEPHS, K. A. & JACK, C. R., JR. 2007. Focal atrophy in dementia with Lewy bodies on MRI: a distinct pattern from Alzheimer's disease. *Brain : a journal of neurology,* 130**,** 708-719.

WIEDEMANN, N., FRAZIER, A. E. & PFANNER, N. 2004. The Protein Import Machinery of Mitochondria. *Journal of Biological Chemistry,* 279**,** 14473-14476.

WILKINSON, K. A. & HENLEY, J. M. 2010. Mechanisms, regulation and consequences of protein SUMOylation. *Biochem J,* 428**,** 133-45.

WILLEMS, J. G. P., WADMAN, W. J. & CAPPAERT, N. L. M. 2018. Parvalbumin interneuron mediated feedforward inhibition controls signal output in the deep layers of the perirhinal-entorhinal cortex. *Hippocampus,* 28**,** 281-296.

WITTENBERG, R., KNAPP, M., HU, B., COMAS-HERRERA, A., KING, D., REHILL, A., SHI, C., BANERJEE, S., PATEL, A., JAGGER, C. & KINGSTON, A. 2019. The costs of dementia in England. *International journal of geriatric psychiatry,* 34**,** 1095-1103.

WOJTOWICZ, A. M., VAN DEN BOOM, L., CHAKRABARTY, A., MAGGIO, N., HAQ, R. U., BEHRENS, C. J. & HEINEMANN, U. 2009. Monoamines block kainate- and carbachol-induced gamma-oscillations but augment stimulus-induced gamma-oscillations in rat hippocampus in vitro. *Hippocampus,* 19**,** 273-88.

WOOD, I. K. 1996. Neuroscience: Exploring the brain. *Journal of Child and Family Studies,* 5**,** 377-379.

WOOD, S. J., WYPYCH, J., STEAVENSON, S., LOUIS, J. C., CITRON, M. & BIERE, A. L. 1999. alpha-synuclein fibrillogenesis is nucleation-dependent. Implications for the pathogenesis of Parkinson's disease. *J Biol Chem,* 274**,** 19509-12.

WOODRUFF, A. R., MCGARRY, L. M., VOGELS, T. P., INAN, M., ANDERSON, S. A. & YUSTE, R. 2011. State-Dependent Function of Neocortical Chandelier Cells. *The Journal of Neuroscience,* 31**,** 17872.

WRASIDLO, W., TSIGELNY, I. F., PRICE, D. L., DUTTA, G., ROCKENSTEIN, E., SCHWARZ, T. C., LEDOLTER, K., BONHAUS, D., PAULINO, A., ELEUTERI, S., SKJEVIK, A. A., KOUZNETSOVA, V. L., SPENCER, B., DESPLATS, P., GONZALEZ-RUELAS, T., TREJO-MORALES, M., OVERK, C. R., WINTER, S., ZHU, C., CHESSELET, M. F., MEIER, D., MOESSLER, H., KONRAT, R. & MASLIAH, E. 2016. A de novo compound targeting alpha-synuclein improves deficits in models of Parkinson's disease. *Brain,* 139**,** 3217-3236.

WU, C. & SUN, D. 2015. GABA receptors in brain development, function, and injury. *Metabolic brain disease,* 30**,** 367-379.

WURM, C. A., NEUMANN, D., LAUTERBACH, M. A., HARKE, B., EGNER, A., HELL, S. W. & JAKOBS, S. 2011. Nanoscale distribution of mitochondrial import receptor Tom20 is adjusted to cellular conditions and exhibits an inner-cellular gradient. *Proceedings of the National Academy of Sciences,* 108**,** 13546-13551.

XIA, M., ZHANG, Y., JIN, K., LU, Z., ZENG, Z. & XIONG, W. 2019. Communication between mitochondria and other organelles: a brand-new perspective on mitochondria in cancer. *Cell & Bioscience,* 9**,** 27.

XU, X., ROBY, K. D. & CALLAWAY, E. M. 2010. Immunochemical characterization of inhibitory mouse cortical neurons: three chemically distinct classes of inhibitory cells. *J Comp Neurol,* 518**,** 389-404.

XU, Y., DENG, Y. & QING, H. 2015. The phosphorylation of α-synuclein: development and implication for the mechanism and therapy of the Parkinson's disease. *Journal of Neurochemistry,* 135**,** 4-18.

YANAGISAWA, N. 2018. Functions and dysfunctions of the basal ganglia in humans. *Proceedings of the Japan Academy. Series B, Physical and biological sciences,* 94**,** 275-304.

YAVICH, L., TANILA, H., VEPSÄLÄINEN, S. & JÄKÄLÄ, P. 2004. Role of alpha-synuclein in presynaptic dopamine recruitment. *J Neurosci,* 24**,** 11165-70.

YE, J., WITTER, M. P., MOSER, M.-B. & MOSER, E. I. 2018. Entorhinal fast-spiking speed cells project to the hippocampus. *Proceedings of the National Academy of Sciences,* 115**,** E1627.

YIN, F., BOVERIS, A. & CADENAS, E. 2014a. Mitochondrial energy metabolism and redox signaling in brain aging and neurodegeneration. *Antioxidants & redox signaling,* 20**,** 353-371.

YIN, G., LOPES DA FONSECA, T., EISBACH, S. E., ANDUAGA, A. M., BREDA, C., ORCELLET, M. L., SZEGO, E. M., GUERREIRO, P., LAZARO, D. F., BRAUS, G. H., FERNANDEZ, C. O., GRIESINGER, C., BECKER, S., GOODY, R. S., ITZEN, A., GIORGINI, F., OUTEIRO, T. F. & ZWECKSTETTER, M. 2014b. alpha-Synuclein interacts with the switch region of Rab8a in a Ser129 phosphorylation-dependent manner. *Neurobiol Dis,* 70**,** 149-61.

YSSELSTEIN, D., DEHAY, B., COSTANTINO, I. M., MCCABE, G. P., FROSCH, M. P., GEORGE, J. M., BEZARD, E. & ROCHET, J.-C. 2017. Endosulfine-alpha inhibits membrane-induced α-synuclein aggregation and protects against α-synuclein neurotoxicity. *Acta neuropathologica communications,* 5**,** 3-3.

YU, S., ZUO, X., LI, Y., ZHANG, C., ZHOU, M., ZHANG, Y. A., UEDA, K. & CHAN, P. 2004. Inhibition of tyrosine hydroxylase expression in alpha-synuclein-transfected dopaminergic neuronal cells. *Neurosci Lett,* 367**,** 34-9.

ZARRANZ, J. J., ALEGRE, J., GOMEZ-ESTEBAN, J. C., LEZCANO, E., ROS, R., AMPUERO, I., VIDAL, L., HOENICKA, J., RODRIGUEZ, O., ATARES, B., LLORENS, V., GOMEZ TORTOSA, E., DEL SER, T.,

MUNOZ, D. G. & DE YEBENES, J. G. 2004. The new mutation, E46K, of alpha-synuclein causes Parkinson and Lewy body dementia. *Ann Neurol,* 55**,** 164-73.

ZHANG, J., LI, X. & LI, J.-D. 2019. The Roles of Post-translational Modifications on α-Synuclein in the Pathogenesis of Parkinson's Diseases. *Frontiers in neuroscience,* 13**,** 381-381.

ZHANG, J., YE, Z. W., SINGH, S., TOWNSEND, D. M. & TEW, K. D. 2018. An evolving understanding of the S-glutathionylation cycle in pathways of redox regulation. *Free Radic Biol Med,* 120**,** 204-216.

ZHANG, L., DONG, Y., XU, X. & XU, Z. 2012. The role of autophagy in Parkinson's disease. *Neural regeneration research,* 7**,** 141-145.

ZHENG, C., BIERI, K. W., HWAUN, E. & COLGIN, L. L. 2016. Fast Gamma Rhythms in the Hippocampus Promote Encoding of Novel Object-Place Pairings. *eNeuro,* 3.

ZHOU, J., BROE, M., HUANG, Y., ANDERSON, J. P., GAI, W. P., MILWARD, E. A., PORRITT, M., HOWELLS, D., HUGHES, A. J., WANG, X. & HALLIDAY, G. M. 2011. Changes in the solubility and phosphorylation of alpha-synuclein over the course of Parkinson's disease. *Acta Neuropathol,* 121**,** 695-704.

ZHOU, Y. & DANBOLT, N. C. 2014. Glutamate as a neurotransmitter in the healthy brain. *Journal of neural transmission (Vienna, Austria : 1996),* 121**,** 799-817.

ZHU, X. H., QIAO, H., DU, F., XIONG, Q., LIU, X., ZHANG, X., UGURBIL, K. & CHEN, W. 2012. Quantitative imaging of energy expenditure in human brain. *Neuroimage,* 60**,** 2107-17.

Appendices

Appendix A

Publications, workshops and presentations

Impaired Fast Network Oscillations and Mitochondrial Dysfunction in a Mouse Model of Alpha-synucleinopathy (A30P)

Emma Robson, [a†] Clare Tweedy, [a†] Nelson Manzanza, [a] John-Paul Taylor, [a] Peter Atkinson, [b] Fiona Randall, [c] Amy Reeve, [a] Gavin J. Clowry [a] and Fiona E. N. LeBeau [a*]

[a] *Institute of Neuroscience, Newcastle University, Medical School, Framlington Place, Newcastle-upon-Tyne, NE2 4HH, UK*

[b] *Eisai Hatfield Research Laboratories, Eisai Ltd., European Knowledge Centre, Mosquito Way, Hatfield, Herts AL10 9SN, UK*

[c] *Eisai AiM Institute, Eisai Inc., 4 Corporate Drive, Andover, MA 01810, USA*

Abstract—Intracellular accumulation of alpha-synuclein (α-syn) is a key pathological process evident in Lewy body dementias (LBDs), including Parkinson's disease dementia (PDD) and dementia with Lewy bodies (DLB). LBD results in marked cognitive impairments and changes in cortical networks. To assess the impact of abnormal α-syn expression on cortical network oscillations relevant to cognitive function, we studied changes in fast beta/gamma network oscillations in the hippocampus in a mouse line that over-expresses human mutant α-syn (A30P). We found an age-dependent reduction in the power of the gamma (20–80 Hz) frequency oscillations in slices taken from mice aged 9–16 months (9 + A30P), that was not present in either young 2–6 months old (2 + A30P) mice, or in control mice at either age. The mitochondrial blockers potassium cyanide and rotenone both reduced network oscillations in a concentration-dependent manner in aged A30P mice and aged control mice but slices from A30P mice showed a greater reduction in the oscillations. Histochemical analysis showed an age-dependent reduction in cytochrome c oxidase (COX) activity, suggesting a mitochondrial dysfunction in the 9 + A30P group. A deficit in COX IV expression was confirmed by immunohistochemistry. Overall, our data demonstrate an age-dependent impairment in mitochondrial function and gamma frequency activity associated with the abnormal expression of α-syn. These findings provide mechanistic insights into the consequences of over-expression of α-syn which might contribute to cognitive decline. © 2018 IBRO. Published by Elsevier Ltd. All rights reserved.

Key words: hippocampus, gamma oscillations, alpha-synuclein, mitochondria, rotenone.

INTRODUCTION

Abnormal intraneuronal deposition of the synaptic protein alpha-synuclein (α-syn) occurs in several neurodegenerative diseases, collectively referred to as the synucleinopathies, which include conditions such as PDD and DLB and a subgroup of patients with Alzheimer's disease (AD). α-syn is a small, 140 amino-acid, soluble protein enriched in the presynaptic terminal of neurons where it plays a role in vesicular trafficking, neurotransmitter release and synaptic maintenance (Cabin et al., 2002; Nemani et al., 2010; Scott et al., 2010). Excess misfolded α-syn forms deposits called Lewy bodies, the pathological hallmark of the synucle-inopathies, which are present throughout the brain including within the hippocampus and neocortex (Spillantini et al., 1998; Lassen et al., 2016).

Cognitive dysfunction is a key feature of both PD dementia (PDD) and DLB, which together, are the second most common cause of dementia in the elderly after AD. Both PDD and DLB are associated with progressive cognitive impairment including memory loss, Parkinsonism, attention deficits and complex visual hallucinations (McKeith et al., 2005). The link between abnormal α-syn expression and cognitive impairment is still unclear, but changes in network oscillations may underlie many of the cognitive deficits seen in neurodegenerative diseases (Nimmrich et al., 2015). Both AD and DLB patients have a general slowing of the electroencephalogram (EEG) activity, particularly from alpha- (8–12 Hz) frequency oscillations to slower theta- (4–8 Hz), and delta- (1–4 Hz) oscillations (Bonanni

et al., 2008, 2016; Morris et al., 2015). The majority of the clinical EEG studies in patients have focused on lower frequency oscillations in the theta 4–8 Hz and alpha 8–12 Hz bands (e.g. Bonanni et al., 2016). However, fast network oscillations in the beta (20–30 Hz) and gamma (30–80 Hz) frequency ranges are also important for cognitive tasks including attention (Clayton et al., 2015), and memory functions (Watrous et al., 2015; Zheng et al., 2016). Several studies have reported impaired gamma activity in patients with AD (Herrmann and Demiralp, 2005; Basar et al., 2016).

Missense mutations, including (A30P) and (A53T), in the human α-syn (SNCA) gene have been identified that are linked to early onset familial Parkinson's disease (Polymeropoulos et al., 1997; Kruger et al., 1998). Several transgenic mouse lines are available that over-express either human or mutant α-syn (Kahle, 2008; Hatami and Chesselet, 2015). To assess the impact of abnormal α-syn on cortical network oscillations we have used the A30P mouse line that over-expresses human mutant α-syn under the control of the CNS promoter Thy-1 (Kahle et al., 2000; Neumann et al., 2002). Previous studies have confirmed widespread expression of human mutant α-syn throughout the mouse brain, including the hippocampus and neocortex, with cognitive deficits evident at ~12 months of age and motor deficits from ~14 months (Kahle et al., 2000; Freichel et al., 2007; Schell et al., 2009). One recent study, using an alternative A53T α-syn transgenic mouse line, reported a general slowing of the EEG in the theta and alpha bands (Morris et al., 2015), consistent with patient data, but the impact of excess α-syn expression on the generation of beta and gamma frequency network oscillations is unknown.

Mitochondrial dysfunction is also a key feature of many neurodegenerative diseases such as PD and AD (Schon and Przedborski, 2011; Spano et al., 2015). Previous studies have shown that acute blockade of complex I of mitochondria in slices from normal animals impairs the generation of fast network oscillations (Kann et al., 2011; Whittaker et al., 2011). Excess α-syn can translocate to the mitochondrial inner membranes and inhibit function (Nakamura et al., 2011), but whether there is a link between excess α-syn, impaired mitochondrial function, and network oscillations remains to be determined.

In this study we wanted to determine whether α-syn over-expression was associated with changes in gamma network oscillations and mitochondrial function. We recorded hippocampal gamma frequency activity *ex vivo* in A30P mice aged between 2 and 16 months and compared results with age-matched control C57BL/6 mice. We found significant impairments in the power of the gamma frequency activity *ex vivo* in A30P mice aged > 9+ months, but not at 2–6 months of age, or in age-matched control mice. Application of the known inhibitors of mitochondrial function (KCN and rotenone) reduced the power of network oscillations in older C57BL6 mice and A30P mice but there was a trend for a greater reduction in the A30P mice. The deficits in network oscillations were associated with a reduced mitochondrial function as indicated by changes in COX/SDH activity in slices only in the older 9 + A30P mice. Our data suggest

that excess human mutant α-syn expression in mice causes abnormal hippocampal gamma frequency oscillations and impaired mitochondrial function that could contribute to cognitive decline.

EXPERIMENTAL PROCEDURES

Transgenic mice

The A30P mice (male and female) were bred in house from breeding pairs supplied by Dr. P. Kahle, University of Tubingen. Transgenic mice of C57BL/6 background expressed human mutant A30P α-syn under the control of the CNS specific promoter Thy-1 (Kahle et al., 2000; Neumann et al., 2002). The transgenic A30P α-syn were maintained as a homozygous colony and aged (2–16 months) in the animal facility. Control mice (male and female) were age-matched C57BL/6 supplied from Charles River and also aged in house. Mice were genotyped after transport and breeding to ensure homozygous expression of A30P α-syn in the mouse colony. Animals were housed according to ARRIVE guidelines and were maintained on a 12-h dark/light cycle with lights on at 7.00 am. For most analyses A30P mice were divided into two age groups referred to as 2 + A30P (2–6 months) and 9 + A30P (9–16 months) but see Results.

Slice preparation and solutions

All mice were anesthetized with inhaled isoflurane prior to intramuscular injection of ketamine ($\geq$100 mg kg^{-1}) and xylazine ($\geq$10 mg kg^{-1}) as described previously (Driver et al., 2007). When all response to noxious stimuli, such as pedal withdrawal reflex, had terminated the animals were intracardially perfused with ~25 mls of modified artificial cerebrospinal fluid (ACSF) that was composed of (mM) 252 sucrose, 3.0 KCl, 1.25 NaH$_2$PO$_4$, 24 NaHCO$_3$, 2.0 MgSO$_4$, 2.0 CaCl$_2$ and 10 glucose. This procedure was in accordance with the UK Animals (Scientific Procedures) Act 1986 and European Union directive 2010/63EU. Following brain removal, 450-μm-thick horizontal slices were cut using a Leica VT1000S vibratome. Slices were then trimmed and transferred to a holding chamber at room temperature for approximately 1 h before being placed in the recording chamber where they were maintained at 32–34 °C at the interface between normal ACSF (where sucrose was replaced with 126 mM NaCl) and humidified 95% O$_2$/5% CO$_2$.

Drugs

Carbachol (10 μM); nitroblue tetrazolium (NBT), phenazine methosulfate (PMS); phosphate buffered saline (PBS); potassium cyanide (KCN 50–100 μM); rotenone (250–1000 nM); (Sigma–Aldrich, Gillingham, Dorset, UK); HistoClear (Fisher Scientific Ltd., Leicester, UK). Rotenone was dissolved in DMSO and stored at −20 °C.

Recording and data acquisition

Extracellular recording electrodes were filled with normal ACSF (resistance 2–5 MΩ). Gamma frequency

oscillations were evoked using the cholinergic agonist carbachol (10 μM) and field traces were recorded from the border between *stratum radiatum* and *stratum lacunosum moleculare* in CA3. Data were recorded with an Axoclamp-2B amplifier (Axon Instruments Inc., Union City, CA, USA). Extracellular data were filtered at 0.001–0.4 kHz low-using Bessel filters. Mains noise was subtracted from the signal with a Humbug (Digitimer, Welwyn Garden City, Herts, UK). Data were redigitized at 10 kHz using an ITC-16 interface (Digitimer, Welwyn Garden City, UK). Data were recorded and analyzed using Axograph 4.6 software (Axon Instruments Inc., Union City, CA, USA). Further offline analysis was performed using MATLAB (Mathworks, Natick, USA).

Data analysis

Power spectra were generated using Axograph by Fourier analysis of 60 s epochs of recorded activity to give the peak frequency of the oscillations. Gamma frequency oscillations in the mouse have previously been shown to have a slower frequency compared to rat ∼20–35 Hz (Driver et al., 2007), therefore, a value for area power was determined as the area under the peak in the power spectra between 15 and 80 Hz. Control oscillations were considered "stable" when area power measurements were within ± 10–15% for three consecutive recordings at 10–15 mins intervals. Rhythmicity was measured from the amplitude of the first side peak of the auto-correlations performed over 1 s traces. The rhythmicity index (RI) was on a scale of 0–1. As multiple slices can be obtained from each animal, in all the data reported below two n values N/n represent animal/slice respectively.

α-synuclein and COX IV immunohistochemistry

Upon termination of electrophysiological recordings, slices were immediately fixed in 4% buffered paraformaldehyde solution and stored in PBS at 4 °C. Following cryoprotection in 30% sucrose in PBS slices were resectioned at 40 μm with a freezing microtome and immunoperoxidase- stained free-floating for either human α-syn using anti-human α-syn (Abcam, Cambridge, UK) 1:5000 dilution, or COX IV antibody (Abcam, Cambridge, UK) 1:100 dilution using standard histological procedures (secondary reagents supplied by Vector Laboratories, Peterborough, UK). Sections were photographed using an Axiovision camera and software and Olympus BX-50 microscope.

COX/SDH activity

Mice were anesthetized with inhaled isoflurane before an intramuscular injection of ketamine and xylazine. Once eye blink and pedal withdrawal reflexes ceased, the brain was removed and snap frozen using isopentane immersed in liquid nitrogen. Brains were then stored in a −80 °C freezer prior to cryosectioning. Snap frozen whole brains were sectioned at 10 μm using a cryostat at −20 °C and collected on to slides. Three sections were collected per slide, with each containing at least one hippocampus. All slides were stored at −80 °C until

ready to use. Slides were removed from the freezer and left to dry at room temperature for 1 h before use. Wherever possible individual slides were processed in large batches to maintain consistency and avoid day-to-day variability in staining. The first section of every slide was used as a control to ensure consistency of COX and SDH media. Half of the control slices received COX incubation medium only, and the other half received SDH incubation medium only. All other sections received both COX and SDH medium. The COX incubation medium was prepared by adding 100 μM cytochrome *c* to 5 mM 3,3′-diaminobenzidine (DAB) and vortexing with a few crystals of catalase. COX medium (50 μL) was applied to each section, and all slides were incubated for 40 min at 37 °C. COX medium was then removed and 2× five-minute washes with 0.1 M PBS were performed. After the final wash, excess PBS was removed from the slides.

The SDH incubation medium was prepared by vortexing together 1.5 mM NBT, 130 mM sodium succinate, 0.2 mM PMS, and 1.0 mM sodium azide. Care was taken to protect the sensitive PMS (and resultant final media) from light. SDH medium (50 μL) was applied to each section, and all sections were incubated for 40 min at 37 °C. SDH medium was then removed and 2× five-minute washes with 0.1 M PBS were carried out. Slides were dehydrated through an ethanol gradient (70%, 95%, 100%, 100%) with 5 min in each ethanol solution and 10 min in the final 100% ethanol solution. Slides were then transferred to two consecutive pots of HistoClear for five minutes of clearing in each and then mounted with DPX.

Quantification of COX/SDH staining and anti-COX IV immunohistochemical staining

Using an Olympus BX51 stereology microscope with an Olympus U-TV1X-2T2 camera, color images of COX/SDH staining were taken at ×10 magnification of the CA3 region of the hippocampus. All slides were assigned a random numerical value to blind the imaging and quantification processes. In the presence of normal COX activity, the brown DAB precipitate which forms inhibits the formation of the blue NBT precipitate with SDH activity (Trifunovic et al., 2004). Therefore, normal COX activity would appear as brown, while a complete absence of COX activity would appear as blue. Using ImageJ's histogram tool (http://rsb.info.nih.gov/ij/), a free-hand selected area of the CA3 pyramidal layer could be analyzed for its mean RGB (red, green, blue) constitution. All values were noted, but the mean blue value (no blue = 0, maximum blue = 255) was compared as a measure of mitochondrial dysfunction. Values obtained from sections were compared to control sections stained for either COX (brown) or SDH (blue) alone. Multiple sections (2–7) per mouse were averaged to give an average per animal, and then animals were compared on average for the young 2 + A30P and older 9 + A30P groups using an unpaired *t* test.

Low power black and white Images of COX IV immunoperoxidase staining were analyzed using ImageJ. The *stratum pyramidale* of the CA3 region was outlined and the area and mean optical density

(white = 0, black = 255) of the immunostaining within this region of interest was measured and normalized against background staining by subtracting the mean optical density of a nearby area of white matter. Six sections were analyzed for each animal, and for each section the total optical density was calculated by multiplying area by the mean optical density. The mean optical density for each animal was calculated by dividing total density by total area from the six sections analyzed. Results from 2 + A30P (*n* = 3) mice were compared with 9 + A30P (*n* = 3) mice.

Statistical analysis

Data were statistically analyzed using Sigmaplot (v12.5) to determine whether it corresponded to a normal (Gaussian) distribution. Normally distributed data were plotted as mean ± s.e.m and compared using a Student's *t*-test. Due to the normal variability, especially in gamma frequency area power, all electrophysiological data were analyzed using non-parametric statistics on the raw data and described as median and interquartile ranges (IQR) or percentage change. When comparing two different groups we used a Mann–Whitney rank sum text. A Wilcoxon signed rank test was used for comparing before and after conditions in the same sample. Repeated measures on the same sample were analyzed using Friedman's repeated measures ANOVA. Multiple groups were compared using Kruskal–Wallis one-way ANOVA on ranks. If the p value for the ANOVA tests showed a significant difference a Dunn's or Tukey's (all pairwise multiple comparison) test was performed to determine which parameters were significantly different. *p* values are reported as significant < 0.05 and < 0.001.

RESULTS

Alpha-syn expression in A30P mice

Immunohistochemical analysis using the human-specific α-syn antibody (see Methods) in slices from the 2 + A30P group, confirmed widespread expression of human α-syn throughout the brain including *stratum pyramidal*e in the hippocampus (Fig. 1A). There was no staining for human α-syn in the hippocampal pyramidal cell layer in age-matched control C57BL6 mice (Fig. 1B). A similar staining pattern was observed for both 9 + A30P and the 9 + C57 mice (data not shown).

Over-expression of α-syn results in an age-dependent decline in gamma frequency activity

Cognitive impairments in the A30P mice have been reported at 12 months of age (Kahle et al., 2000; Freichel et al., 2007), therefore, to assess network oscillations we initially divided A30P mice into four age

groups referred to as 2 + (2–6 months *n* = 21 mice/45 slices); 9–11 months *n* = 7 mice/18 slices, 12–13 months *n* = 7 mice/18 slices, and 14 + (14–16 months, *n* = 3 mice/8 slices). Gamma frequency oscillations can be readily evoked in the CA3 region of the hippocampus following activation of cholinergic receptors with carbachol (Fisahn et al., 1998; Mann et al., 2005). After application of carbachol (10 μM) the area power of the gamma frequency oscillations increased gradually for 2–4 h as previously reported (Lu et al., 2012; Haggerty et al., 2013), and measurements were made once oscillations had stabilized (see Methods).

Our data demonstrated an age-dependent decrease in the area power of the gamma frequency oscillations in the A30P mice (Fig. 2A–E, Table 1). Area power of the gamma activity was significantly different between the 2 + A30P, 9-11A30P, 12-13A30P and 14 + A30P groups (Kruskal–Wallis one-way ANOVA on ranks, *p* < 0.001). A pairwise multiple comparisons test (Dunn's method) showed that slices from the 2 + A30P group had significantly larger oscillations than the 9-11A30P, 12-13A30P, 14 + A30P groups, and versus all 9 + A30P data combined. However, there was no significant difference between any of the older age groups (Fig. 2E). Table 1 shows the median and IQR values for area power in each age group.

In contrast, the frequency of the gamma oscillation was not significantly different (Fig. 2F) between any of the different age groups of A30P mice (Kruskal–Wallis one-way ANOVA on ranks, *p* > 0.001; Table 1). In addition, there was a significant difference in RI values (Fig. 2G, Table 1) overall (Kruskal–Wallis one-way ANOVA on ranks, *p* < 0.05; Table 1); however, a pairwise multiple comparisons test (Dunn's method) did not reveal any significant differences between specific groups. As slices from the 9-11A30P, 12-13A30P or 14 + A30P and all 9 + A30P combined groups all showed reduced gamma frequency area power compared to the 2 + A30P group, these older age groups were combined into the so-called 9 + A30P group for all subsequent analysis (Table 1).
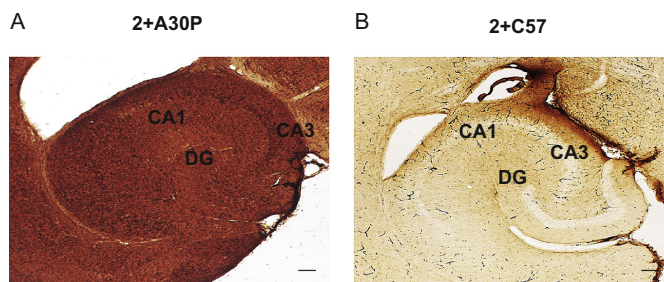

Fig. 1. Alpha synuclein expression in the hippocampus. (A) Immunohistochemistry shows strong human α-syn immunostaining in the hippocampus, especially in the stratum pyramidale, of 2 + A30P mice. (B) 2 + C57 mice do not express human α-syn, although some non-specific staining is observed in erythrocytes and around the section edges. Hippocampal regions *Cornu Ammonis* 1 (CA1), *Cornu Ammonis* 3 (CA3) and dentate gyrus (DG) are indicated. Scale bar = 100 μm.

No sex differences in the power of network oscillations in the A30P mice

Both the 2+ and 9+A30P groups contained data obtained from male and female mice. Therefore, we also assessed these groups separately, but found no significant difference in the stable area power between slices taken from male and female mice (Fig. 3A). Stable area gamma frequency power in 2+A30P male mice was 2066 (IQR 1115–4966; n = 5 mice/11 slices) μV^2 compared with 3325 (IQR 2252–6216; n = 16 mice/34 slices) μV^2 in the female 2+A30P mice

(Kruskal–Wallis one-way ANOVA on ranks p > 0.05). In the 9+A30P group there was also no significant difference between slices taken from male and female mice. Stable area gamma frequency power in 9+A30P male group was 306 (IQR 124–1355; n = 11 mice/30 slices) μV^2 compared with 1484 (IQR 265–2254; n = 5 mice/14 slices) μV^2 in the female 2+A30P group (Kruskal–Wallis one-way ANOVA on ranks p > 0.05). Importantly, slices taken from male and female mice both showed an age-dependent reduction in the area power of the gamma frequency activity between 2+A30P and 9+A30P age groups (p < 0.05, Kruskal–Wallis one-way ANOVA on ranks, Fig. 3A).

The frequency of the gamma oscillation (Fig. 3B) for the 2+A30P male mice was 25.6 (IQR 23.9–27.0; n = 5 mice/11 slices) Hz compared with 25.1 (IQR 23.4–26.8; n = 16 mice/34 slices) Hz in the female 2+A30P mice (p > 0.05). In the 9+A30P group there was a median frequency of 23.6 (IQR 21.6–25.7; n = 11 mice/30 slices) Hz in male mice compared with 26.7 (IQR 23.7–27.7; n = 5 mice/14 slices) Hz in the female 9+A30P group. There were no significant differences between the groups (Kruskal–Wallis one-way ANOVA on ranks, p > 0.05). RI values were also assessed separately for slices from male and female mice (Fig. 3C). For the 2+A30P male mice RI was 0.59 (IQR 0.16–0.75) compared to 0.67 (IQR 0.48–0.74) for female. In the 9+A30P group RI in the male group was 0.29 (IQR 0.13–0.59) compared to 0.48 (IQR 0.24–0.75) in the female group. Again, as above for RI values, there was a significant difference overall (Kruskal–Wallis one-way ANOVA on ranks, p < 0.05) but a multiple comparison procedure did not reveal specific group differences.
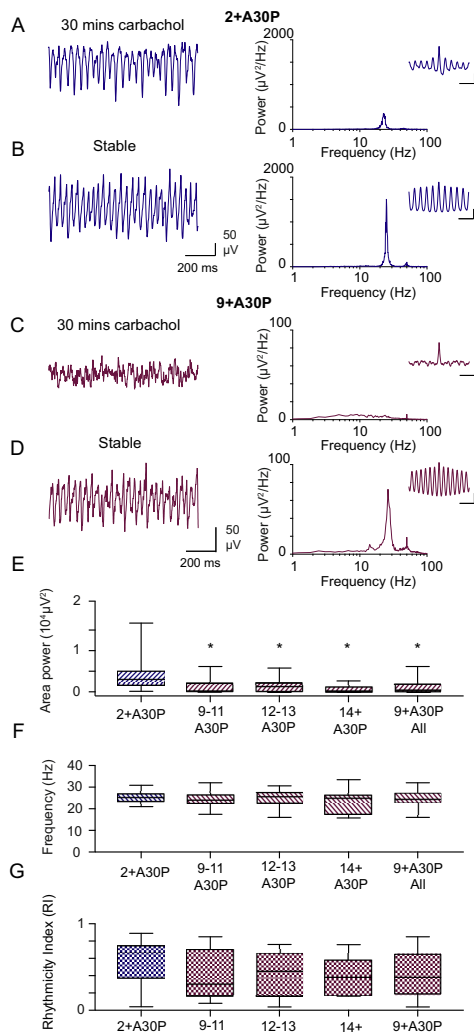
Fig. 2. Age-dependent reduction in gamma frequency activity in A30P mice. (A) Representative 1 s extracellular field trace in 2+A30P (blue) following 30 min bath application of carbachol (10 μM) and the corresponding power spectra. Inset shows auto-correlation. (B) Representative 1 s extracellular field trace when stable gamma activity was reached and corresponding power spectra. Inset shows auto-correlation. (C) Representative 1 s extracellular field trace (maroon) in 9+A30P following 30 min bath application of carbachol (10 μM) and corresponding power spectra. Inset shows auto-correlation. (D) Representative 1 s extracellular field trace when stable gamma activity was reached and corresponding power spectra. Inset shows auto-correlation. Note different scales on power spectra for 2+ and 9+A30P mice. (E) Boxplot shows the median (whiskers max − min) stable area power of the gamma frequency activity in all age groups (1 outlier removed from plot). Asterix (*) indicates power in the 2+A30P group was significantly different from all other groups (p < 0.05; Kruskal–Wallis One-way ANOVA on ranks) and post hoc all pairwise multiple comparison (Dunn's method). (F) Boxplot shows the median (whiskers max − min) frequency of the gamma frequency activity in all age groups. There was no significant difference between any group (p > 0.05; Kruskal–Wallis One-way ANOVA on ranks). (G) Boxplot shows median (whiskers max − min) RI index of the gamma frequency activity in all age groups. There was a significant difference between the groups (p < 0.05; Kruskal–Wallis One-way ANOVA on ranks but post hoc all pairwise multiple comparison (Dunn's method) did not reveal specific group differences. Scale bars for auto-correlation 0.5/100 ms. (For interpretation of the references to color in this figure legend, the reader is referred to the web version of this article.)

Table 1. Stable gamma frequency area power in A30P mice.

A30P	2+ months	9–11 months	12–13 months	14+ months	9+ (all)
Median Power μV^2	3089	306*	1239*	262*	469*
(IQR)	(1656–5452)	(171–2018)	(200–2043)	(30–1121)	(132–1839)
Median Freq. (IQR)	25.3	24.2	25.6	25.0	24.5
Hz	(23.7–26.8)	(22.9–26.3)	(22.9–27.3)	(17.8–26.3)	(22.9–26.9)
N/n = Mice/slice	21/45	7/18	7/18	3/8	17/44
Median	0.66	0.30	0.45	0.39	0.38
RI values	(0.38–0.74)	(0.16–0.69)	(0.16–0.65)	(0.18–0.57)	(0.19–0.65)
(IQR)					
N/n = Mice/slice	21/45	6/16	7/17	3/6	16/39

* Significantly different from 2 + A30P group ($p < 0.05$; Kruskal–Wallis One-way ANOVA on ranks) and post hoc all pairwise multiple comparison (Dunn's method). A clear side peak could not be measured in every auto-correlation in the older A30P so RI values for those slices were excluded.

No age-dependent change in stable gamma frequency activity in control C57 mice

Previous *in vitro* studies have shown an age-dependent decrease in hippocampal gamma oscillations in control mice, but only after approximately > 16 months (Vreugdenhil and Toescu, 2005; Driver et al., 2007). In order to confirm the age-dependent deficit observed in the A30P mice was a consequence of human mutant α-syn expression, and not due to normal aging, we compared a similar age-matched group of control C57BL/6 (male only) mice divided into similar 2+ and 9+ age groups.

In contrast to the data reported above for the A30P mice, we found no age-dependent changes in gamma frequency activity between 2+ and 9+C57 mice (Fig. 4A–G). Stable gamma frequency area power in slices taken from 2+C57 mice was 4779 (IQR 1876–9309; $n = 6$ mice/19 slices) μV^2 compared with 2190 (IQR 415–7928; $n = 6$ mice/15 slices) μV^2 in slices taken from 9+C57 mice (Mann–Whitney rank sum test $p > 0.05$). There was also no difference in the frequency of the gamma oscillations between 2+C57 and 9+C57 control mice (Fig. 4F). The median frequencies in 2+C57 and 9+C57 were 23.3 (IQR 22–24.7; $n = 6$ mice/19 slices) Hz and 25.2 (IQR 22.3 – 26.4; $n = 6$ mice/15 slices) Hz, respectively (Mann–Whitney rank sum test $p > 0.05$). We also assessed possible changes in rhythmicity between the 2 + and 9+C57 mice but there was no significant difference in RI values between the two groups. Median RI in the 2+C57 mice was 0.57 (IQR 0.5–0.65) and 0.49 (IQR 0.2–0.6) in the 9+C57 mice (Mann–Whitney rank sum test $p > 0.05$).

A one way-ANOVA comparing all four groups (2+A20P, 9+A30P, 2+C57 and 9+C57) showed a significance difference ($p < 0.001$; Kruskal–Wallis one-way ANOVA on ranks). Post-hoc analysis confirmed that the gamma frequency area power was significantly smaller only in the 9+A30P (Dunn's pairwise multiple comparison). The above data, therefore, demonstrate an age-dependent reduction in gamma frequency power in the older A30P mice that occurs prior to any normal age-related decline in gamma activity in control mice.

Effects of mitochondrial inhibitors on network gamma frequency oscillations

Previous studies have shown that hippocampal gamma frequency oscillations evoked *in vitro* are sensitive to blockade of mitochondrial complex I and complex IV, with rotenone and KCN respectively (Kann et al., 2011; Whittaker et al., 2011). If the impaired gamma frequency activity observed in the 9+A30P mice reflected an age-dependent reduction in mitochondrial function, we predicted we might observe a greater sensitivity of the oscillatory activity to inhibition of mitochondrial function in slices from the older A30P mice. Thus we compared the concentration-dependent effects of potassium cyanide (KCN 25, 50 and 100 μM), and rotenone (250, 500, and 1000 nM), on stable carbachol-evoked gamma frequency oscillations from older C57 and A30P mice (Fig. 5).

Once oscillations were stable KCN was bath applied incrementally every 30 min with readings taken at 10 min intervals (Fig. 5A, B). There was a rapid reduction in gamma oscillatory power within 10 min in slices from both 9+C57 ($n = 4$ mice/10 slices) and 9+A30P C57 ($n = 3$ mice/6 slices) mice. Compared to control stable values statistically significant reductions were evident at 50 μM and 100 μM KCN in both 9+C57 and 9+A30P groups (Freidman's repeated measures ANOVA on ranks followed by Tukey post hoc multiple comparisons test $p < 0.05$). At the final concentration of KCN tested the power of the gamma activity was reduced by −77 ± 7.6% in 9+C57 group and −82.6 ± 8.3% in the 9+A30P group.

In a further set of experiments, we also tested rotenone and this appeared less effective than KCN. In the control 9+C57 group ($n = 7$ mice/21 slices) there was a clear trend towards a concentration-dependent reduction in gamma power (Fig. 5C) but this was not statistically different at any point when compared to stable control levels (Freidman's repeated measures ANOVA on ranks followed by Tukey post hoc multiple comparisons test $p > 0.05$). However, in the 9+A30P group ($n = 6$ mice/18 slices) at the higher concentrations (Fig. 5D) rotenone did cause a statistically significant decrease compared to stable gamma power (Freidman's repeated measures ANOVA on ranks followed by Tukey post hoc multiple

comparisons test $p < 0.05$). At the final concentration of rotenone tested the power of the gamma activity was reduced by $-29.6 \pm 9.8\%$ in $9+C57$ group and $-41.9 \pm 8.8\%$ in the $9+A30P$ group. The greater decrease in gamma frequency oscillations with rotenone suggests slices from the $9+A30P$ mice are more sensitive to this mitochondrial inhibitor.

Age-dependent mitochondrial dysfunction in the A30P mice

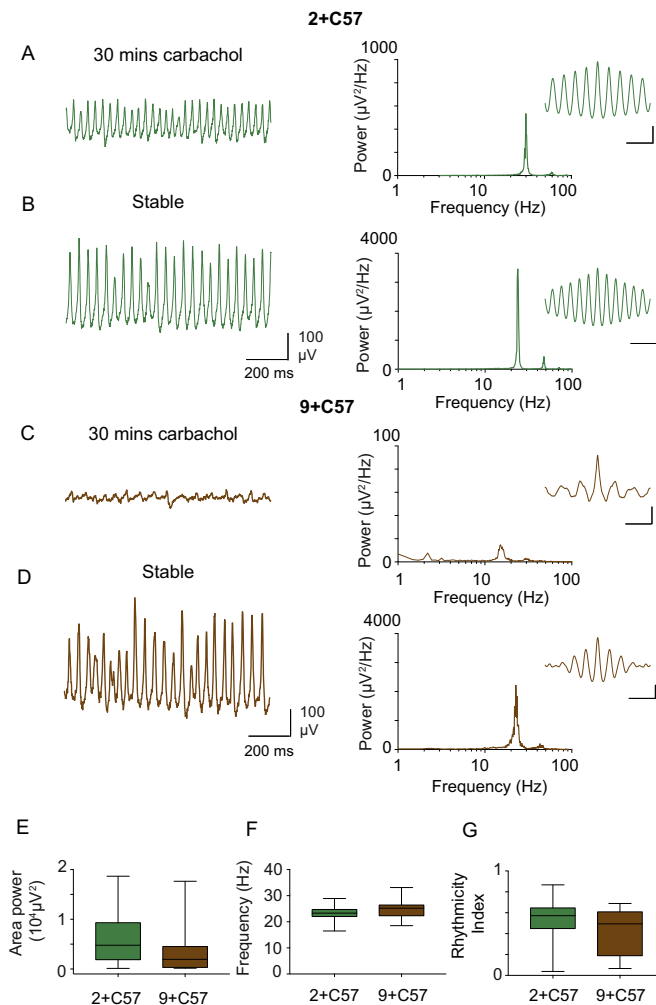The above data suggested that the age-dependent impairment in the power of the gamma frequency
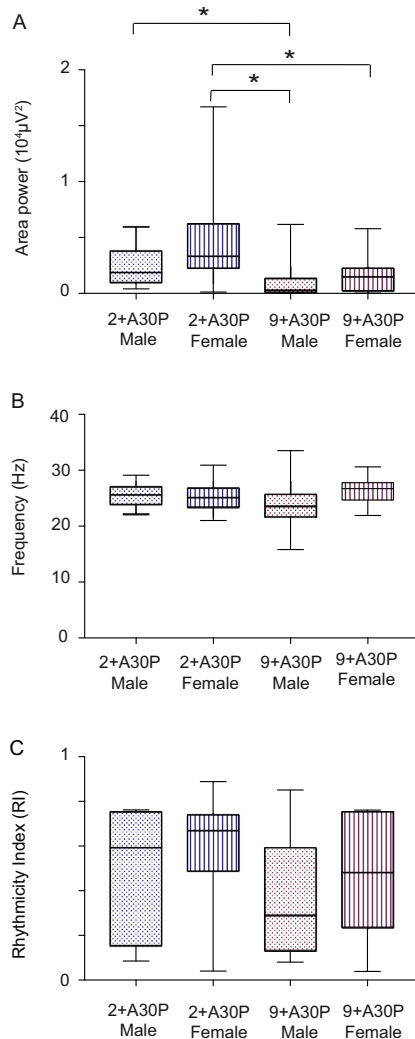
oscillation seen in older A30P mice might reflect a mitochondrial dysfunction in these animals. COX/SDH histochemistry (see Methods) was performed on sections from $2+A30P$ ($n = 5$ mice) and $9+A30P$ ($n = 5$ mice) groups. While we did not detect COX deficiency within individual neurons, a general reduction in COX reactivity was seen across the hippocampus. In order to ascertain if there was any difference in the activity of mitochondria in these sections we measured the changes in RGB balance in the CA3 *stratum pyramidale*, with increased blueness indicating a loss of COX activity (see Methods). The mean blue values for COX alone control was 39.5 ± 2.8 compared to 120.4 ± 4.1 for SDH alone control (Fig. 6A, B) and these control values were highly significantly different ($p < 0.001$). Overall in the $2+A30P$ the mean blue level was 45.17 ± 2.9 compared to 52.59 ± 1.73 in the $9+A30P$ group, which was a statistically significant change in COX/SDH histochemistry in the CA3 *stratum pyramidale* (Fig. 6D-E) in the older $9+A30P$ (Un-paired *t*-test $p < 0.05$). The increased mean blue level suggested an age-dependent decline in mitochondrial COX activity and expression and, therefore, a decrease in mitochondrial function in the $9+A30P$ group. Of note, there was considerable variability between individual mice in the younger $2+A30P$ group (Fig. 6D). In a further set of experiments immunohistochemistry for COX IV immunoperoxidase in the *stratum pyramidale* of the CA3 region also showed a significant 23.3% reduction in optical density in the $9+A30P$ group compared to slices from $2+A30P$ mice (136.7 ± 5.0 to 104.9 ± 5.0, $n = 3$, $p < 0.05$, Fig. 6I). Combined, these data suggest an age-dependent impairment in COX activity and expression indicating a mitochondrial dysfunction was present in the older $9+A30P$ group.

DISCUSSION

In this study we have demonstrated an age-dependent reduction in hippocampal gamma frequency oscillations in slices from older $9+A30P$ mice, compared with younger $2+A30P$ mice, or age-matched control animals. Oscillations in both control C57BL/6 mice and A30P mice were sensitive to inhibitors of mitochondrial

Fig. 3. Area power and frequency in slices from male versus female A30P mice. (A) Boxplot shows the median (whiskers max − min) area power of the gamma frequency activity for slices from male versus female $2+A30P$ and $9+A30P$ mice. Power in the male $2+A30P$ group was significantly different from male $9+A30P$ group ($p < 0.05$; Mann–Whitney rank sum test). Power in the female $2+A30P$ group was significantly different from female $9+A30P$ group ($p < 0.05$; Mann–Whitney rank sum test). (B) Boxplot shows the median (whiskers max − min) frequency of the gamma frequency activity for slices from male versus female $2+A30P$ and $9+A30P$ mice. There was no significant difference in frequency between male and female mice in the $2+A30P$ or $9+A30P$ groups ($p > 0.05$; Mann–Whitney rank sum test). (C) Boxplot shows the median (whiskers max − min) RI of the gamma frequency activity for slices from male versus female $2+A30P$ and $9+A30P$ mice. There was a significant difference between the groups ($p < 0.05$; Kruskal–Wallis One-way ANOVA on ranks but post hoc all pairwise multiple comparison (Dunn's method) did not reveal specific group differences.

2+C57

A 30 mins carbachol

B Stable

100 µV
200 ms

9+C57

C 30 mins carbachol

D Stable

100 µV
200 ms

E

F

G

Fig. 4. No age-dependent changes in gamma frequency activity in control C57BL/6 mice. (A) Representative 1 s extracellular field trace in 2 + C57 (green) following 30 min bath application of carbachol (10 µM) and the corresponding power spectra. Inset shows auto-correlation. (B) Representative 1 s extracellular field trace when stable gamma activity was reached and corresponding power spectra. Inset shows auto-correlation. (C) Representative 1 s extracellular field trace in 9 + C57 (brown) following 30 min bath application of carbachol (10 µM) and corresponding power spectra. Inset shows auto-correlation. (D) Representative 1 s extracellular field trace when stable gamma activity was reached and corresponding power spectra. Inset shows auto-correlation. (E) Boxplot shows the median (whiskers max − min) area power of the gamma frequency activity in both age groups. Power in the 2 + C57 group was not significantly different from the 9 + C57 group ($p > 0.05$; Mann–Whitney rank sum test). (F) Boxplot shows the median (whiskers max − min) frequency of the gamma frequency activity in both age groups. There was no significant difference between any group ($p > 0.05$; Mann–Whitney rank sum test). (G) Boxplot shows the median (whiskers max − min) RI of the gamma frequency activity in both age groups. There was no significant difference between any group ($p > 0.05$; Mann–Whitney rank sum test). Scale bars for auto-correlation 0.5/100 ms. (For interpretation of the references to color in this figure legend, the reader is referred to the web version of this article.)

function but a greater reduction in area power was seen in the older A30P group. COX/SDH staining and anti-COX IV immunohistochemistry revealed a significant age-related decline in mitochondrial function in A30P mice.

Although human α-syn expression was clearly evident in young animals (2 + A30P), the deficits in gamma activity were only seen in the older 9 + A30P mice. One possible explanation for the age-dependence of the change is that reductions in gamma frequency oscillations might be a consequence of a progressive increase in pathology. α-syn is fully expressed in the A30P mice from one month of age (Kahle et al., 2000). However, posttranslational modifications of α-syn, such as phosphorylation or ubiquitination, are associated with Lewy-like pathology in both humans and in mouse α-synucleinopathy models (Lim et al., 2011). In the A30P mice an age-dependent increase in Serine-129 phosphorylation has been reported, that correlated with the cognitive deficits observed in these animals at 12 months of age (Schell et al., 2009). In this study the deficits in gamma activity were evident at 9–11 months of age in the A30P mice, with no significant further changes observed up to 14–16 months of age. This suggests the reductions in gamma frequency activity occur just prior to the onset of quantifiable cognitive dysfunction.

It is not yet known how abnormal α-syn expression might affect synaptic transmission, and the generation of gamma frequency oscillations in the hippocampus. In human post-mortem tissue from patients with a confirmed diagnosis of DLB, α-syn aggregates were found to localize at the synaptic terminal (Kramer and Schulz-Schaeffer, 2007). α-syn is known to undergo misfolding and oligomerisation forming dimers, oligomers and fibrils (Ingelsson, 2016). It is now generally accepted that the oligomeric form is the most toxic, rather than the larger intracellular inclusions. These oligomeric structures may also be transmitted in a prion-like manner through brain structures (Ingelsson, 2016), and thus could impair synaptic
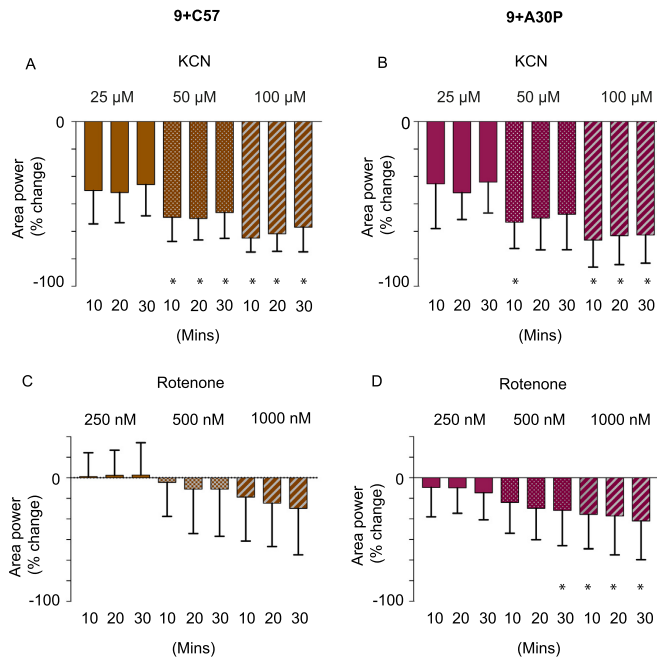
Fig. 5. Effects of mitochondrial inhibitors on network oscillations in the hippocampus. (A) Histogram shows percentage change in area power at 10, 20 and 30 min after application at each concentration of KCN (25 μM, 50 μM and 100 μM) in the 9 + C57 group. (B) Histogram shows percentage change in area power at 10, 20 and 30 min after application at each concentration of KCN (25 μM, 50 μM and 100 μM) in the 9 + A30P group. (C) Histogram shows percentage change in area power at 10, 20 and 30 min after application at each concentration of rotenone (250 nM, 500 nM and 1000 nM) in the 9 + C57 group. (D) Histogram shows percentage change in area power at 10, 20 and 30 min after application at each concentration of rotenone (250 nM, 500 nM and 1000 nM) in the 9 + A30P group. *Indicates significantly different from stable control area power (Freidman's repeated measures ANOVA on ranks and post hoc Tukey test $p < 0.05$).

transmission in subtle ways long before major cognitive decline is evident in the A30P mice. Gamma oscillations in the hippocampus depend upon reciprocal interactions between pyramidal cells and fast-spiking GABAergic interneurons (Whittington et al., 2011) that contain the calcium binding protein parvalbumin (PV). The age-dependent reduction in gamma activity observed in the 9 + A30P mice could reflect changes in either pyramidal cells, interneurons or both and further studies are required to see which cell types are affected or might be selectively vulnerable to α-syn toxicity. However, evidence suggests PV interneurons are particularly vulnerable to metabolic stress due to the high energy demand of their fast firing rates (Kann et al., 2014). Data from AD transgenic mice have implicated loss of PV interneuron function as a key contributor to deficits in network oscillations (Palop and Mucke, 2016). In addition, reductions in PV-positive interneuron staining have been reported in human post-mortem studies in both AD (Brady and Mufson, 1997) and DLB (Bernstein et al., 2011). Further studies are needed to determine if the deficits in gamma frequency

activity observed in aged A30P mice also reflect dysfunction of PV interneurons.

Abnormal α-syn expression in transgenic mice has been associated with both network hyperexcitability (Morris et al., 2015) and mitochondrial dysfunction (Chinta et al., 2010; Rothman et al., 2014; Martin et al., 2014; Chen et al., 2015). α-syn is found in the mitochondria and recently it was shown that α-syn associated with the mitochondria modulates mitochondrial transport and morphology (Pozo Devoto et al., 2017). In transgenic mice that over-express human mutant A53T α-syn both mitochondrial motility (Li et al., 2013) and function (Martin et al., 2014) are impaired. The study by Pozo Devoto et al. (2017) also showed, however, that the effects of over-expression of A53T α-syn in human and mouse derived neuronal cultures were significantly greater than those of over-expression of A30P α-syn. This is in alignment with the observation that the A30P mutation in humans is associated with later onset and less severe clinical symptoms in patients than those seen with the A53T mutation (Kruger et al., 2001; Puschmann et al., 2009). Our data showed a significant age-dependent impairment of both gamma frequency activity, and mitochondrial function, which would be consistent with a slow progression of neurodegenerative changes in the A30P transgenic mice.

Our data using the mitochondrial inhibitors KCN and rotenone showed a concentration-dependent reduction in the power of the gamma frequency activity in both aged wild-type C57 mice and A30P mice. Rotenone blocks mitochondrial complex I while KCN blocks complex IV. Previously, high concentrations of both KCN (100 μM) and rotenone (1 μM) have been shown to cause a rapid collapse of the gamma oscillations (Kann et al., 2011; Whittaker et al., 2011). We had predicted that if A30P mice developed compromised mitochondrial function with age then slices taken from the older A30P mice may be more sensitive to lower concentrations of the inhibitors. While we saw no difference between 9 + C57 and 9 + A30P groups with KCN, the results with rotenone did suggest a slightly greater sensitivity of the oscillations in the 9 + A30P group.

A previous study (Whittaker et al., 2011) showed that KCN (100 μM) had no effect on pyramidal cell properties or excitatory post-synaptic potentials (EPSPs) onto the pyramidal cells, suggesting the changes in oscillations

were not mediated by reductions in glutamatergic neuro-transmission. In contrast, these authors found a reduction in inhibitory post-synaptic potential (IPSPs) on the pyramidal cells, while fast-spiking interneurons were depolarized and spiking activity in the interneurons was abolished (Whittaker et al., 2011). This loss of action

A COX control

B SDH control

C 2+A30P

D 9+A30P

D 2+A30P

E 9+A30P

E 2+A30P

F 9+A30P

I
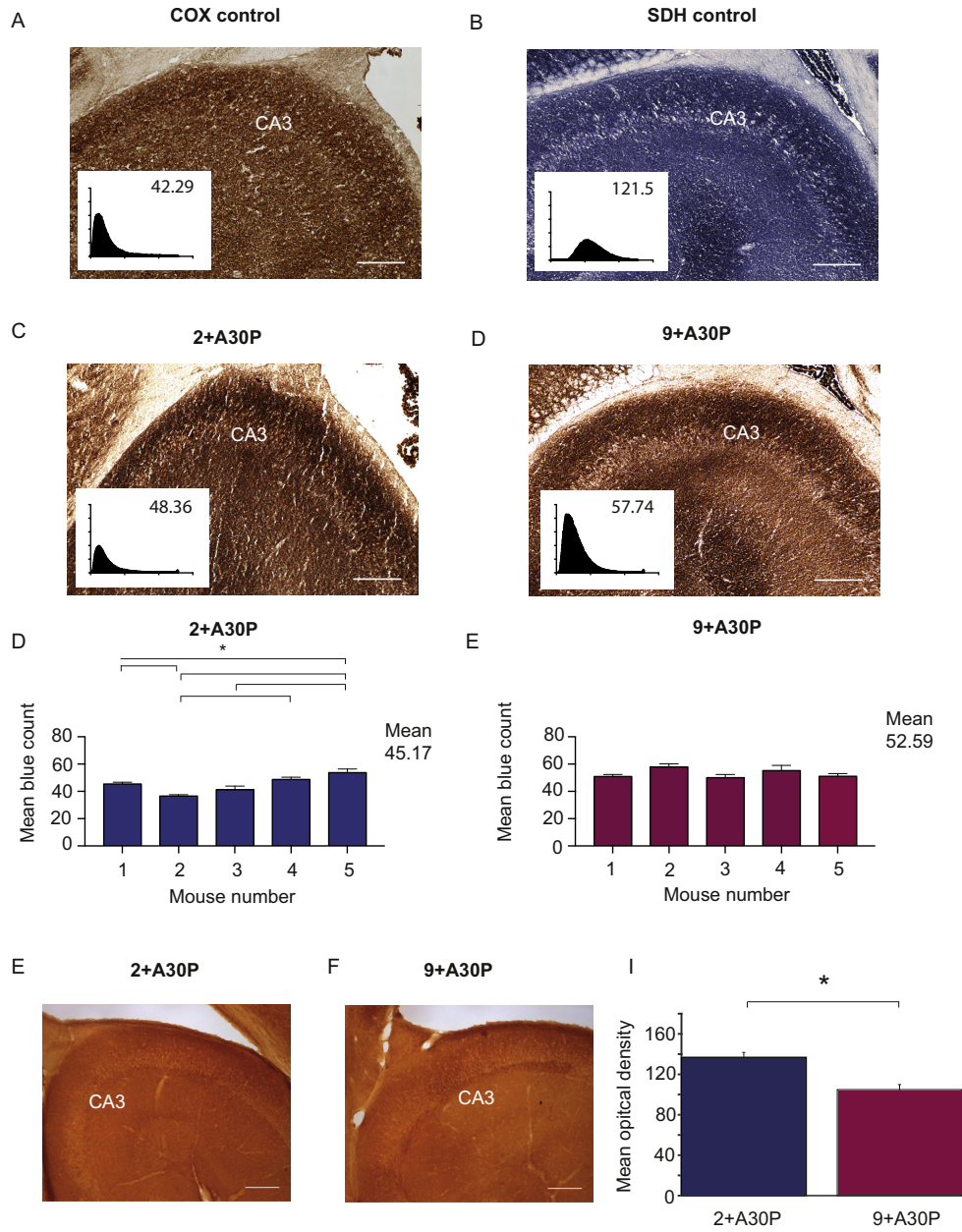
Fig. 6. Age-dependent reduction in mitochondrial function in A30P mice. (A) Representative sections from the hippocampal CA3 region showing COX activity and (B) SDH activity only in sections from the 2 + A30P group. Inset histograms show the individual blue stain intensity in the RGB spectra using ImageJ for each section shown (x-axis scale 0–255). (C) Representative sections from the hippocampal CA3 region and inset histograms of blue stain intensity in the RGB spectra using ImageJ values from 2 + A30P animals and (D) 9 + A30P where the mean blue intensity level is significantly increased, indicating a reduction in COX activity. Scale bars = 100 μm. (E) Mean blue intensity levels for each mouse in 2 + A30P and (F) 9 + A30P groups. There was significant variability between values for individual mice in the 2 + A30P group. (G) Shows examples of anti-COX immunostaining in 2 + A30P and (H) 9 + A30P mice. (I) Mean optical density measurements from the CA3 *stratum pyramidale* revealed a significant decrease in immunoreactivity in the 9 + A30P group. (For interpretation of the references to color in this figure legend, the reader is referred to the web version of this article.)

potential firing in fast spiking interneurons, and the subsequent decrease in IPSP amplitude could account for the reduction in gamma frequency oscillations observed both in their study and in the current experiments. As outlined above the higher sensitivity of interneurons to inhibition of mitochondrial function is consistent with their high metabolic requirements (Kann, 2016). Rotenone block of complex I can cause either an increase in reactive oxygen species (ROS) or ATP depletion. It would be interesting in further studies to assess whether interventions that prevent oxidative stress and energy failure have any impact on the impaired gamma frequency activity in the older A30P mice.

COX/SDH histochemistry detects alterations in the activity of complex IV and II respectively, and we found a significant deficit in COX activity and presumably expression in the 9 + A30P group, although SDH expression in complex II was retained. An age-dependent deficit in COX IV expression was confirmed by immunohistochemistry in the 9 + A30P group. This result is suggestive of mitochondrial dysfunction, which may be caused by mutations in key mitochondrial genes either within mitochondrial DNA (mtDNA) or the nucleus. In aging human neurons, a reduction in COX activity is predominantly associated with deletions within mtDNA, which is vulnerable to oxidative damage, whereas the preservation of SDH activity in these situations is because it is entirely nuclear encoded, meaning that its activity is not affected by mutations in mtDNA (Bender et al., 2006; Kraytsberg et al., 2006; Krishnan et al., 2012). The variability in COX staining seen between different mice in the 2 + A30P group may also indicate early changes, which while not significant as a group, suggest changes in mitochondrial function may already be starting to occur in some animals. Although from the current study we cannot ascertain whether the mitochondrial dysfunction is cell type specific, impairments in pyramidal cells and/or fast-spiking interneurons could result in the reduction in gamma frequency activity observed in the older 9 + A30P mice.

CONCLUSIONS

Several studies have shown that α-syn oligomers impair hippocampal long-term potentiation (LTP), which is thought to represent the cellular mechanism of learning and memory. However, to our knowledge, this is the first study to report deficits in cognitively relevant, beta/gamma frequency network oscillations in the hippocampus in mice that express abnormal human mutant α-syn. We have shown a consistent deficit in

oscillations in aged mice overexpressing α-syn that precedes reported behavioral deficits and correlates temporally with observed changes in mitochondrial function.

REFERENCES

Basar E, Emek-Savas DD, Guntekin B, Yener GG (2016) Delay of cognitive gamma responses in Alzheimer's disease. Neuroimage Clin 11:106–115.

Bender A, Krishnan KJ, Morris CM, Taylor GA, Reeve AK, Perry RH, Jaros E, Hersheson JS, et al. (2006) High levels of mitochondrial DNA deletions in substantia nigra neurons in aging and Parkinson disease. Nat Genet 38:515–517.

Bernstein HG, Johnson M, Perry RH, LeBeau FE, Dobrowolny H, Bogerts B, Perry EK (2011) Partial loss of parvalbumin-containing hippocampal interneurons in dementia with Lewy bodies. Neuropathology 31:1–10.

Bonanni L, Thomas A, Tiraboschi P, Perfetti B, Varanese S, Onofrj M (2008) EEG comparisons in early Alzheimer's disease, dementia with Lewy bodies and Parkinson's disease with dementia patients with a 2-year follow-up. Brain 131:690–705.

Bonanni L, Franciotti R, Nobili F, Kramberger MG, Taylor JP, Garcia-Ptacek S, Falasca NW, Fama F, et al. (2016) EEG markers of dementia with lewy bodies: a multicenter cohort study. J Alzheimers Dis 54:1649–1657.

Brady DR, Mufson EJ (1997) Parvalbumin-immunoreactive neurons in the hippocampal formation of Alzheimer's diseased brain. Neuroscience 80:1113–1125.

Cabin DE, Shimazu K, Murphy D, Cole NB, Gottschalk W, McIlwain KL, Orrison B, Chen A, et al. (2002) Synaptic vesicle depletion correlates with attenuated synaptic responses to prolonged repetitive stimulation in mice lacking alpha-synuclein. J Neurosci 22:8797–8807.

Chen L, Xie Z, Turkson S, Zhuang X (2015) A53T human alpha-synuclein overexpression in transgenic mice induces pervasive mitochondria macroautophagy defects preceding dopamine neuron degeneration. J Neurosci 35:890–905.

Chinta SJ, Mallajosyula JK, Rane A, Andersen JK (2010) Mitochondrial alpha-synuclein accumulation impairs complex I function in dopaminergic neurons and results in increased mitophagy in vivo. Neurosci Lett 486:235–239.

Clayton MS, Yeung N, Cohen Kadosh R (2015) The roles of cortical oscillations in sustained attention. Trends Cogn Sci 19:188–195.

Driver JE, Racca C, Cunningham MO, Towers SK, Davies CH, Whittington MA, LeBeau FE (2007) Impairment of hippocampal

- The following paper was recently published.

Review

Alpha-Synuclein post-translational modifications: Implications for pathogenesis for Lewy body dementias

Nelson de Oliveira Manzanza[1], Lucia Sedlackova[2] and Rajesh N Kalaria[1]

Author affiliation:

[1]Translational and Clinical Research Institute, Campus for Ageing and Vitality, Newcastle University, Newcastle upon Tyne, NE4 5PL, UK

[2]Biosciences Institute, Campus for Ageing and Vitality, Newcastle University, Newcastle upon Tyne, NE4 5PL, UK

Abstract

Lewy Body Dementias (LBD) are age related neurodegenerative disorder characterized by the presence of neuronal inclusions termed Lewy Bodies (LB) and extracellular Lewy Neurites (LN). They are considered the second most common form of neurodegenerative dementia after Alzheimer's disease. LBD are progressive pathologic conditions with variable clinical symptoms. Currently there are no effective treatments for these disorders. LBs and LNs inclusions are mainly composed of α-synuclein (α-syn) aggregates. It has been proposed that posttranslational modifications such as α-syn phosphorylation, ubiquitination SUMOylation, Nitration, o-GlcNacylation and Truncation play important roles in the formation of toxic forms of α-syn, which consequently facilitates the formation of these inclusions. This review outlines the involvement of different posttranslational modifications (PTMs) of α-syn as described in in the spectrum of the synucleinopathies, with a particular focus on LBD. We provide insight into how these PTMs interact with α-syn to cause misfolding and aggregation of α-syn, leading to the potential functional and pathogenic consequences so far detected, and their particular involvement in the development of LBD.

Key words: Lewy body dementias, posttranslational modifications, alpha synuclein

- The following papers are being prepared for publication.

1

Review

Parvalbumin expressing interneurons the brains conductor of the neural networks: Implications for pathogenesis for Dementia with Lewy bodies.

Nelson de Oliveira Manzanza[1], Yoshiki Hase[1], and Rajesh N Kalaria[1]

Author affiliation:
[1]Translational and Clinical Research Institute, Campus for Ageing and Vitality, Newcastle University, Newcastle upon Tyne, NE4 5PL, UK

Abstract
Dementias with Lewy bodies (DLB) is an age related neurodegenerative disorder pathologically characterized by the presence of abnormal intraneuronal aggregates termed Lewy Bodies (LB) and extracellular Lewy Neurites (LN). It is a prevalent form of dementia in the elderly after Alzheimer's disease. DLB is a progressive pathologic condition that curse with variable clinical symptoms, which includes motor impairments, cognitive dysfunctions and neuronal network impairments. As yet there are no drugs that can halt or cure this disease. It has been proposed that dysfunction/loss of parvalbumin-expressing interneurons underlie the pathogenesis of DLB. Indeed PV interneuron impairments leads to disruptions of the neuronal network, negatively affecting the information processing in the neocortex, causing impairments in complex brain functions such as movements and cognition. This review outlines the involvement of fast spiking parvalbumin expressing interneurons as described in the spectrum of the neuronal networks, with a particular focus on DLB. Providing insights into how parvalbumin-expressing interneurons affects the neuronal network in neurodegenerative conditions such as DLB.

Key words: Dementia with Lewy bodies, Parvalbumin interneurons, neuronal networks.

- Chapters 3, 4 and 5 of this thesis are also being prepared for publications

Oral presentations

- **Institute of Neuroscience postgraduate symposium:** Investigating abnormal network in mouse model of alpha synucleinopathy.
- **York University meeting**: Investigating abnormal network in mouse model of alpha synucleinopathy.

Other courses

- Neurocourses, UK 2018- the limbic system, Kings College, London
- North East Bio Imaging Workshop 2018
- Animal Licence course 2018

Training Workshops Report

NELSON Manzanza
Student no. 160376319
Programme - PhD Translational and Clinical Research (FT)
Stage - Year 4 Writing Up

WORKSHOPS	Date	Attended
Managing your PhD/MPhil for part-time and staff candidates	Tuesday 10th Oct 2017	Yes
EndNote	Monday 6th Nov 2017	Yes
Writing a Literature Review	Wednesday 7th Mar 2018	Yes
Your Personal Development Plan (PDP) - Preparing for the Progress Review Panel	Monday 12th Mar 2018	Yes
Advanced Document Management - Using Word and Endnote	Tuesday 19th Jun 2018	Yes
Academic Writing: Accessible Abstracts	Wednesday 11th Jul 2018	Yes
PG NICE Focus Group	Thursday 7th Feb 2019	Yes
Thesis Writing	Friday 8th Feb 2019	Yes
Research Ethics - Theory	Tuesday 12th Feb 2019	Yes
Research Ethics - Application	Tuesday 12th Feb 2019	Yes
Writing a Literature Review	Wednesday 6th Mar 2019	Yes
TOTAL		19

Report generated: Nov. 18, 2020, 12:20 p.m.
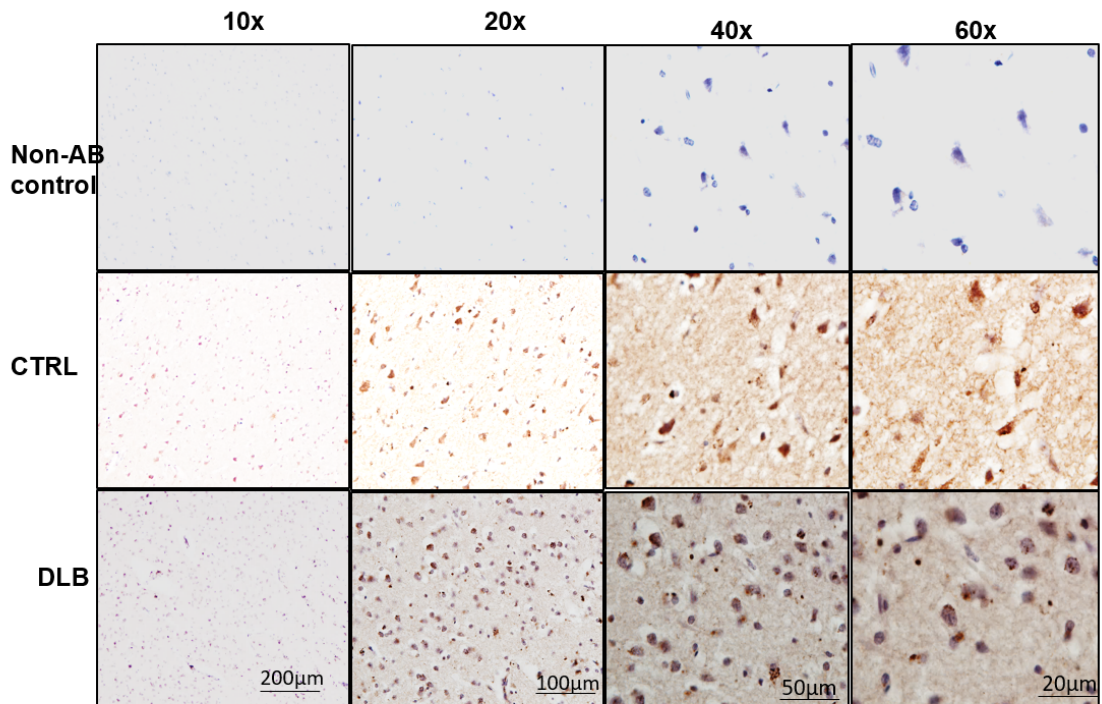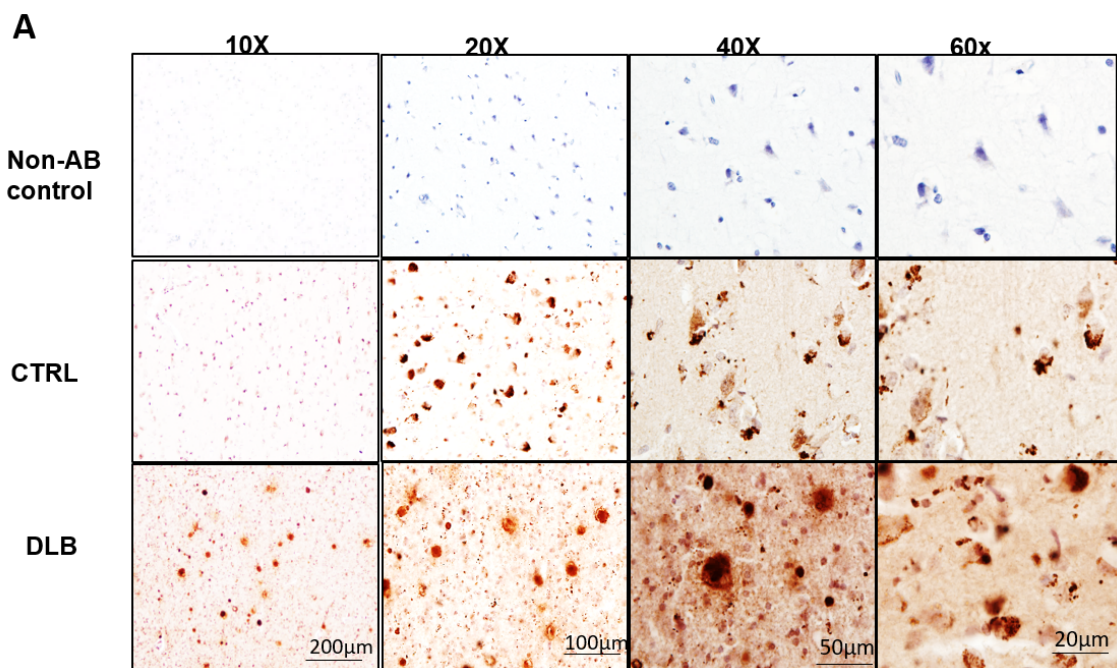
PV+ Interneurons in A30P mice
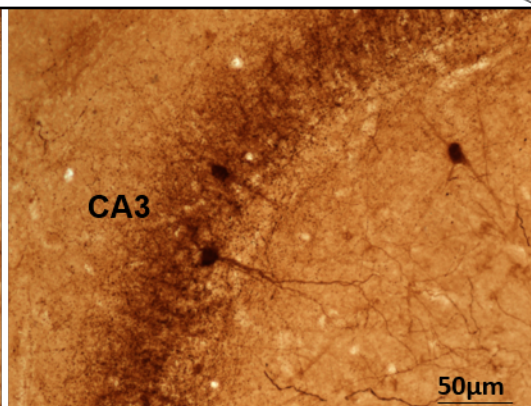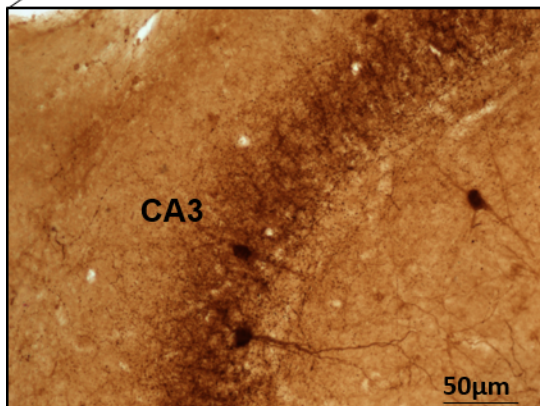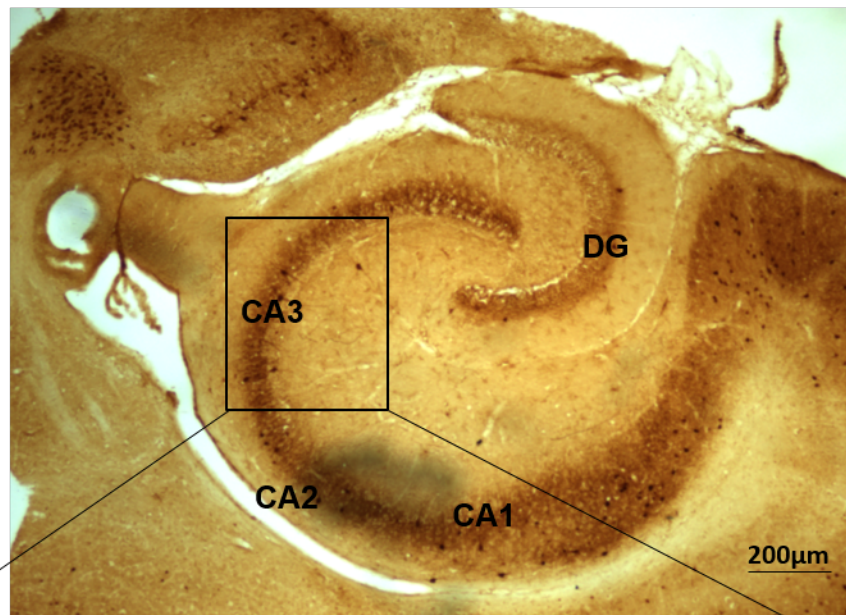
Immunoreactivity for Nitrated aSyn in DLB and control cases Using Citrate antigen retrieval

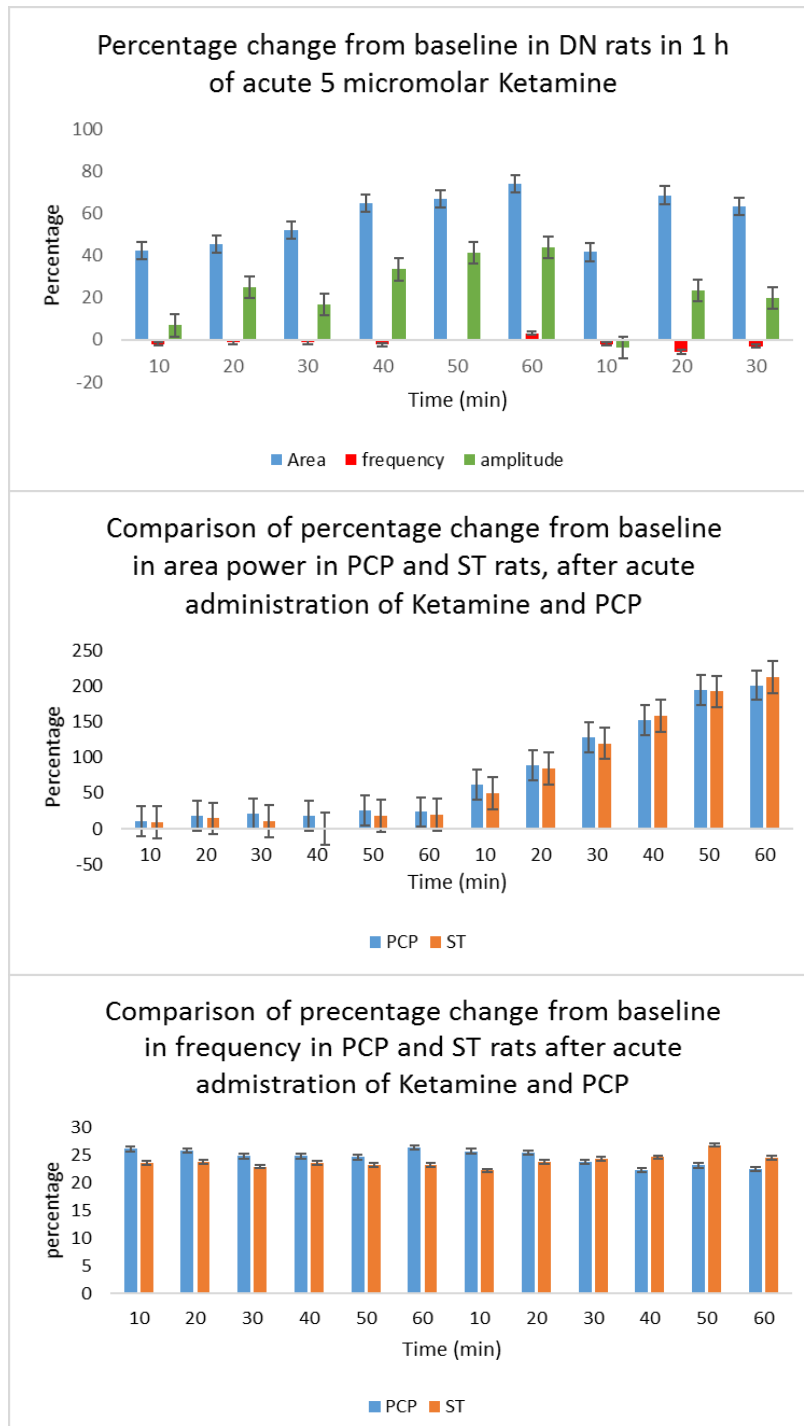## Immunoreactivity for Nitrated aSyn in DLB and control cases Using EDTA antigen retrieval

A

Characterization of fast neuronal network oscillations in ACC slices in PCP, control and saline treated Rats with acute administration of ketamine20µM

Percentage change from baseline in DN rats in 1 h of acute 5 micromolar Ketamine

Comparison of percentage change from baseline in area power in PCP and ST rats, after acute administration of Ketamine and PCP

Comparison of precentage change from baseline in frequency in PCP and ST rats after acute admistration of Ketamine and PCP

Characterization of the effects of phencyclidine (PCP 10 µM) in gamma network oscillations in ACC of Rats.
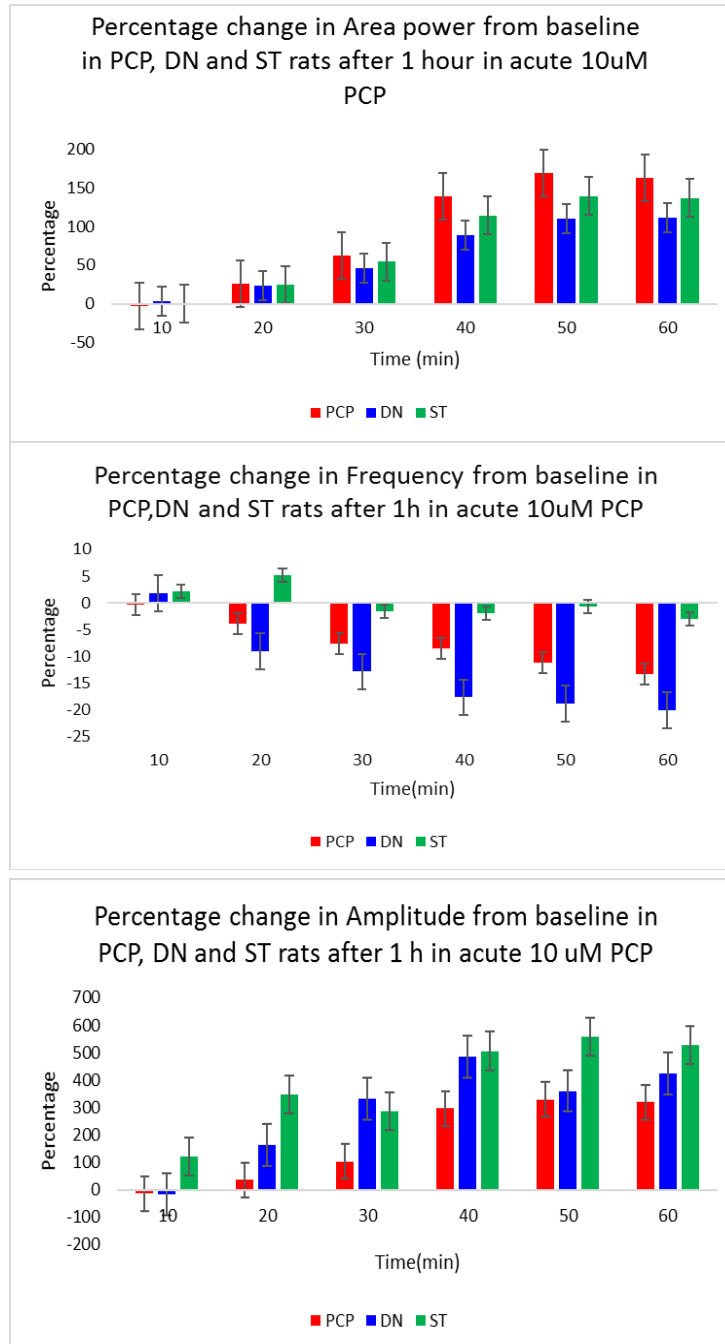
Appendix F

Analysis of the area power, frequency and amplitude in acute administration of DAP5 25μM in PCP, Drug Naïve(DN) and Saline(ST) treated Rats.

Percentage change in Area power from baseline in response to acute administration of DAP5 25 uM in DN,PCP and saline treated rats

Percentage change in frequency from baseline in response to acute administration of DAP5 25 uM in PCP,DN and Saline treated rats

Percentage change in amplitude from baseline in response to acute administration of DAP5 25 uM in PCP, DN and saline treated rats